ISSN 1816-8957

No. 31, October 2022

Scientific Drilling

Reports on Deep Earth Sampling and Monitoring

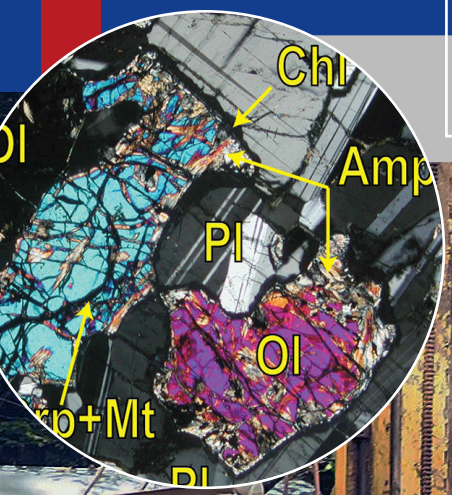

Editorial preface

Dear Reader,

We would like to invite you to take a break from your usual office work and disregard the financial crises, the pandemic, and the brutal war on Ukraine for a moment. Instead, enjoy an informative plunge into Earth's history as unveiled by this issue of Scientific Drilling.

Sedimentary archives formed by monsoonal action, glaciation, or opening and closing of marine gateways are the focus of three articles published in this issue of Scientific Drilling.

IODP conducted a series of expeditions between 2013 and 2016 spanning the region from the Arabian Sea to the Sea of Japan and southward to western Australia. They were designed to address the long-term development of monsoon climate systems between Southeast Asia and Australia. Comparisons of the monsoonal records in the different drilling areas are discussed in a synthesis paper (**p. 1**) and indicate drying trends in most parts of Asia since ~10 Ma, which contrasts with the northwestern Australian wet phase at 5.0–2.5 Ma. The sedimentary infill of glacially overdeepened valleys renders an excellent yet underexplored archive with regard to the age, extent, and nature of past waxing and waning glaciations. The ICDP project 'Drilling Overdeepened Alpine Valleys', DOVE, highlights paleontological evidence of overdeepened valleys along the northern front of the Alps in Switzerland and Germany that preserves sediment records throughout repeated glacial cycles (**p. 51**). A report on a MagellanPlus workshop (**p. 93**) lays out the ambitious plan of ocean drilling to elucidate the complex evolution of the Mediterranean gateways over the past 7 Myr as a driver of environmental challenges severely impacting marine and terrestrial biota in Eurasia.

Another science report in this issue addresses the ICDP Eger Project in the Bohemian (Czech Republic) geodynamic region (**p. 31**), where seismic swarms and carbon dioxide emanations are connected to late-stage volcanism. Five boreholes have so far been drilled, and ongoing installations serve as an in situ geodynamic borehole laboratory.

Two articles on technical developments round off this issue: a study (**p. 85**) that proposes a method to calculate parameters of cylindrical concentric folds by considering the point at which the bedding trend changes as an inflexion point of the fold. Another one (**p. 71**) constitutes saw cuttings from core splitting as a valuable subsample to obtain an average mineralogical and geochemical composition of a core, as it was applied on the core of the lower oceanic crust in the Hess Deep rift obtained during IODP Expedition 345.

With best regards,

the editors of *Scientific Drilling*

Ulrich Harms, Thomas Wiersberg, Jan Behrmann, Tomoaki Morishita, and Will Sager

Aims & scope

Scientific Drilling (SD) is a multidisciplinary journal focused on bringing the latest science and news from the scientific drilling and related programmes to the geosciences community. Scientific Drilling delivers peer-reviewed science reports from recently completed and ongoing international scientific drilling projects. The journal also includes reports on engineering developments, technical developments, workshops, progress reports, and news and updates from the community.

Editorial board

Additional information

ISSN 1816-8957 | eISSN 1816-3459

Copernicus Publications
The Innovative Open Access Publisher

Copernicus Publications
Bahnhofsallee 1e
37081 Göttingen
Germany
Phone: +49 551 90 03 39 0
Fax: +49 551 90 03 39 70

editorial@copernicus.org
production@copernicus.org

https://publications.copernicus.org

View the online library or learn more about Scientific Drilling on:
www.scientific-drilling.net

Cover figure: Core drilling at Basadingen, Switzerland as part of phase 1 of the ICDP project DOVE (Drilling Overdeepened Alpine Valleys). Photo: Friedrich Hawemann.
Insert 1: Eger Rift drilling of a seismological monitoring well at the Studenec (Czech Republic). Tomáš Fischer et al., 2002, this volume.
Insert 2: Cross-polarized light images of minerals from IODP Expedition 345 to the Hess Deep rift. Wintsch et al., 2022, this volume.

Contents

Science Reports

Technical Developments

Workshop Reports

Sci. Dril., 31, 1–29, 2022
https://doi.org/10.5194/sd-31-1-2022

Scientific Drilling
Open Access

A synthesis of monsoon exploration in the Asian marginal seas

Peter D. Clift[1], Christian Betzler[2], Steven C. Clemens[3], Beth Christensen[4], Gregor P. Eberli[5], Christian France-Lanord[6], Stephen Gallagher[7], Ann Holbourn[8], Wolfgang Kuhnt[8], Richard W. Murray[9], Yair Rosenthal[10], Ryuji Tada[11], and Shiming Wan[12]

[1]Department of Geology and Geophysics, Louisiana State University, Baton Rouge, LA 70803, USA
[2]Institute for Geology, German Research Fleet Coordination Center, University of Hamburg, Bundesstrasse 55, 20146 Hamburg, Germany
[3]Department of Earth, Environmental and Planetary Sciences, Box 1846, Brown University, Providence, RI 02912-1846, USA
[4]Department of Environmental Science, Rowan University, 201 Mullica Hill Road, Glassboro, NJ 08028, USA
[5]CSL – Center for Carbonate Research, University of Miami, 4600 Rickenbacker Causeway, Miami, FL 33149, USA
[6]Centre de Recherches Pétrographiques et Géochimiques, Université de Nancy, CNRS UMR 7358, 54500, Vandoeuvre-lès-Nancy, France
[7]School of Geography, Earth and Atmospheric Sciences, The University of Melbourne, Victoria, 3010, Australia
[8]Institute of Geosciences, Christian-Albrecht University, Olshausenstrasse 40, 24118 Kiel, Germany
[9]Woods Hole Oceanographic Institution, Woods Hole, MA 02543, USA
[10]School of Environmental and Biological Sciences, Rutgers, The State University of New Jersey, 71 Dudley Road, New Brunswick, NJ 08901-8520, USA
[11]Department of Earth and Planetary Science, The University of Tokyo, 7-3-1 Hongo, Bunkyo-Ku, Tokyo, 113-0033, Japan
[12]Key Laboratory of Marine Geology and Environment, Institute of Oceanology, Chinese Academy of Sciences, 7 Nanhai Road, Qingdao, Shandong Province, 266071, China

Correspondence: Peter D. Clift (pclift@lsu.edu)

Received: 17 January 2022 – Revised: 29 May 2022 – Accepted: 7 June 2022 – Published: 28 October 2022

Abstract. The International Ocean Discovery Program (IODP) conducted a series of expeditions between 2013 and 2016 that were designed to address the development of monsoon climate systems in Asia and Australia. Significant progress was made in recovering Neogene sections spanning the region from the Arabian Sea to the Sea of Japan and southward to western Australia. High recovery by advanced piston corer (APC) has provided a host of semi-continuous sections that have been used to examine monsoonal evolution. Use of the half-length APC was successful in sampling sand-rich sediment in Indian Ocean submarine fans. The records show that humidity and seasonality developed diachronously across the region, although most regions show drying since the middle Miocene and especially since ∼ 4 Ma, likely linked to global cooling. A transition from C_3 to C_4 vegetation often accompanied the drying but may be more linked to global cooling. Western Australia and possibly southern China diverge from the general trend in becoming wetter during the late Miocene, with the Australian monsoon being more affected by the Indonesian Throughflow, while the Asian monsoon is tied more to the rising Himalaya in South Asia and to the Tibetan Plateau in East Asia. The monsoon shows sensitivity to orbital forcing, with many regions having a weaker summer monsoon during times of northern hemispheric Glaciation. Stronger monsoons are associated with faster continental erosion but not weathering intensity, which either shows no trend or a decreasing strength since the middle Miocene in Asia. Marine productivity proxies and terrestrial chemi-

cal weathering, erosion, and vegetation proxies are often seen to diverge. Future work on the almost unknown Paleogene is needed, as well as the potential of carbonate platforms as archives of paleoceanographic conditions.

1 Introduction

Monsoon climatic systems exist in most continents where large seasonal temperature differences develop between the continental interior and the surrounding oceans. The Asian monsoon is the strongest such system because of the great size of the Asian continent and the height of the topography associated with the Himalayan mountains and Tibetan Plateau, whose development is tightly linked with the climate (Molnar et al., 1993; Prell and Kutzbach, 1992). The monsoon is split into two distinct seasons, one wet and one dry. In the summer, onshore winds bring moisture from the Bay of Bengal into South Asia and from the South China Sea and western Pacific into southern China and former Indochina (Wang, 2006; Webster et al., 1998). During northern hemispheric winter the winds reverse, with cold dry air blowing from the atmospheric high-pressure area in Siberia towards the ocean. The seasonal advance of the monsoon rain front into the continent represents a migration in the intertropical convergence zone (ITCZ) and is mirrored by a similar system that brings heavy rain to northern Australia and parts of Indonesia during the southern hemispheric summer (Suppiah, 1992).

There has been significant scientific interest in monsoon climates because the Asian monsoon has come to symbolize the archetypal example of how the solid Earth and atmosphere coevolve, with feedbacks between the two over various timescales (Clift et al., 2008; Whipple, 2009). The societal significance of the Asian monsoon has also made it the target of research given the high population density that is sustained by the agriculture permitted by summer rainfall today, as well as its role in controlling the rise and subsequent decline of early urban civilizations (Madella and Fuller, 2006; Clift and d'Alpoim Guedes, 2021). Although much is known about the atmospheric physics that controls the intensity of the monsoon in the present day, the long-term development of this climatic system is less well characterized, especially prior to the Quaternary.

Scientific drilling in the 1980s played a crucial role in the first attempt to constrain the timing of Asian monsoon intensification, particularly through records of oceanic upwelling and productivity along the Arabian margin (Kroon et al., 1991; Prell et al., 1992), where strong summer winds are linked to the monsoon in the present day. The winds blow to the northeast offshore Arabia, bringing nutrient-rich water to the surface that causes a seasonal bloom in planktic foraminifers in the modern Arabian Sea during the summer (Curry et al., 1992). In turn an oxygen minimum zone (OMZ) forms in response to the high marine productivity driven by monsoon-induced upwelling (Altabet et al., 1995) and because of limited vertical mixing. This phenomenon is particularly well developed along the NE margin offshore India and Pakistan. The OMZ is greater when the productivity is high and when winter mixing of the water column is shallow (Reichart et al., 1998). Correlation of these records with terrestrial vegetation proxies in the Himalayan foreland basin played a key role in leading to an estimate for initial intensification at ~ 8 Ma (Quade et al., 1989), which at that time was believed to correlate with a phase of rapid Tibetan uplift (Harrison et al., 1992). Subsequently, re-examination of the Oman margin cores has resulted in recognition of an initial monsoon wind system starting at 12.9 Ma and intensifying ~ 7 Ma (Gupta et al., 2015). Drilling in the South China Sea by the Ocean Drilling Program (ODP) Leg 184 in 1999 established a contrasting chemical weathering and salinity record that implied a much earlier intensification of heavy rains in southern China, starting around 24 Ma and again at 15 Ma (Clift et al., 2002; Wan et al., 2007) and indicated a drying of the climate in the late Miocene (Steinke et al., 2010).

It is apparent that a number of different processes control the strength of the monsoon systems by influencing the temperature of the continent as well as the oceans. In particular, the development of high topography in central Asia has been invoked to cause long-term strengthening of the monsoon system, and while early efforts focused mostly on the Tibetan Plateau (Manabe and Terpstra, 1974), greater emphasis has recently been placed on the height of the Himalayas and their role in controlling the South if not East Asian monsoon (EAM) (Boos and Kuang, 2010). Climate models have, however, also invoked the importance of topography in the Iranian Plateau (Acosta and Huber, 2020), as well as the opening and closure of marine gateways, most notably in the western Tethys Ocean between Arabia and Eurasia (Gülyüz et al., 2020; Torfstein and Steinberg, 2020). In addition, constriction of the Indonesian Throughflow (ITF), the oceanic gateway between Indian and Pacific oceans, has increased as Australia collided with Indonesia and New Guinea starting in the Miocene (Van Ufford and Cloos, 2005). Added to this, it has become apparent that the monsoon rainfall is sensitive to global climate in being generally heavier when Earth is hotter. On shorter glacial–interglacial timescales, it has been recognized that monsoon rains tend to be stronger during interglacial times in Asia and become drier during periods of extensive northern hemispheric glaciation. Multi-proxy reconstructions from recent drilling indicate that coupled ice volume and greenhouse gas forcing is a critical factor driving changes in monsoonal rainfall at orbital timescales as well (Clemens et al., 2021; Gebregiorgis et al., 2018; McGrath et

al., 2021). On shorter timescales oceanic phenomena such as the El Niño–Southern Oscillation (ENSO) are often linked to the strength of monsoon rains in Asia (Wang et al., 2013; Lau and Wang, 2006).

The Australian monsoon is linked to the Asian system but has different sensitivities. A positive Indian Ocean Dipole (IOD), when the western Indian Ocean warms but the sea offshore western Australia is colder than normal, is associated with droughts in SE Asia and Australia, especially in southeast Australia (Cai et al., 2009). Likewise, the El Niño state in the Pacific, when colder waters dominate in the western Pacific and the eastern Pacific is warmer than normal, weakens spring rains in Australia (Ashcroft et al., 2016). The IOD in particular has been affected by the closure of the ITF (Kajtar et al., 2015), although ENSO appears to be more dependent on the atmospheric Walker circulation (Sprintall et al., 2014). Nonetheless, restriction of the gateway is one of the factors driving long-term aridification of Australia (Krebs et al., 2011). Both ENSO and IOD are also affected by shorter-term orbital-related processes that affect the strength and seasonality of the rains and control the environment. El Niño conditions and thus weak Australian rains are more common when the Earth is generally warmer. Likewise, the IOD has become more positive, and thus Australia has been drier since the Last Glacial Maximum (LGM; 20 ka) (Abram et al., 2020).

Model-based testing of what controls monsoon intensity has been hampered by the lack of long-duration marine records. Although shallow piston coring has been effective in collecting sequences to examine how the monsoon has changed over millennial timescales, scientific ocean drilling is required to look at how this system has evolved on orbital (10^4) to tectonic ($> 10^6$ years) timescales. The work necessarily involves correlation of marine records with terrestrial sediment archives, as well as tectonic models derived from studying the mountains, whose uplift has influenced the atmospheric dynamics across the continents. Although continental records are important in providing some local control over environmental conditions and erosion of mountain belts, it is the marine depocenters that comprise the more continuous, better dated records that are required to develop sophisticated models of monsoon evolution and its impacts. The marine record is also critical if we are to relate the continental environmental conditions with the oceanography of the surrounding seas because understanding of the modern monsoon would indicate that they should be tightly coupled (Fasullo, 2012; Tada and Murray, 2016). Before the start of this most recent campaign of scientific drilling, there were major gaps in our data coverage, hampering better understanding. Although there were Miocene to Recent records from the Arabian and South China seas, no high-resolution records were available over many other parts of the region, at least spanning the Neogene, let alone the Paleogene. Since the onset of the monsoon has been estimated to be as old as the late Eocene (Licht et al., 2014; Sorrel et al., 2017), this made the marine record of rather limited use to study long-term evolution. Although it has long been argued that erosion and weathering of the mountains might be a primary control over global climate during the Cenozoic (Raymo and Ruddiman, 1992), the lack of a long-term erosional record from either of the large submarine fans in the Indian Ocean, let alone the major rivers of former Indochina prevented these models being tested.

2 Regional drilling campaigns

From 2013 to 2016, the International Ocean Discovery Program (IODP) conducted drilling around Asia and Australia that was specifically designed to document variations in monsoon intensity on millennial and longer tectonic timescales. This has resulted in significant revision of our reconstructions of when the monsoon intensified and weakened across a range of timescales, and in turn this contributes to our understanding of what the primary driving factors controlling wind and rainfall intensity in South and East Asia have been.

The drilling campaigns addressed all the marginal seas around Asia, stretching from the Arabian Sea in the southwest (Betzler et al., 2017; Pandey et al., 2016) to the Sea of Japan in the northeast (Tada et al., 2015), continuing southward through Indonesia, to the west coast of Australia (Gallagher et al., 2017) (Fig. 1). As well, both the major Indian Ocean submarine fans, the Indus and the Bengal (Clemens et al., 2016; France-Lanord et al., 2016), which together represent the bulk of the sediment derived from the Himalayan orogen, were drilled together with the Nicobar fan located on the east side of the Ninety-East Ridge and thus provide a relatively complete history of Himalayan erosion, at least covering much of the Neogene (McNeill et al., 2017). Furthermore, the eastern Indian Margin and Andaman Sea were drilled to reconstruct the Miocene to present monsoonal paleoclimate and paleoceanography (Clemens et al., 2016). In the South China Sea, three expeditions recovered sections of sediment mostly from the northern margin, related to the Pearl River catchment of southern China (Li et al., 2015; Sun et al., 2018), enhancing records obtained during the earlier ODP Leg 184 (Wang et al., 2000). Although drilling was largely focused on Neogene targets, for the first time the regional character of the campaign provided a wide sampling of many of the large continental drainage systems of Asia from which environmental, weathering, and erosion records can be derived, thus constraining both South and East Asian monsoons and providing the high-resolution records necessary for comparison between systems. Moreover, these are now accompanied by similarly high-resolution records from Western Australia looking at the evolution in climate of this continent and constraining the development of the monsoon system in that region, providing a means of comparison with the Asian monsoons (Gallagher et al., 2017). A related expe-

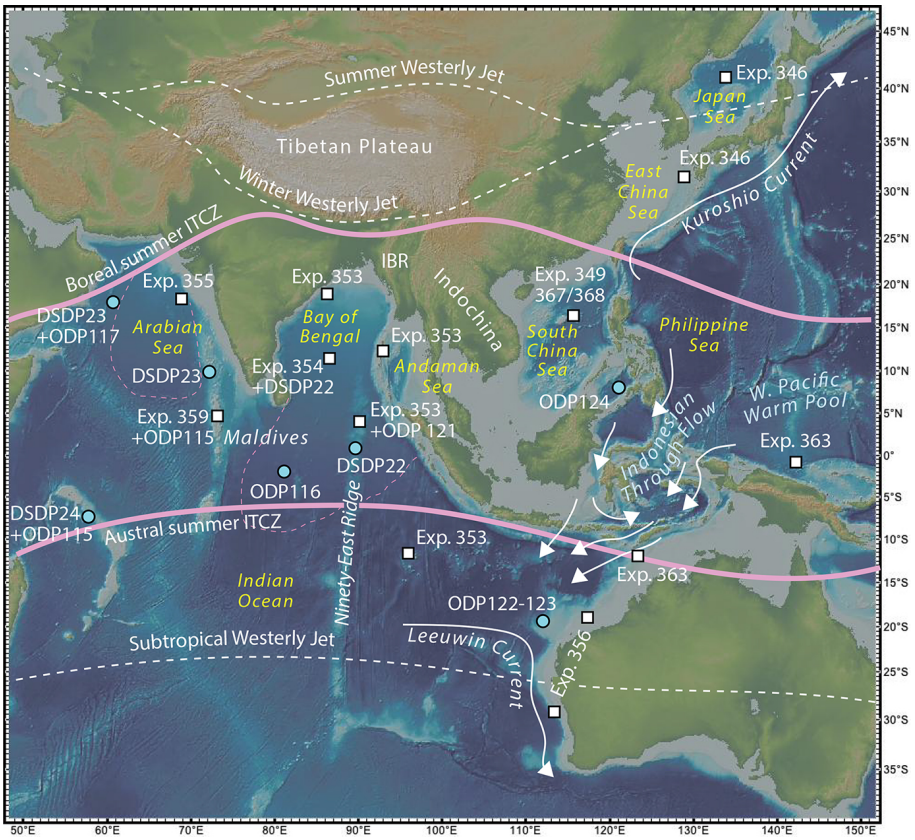

Figure 1. Shaded bathymetric map of the regions affected by the Asian and Australian monsoon systems showing the area of operations of the expeditions completed by IODP in the most recent campaign. Areas of older ODP and DSDP drilling are shown as blue dots. IBR is the Indo-Burman Range. Route of IFT after Gordon (2005). Dashed pink lines show outline of Indus and Bengal fans. ITCZ locations are from Yan (2005). Base map is from GeoMapApp.

dition offshore NW Australia and north of New Guinea provides an important record of the Western Pacific Warm Pool (WPWP) (Rosenthal et al., 2018), which is closely correlated with the intensity of the EAM system and additional Neogene records of the NW Australian system. In this study we summarize the primary findings in each of these critical areas and then assess how they may be related to one another in order to understand how different parts of the Asian–Australian monsoon system may be linked.

3 Arabian Sea

Some of the earliest constraints on the geological evolution of the monsoon were derived in the Arabian Sea through scientific drilling (Fig. 1). This is a particularly good area to look at the monsoon because of the strong oceanographic effects that the wind system has on upwelling and marine production in the area, as well as on the delivery of sediments from the Indian peninsula and particularly the Indus River, which represents the largest drainage system in the NW Himalaya. Prior to IODP drilling, the southwestern Indian margin was sampled by Indian National Gas Hydrate Expedition 01 Site NGHP-01-01A, located offshore Goa. Sedimentary and geochemical data indicate stronger water mass mixing associated with a winter monsoon circulation after 23.7 Ma (Beasley et al., 2021). The same study also argued for the first summer monsoon after 23 Ma based on increases in Ti / Ca and dissolution of the biogenic carbonate fraction, as well as formation of an OMZ in the eastern Arabian Sea.

3.1 Expedition 355: environmental records in the Laxmi Basin

Expedition 355 recovered two long sections (1109 m penetration at Site U1456 and 1008 m at Site U1457) from the central Laxmi Basin, offshore western India, forming the eastern side of the Indus submarine fan. Recovery was 92 % with the advanced piston corer at Site U1456, 93 % at Site U1457 and 57 %, and 48 % with the Rotary Core Barrel (RCB) at each site respectively. The occurrence of a large mass transport complex (MTC) disrupted plans to recover sediment older than around 11 Ma (Dailey et al., 2019), but operations did retrieve a relatively continuous record of continen-

tal erosion spanning the last 11 Myr and covering the critical climatic transition around 8 Ma, albeit disrupted by a number of hiatuses (Routledge et al., 2020). Work within the NW Himalayan foreland had used carbon isotopes to identify changes in vegetation (Quade et al., 1989), and these same methods were applied to detrital organic carbon in the cores to assess how vegetation had evolved in the Indian peninsula and Himalayan foreland since 11 Ma. Studies of sedimentary organic carbon implied a change in the vegetation in the source regions starting at 7 Ma (Khim et al., 2020). The $\delta^{13}C$ of long-chain n-C_{32} fatty acids shifted from $-34\,‰$ to $-22\,‰$ between 10 and 6.3 Ma, and this was interpreted to indicate the progressive increase in C_4 grasses at the expense of C_3 plants (e.g., trees), especially between around 8.2 and 6.3 Ma (Suzuki et al., 2020) (Fig. 2d). This climatic transition was furthermore supported by a high-resolution study that focused on the period of climatic transition (Feakins et al., 2020). That study employed a multi-proxy approach involving bulk organic carbon and plant wax alkanes and acids, as well as a variety of pollen, charcoal, and lignin proxies, to assess how the vegetation changed under the influence of the evolving monsoon.

The Feakins et al. (2020) study was able to separate the influence of the Indus River compared to regional rivers draining the Indian peninsula. $\delta^{13}C$ values from n-C_{31} n-alkanes together with the other proxies supported the idea of expansion of grasslands through the late Miocene in northwest India, with change especially noted between 7.2 and 7.4 Ma. Interestingly, there was no clear change in δD values, which have been used as proxies for rainfall intensity in the Arabian Sea (Huang et al., 2007). This implied that there has been a relatively constant monsoon system across the area that was not disrupted during the time of transition in the vegetation and in turn raises the possibility that it was cooling, reconstructed from TEX_{86} data, and not drying that was responsible for the shift in the environment at that time.

Chemical weathering data has also been employed to constrain the evolving environment in the Indus catchment. Hematite / goethite values measured by color spectroscopy were used to constrain relative humidity, with hematite favored during times of drier climate. These records indicated a drying, or at least an increase in the duration of the dry season, after $\sim$7.7 Ma, and while there was a phase of increased humidity between 6.3 and 5.9 Ma, a long-term trend was towards less chemical weathering and slower and drier conditions as the Miocene progressed into the Pliocene (Clift et al., 2020).

Bulk sediment major element geochemical data, color spectral data, and clay mineralogy confirmed a long-term decrease in weathering intensity that is often associated with drier, colder conditions (Zhou et al., 2021). The role of hematite in highlighting dry conditions is particularly noteworthy in implying a long-term decrease in humidity and thus summer monsoon rains (Fig. 2a). Clay minerals are sensitive to environmental conditions (Thiry, 2000) but can also be used as provenance proxies under certain conditions. Clays have been used to argue that since 3.7 Ma, changes in monsoon strength have caused the sediment supplied to the Indian Ocean to alternate with more supply from the peninsula and Deccan Traps during times of heavier summer rains (Cai et al., 2020). It is noteworthy that there is a disconnect between monsoon intensity inferred from oceanic productivity records and those related to the climate. In the modern day, strong summer winds are associated both with heavy rain and with upwelling (Curry et al., 1992). This linkage extends to orbital timescales (Clemens et al., 2021) but does not appear to have been the case at longer timescales.

Nitrogen isotope compositions of sediment track marine nitrogen cycling, which can be related to biological productivity. N isotopes reflect the source of dissolved N to phytoplankton, and in nutrient-replete environments, the relative utilization. In the Arabian Sea, N isotopes reflect the upwelling of partially denitrified nitrate from the OMZ. Increases above the oceanic mean are taken as an increase in the intensity of the OMZ, often related to oxygen demand due to monsoon-driven upwelling (Altabet et al., 1995). N isotope and organic carbon contents of Laxmi Basin sediments indicate that the first sign of denitrification occurred at 3.2–2.8 Ma and that the modern OMZ was not established until $\sim$1 Ma (Tripathi et al., 2017). Subsequent higher-resolution studies spanning 800 ka indicated a persistent OMZ in the eastern Arabian Sea but with a breakdown of the OMZ in the western Arabian Sea during glacial times when the summer monsoon weakened (Kim et al., 2018). Geological evidence for marine production and continental erosion implies that the summer monsoon strengthened at 2.95 Ma, possibly linked to closure of the ITF but then progressively weakened independently of the glacial climatic cycles (Sarathchandraprasad et al., 2021). The lack of correlation between the OMZ history and the terrestrial weathering and vegetation proxies is a clue that the paleoceanography and terrestrial rainfall are not tightly coupled over the longer-term geological past. This conclusion is consistent with a number of recent modeling studies (Nilsson-Kerr et al., 2021; Acosta and Huber, 2020).

3.2 Expedition 359: Maldives monsoon winds

The Maldives archipelago in the northern central Indian Ocean has acted for over 25 Myr as a giant natural sediment trap and contains a record of monsoon-related environmental changes in that region. The carbonate platforms record sea-level fluctuations, while the drift and periplatform deposits carry the record of monsoon-driven changes of the surface and intermediate water mass current regime and of wind-driven dust influx.

IODP Expedition 359 cored sediments from eight locations in the Inner Sea of the Maldives (Betzler et al., 2017). Penetration was up to 1097 m below the seafloor at Site U1467, located in the center of the Inner Sea, with

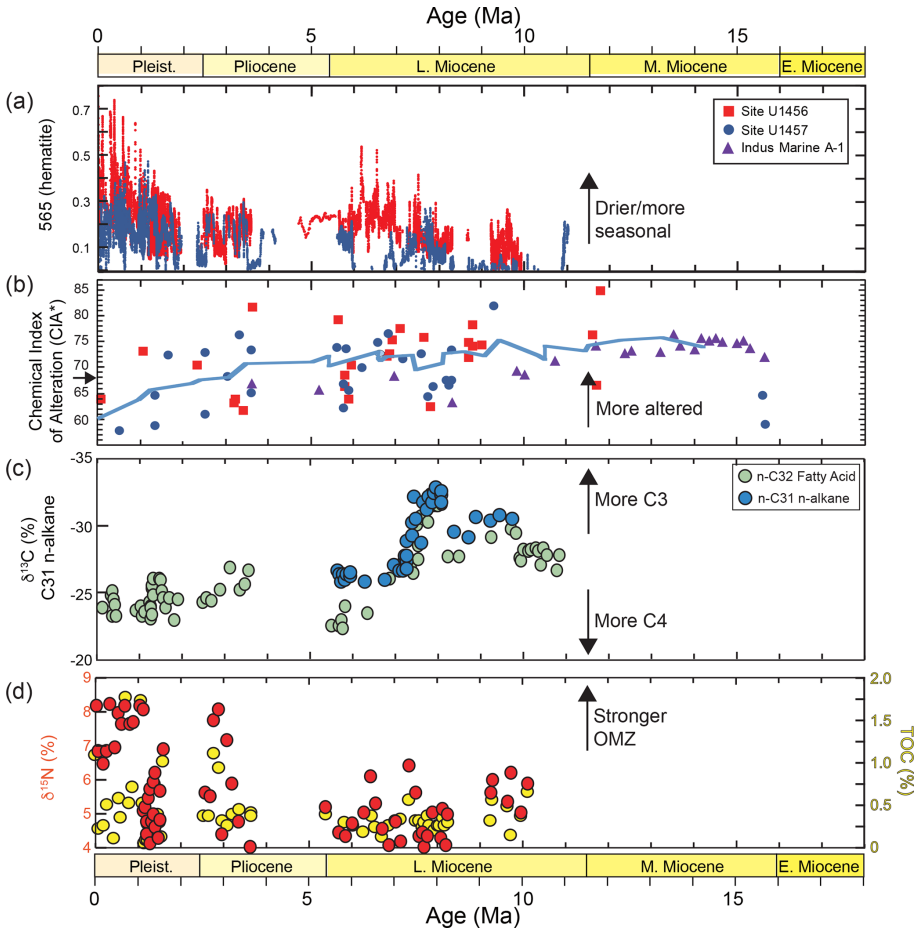

Figure 2. Temporal evolution in weathering proxies from the Laxmi Basin together with possible forcing factors. **(a)** 565 spectra intensity (hematite) and **(b)** CIA*, from Zhou et al. (2021), **(c)** δ^{13}C of n-C_{32} fatty acids (Suzuki et al., 2020) and from n-C_{31} n-alkanes (Feakins et al., 2020), and **(d)** δ^{15}N and total organic carbon (TOC) from Tripathi et al. (2017).

high degrees of recovery (> 90 %) over many of the intervals drilled by the APC. The expedition was designed to reconstruct the evolution of the South Asian monsoon (SAM) and related fluctuations of sea level. The timing of these changes is assessed by dating sedimentary alterations that mark stratigraphic turning points in the Neogene Maldives platform–basin system. The first turning points, dated as early and middle Miocene, are related mostly to sea-level changes. These are reliably recorded in the stratigraphy of the carbonate sequences in which sequence boundaries provide the ages of the sea-level lowstands (Vail et al., 1977).

An abrupt change in sedimentation patterns is recognized across the entire archipelago at a sequence boundary dated as 12.9–13.0 Ma (Betzler et al., 2016). At this turning point, the platform sedimentation switched to a current-controlled mode when the monsoon-wind driven circulation started in the Indian Ocean (Fig. 3). Several areas of the platform drowned in response to physical current effects, i.e., erosion and sediment re-deposition (Ling et al., 2021; Lüdmann et al., 2018; Reolid et al., 2020, 2019). The similar age of the onset of drift deposition from monsoon-wind driven circulation across the entire archipelago indicates an abrupt onset of strong monsoon winds in the Indian Ocean (Betzler et al., 2016, 2018). Ten unconformities dissect the drift sequences, attesting to changes in current strength and/or direction that were likely caused by the combined impact of changes in monsoon wind intensity and sea-level fluctuations over the last 13 Myr. One major shift in the drift packages is dated with 5.8 Ma and coincided with a long-term sea-level rise that transformed the focused delta drift deposition to more widespread sheeted drifts (Fig. 3). A second major shift at 3.8 Ma coincided with the end of stepwise platform drowning and a reduction of the OMZ in the Inner Sea.

The strata of the Maldives platform provide a detailed record of the extrinsic controlling factors on carbonate platform growth through time. This potential of carbonate platforms for dating Neogene climate and current changes has been exploited in other platforms drilled by earlier scientific drilling. For example, Great Bahama Bank, the Queensland Plateau, and the platforms on the Marion Plateau show

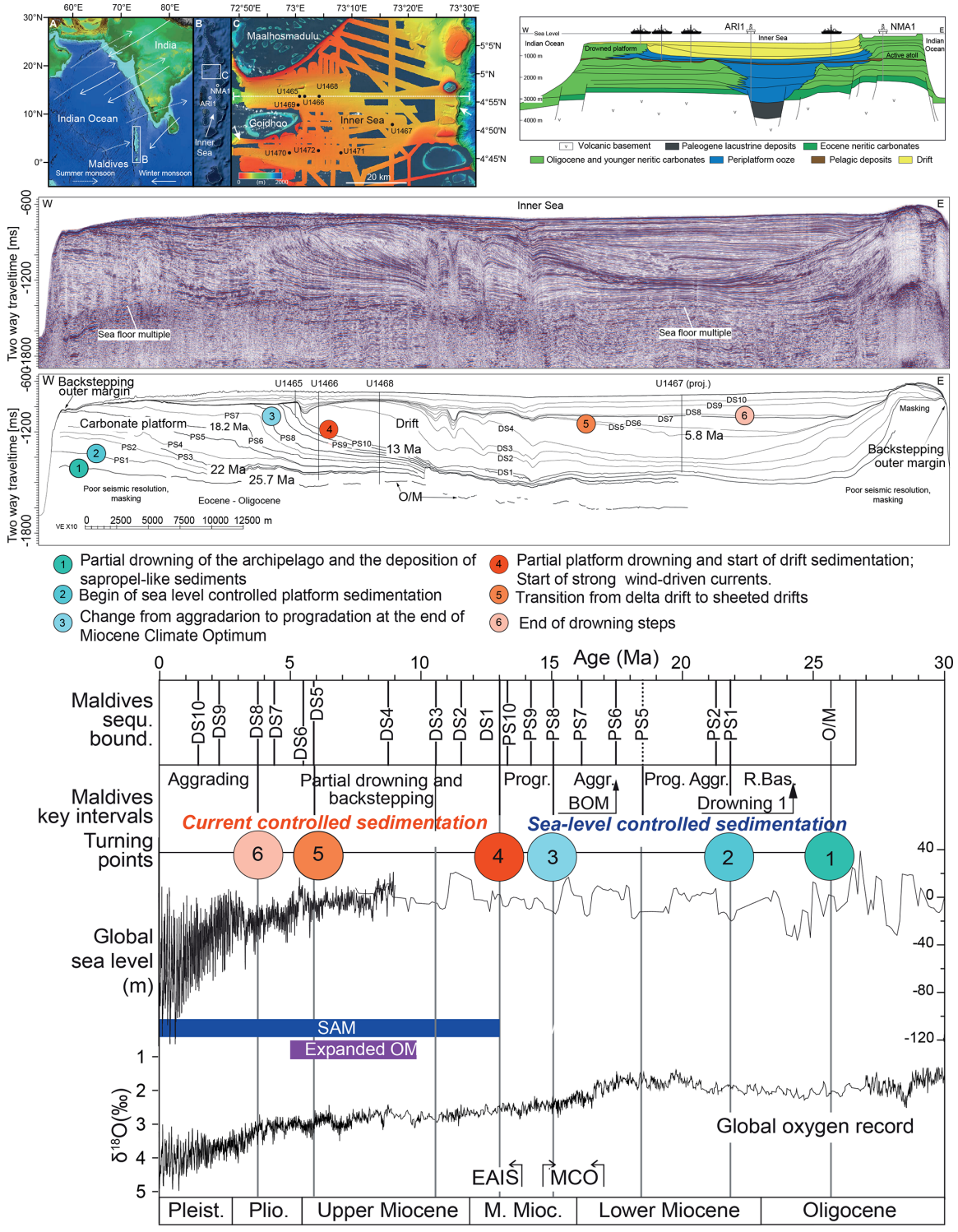

Figure 3. The Maldives archipelago, located in the Indian Ocean, is affected by the seasonally reversing monsoonal winds and currents. The archipelago has two rows of drowned and active atolls that line the Inner Sea. Seismic line across the Maldives Inner Sea with line drawing showing the platform sequence (PS) boundaries and the drift sequence (DS) boundaries. Carbonate platform sedimentation is controlled by sea level, while the drift sequences are controlled by strong currents which start at 13 Ma. Major turning points in sea level (blue circles) and current control (reddish circles) are indicated. Position of seismic line corresponds to white line in the map. Maps were produced using the program Esri ArcMap 10.1 (http://www.esri.com, last access: 29 May 2022). Bathymetric data were exported as Geotiffs from GeoMapApp 3.6.0 (http://www.geomapapp.org, last access: 29 May 2022). Worldwind satellite images (http://worldwind.arc.nasa.gov/java, last access: 29 May 2022) were merged with multibeam data acquired during cruises M74/4 and SO236.

similar histories with sediment architectures driven by sea level in their early history (early to middle Miocene) replaced by current-driven drowning or partial drowning during their later history (late Miocene) (Betzler and Eberli, 2019). In all three platform systems, the influence of currents on sedimentation is reported to be between 11 and 13 Ma.

The lithogenic fraction of the Maldives carbonate drifts provides a unique record of atmospheric dust transport during the past 4 Myr because grain size can act as a proxy for dust flux, as well as wind transport capacity (Lindhorst et al., 2019). Entrainment and long-range transport of dust in the medium to coarse silt size range is linked to the strength of the Arabian Shamal winds and the occurrence of convective storms that prolong dust transport. Dust flux and the size of dust particles increased between 4.0 and 3.3 Ma, corresponding to the closure of the ITF seaway and the intensification of the SAM. Between 1.6 Ma and the Recent, dust flux again increased but shows higher variability, especially during the last 500 kyr. Eolian transport capacity based on grain size increased between 1.2 and 0.5 Ma but has slightly decreased since that time. Dust transport varied on orbital timescales, with eccentricity control being the most prominent (400 kyr throughout the record and 100 kyr between 2.0 and 1.3 Ma and since 1.0 Ma). Higher-frequency cycles (obliquity and precession) are most pronounced in wind transport capacity.

Using XRF scans of the cores recovered at Site U1467, wavelet and spectral analyses of the Fe / K record show increased dominance of 100 kyr cycles after the Mid-Pleistocene Transition (MPT) at 1.25 Ma in tandem with the global ice volume inferred from calculated seawater $\delta^{18}O$ data (LR04 record) (Kunkelova et al., 2018). In contrast to the LR04 record, the Fe / K profile from Site U1467 resolves cycles that are similar to 100 kyr cycles around the 130 kyr eccentricity frequency band in the interval from 1.25 to 2.0 Ma. These cycles similar to 100 kyr cycles likely formed through the bundling of two or three obliquity cycles, indicating that low-latitude Indian–Asian climate variability reflected an increased tilt sensitivity to regional eccentricity insolation changes (pacing tilt cycles) prior to the MPT. The implication of appearance of the 100 kyr cycles in the LR04 and the Fe / K records since the MPT suggests strengthening of a climate link between the low and high latitudes during this period of climate transition.

4 Bay of Bengal

4.1 Expedition 353: South Asian monsoon

Expedition 353 (Clemens et al., 2016) drilled the Ninety-East Ridge, Bengal fan, northeast Indian Margin, and Andaman Sea. The expedition recovered 4.28 km of sediment from six sites with 97 % recovery on average. Double and triple coring was conducted in order to produce complete sections that would allow for reconstruction of continental erosion and monsoonal hydroclimate at a range of timescales from sites with sedimentation rates ranging 2–15 cm kyr^{-1} (Robinson et al., 2016), with recovery spanning Campanian to Recent, although much of the Eocene was not recovered.

4.1.1 Paleocene–Oligocene: start of Himalayan erosion

Barnet et al. (2020) examined the interval of Earth history containing the well-known hyperthermal events of the Paleocene–Eocene Thermal Maximum (PETM) and Eocene Thermal Maximum (ETM), often studied as potential analogues for future anthropogenic climate change. Trace element and isotopic records from Ninety-East Ridge IODP Site U1443 and ODP Site 758 spanning ∼ 58–53 Ma place these hyperthermal events in the context of a long-term warming of the water column on the order of 4–5 °C. These results are comparable to those reconstructed from the low-latitude Pacific, demonstrating global-scale synchronous warming of the low-latitude and high-latitude regions of deep-water formation. These new findings support the idea that atmospheric CO_2 was the primary driver of global climate during this time of climatic transition.

Ali et al. (2021) used a newly-developed isotope chronostratigraphy from Site U1443 (Lübbers et al., 2019) coupled with samples from ODP Site 758 (at the same location) to evaluate the radiogenic Sr, Nd, and Pb isotopic composition of clay minerals produced from silicate weathering and deposited in the Bay of Bengal since 27 Ma, the longest such marine record in South Asia. They demonstrate remarkable source consistency, indicating dominance of supply from Himalayan rocks and the Indo-Burman Range, implying that the spatial pattern of weathering associated with monsoon rainfall has varied little over the past 27 Ma.

4.1.2 Miocene–Pliocene: changing Himalayan erosion patterns

A number of investigators have worked to differentiate provenance, weathering, tectonics, and climate change signals at Expedition 353 sites, located both in proximal and distal positions relative to the source drainages and using both hemipelagic and turbiditic sequences. Bretschneider et al. (2021) assessed high-resolution records of radiogenic Sr, Nd, and Pb isotopic composition of clay minerals deposited on the Ninety-East Ridge at Site U1443 across five time slices within the middle to late Miocene (15.8–9.5 Ma). This is the same site where Ali et al. (2021) recorded an increase in clay mineral abundance at ∼ 13.9 Ma that would signify an increase in physical weathering intensity in the sources, coincident with middle Miocene global cooling and regional tectonic reorganization (Fig. 4). Despite Himalayan tectonic reorganization, the erosional sources remained remarkably consistent across the five time slices. However, shorter (orbital) timescale variability shows significant fluctuations in all three isotope systems, likely linked to monsoon intensity. Variability within the middle Miocene Climatic Opti-

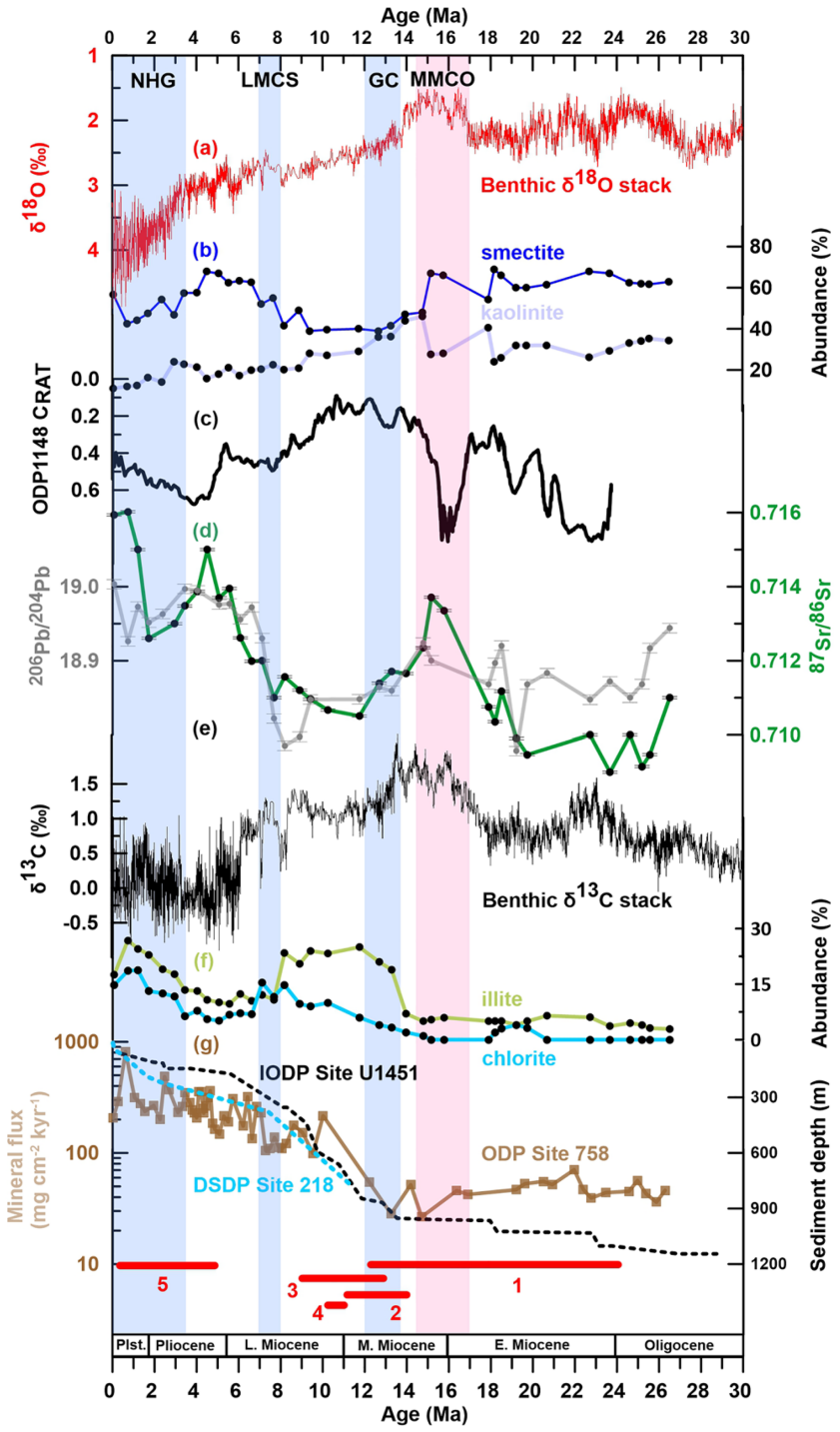

Figure 4. **(a, e)** Global $\delta^{18}O$ and $\delta^{13}C$ from bottom-living (benthic) foraminifera compiled from more than 40 DSDP and ODP sites (Zachos et al., 2008) representing global ice volume and deep-sea temperature, highlighting the global climate changes of the last 30 Myr. Periods of global cooling, after Zachos et al. (2008), are marked with blue bars, and the MMCO is marked with a red bar **(b, f)**. Clay mineralogy of ODP Site 758, relative abundances (% of smectite and kaolinite, illite, and chlorite), I CRAT record of ODP Site 1148 (Clift et al., 2008) from the South China Sea as a record of East Asian monsoon development, **(e)** Nd and Pb isotope composition of ODP Site 758 clays, **(g)** mineral flux record (Hovan and Rea, 1992) of ODP Site 758 recalculated using updated linear sedimentation rates, and sedimentation rates from the Bengal fan DSDP Site 218 and IODP Site U1451 (France-Lanord et al., 2016; Galy et al., 2010), and at the bottom a summary of the regional tectonic events (Allen and Armstrong, 2012). 1 – high Himalayan uplift, Main Central Thrust (MCT); 2 – onset of normal fault, southern Tibet; 3 – surface uplift, eastern Tibet; 4 – initial thrusting on main boundary Thrust; and 5 – fast exhumation at Himalayan syntaxes, outward growth of NE Tibet. This figure is from Ali et al. (2021).

mum (MMCO; 16–15 Ma) and the interval of global cooling at 13.9–13.8 Ma was larger than during younger intervals, a change attributed to movement of the precipitation locus from the high Himalaya to the frontal Himalayan ranges and to the Indo-Burman Range.

The older intervals from pelagic sections on the Ninety-East Ridge indicate relatively stable sediment provenance over long intervals of time. However, reconstructions from the middle–northern Bengal fan IODP Site U1444A, spanning the late Miocene to present (~ 7–0 Ma), do indicate provenance changes. Chang and Zhou (2019) used optically and thermally stimulated luminescence (OSL and TL) of quartz and K-feldspar grains to characterize the sediment mineral composition through time. These authors interpret a distinct increase in quartz luminescence sensitivity at ~ 3.5–0.5 Ma as increased hemipelagic contribution from Indian peninsular rivers relative to Himalayan-sourced pulses of turbidite sediments which dominated at 7–6 and 3.8–3.5 and since 0.5 Ma. In this case, changes between hemipelagic (Indian peninsula) and turbiditic (Himalayan) deposition were attributed more to changes in tectonic activity in the Himalayan region as opposed to the monsoonal climate.

Peketi et al. (2021) studied the time interval since ~ 6 Ma at the eastern Indian continental margin Site U1445A using Sr and Nd isotopic analysis of the lithogenic fraction, elemental Fe / Al ratios, and clay mineralogy. They documented variable Ganga and Brahmaputra provenance at Site U1445A, with little input from the proximal Mahanadi drainage basin. The interval since 1.8 Ma indicates increased flux from the Brahmaputra River (supplied by erosion from the Trans-Himalayan batholiths) during periods of monsoon intensification and more from the Ganga during times of weakened monsoons. Variability within the interval 6–1.8 Ma was found to be influenced by both climate and tectonic forcings, the relative effects of which could not be differentiated.

Dunlea et al. (2020) also investigated the sequence recovered at Site U1445 to assess the expansion of C_4 vegetation, linked to drying of the environment. Their assessment of provenance was based on major, trace, and rare earth elemental concentration data, which were interpreted to indicate a Mahanadi drainage provenance, contrary to the conclusions of Peketi et al. (2021). The associated bulk organic and compound specific biomarkers, whether reflective of the Mahanadi drainage within the core monsoon zone of India or larger drainages to the north, document the existence of C_4 vegetation before the end of the Miocene but with an expansion to higher abundances at ~ 3.5–1.5 Ma, all superimposed on an overall long-term decrease in monsoon precipitation since the late Miocene. These findings build upon the existing evidence for regionally heterogeneous responses in the timing of C_4 expansions and contractions, indicating sensitivity to regional climate changes in addition to global pCO_2 forcing (Feakins et al., 2020).

Hemipelagic sediment from western Andaman Sea Site U1447 spans the past 10 Myr and was analyzed by Lee et al. (2020b) for Sr and Nd isotopes, clay mineralogy, and $\delta^{13}C$ of sediment organic matter. The Nd and Sr data indicate sources in the Myanmar region, including major river drainages (e.g., Irrawaddy, Salween, Sittang) and smaller drainages from the Indo-Burman Range. Like the Ninety-East Ridge Site U1443 studies, the results indicate no significant changes in provenance since the late Miocene, and hence clay mineralogical changes can be interpreted in the context of monsoonal environmental change. A decreasing trend of smectite / (illite + chlorite) [S / (I + C)] implies stronger physical and weakened chemical weathering since the late Miocene, consistent with global cooling at that time. Climatologically, this is interpreted as a strengthening of the winter monsoon or weakening of the summer monsoon over this time period. Distinct events at 9.2–8.5, 3.6, 2.4, and 1.2 Ma were interpreted to result from the combined effects of global cooling and Tibetan Plateau uplift, the relative impacts of which cannot yet be differentiated. Initial results from spectral natural gamma ray (NGR) sediment core-logging and benthic foraminiferal stable isotope analyses of the upper Miocene record at Site U1447 indicate that an important long-term increase in physical weathering and erosion coincided with the globally recognized late Miocene cooling trend between ~ 7.0 and 5.5 Ma (Kuhnt et al., 2020).

4.1.3 Miocene–Pliocene: monsoon-driven oceanic circulation

Lübbers et al. (2019) examined the critical interval of time from 13.5 to 8.2 Ma at Ninety-East Ridge Site U1443 using O and C stable isotopes from benthic foraminifera, XRF elemental data, and carbonate accumulation rates. At this equatorial site, a marked decrease in carbonate deposition took place between ~ 13.2 and 8.7 Ma, coinciding with the middle to late Miocene "carbonate crash". Synthesizing the timing of this event at a global array of sites led the authors to hypothesize changes in chemical weathering and riverine influx of calcium and carbonate ions as fundamental mechanisms driving the carbonate crash and recovery. After 11.2 Ma, elemental ratio data (Ba / Ti) implied increased primary production and organic carbon burial. This timing, somewhat earlier than the global onset of the biogenic bloom, is attributed to intensification of upper-ocean mixing associated with changes in the seasonality and intensity of SAM winds and precipitation.

Jöhnck et al. (2020) produced a set of multi-proxy records from Site U1448 in the Andaman Sea spanning 6.24–4.91 Ma. Their benthic and planktic foraminiferal stable isotopes, combined with paired planktic carbonate Mg / Ca elemental ratio data, yield the first high-resolution orbital-scale reconstructions of monsoon variability across the Miocene–Pliocene transition. They found a 4 °C increase in mixed-layer temperature between 5.55 and 5.28 Ma, coincident with

a change from precession-dominated to obliquity-dominated variability in planktic $\delta^{18}O$ and seawater $\delta^{18}O$. This suggests that intensified cross-equatorial heat and moisture transport paced by obliquity resulted in increased summer monsoon precipitation during warm stages. In contrast, cold stages were characterized by colder mixed-layer temperatures and reduced monsoon rainfall, resembling Late Pleistocene stadials. The interval 5.55–4.91 Ma was one showing strong coherence of seawater $\delta^{18}O$ with orbital precession, indicating that seawater $\delta^{18}O$ minima lag precession minima by 119° (7.6 kyr). This lag is consistent with that measured in the Pleistocene from the same region (Gebregiorgis et al., 2018) and at Site U1446 on the northeast Indian margin (Clemens et al., 2021).

Most recently, a study of sediment from Ninety-East Ridge Site U1443 spanning the period 9 to 5 Ma reconstructed changes in biogenic production at high resolution and highlighted variance over cycles of 19–23 kyr, similar to that seen in the Late Pleistocene (Bolton et al., 2022). This work confirmed the important of insolation forcing of monsoon wind strength in the Indian Ocean and demonstrated that the wind system did not intensify significantly during the late Miocene.

4.1.4 Pleistocene: orbital forcing of monsoon productivity and rainfall

Monsoon variability has been assessed across the MPT, as well as orbital-scale variability over the past million years and high-resolution variability across marine isotopic stage 5 (MIS5). Lee et al. (2020a) evaluated paleo-productivity over the past 2.3 Myr at northeast Indian margin Site U1445 using the mass accumulation rate (MAR) of biogenic opal, total organic carbon (TOC), and total nitrogen to assess links between productivity and monsoon forcing across the MPT. These authors identified a regime change from a dominance of biogenic opal prior to the MPT to biogenic carbonate after this time. These changes were interpreted in the context of riverine silicate supply, with a strengthened monsoon-induced supply at 2.3–1.5 Ma, prior to the MPT, resulting in enhanced biogenic opal productivity. Across the MPT and thereafter, weakened monsoon runoff reduced stratification and enhanced nitrate supply from upwelling, leading to a carbonate-dominated productivity regime. The inferred reduction in monsoonal runoff is supported by the 0.19 ‰ shift in seawater $\delta^{18}O$ across the MPT observed at Site U1446 (Clemens et al., 2021).

Orbital-scale investigations of the monsoon at Andaman Sea Site NGHP-17/U1448 and northeast Indian margin Site U1446 have used water-related isotopes (speleothem $\delta^{18}O$, leaf wax δD, and seawater $\delta^{18}O$), leaf wax $\delta^{13}C$, and elemental XRF ratios to differentiate changes in the isotopic composition of rainfall from rainfall amount. McGrath et al. (2021) showed that variability in leaf wax δD is strongly coherent with that of speleothem $\delta^{18}O$, with variability in both proxies being coherent and in phase with ice-volume minima and pCO_2 maxima. In contrast, seawater $\delta^{18}O$ from the Andaman Sea (Gebregiorgis et al., 2018) and Indian margin (Clemens et al., 2021) indicates that maximum rainfall/runoff occurred significantly later and, in the case of precession, in phase with maximum summer-monsoon wind strength proxies. These relationships indicate that speleothem $\delta^{18}O$ and leaf wax δD predominantly reflect the isotopic composition of rainfall, varying as a function of changing moisture source areas and transport path dynamics, whereas seawater $\delta^{18}O$ predominantly reflects monsoonal rainfall and runoff amount.

Nilsson-Kerr et al. (2019) focused on millennial-scale seawater $\delta^{18}O$ and elemental ratio reconstructions of ice volumes during Termination II (TII; 139–127 ka) in the northeast Indian margin at Site U1446. They found that the TII is characterized by a transient monsoon intensification associated with the polar seesaw. The deglacial progression is characterized first by southern hemispheric warming, then by warming in the tropics, coincident with monsoon intensification, followed by northern hemispheric warming. These temporal relationships imply that the monsoon served as a conduit for the transport of heat across the Equator into the Northern Hemisphere, promoting deglaciation. This work was followed by a low-latitude synthesis of MIS 5 (130–70 ka) reconstructions combined with modeling (Nilsson-Kerr et al., 2021). Results document strong regional variability beyond that which can be ascribed to simple meridional migration of the ITCZ. Dipole-like patterns are pervasive across monsoon regions, highlighting the importance of mechanisms internal to the climate system, as opposed to monsoon systems responding simply external radiation forcing.

4.2 Expedition 354: Himalayan erosion and tectonics

Expedition 354 recovered long-duration erosion records going back to the Miocene in the central part of the submarine fan (Fig. 1). Coring followed a program of short APC cores, followed by extended core barrel (XCB) and finally RCB to the base of the section. The 17 holes drilled at Sites U1449–U1455 penetrated a total of 5167.2 m sub-seafloor. Coring spanned 2889.7 m of this penetration and recovered 1727.12 m of sediment and rocks (60 % average recovery). This expedition was designed to retrieve a complete record of turbidite deposition spanning the Neogene, together with more detail over the Pleistocene. The main objectives were to provide a record of erosion, both in terms of distribution and rate across the Himalayan arc, and a record of continental monsoon precipitation and vegetation and to estimate the impact of Himalayan erosion on the global carbon cycle. The E–W transect approach employed allowed the migration of the depocenter through time to be reconstructed and is the basis for reconstructing the paleo-erosion record (Fig. 5).

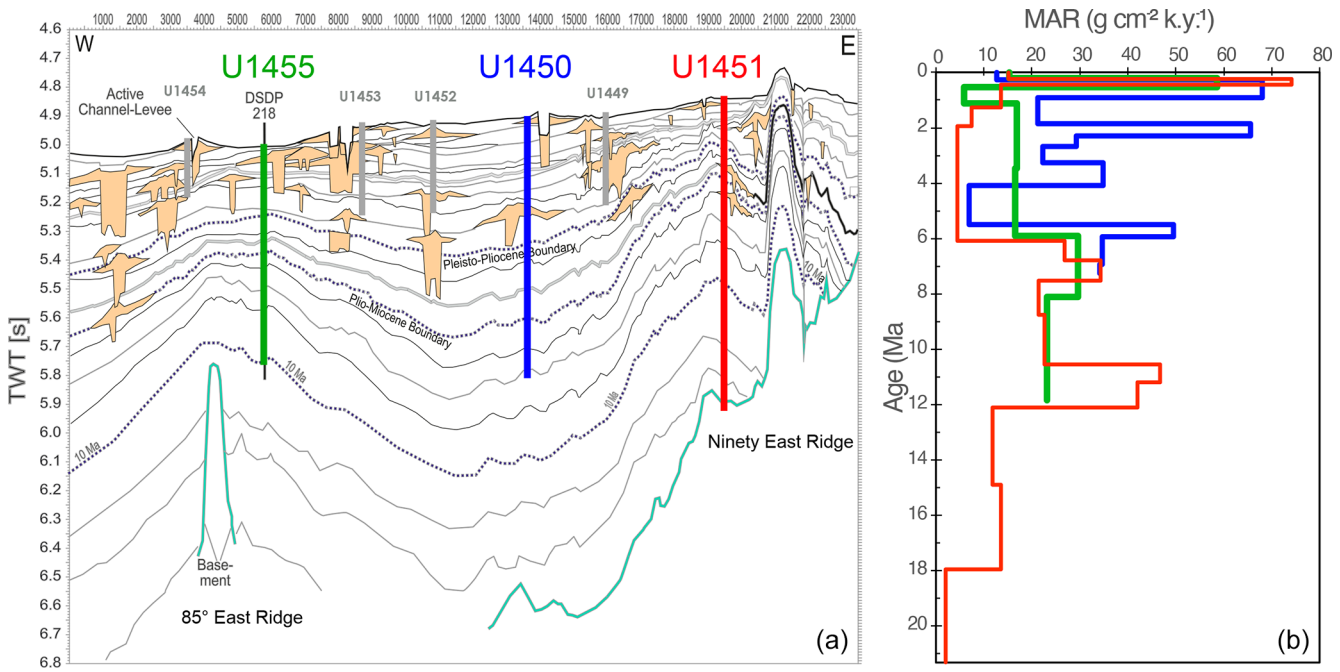

Figure 5. **(a)** Interpreted seismic section of the Bengal fan at 8° N (Schwenk and Spieß, 2009) with position of the Expedition 354 sites. The upper fan comprises a stacking of channel levee systems, with alternations of high accumulation of fan deposits and hemipelagic intervals that are 2 orders of magnitude lower. The easternmost Site U1451 drilled ~ 1200 m on the west flank of the 90° E Ridge, where the onset of turbiditic deposition at this position has been dated around 18 Ma. Two other 900 m penetration sites (U1550 and U1455) complete the Neogene record. **(b)** Mass accumulation rates for the three deep records of Expedition 354. Age models are from France-Lanord et al. (2016), Lenard et al. (2020a), Cruz et al. (2021), and Reilly et al. (2020).

4.2.1 Turbidites of the Bengal fan

Sediments retrieved at all sites of Expedition 354 are dominated by turbidites composed of massive sand lobes and silty sand to clayey silt turbidites deposited by channel levee systems (Adhikari et al., 2018). Hemipelagic, calcareous clay layers mark intervals with no turbidite deposition. Sand deposition is estimated to represent up to 60 % of the sediments in the Pleistocene section (Bergmann et al., 2020) and was already widespread during the Miocene, reflecting strong erosion under a monsoon climate. In the absence of sand recovery in the deeper sections, high penetration rates and hole instability implied the presence of unconsolidated sand throughout the Miocene (France-Lanord et al., 2016). Petrologic and geochemical characteristics of turbidites are very similar to those of modern Ganga and Brahmaputra river sediments (France-Lanord et al., 2016; Yoshida et al., 2021). Their Sr–Nd isotopic compositions and heavy mineral geochronological characteristics further demonstrate the Himalayan lineage of these detrital sediments (Blum et al., 2018; Lenard et al., 2020b; Huyghe et al., 2020), making them suitable archives of how Himalayan erosion has responded to the changing climate.

4.2.2 Erosion of the Himalaya

The geochemical characteristics of the Bengal fan turbidites demonstrate their Himalayan origin. While this was known from earlier Deep Sea Drilling Project (DSDP) and ODP records (Galy et al., 2010) or Pleistocene cores (Hein et al., 2017; Joussain et al., 2017), for the first Expedition 354 allows for the time study of a complete Neogene to Holocene record, with minimum gaps in deposition and sediment transport bias. In addition, the abundance of sand layers and their efficient recovery by the half-length APC allowed for the sampling of up to 1 kg of sand and so access to dense mineral extractions for thermochronology or large samples of quartz grains for cosmogenic isotopes. Such methods are critical to reconstructing erosion and seeing how this related to monsoon intensity.

The distribution of U–Pb ages of detrital zircon reveals that in addition to the Himalaya, supply by erosion of the Asian plate, north of the Indus-Yarlung suture, was already as significant during the early Miocene, as it is today via the southern Tibetan connection of the Yarlung Tsangpo to the Brahmaputra (Blum et al., 2018). A multi-proxy reconstruction of provenance and exhumation rates employed apatite and rutile U–Pb, mica Ar–Ar, and zircon fission-track data. For sediments older than 10 Ma, the rutile and zircon fission-track thermochronometry shows lag times between cooling

and sedimentation that imply derivation from the Greater Himalaya, which were exhuming rapidly from 17 to 14 Ma, but then these slowed. Over the interval 5.6–3.5 Ma, lag times shortened to < 1 Myr, and only these are found since that time (Najman et al., 2019). This implies a speeding up of erosion since 5.6 Ma, especially from the eastern syntaxis centered on Namche Barwa. Najman et al. (2019) ascribe variations in erosion to tectonic forces in the Himalaya and syntaxis rather than the evolving monsoon climate, although we note that the SAM rainfall likely peaked around 15 Ma and then weakened in the late Miocene (Clift et al., 2008; Yang et al., 2020; Molnar and Rajagopalan, 2012).

Apatite fission-track lag times are more stable through time and translate in erosion rate to 1 to 3 mm yr^{-1} since the Miocene (Huyghe et al., 2020). Finally, for the first time on IODP cores, quartz in situ cosmogenic ^{10}Be concentrations were measured since 6 Ma (Lenard et al., 2020b). This study reported steady erosion rates of ~ 1 mm yr^{-1} since the Miocene, implying that the onset of Pleistocene climate variability had little effect on the erosion regime.

4.2.3 Link to the carbon cycle

Himalayan erosion is potentially a globally significant actor in the carbon cycle. While silicate weathering is moderate in the drainage basin, the most important sink for carbon is thought to be via the burial of organic carbon (Galy et al., 2007). Detailed study of the weathering history is still in progress, but shipboard data on major element geochemistry and clay mineralogy already show that Bengal turbidites recovered at 8° N have relatively stable compositions and reflect essentially moderate intensity of silicate weathering. Overall K / Al ratios (a proxy for alteration intensity) of turbidites from Miocene to Holocene are similar to or higher than those of the modern rivers (Lupker et al., 2013), which indicates comparable to lower weathering conditions relative to today, consistent with results from the Arabian and South China seas (Clift and Jonell, 2021a). Similarly, clay mineral assemblages are dominated by illite and chlorite, which derives from physical erosion, not chemical weathering.

Shipboard organic carbon data confirm the general negative relationship between grain size and TOC in turbidites. Previous studies on Bengal fan turbidites demonstrated that they are dominated by organic matter exported from land and also carry indications of the evolution of vegetation. Shipboard data indicate that the organic carbon loading of the turbidites is slightly lower than observed in recent sediment in the northern part of the fan (Galy et al., 2008). However, a number of samples carry millimeter to centimeter organic particles that locally lead to very high organic carbon concentrations (Lee et al., 2019). These are derived from wood debris, whose δ^{13}C composition can be used to constrain the dominant vegetation. Miocene δ^{13}C values have a mean of −26.6 ‰, indicating C_3 dominance, but from about 4 Ma to present, the δ^{13}C of the wood is −20.5 ‰, which is 3.3 ‰ more positive than the most ^{13}C-enriched sample during the Miocene. This suggests a mixture of C_3 and C_4 fragments. More ^{13}C-enriched values appear since 1 Ma, where δ^{13}C wood values are bimodal with a C_4-like cluster (mean = −13.1 ‰) as well as the typical C_3-like values (mean = −26.3 ‰). This suggests a change in the ecosystems from which the wood is being exported, with one-third of the wood derived from C_4 plants in the last 1 Myr. In addition to the permanent transfer of organic carbon with fine grained particles, low-frequency wood export contributed significantly to the carbon burial in Bengal turbidites.

On shorter timescales, Weber et al. (2018) investigated the role of orbital forcing in monsoon rainfall since 200 ka at Site U1452. The variability of TOC, total nitrogen, and the δ^{13}C composition of organic matter was used to indicate the marine origin of the organic matter, and this showed that primary marine productivity likely increased during times of enhanced NE monsoon during glacial periods. At the same time, there was faster delivery of sediment to the Bay of Bengal caused by higher soil erosion on land. Similarities between the sediment record and the Antarctic climate record spanning multiple glacial cycles imply a close relationship between high-southern-latitude and monsoonal Asian climate driven by shifts in position of the ITCZ.

5 South China Sea: chemical weathering and fluvial runoff

Since the first scientific oceanic drilling in 1999 (ODP Leg 184) in the South China Sea which focused on the theme of "Exploring the Asian monsoon", four more IODP expeditions (349, 367, 368, and 368X) have been completed since 2014. This later campaign was designed to examine the tectonic evolution of the South China Sea (Sun et al., 2018; Li et al., 2015). Nonetheless, these new expeditions recovered long sequences of sediment that can be used to study the Asian monsoon over geologic timescales.

During Expedition 349, a total of 703 and 611 m of sediment/sedimentary rock were recovered at the two deepest sites, Site U1431 in the central east subbasin and U1433 in the southwest subbasin (Li et al., 2015). Sedimentary magnetic parameters (magnetic susceptibility and ARM, anhysteretic remanent magnetization) and hematite / goethite values of sediment from Hole U1431D were used to infer EAM variation since 6.5 Ma (Gai et al., 2020). The magnetic results indicate that the EAM was stable between 6.5 and 5.0 Ma and intensified between 5.0 and 3.8 Ma, possibly due to closure of the Central American Seaway, and then weakened gradually starting after 3.8 Ma in response to the onset of Northern Hemisphere glaciation (NHG) and global cooling.

Pollen from IODP Site U1433, mainly derived from the Mekong River, shows a long-term increase in herbaceous plants since 8 Ma and indicates a persistent drying and weakening of precipitation in former Indochina (Miao et

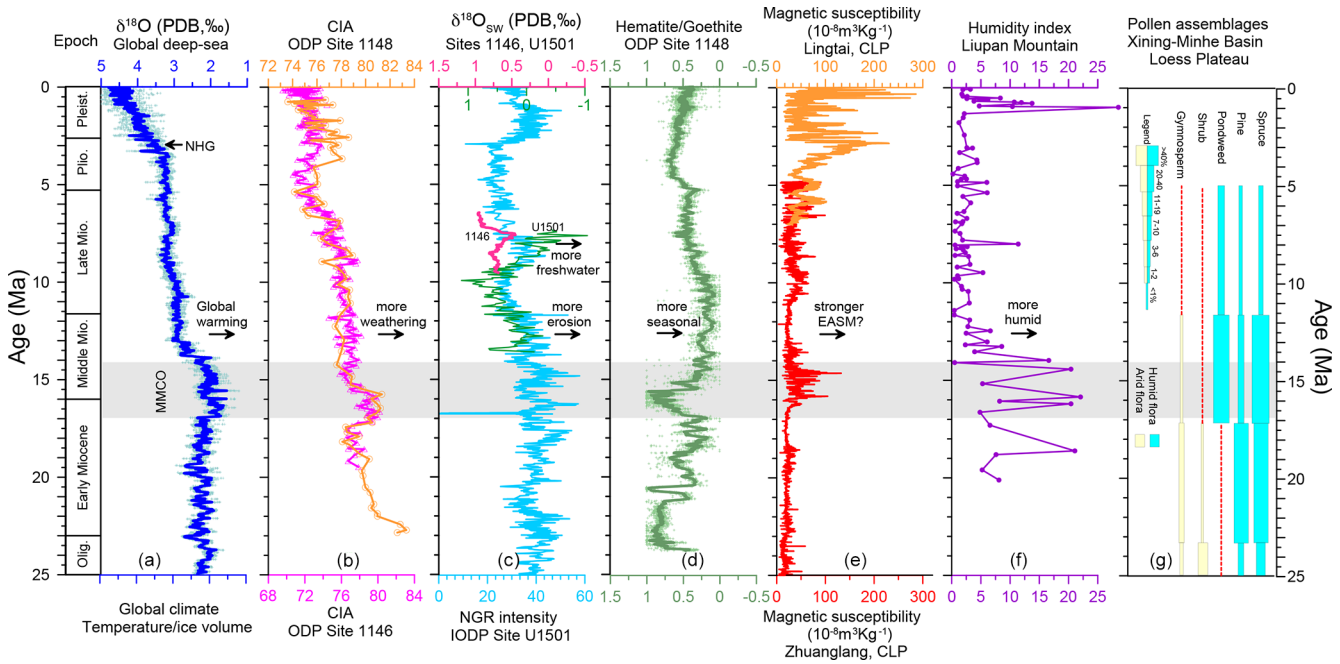

Figure 6. Proxies from land and sea showing the evolution of global climate and East Asian summer monsoon since 25 Ma. **(a)** Global deep-sea δ^{18}O (Westerhold et al., 2020); **(b)** chemical index of alteration at ODP Site 1146 (Wan et al., 2010) and 1148 (Wei et al., 2006) in the northern South China Sea; **(c)** seawater δ^{18}O at ODP Site 1146 (Steinke et al., 2010) and IODP Site U1501 (Yang et al., 2021), as well as NGR intensity at Site U1501 (Jian et al., 2018); **(d)** hematite / goethite ratio at ODP Site 1148 (Clift et al., 2008); **(e)** magnetic susceptibility of loess–paleosol sequences (Ding et al., 1999; Qiang et al., 2011); **(f)** pollen-based humidity index from Liupan Mountain (Jiang and Ding, 2008); **(g)** pollen assemblage evolution at Xining Basin (Sun and Wang, 2005). All drilling sites are located in the northern South China Sea on the continental margin.

al., 2017). Such an observation parallels trends in chemical weathering and hematite proxies at the same site (Liu et al., 2019). Interestingly, it remains debated as to whether the East Asian summer monsoon (EASM) intensified or weakened since the late Miocene (see synthesized proxies in Fig. 6). For example, magnetic susceptibility of loess–paleosol sequences suggests a weaker EASM during the Miocene–early Pliocene relative to late Pliocene–Pleistocene (An et al., 2001; Qiang et al., 2011; Zhao et al., 2020). In contrast, pollen assemblages in North China (Jiang and Ding, 2008; Sun and Wang, 2005) and weathering (Clift et al., 2014; Wan et al., 2010; Wei et al., 2006) and paleoceanographic proxies in the South China Sea (Holbourn et al., 2018; Steinke et al., 2010; Holbourn et al., 2021) show a general weakening EASM since the middle Miocene, possibly linked to global cooling.

Although IODP Expedition 368 recovered long sediment cores at Sites U1501 and U1505 on the continental margin in the NE South China Sea, most related studies are still on-going. However, at Site U1501 a study of seawater δ^{18}O and Mg / Ca ratios in planktic foraminifera has been completed. Differences between surface and thermocline records can be used to track the thermal gradient between the surface and subsurface waters, and the results imply that upper-water mixing was weaker at 9.4–7.3 Ma, which may have related to increased fluvial runoff linked to higher rainfall. These data also suggest a decrease in the intensity of EASM between 13.6 and 10.2 Ma and an increase during 10.2–7.3 Ma (Yang et al., 2021). The trend in seawater δ^{18}O at Site U1501 is a little different from previous study at nearby ODP Site 1146 (Fig. 6), which shows a rapidly decreasing sea surface salinity (SSS) and weakening of EASM since 7.5 Ma (Steinke et al., 2010; Holbourn et al., 2018). In any case, a similar long-term decreasing trend in the intensity of NGR (indicative of terrigenous clay input) is observed at both sites (Jian et al., 2018), consistent with a coupled evolution of continental erosion and monsoonal rainfall. This record implies that late Miocene rainfall of South China might have become wetter, while that in South Asia was drying after 7 Ma, a discrepancy that Yang et al. (2021) linked to formation of the WPWP at this time influencing East Asia, while Indian Ocean surface water cooling and Tibetan uplift were more influential in South Asia.

6 Sea of Japan: paleoceanography and Asian dust records

Expedition 346 targeted the upper Miocene to Holocene hemipelagic sediments of the Sea of Japan (East Sea of Korea) and the northern East China Sea (ECS) (Fig. 7). Seven

sites were drilled in the Sea of Japan, with two closely spaced sites in the ECS. In total, the expedition recovered 6135.3 m of core by the APC, with an average recovery of 101 %.

The primary objective was to explore the timing of onset and evolution of millennial- and orbital-scale variabilities of the EAM based on the hypothesis of Tada et al. (1999, 2015) that millennial- and orbital-scale variabilities of the EAM were recorded in the hemipelagic sediments of the Sea of Japan. These deposits are characterized by centimeter- to decimeter-scale alternations of dark and light layers modulated by the fresh-water discharge of the Yangtze River during summer that diluted the surface water of the northern ECS and modulated the SSS and nutrient concentration of the ocean water flowing into the Sea of Japan through the Tsushima Strait. Changes in SSS and nutrient content of the ocean water flowing into the Sea of Japan caused changes in ventilation and surface productivity of the sea.

Clemens et al. (2018) analyzed $\delta^{18}O$ and Mg / Ca ratios of *G. ruber* at Site U1429 in the northern ECS and reconstructed $\delta^{18}O_{sw}$, which reflects runoff-induced changes in SSS, during the last 400 kyr. They demonstrated that local SSS changed in association with eccentricity and obliquity cycles but not with the precession cycle, although precession is clearly evident in the planktonic $\delta^{18}O$. This contrasts the work of Cheng et al. (2016), who demonstrated that $\delta^{18}O$ of Chinese stalagmites shows a strong precession signal, with almost no evidence of eccentricity and obliquity. Hence, the extent to which local precipitation is reflected in stalagmite $\delta^{18}O$ remains in question. Clemens et al. (2018) also demonstrated the presence of millennial-scale variability of $\delta^{18}O_{sw}$, which Kubota et al. (2019) interpreted to reflect changes in precipitation of EASM in association with Dansgaard–Oeschger cycles during the last glacial period. Kubota et al. (2019) also demonstrated that $\delta^{18}O_{sw}$ changes in the northern ECS are closely associated with the changes in the gray scale of the sediments in the deeper part of the Sea of Japan, consistent with the hypothesis of Tada et al. (1999, 2015).

Irino et al. (2018) revised shipboard splices and constructed a complete, continuous dark–light sedimentary sequence at the seven sites drilled in the Sea of Japan, covering the last 3 Myr. Tada et al. (2018) used this sequence to examine centimeter- to decimeter-scale dark layers for the six sites deeper than ∼ 900 m water depth. They confirmed that it is possible to correlate almost all of the dark layers between the six sites in the deeper part of the basin, which could be traced back to 1.45 Ma when the first distinct dark layer was deposited. It was concluded that the Sea of Japan has responded to the orbital- and millennial-scale climatic changes as a single system since 1.45 Ma and that intermittent occurrences of millennial-scale variability of EAM can be traced back to at least 1.45 Ma. Based on XRF core scanning, Seki et al. (2019) demonstrated that gray-scale variation of Sea of Japan sediments basically reflects marine organic carbon content and so in turn reflects millennial-scale variability of the surface productivity.

Tada et al. (2018) also demonstrated that gamma ray attenuation density (GRA) is controlled by diatom content and that this changes in association with glacio-eustatic sea-level changes. Using this relationship, they constructed an orbitally tuned age model covering the last 3 Myr. Kurokawa et al. (2019) extended this age model back to 11.7 Ma, allowing for precise dating of paleoceanographic events across the basin. For example, they identified the occurrence of a hiatus from 7.3 to 5.3 Ma at Site U1330 on the South Korean Plateau, at water depths of 1072 m. It is possible that this hiatus was caused by intensification of the Sea of Japan Intermediate Water during the late Miocene global cooling (LMGC) interval from 7.8 to 5.8 Ma (Herbert et al., 2016).

Matsuzaki et al. (2020) examined radiolarian assemblages at Site U1425 in the middle of the Sea of Japan spanning the time interval 9.1–5.3 Ma and used these to reconstruct annual mean sea surface temperature (SST). They found a drastic decrease in annual SST from 24 to 16 °C from 7.9 to 6.6 Ma, which they attributed to intensification of East Asian winter monsoon (EAWM) during the early half of the LMGC. Based on comparison with NW Pacific high-latitude and midlatitude alkenone-based SST (Herbert et al., 2016; LaRiviere et al., 2012), they speculated that the later half of LMGC is characterized by summer cooling.

Shen et al. (2018) analyzed $\delta^{13}C$ of black carbon of probable eolian origin in sediments from Site U1430 and found a drastic increase in $\delta^{13}C$ that started at ∼ 5.3 Ma. They argued that this increase most likely reflects expansion of C_4 vegetation in Central Asia. However, they used a preliminary age model which did not take into account the hiatus from 7.3 to 5.3 Ma. According to a new age model of Kurokawa et al. (2019), the drastic increase in $\delta^{13}C$ occurred during the hiatus between 7.3 and 5.3 Ma. It is likely that expansion of C_4 vegetation in Central to East Asia occurred in association with LMGC.

Anderson et al. (2020) reconstructed the provenance of aluminosilicate sediment at Site U1430 since 12 Ma using multivariate partitioning of the major, trace, and rare earth element composition of bulk samples. They identified four aluminosilicate components (Taklimakan, Gobi, Chinese Loess, and Korean Peninsula) and demonstrated that the Taklimakan Desert component was the most abundant component before 7.5 Ma, whereas Gobi + Chinese Loess components became dominant by 4 Ma (and maybe as early as 7.5 Ma when taking into account the hiatus between 7.3 and 5.3 Ma) (Fig. 8). Accumulation rates of these dust components were relatively high before 7.5 Ma and very low between 4 and 2 Ma and increased again after ∼ 2 Ma. It is possible that expansion of the Gobi Desert and Chinese Loess Plateau occurred in association with LMGC. Because sedimentation at Site U1430 was influenced by bottom current winnowing from 7.5 Ma to as young as 3.5 Ma, similar provenance studies should be

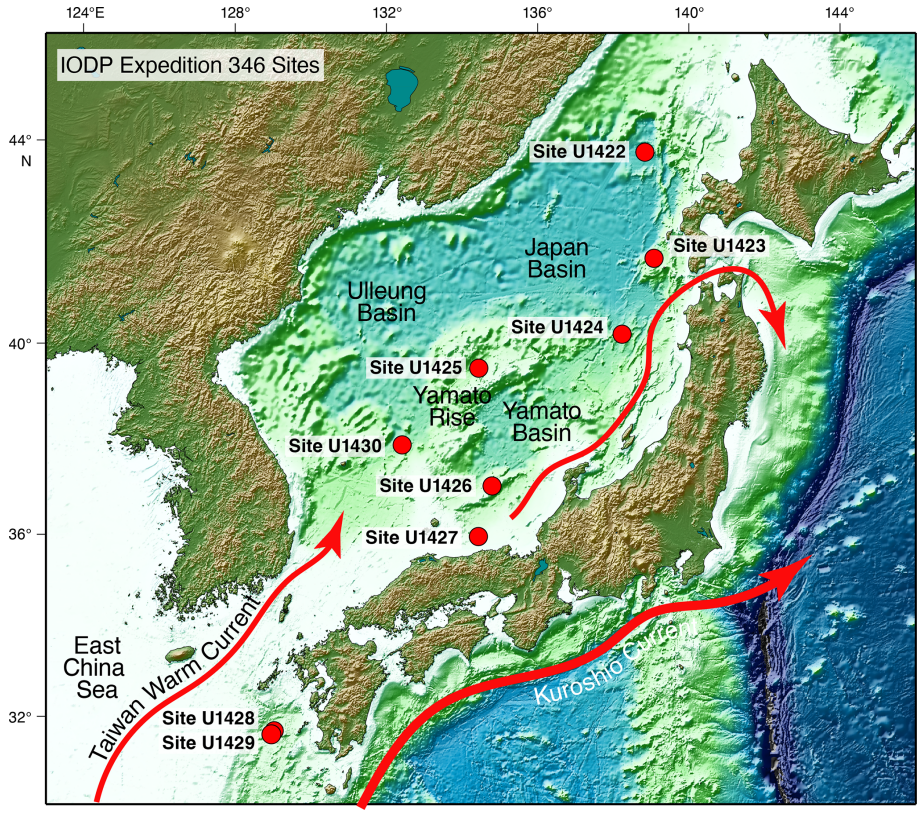

Figure 7. Bathymetric map of the area sampled by Expedition 346 with the major bathymetric features labeled as well as the locations of the drilling site. The red arrows show the major surface currents that affect the region. Modified after Tada et al. (2015).

conducted at other deeper-water sites to evaluate dust flux during the time interval between 7.5 and 1.5 Ma.

Results of Expedition 346 proved that dark and light alternations of the Quaternary sediments from the Sea of Japan faithfully recorded millennial-scale variability of EASM. Changes in salinity and nutrient concentration of the influx through the Tsushima Strait into the Sea of Japan since 1.45 Ma controlled surface productivity and ventilation in the sea so that millennial-scale variability of EAM can be traced back to that time. The work showed that distinct precession signals recorded in $\delta^{18}O$ of Chinese stalagmites were not caused by local precipitation changes of EASM but more likely reflecting changes in the $\delta^{18}O$ of precipitation, whereas millennial changes in $\delta^{18}O$ of Chinese stalagmites probably reflect changes in EASM precipitation. It is highly likely that EAWM intensified during the early half of the LMGC. On the other hand, EASM seems to have been weakened later during LMGC. It is possible that Gobi Desert expanded and C_3 to C_4 transition of vegetation occurred in Central to East Asia in association with the LMGC. However, the presence of a hiatus from 7.3 to 5.3 Ma in the sedimentary record of Site U1430 precludes precise dating of their timings. Similar examinations at Site 1425 are desirable.

7 Western Australian monsoon

North Australia is influenced by strong summer westerly and southwesterly winds that source warm, moist equatorial air, leading to monsoonal rains and cyclonic activity north of the monsoon shear line (Fig. 9). Seasonal monsoonal runoff delivers substantial amounts of fluvial sediment to the shelf via the Fitzroy, De Grey, Ashburton and Fortescue rivers. In contrast, continental wind-blown dust is transported by the trade winds offshore northwest Australia when the trade winds dominate during the winter dry season (Fig. 9).

IODP Expedition 356 cored seven sites to determine the latitudinal variation in climate and ocean conditions from ~ 30 to 18° S over the last 5 myr (Gallagher et al., 2017). The expedition recovered 5185.15 m of core, with 62 % recovery. Sites were cored in shelf regions near to the shore to determine the long-term history of the Australian monsoon and southwestern Australian climate. Many sites yielded older sections, revealing a climate archive extending as far back as ~ 50 Ma. For example, Sites U1461 and U1462 on the NW continental shelf at ~ 22° S yielded thick (up to 1 km) sections of upper Miocene to Recent strata that record the southerly extent of the Australian monsoon and its intensity. Further north, Sites U1463 and U1464 (~ 18° S) cored middle Miocene to Recent sections with contrasting facies

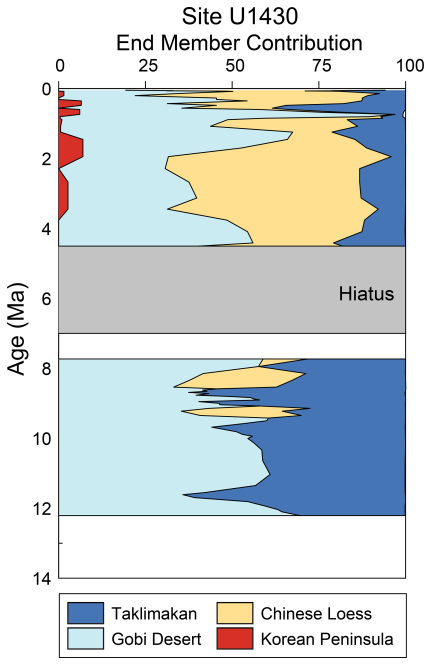

Figure 8. Aluminosilicate contribution (wt % of aluminosilicate inventory) at Site U1430 through time. The end-member contributions are plotted as the total sum, with each color representing the sum of the specific end-member plus the end-members to the left. The shaded region denotes a hiatus, and the following box notes a period in which we did not overinterpret our data to fill the temporal gap between the end of the hiatus and the start of our Miocene-aged samples. From Anderson et al. (2020).

ranging from Miocene subaerial, arid, sabkha evaporitic facies (Groeneveld et al., 2017; Tagliaro et al., 2018), and Pliocene deep-water carbonates (De Vleeschouwer et al., 2018) to Quaternary aridity-related oolite facies (Gallagher et al., 2018). These cores provide an unprecedented opportunity to investigate the long-term history of the Australian monsoon and aridity.

Previous studies suggested that at 23–14 Ma, Australia experienced seasonally wetter, monsoonal rainfall compared to today when the monsoonal front was in a similar position (Herold et al., 2011). However, analyses of sediments from Site U1459 show that arid conditions persisted from 16 to 6 Ma (Groeneveld et al., 2017), transitioning to a wetter period with all-year-round rainfall at ∼ 5.5 Ma (Site U1463) (Christensen et al., 2017; De Vleeschouwer et al., 2018; Auer et al., 2019) that became seasonal (monsoonal) starting at ∼ 3.3 Ma. The drying trend exhibited in Miocene NW Australia is broadly similar to that seen in the Mekong basin, and there may be a relationship between the northward migration of the westerlies from ∼ 12 Ma associated with expanded Antarctic sea ice and its abrupt shift back associated with LMGC (Groeneveld et al., 2017). The onset of humidity in NW Australia occurred seemingly differentially, first at the more northerly Site U1464 ∼ 6 Ma (Groeneveld et al., 2017) and later at Site U1463 at ∼ 5.5 Ma (Christensen et al., 2017). However, Karatsolis et al. (2020) suggested the region was humid, probably since ∼ 7 Ma when the ITCZ moved southward. NW Australia remained in the Humid Interval until ∼ 3.3 Ma (Christensen et al., 2017) when conditions became drier, although a major SST drop from ∼ 3.15 to 3 Ma based on TEX_{86} indicates temperature-driven drying may have begun slightly later (Smith et al., 2020). NW Australia achieved arid conditions with a strong winter monsoon similar to today by ∼ 2.4 Ma at the onset of the Arid Interval (Christensen et al., 2017) when higher-amplitude interglacial–glacial fluctuations in SST (Smith et al., 2020) led to a seasonal (monsoonal) regime. Over the last 2 Myr, interglacial wetter (strong monsoon with clay influx) and arid glacial (weak monsoon with limestone facies and dust input) conditions persisted in Australia's northwest (Gallagher and deMenocal, 2019). Evidence of the Holocene Australian summer monsoon (ASM) activity has been interpreted at Site U1461 from K / Ca ratios, with the percentage of potassium constrained from shipboard NGR (Ishiwa et al., 2019). These data show increased fluvial terrigenous input after 11.5 ka, followed by a maximum at ∼ 8.5 ka due to enhanced ASM-derived precipitation as a response to the southern migration of the ITCZ. Subsequently, weakening of rainfall after 8.5 ka was caused by the northern migration of the ITCZ.

8 Western Pacific Warm Pool

As a major source of heat and moisture to the atmosphere, the WPWP, often defined by the 28 °C isotherm and located in the heart of the Indo-Pacific Warm Pool, exerts a major role in influencing climate both in the tropics and globally. Changes in the SST of the WPWP influence the location and strength of convection in the rising limb of the Hadley and Walker cells, affecting planetary-scale atmospheric circulation, atmospheric heating, and tropical hydrology, including the Asian and Australian monsoons (Neale and Slingo, 2003; Wang and Mehta, 2008). Likewise, an important control on the WPWP and east Asian hydroclimate is the change in the equatorial Pacific zonal and Equator to pole temperature gradients. A primary goal of Expedition 363 was to assess changes in regional climate variability, expressed in temperature, precipitation, and biological productivity in the context of the global background state from the middle Miocene through the Holocene.

Currently, there is an ongoing debate about the evolution of SST in the WPWP since the late Miocene, due to substantial disagreement between proxy records, whereas foraminiferal Mg / Ca suggests stable mixed-layer temperatures throughout this period; records of the organic proxy TEX_{86}, interpreted to reflect SST, argue for a major cooling throughout with a similar magnitude to the change observed in the eastern equatorial Pacific (Zhang et al., 2014b; Ravelo et al., 2014; Zhang et al., 2014a). These two con-

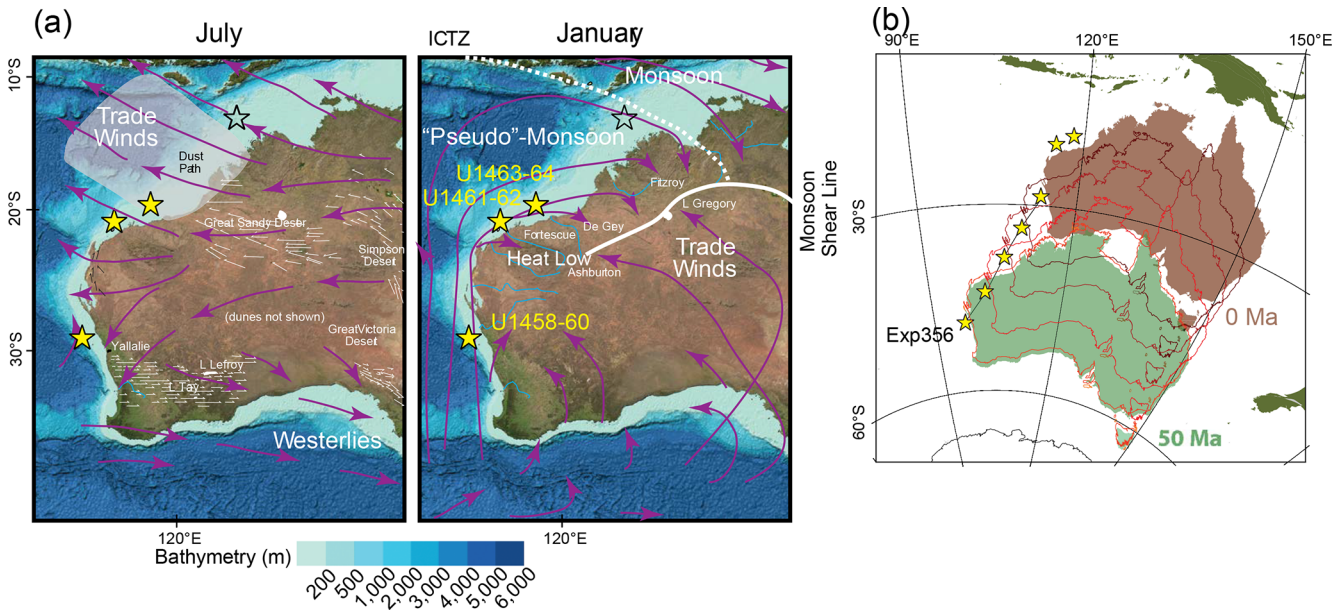

Figure 9. **(a)** Atmospheric circulation for January and July (Gentilli, 1972) with the mean monsoon shear line (McBride, 1986) and intertropical convergence zone (ITCZ). Base map adapted from the General Bathymetric Chart of the Oceans (GEBCO) http://www.gebco.net (last access: 29 May 2022). IODP Expedition 356 sites are shown as stars. **(b)** Plate tectonic motion of Australia since 50 Ma at 10 Myr intervals, with the path line for Site U1459 (Expedition 356). Figure adapted from Gallagher and deMenocal (2019).

trasting scenarios of the evolution of the equatorial Pacific zonal temperature gradient have very different implications on the hydroclimate of the Indo-Pacific Warm Pool and likely the Asian monsoon system. However, using samples from IODP Site U1488, Meinicke et al. (2021) show very good agreement between measurements of mixed-layer and thermocline planktic foraminiferal Mg / Ca and clumped isotopes (Δ_{47}), two independent foraminiferal proxies of temperature, thereby supporting the view that the WPWP mixed-layer temperatures did not cool substantially since the early Pliocene, while subsurface temperatures cooled more strongly, a change analogous to a shift from El Niño-like to more La Niña-like conditions, which could have intensified regional precipitation in the WPWP and east Asia.

Seasonal to interannual climate variations in the WPWP are dominated by fluctuations in precipitation associated with the seasonal march of the monsoons, migration of the intertropical convergence zone (ITCZ), and interannual changes associated with variability of the El Niño–Southern Oscillation (ENSO). It has been argued that on orbital timescales, the ITCZ and associated tropical precipitation belt migrate from a northern- to southern-centered position, relative to the Equator. These hemispherically asymmetric shifts are in pace with orbital variability. In contrast, new XRF geochemical records from Site U1483 and nearby sites on the northwestern Australia margin, when compared with published precipitation records from the WPWP, suggest that precipitation changed nearly in phase between the two hemispheres on the precession band, arguing for expansion and contraction in the latitudinal extent rather than migration of the tropical precipitation belt (Zhang et al., 2020). Furthermore, XRF records from other sites further to the south on the Australian, including Site U1482, reveal shorter periods of maximum Australian monsoon in the early Holocene (~ 10 ka), MIS 5e (~ 130 ka), MIS 7 (~ 200, ~ 220, and ~ 240 ka), and MIS 9 (~ 280, ~ 305, and ~ 330 ka), when maxima in atmospheric greenhouse gases coincided with maxima in Southern Hemisphere insolation (September). The intensification of the regional monsoon is attributed to intensely heated low-pressure cells over the Pilbara region that trigger the southward shift of the ITCZ (Pei et al., 2021). When compared with sites recovered in the other expedition, it is clear that the ongoing research on sites recovered during Expedition 363 will be important in testing hypotheses related to regionality and globality of the monsoon system, both on orbital and shorter timescales.

9 Synthesis

Comparison of the monsoon records in the different drilling areas targeted in this campaign indicates drying trends in most parts of Asia since ~ 10 Ma, which contrasts with the NW Australian wet phase at 5.0–2.5 Ma. However, this area too shows a trend to drier environments after 2.5 Ma (Fig. 10). Decoupling of the Australian and Asian monsoons reflects the greater influence of the ITF over regional climate in the Southern Hemisphere. Even within Asia, drying of the continent has not occurred in a uniform fashion. While most

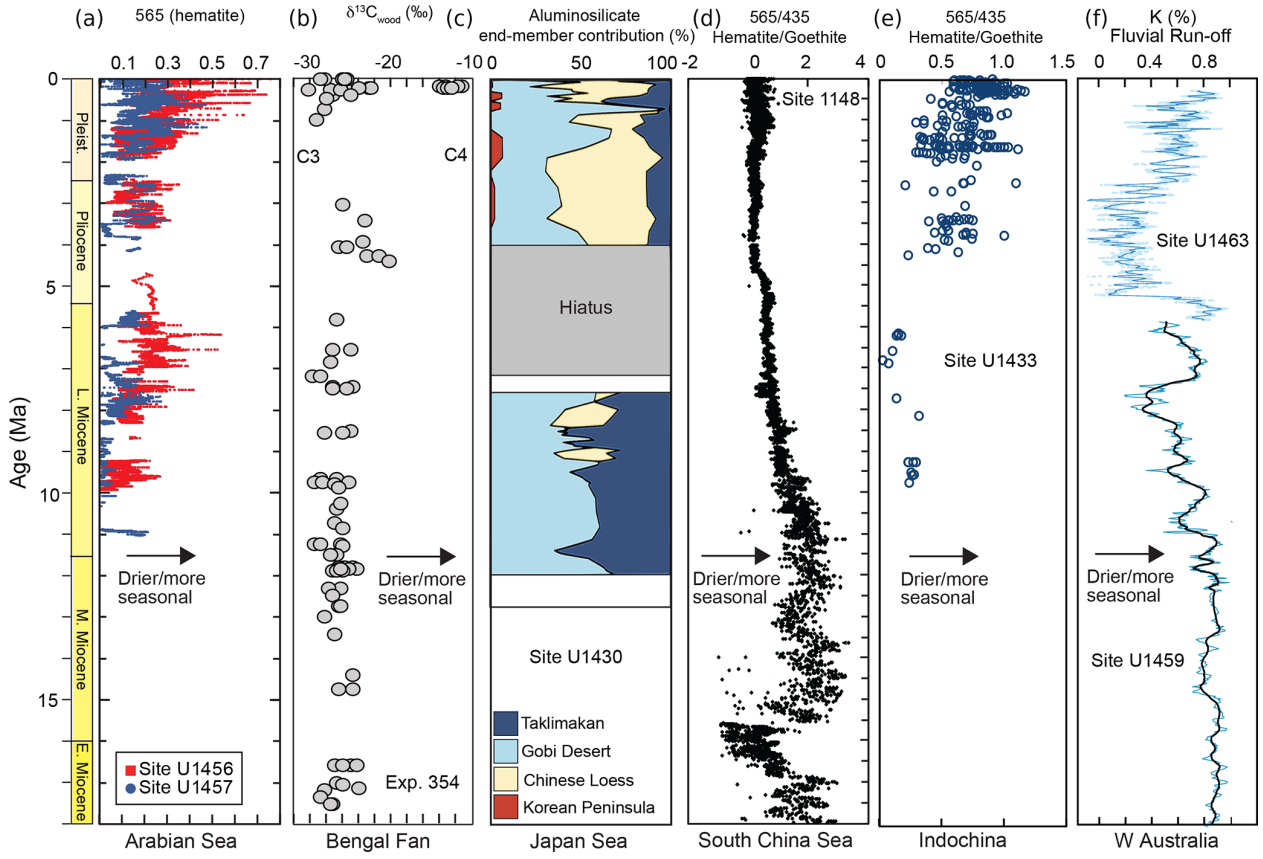

Figure 10. Compilation and comparison of monsoon related proxies from across the Asia–Australia region. **(a)** Hematite content from Laxmi Basin measured by 565 nm spectral analysis (Zhou et al., 2021), **(b)** $\delta^{13}C$ of wood from Bengal fan sediments (data from Lee et al., 2019), **(c)** source of wind-blown sediment in the Sea of Japan (Anderson et al., 2020), **(d)** hematite / goethite relative abundance tracked by 565/435 nm ratio from spectral analysis from northern South China Sea (Clift et al., 2008), **(e)** hematite / goethite relative abundance tracked by 565/435 nm ratio from SW South China Sea (data from Liu et al., 2019) and, **(f)** K (%) contents from western Australia acting a proxy for fluvial run-off at Site U1463 in NW Australia (data from Christensen et al., 2017) and Site U1459 in SW Australia (data from Groeneveld et al., 2017).

areas have seen increasing aridity, southern China appears to have become wetter, possibly due to migration of the ITCZ northwards since the late Miocene (Liu et al., 2019). Drying trends elsewhere are not synchronous. In the Indus Basin of SW Asia, drying started after 10 Ma, although the major change in vegetation to being C_4-dominated after around 7.2–7.4 Ma was not linked to changing rainfall but rather cooling of the Arabian Sea (Feakins et al., 2020). Drying started later, after 5 Ma in former Indochina and especially after 4 Ma in the Ganges Basin, although carbon isotope evidence from the Himalayan foreland basin indicates that eastern parts of the basin have essentially never made the C_3 to C_4 transition (Vögeli et al., 2017).

In central Asia, the Taklimakan Desert formed in the early Miocene (Zheng et al., 2015), but further east desiccation of the Chinese Loess Plateau appears to have occurred most strongly in the Pliocene based on records from the Ulleung Basin (Anderson et al., 2020). This migration in aridity may reflect the progressive northeastward growth of the Tibetan Plateau, starting in the Eocene (Ji et al., 2017) but with further uplift at 25–16 Ma and after 10 Ma (Wang et al., 2022). Lack of correlation between SAM and EAM is consistent with climate models that tie the SAM more closely with the height of the Himalayan topographic barrier (Boos and Kuang, 2010) when considering tectonic ($> 10^6$ years) timescales, while the EAM is influenced more by the height and extent of the Tibetan Plateau and the WPWP, at least by some studies (Tada et al., 2016). Recent climate models emphasize how the northern expansion of the plateau has increased rainfall in East Asia, especially during the drier winter season (Li et al., 2021), at the same time that northeast Tibet and northern China dried (Jiang et al., 2008; Zhang et al., 2021). In general the topography of Asia, including the Iranian Plateau, and even East Africa, acts to steer moisture inland and to focus precipitation, while the monsoon circulation itself reflects seawater temperature gradients (Acosta and Huber, 2020; Bordoni and Schneider, 2008). Thus, on shorter timescales when orbital processes dominate there is a

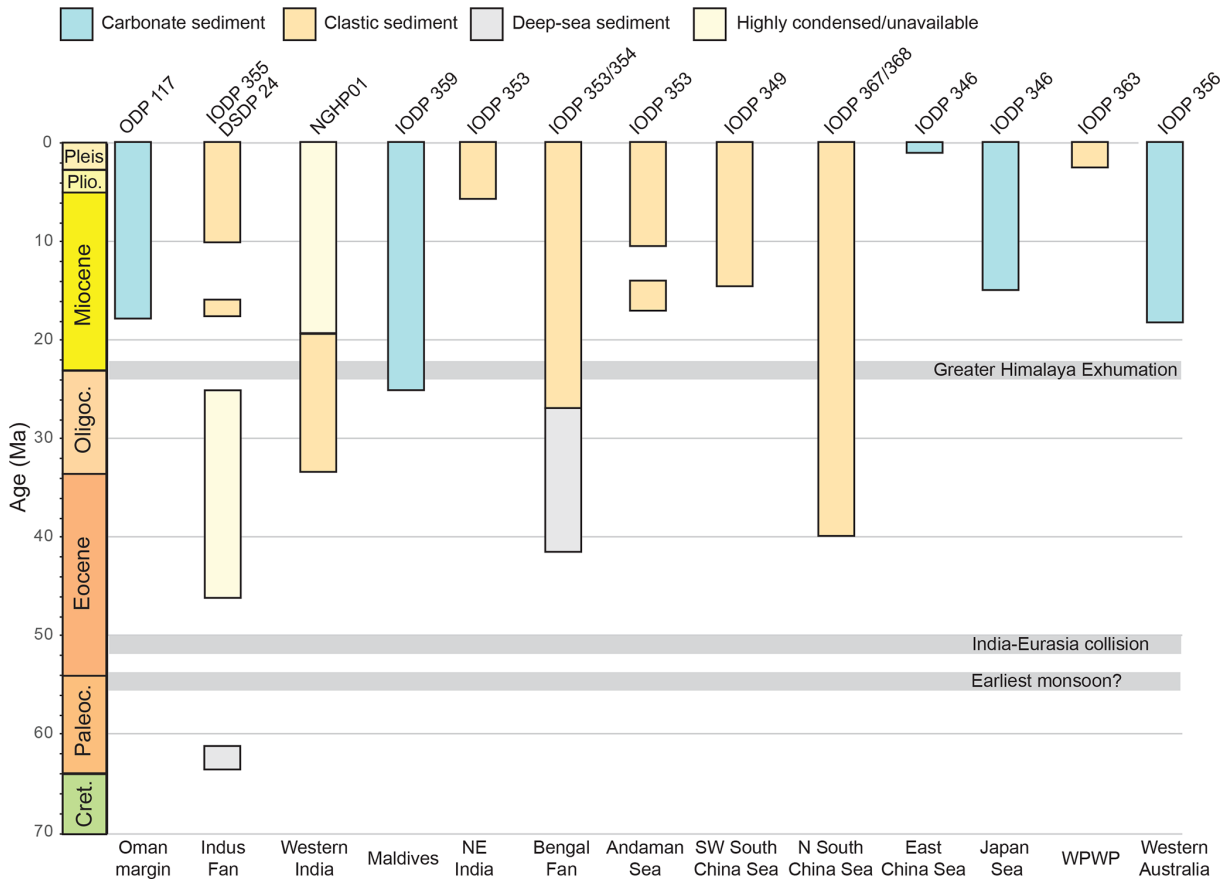

Figure 11. Summary of the temporal coverage now available across the marginal seas of monsoonal Asia, distinguishing between carbonate, biogenic, and oceanic sites and those comprising clastic sediments with records of continental erosion and weathering. Earliest monsoon age is from Licht et al. (2014). India–Eurasia collision age is from Najman et al. (2010). Greater Himalayan exhumation is from Godin et al. (2006).

tendency for the EAM and SAM to wax and wane together, as the surrounding oceans warm and cool.

The weakening monsoon is more generally caused by progressive global cooling since the early Miocene, although the results from the new drilling now indicate that this is not driven by more chemical weathering flux caused by faster erosion in either the western (Clift and Jonell, 2021b) or eastern Himalaya (France-Lanord et al., 2016). Instead, the erosion of areas such as New Guinea under the influence of the Australian monsoon may be critical (Macdonald et al., 2019), adding to the effect of enhanced organic carbon burial (Galy et al., 2007). However, earlier cooling may yet be related to Himalayan uplift in the Eocene–early Miocene. The improved monsoon records clearly show that a simple link between summer rains and topography in Asia is not viable, even assuming the latter can be reconstructed, but must instead involve additional tectonic and climatic processes.

Furthermore, combined records from across the region provide powerful tools for understanding monsoon in a holistic way when combined with onshore records. It is clear that proxies related to oceanographic productivity do not simply track those of continental rainfall. Monsoon rainfall in South Asia strengthened in the early Miocene (Clift and Webb, 2019), while the upwelling records show monsoon winds starting after 13 Ma (Betzler et al., 2016), linked to the stronger winds of the Somali Jet. This is related to the Iranian and African topographic rise, while Arabian Sea upwelling increased as the Arabian Peninsula became more continental (Sarr et al., 2022). Wind strength and/or stratification of ocean waters are key to controlling biological production but are less important to supplying moisture to inland Asia. Warmer oceans result in greater moisture supply, but the evolving topography diverts this in different directions and focuses precipitation into different areas. While some areas dry, others receive more rainfall, independently of how the oceans evolve. Measuring continental rainfall is not easy and is probably best tracked within limited drainage basins via the evolving vegetation (i.e., C_3 to C_4 balance) coupled with δD measurements. Chemical weathering proxies can play a part but are impacted by both temperature and seasonality, as well as precipitation, so that they must be applied with caution and over limited areas (cf., the contrast-

ing evolution in environments in former Indochina, southern China, and the Chinese Loess Plateau).

10 Future targets

While the monsoon drilling campaign has significantly advanced our understanding of how this climate system has evolved, there remain significant gaps in our comprehension. The almost total lack of Paleogene sedimentary archives is especially noteworthy (Fig. 11). This is a serious shortcoming because few of the marine sections even reach the time of Greater Himalayan exhumation, when monsoon intensification likely happened, let alone the older sections spanning the time of earliest monsoon activity. Climate modeling (Farnsworth et al., 2019) supports sparse terrestrial data (Licht et al., 2014; Sorrel et al., 2017) that indicate the monsoon having initiated in the late Eocene or even earlier, but to date few matching marine records have been cored, although suitable sequences would be accessible in the distal Bengal fan, along the Owen Ridge in the western Arabian Sea, and potentially in the Southwest Indian Margin.

Understanding the evolving continental topography is important when trying to quantify the links between monsoon histories and mountain building in Asia. As part of this effort there has been considerable research done on the evolving river systems of SE Asia which are sensitive to the growth of topography in the eastern Tibetan Plateau. Large-scale drainage capture has been associated with plateau uplift and the re-tilting of east Asia towards the east during the Cenozoic (Wang, 2004). Such studies are hamstrung onshore because of difficulties in constraining sedimentation ages and the lack of long-duration, semi-continuous records. The river systems of SE Asia, especially the Irrawaddy and Mekong, are noteworthy in being central to this debate but with few known sections that record their development studied to date. Drilling in the delta or fan of these systems would help resolve debates about drainage capture while also providing environmental records for SE Asia.

The published and ongoing studies of IODP Expedition 359 Maldive cores show that deposits surrounding carbonate platforms, in particular carbonate drifts, bear a previously underestimated potential for the understanding of the monsoon evolution on million-year timescales but also over shorter intervals and would add substantial knowledge to monsoon fluctuations at all timescales. Potential targets for further research on this topic exist in the Laccadives, the Mascarene Plateau, or the South China Sea platforms.

Data availability. Data presented in this paper are available in the articles cited throughout.

Author contributions. PDC led the overall writing, wrote the section about the Indus fan, and edited the final paper. CB and GPE wrote the section about the Maldives. SCC, CFL, AH, and WK wrote the sections on the Bay of Bengal and Bengal fan. SW and AH wrote the section on the South China Sea. BC, YR, AH, and SG wrote the sections about the Australian monsoon and western Pacific Warm Pool. RWM and RT wrote the section about the Sea of Japan. All authors contributed to the synthesis and future plans.

Competing interests. The contact author has declared that neither they nor their co-authors have any competing interests.

Disclaimer. Publisher's note: Copernicus Publications remains neutral with regard to jurisdictional claims in published maps and institutional affiliations.

Acknowledgements. We thank Carl Brenner and Angela Slagle at USSSP for encouraging the writing of this synthesis. The manuscript benefited from reviews by Rebecca Robinson and Clara Bolton.

Review statement. This paper was edited by Will Sager and reviewed by Clara Bolton and Rebecca Robinson.

References

Abram, N. J., Hargreaves, J. A., Wright, N. M., Thirumalai, K., Ummenhofer, C. C., and England, M. H.: Palaeoclimate perspectives on the Indian Ocean Dipole, Quaternary Sci. Rev., 237, 106302, https://doi.org/10.1016/j.quascirev.2020.106302, 2020.

Acosta, R. P. and Huber, M.: Competing Topographic Mechanisms for the Summer Indo-Asian Monsoon, Geophys. Res. Lett., 47, e2019GL085112, https://doi.org/10.1029/2019GL085112, 2020.

Adhikari, S. K., Sakai, T., and Yoshida, K.: Data report: grain size analysis of Bengal Fan sediments at Sites U1450 and U1451, IODP Expedition 354, Proceedings of the International Ocean Discovery Program, College Station, TX, 354, https://doi.org/10.14379/iodp.proc.354.202.2018, 2018.

Ali, S., Hathorne, E. C., and Frank, M.: Persistent Provenance of South Asian Monsoon-Induced Silicate Weathering Over the Past 27 Million Years, Paleoceanography and Paleoclimatology, 36, e2020PA003909, https://doi.org/10.1029/2020PA003909, 2021.

Allen, M. B. and Armstrong, H. A.: Reconciling the Intertropical Convergence Zone, Himalayan/Tibetan tectonics, and the onset of the Asian monsoon system, J. Asian Earth Sci., 44, 36–47, https://doi.org/10.1016/j.jseaes.2011.04.018, 2012.

Altabet, M. A., Francois, R., Murray, D. W., and Prell, W. L.: Climate-related variations in denitrification in the Arabian Sea from sediment ^{15}N / ^{14}N ratios, Nature, 373, 506–509, 1995.

An, Z., Kutzbach, J. E., Prell, W. L., and Porter, S. C.: Evolution of Asian monsoons and phased uplift of the Himalaya-Tibetan Plateau since late Miocene times, Nature, 411, 62–66, https://doi.org/10.1038/35075035, 2001.

Anderson, C. H., Murray, R. W., Dunlea, A. G., Giosan, L., Kinsley, C. W., McGee, D., and Tada, R.: Aeolian delivery to Ulle-

ung Basin, Korea (Japan Sea), during development of the East Asian Monsoon through the last 12 Ma, Geol. Mag., 157, 806–817, https://doi.org/10.1017/S001675681900013X, 2020.

Ashcroft, L., Gergis, J., and Karoly, D. J.: Long-term stationarity of El Niño–Southern Oscillation teleconnections in southeastern Australia, Clim. Dynam., 46, 2991–3006, https://doi.org/10.1007/s00382-015-2746-3, 2016.

Auer, G., De Vleeschouwer, D., Smith, R. A., Bogus, K., Groeneveld, J., Grunert, P., Castañeda, I. S., Petrick, B., Christensen, B., Fulthorpe, C., Gallagher, S. J., and Henderiks, J.: Timing and Pacing of Indonesian Throughflow Restriction and Its Connection to Late Pliocene Climate Shifts, Paleoceanography and Paleoclimatology, 34, 635–657, https://doi.org/10.1029/2018PA003512, 2019.

Barnet, J. S. K., Harper, D. T., LeVay, L. J., Edgar, K. M., Henehan, M. J., Babila, T. L., Ullmann, C. V., Leng, M. J., Kroon, D., Zachos, J. C., and Littler, K.: Coupled evolution of temperature and carbonate chemistry during the Paleocene–Eocene; new trace element records from the low latitude Indian Ocean, Earth Planet. Sci. Lett., 545, 116414, https://doi.org/10.1016/j.epsl.2020.116414, 2020.

Beasley, C., Kender, S., Giosan, L., Bolton, C. T., Anand, P., Leng, M. J., Nilsson-Kerr, K., Ullmann, C. V., Hesselbo, S. P., and Littler, K.: Evidence of a South Asian Proto-Monsoon During the Oligocene-Miocene Transition, Paleoceanography and Paleoclimatology, 36, e2021PA004278, https://doi.org/10.1029/2021PA004278, 2021.

Bergmann, F., Schwenk, T., Spiess, V., and France-Lanord, C.: Middle to Late Pleistocene Architecture and Stratigraphy of the Lower Bengal Fan—Integrating Multichannel Seismic Data and IODP Expedition 354 Results, Geochem. Geophy. Geosy., 21, e2019GC008702, https://doi.org/10.1029/2019GC008702, 2020.

Betzler, C. and Eberli, G. P.: Miocene start of modern carbonate platforms, Geology, 47, 771–775, https://doi.org/10.1130/g45994.1, 2019.

Betzler, C., Eberli, G. P., Kroon, D., Wright, J. D., Swart, P. K., Nath, B. N., Alvarez-Zarikian, C. A., Alonso-García, M., Bialik, O. M., Blättler, C. L., Guo, J. A., Haffen, S., Horozai, S., Inoue, M., Jovane, L., Lanci, L., Laya, J. C., Mee, A. L. H., Lüdmann, T., Nakakuni, M., Niino, K., Petruny, L. M., Pratiwi, S. D., Reijmer, J. J. G., Reolid, J., Slagle, A. L., Sloss, C. R., Su, X., Yao, Z., and Young, J. R.: The abrupt onset of the modern South Asian Monsoon winds, Sci. Rep., 6, 29838, https://doi.org/10.1038/srep29838, 2016.

Betzler, C., Eberli, G. P., Alvarez Zarikian, C. A., and Expedition 359 Scientists: Maldives Monsoon and Sea Level, International Ocean Discovery Program, College Station, TX, https://doi.org/10.14379/iodp.proc.359.2017, 2017.

Betzler, C., Eberli, G. P., Lüdmann, T., Reolid, J., Kroon, D., Reijmer, J. J. G., Swart, P. K., Wright, J., Young, J. R., Alvarez-Zarikian, C., Alonso-García, M., Bialik, O. M., Blättler, C. L., Guo, J. A., Haffen, S., Horozal, S., Inoue, M., Jovane, L., Lanci, L., Laya, J. C., Hui Mee, A. L., Nakakuni, M., Nath, B. N., Niino, K., Petruny, L. M., Pratiwi, S. D., Slagle, A. L., Sloss, C. R., Su, X., and Yao, Z.: Refinement of Miocene sea level and monsoon events from the sedimentary archive of the Maldives (Indian Ocean), Prog. Earth Planet. Sci., 5, 5, https://doi.org/10.1186/s40645-018-0165-x, 2018.

Blum, M., Rogers, K., Gleason, J., Najman, Y., Cruz, J., and Fox, L.: Allogenic and Autogenic Signals in the Stratigraphic Record of the Deep-Sea Bengal Fan, Sci. Repts., 8, 7973, https://doi.org/10.1038/s41598-018-25819-5, 2018.

Bolton, C. T., Gray, E., Kuhnt, W., Holbourn, A. E., Lübbers, J., Grant, K., Tachikawa, K., Marino, G., Rohling, E. J., Sarr, A.-C., and Andersen, N.: Secular and orbital-scale variability of equatorial Indian Ocean summer monsoon winds during the late Miocene, Clim. Past, 18, 713–738, https://doi.org/10.5194/cp-18-713-2022, 2022.

Boos, W. R. and Kuang, Z.: Dominant control of the South Asian monsoon by orographic insulation versus plateau heating, Nature, 463, 218–222, https://doi.org/10.1038/nature08707, 2010.

Bordoni, S. and Schneider, T.: Monsoons as eddy-mediated regime transitions of the tropical overturning circulations, Nat. Geosci., 1, 515–519, 2008.

Bretschneider, L., Hathorne, E. C., Huang, H., Lübbers, J., Kochhann, K. G. D., Holbourn, A., Kuhnt, W., Thiede, R., Gebregiorgis, D., Giosan, L., and Frank, M.: Provenance and Weathering of Clays Delivered to the Bay of Bengal During the Middle Miocene: Linkages to Tectonics and Monsoonal Climate, Paleoceanography and Paleoclimatology, 36, e2020PA003917, https://doi.org/10.1029/2020PA003917, 2021.

Cai, M., Xu, Z., Clift, P. D., Khim, B.-K., Lim, D., Yu, Z., Kulhanek, D. K., and Li, T.: Long-term history of sediment inputs to the eastern Arabian Sea and its implications for the evolution of the Indian summer monsoon since 3.7 Ma, Geol. Mag., 157, 908–919, https://doi.org/10.1017/S0016756818000857, 2020.

Cai, W., Cowan, T., Briggs, P., and Raupach, M.: Rising temperature depletes soil moisture and exacerbates severe drought conditions across southeast Australia, Geophys. Res. Lett., 36, L21709, https://doi.org/10.1029/2009GL040334, 2009.

Chang, Z. and Zhou, L.: Evidence for provenance change in deep sea sediments of the Bengal Fan: A 7 million year record from IODP U1444A, J. Asian Earth Sci., 186, 104008, https://doi.org/10.1016/j.jseaes.2019.104008, 2019.

Cheng, H., Edwards, R. L., Sinha, A., Spötl, C., Yi, L., Chen, S., Kelly, M., Kathayat, G., Wang, X., Li, X., Kong, X., Wang, Y., Ning, Y., and Zhang, H.: The Asian monsoon over the past 640 000 years and ice age terminations, Nature, 534, 640–646, https://doi.org/10.1038/nature18591, 2016.

Christensen, B. A., Renema, W., Henderiks, J., De Vleeschouwer, D., Groeneveld, J., Castañeda, I. S., Reuning, L., Bogus, K., Auer, G., Ishiwa, T., McHugh, C. M., Gallagher, S. J., and Fulthorpe, C. S.: Indonesian Throughflow drove Australian climate from humid Pliocene to arid Pleistocene, Geophys. Res. Lett., 44, 6914–6925, https://doi.org/10.1002/2017GL072977, 2017.

Clemens, S. C., Kuhnt, W., LeVay, L. J., and Expedition 353 Scientists: Indian Monsoon Rainfall, International Ocean Discovery Program, College Station, TX, https://doi.org/10.14379/iodp.proc.353.2016, 2016.

Clemens, S. C., Holbourn, A., Kubota, Y., Lee, K. E., Liu, Z., Chen, G., Nelson, A., and Fox-Kemper, B.: Precession-band variance missing from East Asian monsoon runoff, Nat. Commun., 9, 3364, https://doi.org/10.1038/s41467-018-05814-0, 2018.

Clemens, S. C., Yamamoto, M., Thirumalai, K., Giosan, L., Richey, J. N., Nilsson-Kerr, K., Rosenthal, Y., Anand, P., and McGrath, S. M.: Remote and local drivers of Pleistocene South Asian summer

monsoon precipitation: A test for future predictions, Sci. Adv., 7, eabg3848, https://doi.org/10.1126/sciadv.abg3848, 2021.

Clift, P., Lee, J. I., Clark, M. K., and Blusztajn, J.: Erosional response of south China to arc rifting and monsoonal strengthening; a record from the South China Sea, Mar. Geol., 184, 207–226, https://doi.org/10.1016/S0025-3227(01)00301-2, 2002.

Clift, P. D. and d'Alpoim Guedes, J.: Monsoon Rains, Great Rivers and the Development of Farming Civilisations in Asia, Cambridge University Press, Cambridge, 339 pp., https://doi.org/10.1017/9781139342889, 2021.

Clift, P. D. and Jonell, T. N.: Monsoon controls on sediment generation and transport: Mass budget and provenance constraints from the Indus River catchment, delta and submarine fan over tectonic and multi-millennial timescales, Earth-Sci. Rev., 220, 103682, https://doi.org/10.1016/j.earscirev.2021.103682, 2021a.

Clift, P. D. and Jonell, T. N.: Himalayan-Tibetan Erosion is not the Cause of Neogene Global Cooling, Geophys. Res. Lett., 48, e2020GL087742, https://doi.org/10.1029/2020GL087742, 2021b.

Clift, P. D. and Webb, A. G.: A history of the Asian monsoon and its interactions with solid Earth tectonics in Cenozoic South Asia, in: Himalayan Tectonics: A Modern Synthesis, edited by: Searle, M. P., and Treloar, P. J., Special Publications, Geological Society, London, 631–652, https://doi.org/10.1144/SP483.1, 2019.

Clift, P. D., Hodges, K., Heslop, D., Hannigan, R., Hoang, L. V., and Calves, G.: Greater Himalayan exhumation triggered by Early Miocene monsoon intensification, Nat. Geosci., 1, 875–880, https://doi.org/10.1038/ngeo351, 2008.

Clift, P. D., Wan, S., and Blusztajn, J.: Reconstructing Chemical Weathering, Physical Erosion and Monsoon Intensity since 25 Ma in the northern South China Sea: A review of competing proxies, Earth-Sci. Rev., 130, 86–102, https://doi.org/10.1016/j.earscirev.2014.01.002, 2014.

Clift, P. D., Kulhanek, D. K., Zhou, P., Bowen, M. G., Vincent, S. M., Lyle, M., and Hahn, A.: Chemical weathering and erosion responses to changing monsoon climate in the Late Miocene of Southwest Asia, Geol. Mag., 157, 939–955, https://doi.org/10.1017/S0016756819000608, 2020.

Cruz, J. W., Wise, S., and Parker, W. C.: Miocene to Recent calcareous nannofossil biostratigraphy in the eastern Bengal Fan (Indian Ocean): Linking turbidites to tectonic activity during the evolution of the Himalayas, Journal of Nannoplankton Research, 39, 15–28, 2021.

Curry, W. B., Ostermann, D. R., Guptha, M. V. S., and Itekkot, V.: Foraminiferal production and monsoonal upwelling in the Arabian Sea; evidence from sediment traps, in: Upwelling systems; evolution since the early Miocene, edited by: Summerhayes, C. P., Prell, W. L., and Emeis, K. C., Special Publication, Geological Society, London, 93–106, https://doi.org/10.1144/GSL.SP.1992.064.01.06, 1992.

Dailey, S. K., Clift, P. D., Kulhanek, D. K., Blusztajn, J., Routledge, C. M., Calvès, G., O'Sullivan, P., Jonell, T. N., Pandey, D. K., Andò, S., Coletti, G., Zhou, P., Li, Y., Neubeck, N. E., Bendle, J. A. P., Bratenkov, S., Griffith, E. M., Gurumurthy, G. P., Hahn, A., Iwai, M., Khim, B.-K., Kumar, A., Kumar, A. G., Liddy, H. M., Lu, H., Lyle, M. W., Mishra, R., Radhakrishna, T., Saraswat, R., Saxena, R., Scardia, G., Sharma, G. K., Singh, A. D., Steinke, S., Suzuki, K., Tauxe, L., Tiwari, M., Xu, Z., and Yu, Z.: Large-scale Mass Wasting on the Miocene Continental Margin of Western India, Geol. Soc. Amer. Bull., 132, 85–112, https://doi.org/10.1130/B35158.1, 2019.

De Vleeschouwer, D., Auer, G., Smith, R., Bogus, K., Christensen, B., Groeneveld, J., Petrick, B., Henderiks, J., Castañeda, I. S., O'Brien, E., Ellinghausen, M., Gallagher, S. J., Fulthorpe, C. S., and Pälike, H.: The amplifying effect of Indonesian Throughflow heat transport on Late Pliocene Southern Hemisphere climate cooling, Earth Planet. Sci. Lett., 500, 15–27, https://doi.org/10.1016/j.epsl.2018.07.035, 2018.

Ding, Z. L., Xiong, S. F., Sun, J. M., Yang, S. L., Gu, Z. Y., and Liu, T. S.: Pedostratigraphy and paleomagnetism of a ~7.0 Ma eolian loess–red clay sequence at Lingtai, Loess Plateau, north-central China and the implications for paleomonsoon evolution, Palaeogeogr. Palaeocl., 152, 49–66, https://doi.org/10.1016/S0031-0182(99)00034-6, 1999.

Dunlea, A. G., Giosan, L., and Huang, Y.: Pliocene expansion of C_4 vegetation in the Core Monsoon Zone on the Indian Peninsula, Clim. Past, 16, 2533–2546, https://doi.org/10.5194/cp-16-2533-2020, 2020.

Farnsworth, A., Lunt, D. J., Robinson, S. A., Valdes, P. J., Roberts, W. H. G., Clift, P. D., Markwick, P., Su, T., Wrobel, N., Bragg, F., Kelland, S.-J., and Pancost, R. D.: Past East Asian monsoon evolution controlled by paleogeography, not CO_2, Sci. Adv., 5, eaax1697, https://doi.org/10.1126/sciadv.aax1697, 2019.

Fasullo, J.: A mechanism for land–ocean contrasts in global monsoon trends in a warming climate, Clim. Dynam., 39, 1137–1147, https://doi.org/10.1007/s00382-011-1270-3, 2012.

Feakins, S. J., Liddy, H. M., Tauxe, L., Galy, V., Feng, X., Tierney, J. E., Miao, Y., and Warny, S.: Miocene C_4 Grassland Expansion as Recorded by the Indus Fan, Paleoceanography and Paleoclimatology, 35, e2020PA003856, https://doi.org/10.1029/2020PA003856, 2020.

France-Lanord, C., Spiess, V., Klaus, A., Schwenk, T., and Expedition 354 Scientists: Bengal Fan, International Ocean Discovery Program, College Station, TX, https://doi.org/10.14379/iodp.proc.354.2016, 2016.

Gai, C., Liu, Q., Roberts, A. P., Chou, Y., Zhao, X., Jiang, Z., and Liu, J.: East Asian monsoon evolution since the late Miocene from the South China Sea, Earth Planet. Sci. Lett., 530, 115960, https://doi.org/10.1016/j.epsl.2019.115960, 2020.

Gallagher, S. J. and deMenocal, P. B.: Finding dry spells in Ocean Sediments, Oceanography, 32, 38–41, https://doi.org/10.5670/oceanog.2019.120, 2019.

Gallagher, S. J., Fulthorpe, C. S., Bogus, K., and Expedition 356 Scientists: Indonesian Throughflow, International Ocean Discovery Program, College Station, TX, https://doi.org/10.14379/iodp.proc.356.2017, 2017.

Gallagher, S. J., Reuning, L., Himmler, T., Henderiks, J., De Vleeschouwer, D., Groeneveld, J., Rastegar Lari, A., Fulthorpe, C. S., Bogus, K., Renema, W., McGregor, H. V., Kominz, M. A., Auer, G., Baranwal, S., Castañeda, S., Christensen, B. A., Franco, D. R., Gurnis, M., Haller, C., He, Y., Ishiwa, T., Iwatani, H., Jatiningrum, R. S., Korpanty, C. A., Lee, E. Y., Levin, E., Mamo, B. L., McHugh, C. M., Petrick, B. F., Potts, D. C., Takayanagi, H., and Zhang, W.: The enigma of rare Quaternary oolites in the Indian and Pacific Oceans: A result of global oceanographic physicochemical conditions or a sampling bias?, Quaternary Sci. Rev., 200, 114–122, https://doi.org/10.1016/j.quascirev.2018.09.028, 2018.

Galy, V., France-Lanord, C., Beyssac, O., Faure, P., Kudrass, H.-R., and Palhol, F.: Efficient organic carbon burial in the Bengal fan sustained by the Himalayan erosional system, Nature, 450, 407–411, https://doi.org/10.1038/nature06273, 2007.

Galy, V., France-Lanord, C., and Lartiges, B.: Loading and fate of particulate organic carbon from the Himalaya to the Ganga–Brahmaputra delta, Geochim. Cosmochim. Acta, 72, 1767–1787, https://doi.org/10.1016/j.gca.2008.01.027, 2008.

Galy, V., France-Lanord, C., Peucker-Ehrenbrink, B., and Huyghe, P.: Sr–Nd–Os evidence for a stable erosion regime in the Himalaya during the past 12 Myr, Earth Planet. Sci. Lett., 290, 474–480, https://doi.org/10.1016/j.epsl.2010.01.004, 2010.

Gebregiorgis, D., Hathorne, E. C., Giosan, L., Clemens, S., Nürnberg, D., and Frank, M.: Southern Hemisphere forcing of South Asian monsoon precipitation over the past ∼ 1 million years, Nat. Commun., 9, 4702, https://doi.org/10.1038/s41467-018-07076-2, 2018.

Gentilli, J.: Australian climate patterns, Thomas Nelson, Melbourne, ISBN 0170049048, 1972.

Godin, L., Grujic, D., Law, R. D., and Searle, M. P.: Channel flow, ductile extrusion and exhumation in continental collision zones; an introduction, in: Channel Flow, Ductile Extrusion, and Exhumation of Lower-Middle Crust in Continental Collision Zones, edited by: Law, R. D., Searle, M. P., and Godin, L., Special Publication, Geological Society, London, 1–23, https://doi.org/10.1144/GSL.SP.2006.268.01.01, 2006.

Gordon, A. L.: Oceanography of the Indonesian seas and their throughflow, Oceanography, 18, 14–27, https://doi.org/10.5670/oceanog, 2005.

Groeneveld, J., Henderiks, J., Renema, W., McHugh, C. M., Vleeschouwer, D. D., Christensen, B. A., Fulthorpe, C. S., Reuning, L., Gallagher, S. J., Bogus, K., Auer, G., and Ishiwa, T.: Australian shelf sediments reveal shifts in Miocene Southern Hemisphere westerlies, Sci. Adv., 3, e1602567, https://doi.org/10.1126/sciadv.1602567, 2017.

Gülyüz, E., Durak, H., Özkaptan, M., and Krijgsman, W.: Paleomagnetic constraints on the early Miocene closure of the southern Neo-Tethys (Van region; East Anatolia): Inferences for the timing of Eurasia-Arabia collision, Glob. Planet. Change, 185, 103089, https://doi.org/10.1016/j.gloplacha.2019.103089, 2020.

Gupta, A. K., Yuvaraja, A., Prakasam, M., Clemens, S. C., and Velu, A.: Evolution of the South Asian monsoon wind system since the late Middle Miocene, Palaeogeogr. Palaeocl., 438, 160–167, https://doi.org/10.1016/j.palaeo.2015.08.006, 2015.

Harrison, T. M., Copeland, P., Kidd, W. S. F., and Yin, A.: Raising Tibet, Science, 255, 1663–1670, https://doi.org/10.1126/science.255.5052.1663, 1992.

Hein, C. J., Galy, V., Galy, A., France-Lanord, C., Kudrass, H., and Schwenk, T.: Post-glacial climate forcing of surface processes in the Ganges–Brahmaputra river basin and implications for carbon sequestration, Earth Planet. Sci. Lett., 478, 89–101, https://doi.org/10.1016/j.epsl.2017.08.013, 2017.

Herbert, T. D., Lawrence, K. T., Tzanova, A., Peterson, L. C., Caballero-Gill, R., and Kelly, C. S.: Late Miocene global cooling and the rise of modern ecosystems, Nat. Geosci., 9, 843–847, https://doi.org/10.1038/ngeo2813, 2016.

Herold, N., Huber, M., Greenwood, D. R., Müller, R. D., and Seton, M.: Early to Middle Miocene monsoon climate in Australia, Geology, 39, 3–6, https://doi.org/10.1130/g31208.1, 2011.

Holbourn, A., Kuhnt, W., Clemens, S. C., and Heslop, D.: A ∼ 12 Myr Miocene Record of East Asian Monsoon Variability From the South China Sea, Paleoceanography and Paleoclimatology, 36, e2021PA004267, https://doi.org/10.1029/2021PA004267, 2021.

Holbourn, A. E., Kuhnt, W., Clemens, S. C., Kochhann, K. G. D., Jöhnck, J., Lübbers, J., and Andersen, N.: Late Miocene climate cooling and intensification of southeast Asian winter monsoon, Nat. Commun., 9, 1584, https://doi.org/10.1038/s41467-018-03950-1, 2018.

Hovan, S. A. and Rea, D. K.: The Cenozoic Record of Continental Mineral Deposition on Broken and Ninetyeast Ridges, Indian Ocean: Southern African Aridity and Sediment Delivery from the Himalayas, Paleoceanography, 7, 833–860, https://doi.org/10.1029/92PA02176, 1992.

Huang, Y., Clemens, S. C., Liu, W., Wang, Y., and Prell, W. L.: Large-scale hydrological change drove the late Miocene C_4 plant expansion in the Himalayan foreland and Arabian Peninsula, Geology, 35, 531–534, https://doi.org/10.1130/G23666A.1, 2007.

Huyghe, P., Bernet, M., Galy, A., Naylor, M., Cruz, J., Gyawali, B. R., Gemignani, L., and Mugnier, J. L.: Rapid exhumation since at least 13 Ma in the Himalaya recorded by detrital apatite fission-track dating of Bengal fan (IODP Expedition 354) and modern Himalayan river sediments, Earth Planet. Sci. Lett., 534, 116078, https://doi.org/10.1016/j.epsl.2020.116078, 2020.

Irino, T., Tada, R., Ikehara, K., Sagawa, T., Karasuda, A., Kurokawa, S., Seki, A., and Lu, S.: Construction of perfectly continuous records of physical properties for dark-light sediment sequences collected from the Japan Sea during Integrated Ocean Drilling Program Expedition 346 and their potential utilities as paleoceanographic studies, Prog. Earth Planet. Sci., 5, 23, https://doi.org/10.1186/s40645-018-0176-7, 2018.

Ishiwa, T., Yokoyama, Y., Reuning, L., McHugh, C. M., De Vleeschouwer, D., and Gallagher, S. J.: Australian Summer Monsoon variability in the past 14 000 years revealed by IODP Expedition 356 sediments, Prog. Earth Planet. Sci., 6, 17, https://doi.org/10.1186/s40645-019-0262-5, 2019.

Ji, J., Zhang, K., Clift, P. D., Zhuang, G., Song, B., Ke, X., and Xu, Y.: High-resolution magnetostratigraphic study of the Paleogene-Neogene strata in the Northern Qaidam Basin: Implications for the growth of the Northeastern Tibetan Plateau, Gondwana Res., 46, 141–155, https://doi.org/10.1016/j.gr.2017.02.015, 2017.

Jian, Z., Larsen, H. C., Alvarez Zarikian, C. A., and Expedition 368 Scientists: Expedition 368 Preliminary Report: South China Sea Rifted Margin, International Ocean Discovery Program, College Station, TX, https://doi.org/10.14379/iodp.pr.368.2018, 2018.

Jiang, D., Ding, Z., Drange, H., and Gao, Y.: Sensitivity of East Asian climate to the progressive uplift and expansion of the Tibetan Plateau under the mid-Pliocene boundary conditions, Adv. Atmos. Sci., 25, 709–722, https://doi.org/10.1007/s00376-008-0709-x, 2008.

Jiang, H. and Ding, Z.: A 20 Ma pollen record of East-Asian summer monsoon evolution from Guyuan, Ningxia, China, Palaeogeogr. Palaeocl., 265, 30–38, https://doi.org/10.1016/j.palaeo.2008.04.016, 2008.

Jöhnck, J., Kuhnt, W., Holbourn, A., and Andersen, N.: Variability of the Indian Monsoon in the Andaman Sea Across the Miocene-Pliocene Transition, Paleoceanography and Paleoclimatology,

35, e2020PA003923, https://doi.org/10.1029/2020PA003923, 2020.

Joussain, R., Liu, Z., Colin, C., Duchamp-Alphonse, S., Yu, Z., Moréno, E., Fournier, L., Zaragosi, S., Dapoigny, A., Meynadier, L., and Bassinot, F.: Link between Indian monsoon rainfall and physical erosion in the Himalayan system during the Holocene, Geochem. Geophy., Geosy., 18, 3452–3469, https://doi.org/10.1002/2016GC006762, 2017.

Kajtar, J. B., Santoso, A., England, M. H., and Cai, W.: Indo-Pacific Climate Interactions in the Absence of an Indonesian Throughflow, J. Climate, 28, 5017–5029, https://doi.org/10.1175/jcli-d-14-00114.1, 2015.

Karatsolis, B. T., De Vleeschouwer, D., Groeneveld, J., Christensen, B., and Henderiks, J.: The late Miocene to early Pliocene "Humid Interval" on the NW Australian shelf: Disentangling climate forcing from regional basin evolution, Paleoceanography and Paleoclimatology, 35, e2019PA003780, https://doi.org/10.1029/2019PA003780, 2020.

Khim, B.-K., Lee, J., Ha, S., Park, J., Pandey, D. K., Clift, P. D., Kulhanek, D. K., Steinke, S., Griffith, E. M., Suzuki, K., and Xu, Z.: Variations in δ13C values of sedimentary organic matter since late Miocene time in the Indus Fan (IODP Site 1457) of the eastern Arabian Sea, Geol. Mag., 157, 1012–1021, https://doi.org/10.1017/S0016756818000870, 2020.

Kim, J.-E., Khim, B.-K., Ikehara, M., and Lee, J.: Orbital-scale denitrification changes in the Eastern Arabian Sea during the last 800 kyrs, Sci. Repts., 8, 7027, https://doi.org/10.1038/s41598-018-25415-7, 2018.

Krebs, U., Park, W., and Schneider, B.: Pliocene aridification of Australia caused by tectonically induced weakening of the Indonesian throughflow, Palaeogeogr. Palaeocl., 309, 111–117, https://doi.org/10.1016/j.palaeo.2011.06.002, 2011.

Kroon, D., Steens, T., and Troelstra, S. R.: Onset of Monsoonal related upwelling in the western Arabian Sea as revealed by planktonic foraminifers, in: Proceedings of the Ocean Drilling Program, Scientific Results, edited by: Prell, W., and Niitsuma, N., Ocean Drilling Program, College Station, TX, 257–263, https://doi.org/10.2973/odp.proc.sr.117.126.1991, 1991.

Kubota, Y., Kimoto, K., Tada, R., Uchida, M., and Ikehara, K.: Millennial-scale variability of East Asian summer monsoon inferred from sea surface salinity in the northern East China Sea (ECS) and its impact on the Japan Sea during Marine Isotope Stage (MIS) 3, Prog. Earth Planet. Sci., 6, 39, https://doi.org/10.1186/s40645-019-0283-0, 2019.

Kuhnt, W., Holbourn, A. E., Jöhnck, J., and Lübbers, J.: Miocene to Pleistocene Palaeoceanography of the Andaman Region: Evolution of the Indian Monsoon on a Warmer-Than-Present Earth, in: The Andaman Islands and Adjoining Offshore: Geology, Tectonics and Palaeoclimate, edited by: Ray J., R. M., Society of Earth Scientists Series, Springer, https://doi.org/10.1007/978-3-030-39843-9_13, 2020.

Kunkelova, T., Jung, S. J. A., de Leau, E. S., Odling, N., Thomas, A. L., Betzler, C., Eberli, G. P., Alvarez-Zarikian, C. A., Alonso-García, M., Bialik, O. M., Blättler, C. L., Guo, J. A., Haffen, S., Horozal, S., Mee, A. L. H., Inoue, M., Jovane, L., Lanci, L., Laya, J. C., Lüdmann, T., Bejugam, N. N., Nakakuni, M., Niino, K., Petruny, L. M., Pratiwi, S. D., Reijmer, J. J. G., Reolid, J., Slagle, A. L., Sloss, C. R., Su, X., Swart, P. K., Wright, J. D., Yao, Z., Young, J. R., Lindhorst, S., Stainbank, S., Rueggeberg, A., Spezzaferri, S., Carrasqueira, I., Yu, S., and Kroon, D.: A two million year record of low-latitude aridity linked to continental weathering from the Maldives, Prog. Earth Planet. Sci., 5, 86, https://doi.org/10.1186/s40645-018-0238-x, 2018.

Kurokawa, S., Tada, R., Matsuzaki, K. M., Irino, T., and Johanna, L.: Cyclostratigraphy of the Late Miocene to Pliocene sediments at IODP sites U1425 and U1430 in the Japan Sea and paleoceanographic implications, Prog. Earth Planet. Sci., 6, 2, https://doi.org/10.1186/s40645-018-0250-1, 2019.

LaRiviere, J. P., Ravelo, A. C., Crimmins, A., Dekens, P. S., Ford, H. L., Lyle, M., and Wara, M. W.: Late Miocene decoupling of oceanic warmth and atmospheric carbon dioxide forcing, Nature, 486, 97–100, https://doi.org/10.1038/nature11200, 2012.

Lau, N.-C. and Wang, B.: Interactions between the Asian monsoon and the El Niño/Southern oscillation, in: The Asian Monsoon, Springer, 479–512, https://doi.org/10.1007/3-540-37722-0_12, 2006.

Lee, H., Galy, V., Feng, X., Ponton, C., Galy, A., France-Lanord, C., and Feakins, S. J.: Sustained wood burial in the Bengal Fan over the last 19 My, P. Natl. Acad. Sci. USA, 116, 22518–22525, https://doi.org/10.1073/pnas.1913714116, 2019.

Lee, J., Kim, S., and Khim, B.-K.: A paleoproductivity shift in the northwestern Bay of Bengal (IODP Site U1445) across the Mid-Pleistocene transition in response to weakening of the Indian summer monsoon, Palaeogeogr. Palaeocl., 560, 110018, https://doi.org/10.1016/j.palaeo.2020.110018, 2020a.

Lee, J., Kim, S., Lee, J. I., Cho, H. G., Phillips, S. C., and Khim, B.-K.: Monsoon-influenced variation of clay mineral compositions and detrital Nd-Sr isotopes in the western Andaman Sea (IODP Site U1447) since the late Miocene, Palaeogeogr. Palaeocl., 538, 109339, https://doi.org/10.1016/j.palaeo.2019.109339, 2020b.

Lenard, S., Cruz, J., France-Lanord, C., and Lavé, J.: Data report: calcareous nannofossils and lithologic constraints on the age model of IODP Site U1450, Expedition 354, Bengal Fan, Proceedings of the International Ocean Discovery Program, College Station, TX, 354, https://doi.org/10.14379/iodp.proc.354.203.2020, 2020a.

Lenard, S. J. P., Lavé, J., France-Lanord, C., Aumaître, G., Bourlès, D. L., and Keddadouche, K.: Steady erosion rates in the Himalayas through late Cenozoic climatic changes, Nature Geosci., 13, 448–452, https://doi.org/10.1038/s41561-020-0585-2, 2020b.

Li, C.-F., Lin, J., Kulhanek, D. K., and Expedition 349 Scientists: South China Sea Tectonics, International Ocean Discovery Program, College Station, TX, https://doi.org/10.14379/iodp.proc.349.102.2015, 2015.

Li, S.-F., Valdes, P. J., Farnsworth, A., Davies-Barnard, T., Su, T., Lunt, D. J., Spicer, R. A., Liu, J., Deng, W.-Y.-D., Huang, J., Tang, H., Ridgwell, A., Chen, L.-L., and Zhou, Z.-K.: Orographic evolution of northern Tibet shaped vegetation and plant diversity in eastern Asia, Sci. Adv., 7, eabc7741, https://doi.org/10.1126/sciadv.abc7741, 2021.

Licht, A., Cappelle, M. v., Abels, H. A., Ladant, J.-B., Trabucho-Alexandre, J., France-Lanord, C., Donnadieu, Y., Vandenberghe, J., Rigaudier, T., Lecuyer, C., Terry, D., Adriaens, R., Boura, A., Guo, Z., Soe, A. N., Quade, J., Dupont-Nivet, G., and Jaeger, J.-J.: Asian monsoons in a late Eocene greenhouse world, Nature, 513, 501–506, https://doi.org/10.1038/nature13704, 2014.

Lindhorst, S., Betzler, C., and Kroon, D.: Wind variability over the northern Indian Ocean during the past 4 million years – Insights from coarse aeolian dust (IODP exp. 359, site U1467, Maldives), Palaeogeogr. Palaeocl., 536, 109371, https://doi.org/10.1016/j.palaeo.2019.109371, 2019.

Ling, A., Eberli, G. P., Swart, P. K., Reolid, J., Stainbank, S., Rüggeberg, A., and Betzler, C.: Middle Miocene platform drowning in the Maldives associated with monsoon-related intensification of currents, Palaeogeogr. Palaeocl., 567, 110275, https://doi.org/10.1016/j.palaeo.2021.110275, 2021.

Liu, C., Clift, P. D., Giosan, L., Miao, Y., Warny, S., and Wan, S.: Paleoclimatic evolution of the SW and NE South China Sea and its relationship with spectral reflectance data over various age scales, Palaeogeogr. Palaeocl., 525, 25–43, https://doi.org/10.1016/j.palaeo.2019.02.019, 2019.

Lübbers, J., Kuhnt, W., Holbourn, A. E., Bolton, C. T., Gray, E., Usui, Y., Kochhann, K. G. D., Beil, S., and Andersen, N.: The Middle to Late Miocene "Carbonate Crash" in the Equatorial Indian Ocean, Paleoceanography and Paleoclimatology, 34, 813–832, https://doi.org/10.1029/2018PA003482, 2019.

Lüdmann, T., Betzler, C., Eberli, G. P., Reolid, J., Reijmer, J. J. G., Sloss, C. R., Bialik, O. M., Alvarez-Zarikian, C. A., Alonso-García, M., Blättler, C. L., Guo, J. A., Haffen, S., Horozal, S., Inoue, M., Jovane, L., Kroon, D., Lanci, L., Laya, J. C., Mee, A. L. H., Nakakuni, M., Nath, B. N., Niino, K., Petruny, L. M., Pratiwi, S. D., Slagle, A. L., Su, X., Swart, P. K., Wright, J. D., Yao, Z., and Young, J. R.: Carbonate delta drift: A new sediment drift type, Mar. Geol., 401, 98–111, https://doi.org/10.1016/j.margeo.2018.04.011, 2018.

Lupker, M., France-Lanord, C., Galy, V., Lave, J., and Kudrass, H.: Increasing chemical weathering in the Himalayan system since the Last Glacial Maximum, Earth Planet. Sci. Lett., 365, 243–252, https://doi.org/10.1016/j.epsl.2013.01.038, 2013.

Macdonald, F. A., Swanson-Hysell, N. L., Park, Y., Lisiecki, L., and Jagoutz, O.: Arc-continent collisions in the tropics set Earth's climate state, Science, 364, 181–184, https://doi.org/10.1126/science.aav5300, 2019.

Madella, M. and Fuller, D. Q.: Palaeoecology and the Harappan Civilisation of South Asia: a reconsideration, Quaternary Sci. Rev., 25, 1283–1301, https://doi.org/10.1016/j.quascirev.2005.10.012, 2006.

Manabe, S. and Terpstra, T. B.: The effects of mountains on the general circulation of the atmosphere as identified by numerical experiments, J. Atmos. Sci., 31, 3–42, https://doi.org/10.1175/1520-0469(1974)031<0003:TEOMOT>2.0.CO;2, 1974.

Matsuzaki, K. M., Suzuki, N., and Tada, R.: An intensified East Asian winter monsoon in the Japan Sea between 7.9 and 6.6 Ma, Geology, 48, 919–923, https://doi.org/10.1130/g47393.1, 2020.

McBride, J. L.: Tropical cyclones in the Southern Hemisphere summer monsoon, Second International Conference on Southern Hemisphere Meteorology, 1–5 December 1986, Wellington, New Zealand, American Meteorological Society, Boston, 358–364, 1986.

McGrath, S. M., Clemens, S. C., Huang, Y., and Yamamoto, M.: Greenhouse Gas and Ice Volume Drive Pleistocene Indian Summer Monsoon Precipitation Isotope Variability, Geophys. Res. Lett., 48, e2020GL092249, https://doi.org/10.1029/2020GL092249, 2021.

McNeill, L. C., Dugan, B., Backman, J., Pickering, K. T., Pouderoux, H. F. A., Henstock, T. J., Petronotis, K. E., Carter, A., Chemale, F., Milliken, K. L., Kutterolf, S., Mukoyoshi, H., Chen, W., Kachovich, S., Mitchison, F. L., Bourlange, S., Colson, T. A., Frederik, M. C. G., Guèrin, G., Hamahashi, M., House, B. M., Hüpers, A., Jeppson, T. N., Kenigsberg, A. R., Kuranaga, M., Nair, N., Owari, S., Shan, Y., Song, I., Torres, M. E., Vannucchi, P., Vrolijk, P. J., Yang, T., Zhao, X., and Thomas, E.: Understanding Himalayan erosion and the significance of the Nicobar Fan, Earth Planet. Sci. Lett., 475, 134–142, https://doi.org/10.1016/j.epsl.2017.07.019, 2017.

Meinicke, N., Reimi, M. A., Ravelo, A. C., and Meckler, A. N.: Coupled Mg / Ca and Clumped Isotope Measurements Indicate Lack of Substantial Mixed Layer Cooling in the Western Pacific Warm Pool During the Last ∼5 Million Years, Paleoceanography and Paleoclimatology, 36, e2020PA004115, https://doi.org/10.1029/2020PA004115, 2021.

Miao, Y., Warny, S., Clift, P. D., Liu, C., and Gregory, M.: Evidence of continuous Asian summer monsoon weakening as a response to global cooling over the last 8 Ma, Gondwana Res., 52, 48–58, https://doi.org/10.1016/j.gr.2017.09.003, 2017.

Molnar, P., England, P., and Martinod, J.: Mantle Dynamics, Uplift of the Tibetan Plateau, and the Indian Monsoon, Rev. Geophys., 31, 357–396, https://doi.org/10.1029/93RG02030, 1993.

Molnar, P. H. and Rajagopalan, B.: Late Miocene upward and outward growth of eastern Tibet and decreasing monsoon rainfall over the northwestern Indian subcontinent since ∼10 Ma, Geophys. Res. Lett., 39, L09702, https://doi.org/10.1029/2012GL051305, 2012.

Najman, Y., Appel, E., Boudagher-Fadel, M., Bown, P., Carter, A., Garzanti, E., Godin, L., Han, J., Liebke, U., Oliver, G., Parrish, R., and Vezzoli, G.: Timing of India-Asia collision: Geological, biostratigraphic, and palaeomagnetic constraints, J. Geophys. Res., 115, B12416, https://doi.org/10.1029/2010JB007673, 2010.

Najman, Y., Mark, C., Barfod, D. N., Carter, A., Parrish, R., Chew, D., and Gemignani, L.: Spatial and temporal trends in exhumation of the Eastern Himalaya and syntaxis as determined from a multitechnique detrital thermochronological study of the Bengal Fan, GSA Bulletin, 131, 1607–1622, https://doi.org/10.1130/b35031.1, 2019.

Neale, R. and Slingo, J.: The maritime continent and its role in the global climate: A GCM study, J. Climate, 16, 834–848, 2003.

Nilsson-Kerr, K., Anand, P., Sexton, P. F., Leng, M. J., Misra, S., Clemens, S. C., and Hammond, S. J.: Role of Asian summer monsoon subsystems in the inter-hemispheric progression of deglaciation, Nat. Geosci., 12, 290–295, https://doi.org/10.1038/s41561-019-0319-5, 2019.

Nilsson-Kerr, K., Anand, P., Holden, P. B., Clemens, S. C., and Leng, M. J.: Dipole patterns in tropical precipitation were pervasive across landmasses throughout Marine Isotope Stage 5, Communications Earth & Environment, 2, 64, https://doi.org/10.1038/s43247-021-00133-7, 2021.

Pandey, D. K., Clift, P. D., Kulhanek, D. K., and Expedition 355 Scientists: Arabian Sea Monsoon, Proceedings of the International Ocean Discovery Program, College Station TX, 355, https://doi.org/10.14379/iodp.proc.355.2016, 2016.

Pei, R., Kuhnt, W., Holbourn, A., Hingst, J., Koppe, M., Schultz, J., Kopetz, P., Zhang, P., and Andersen, N.:

Monitoring Australian Monsoon variability over the past four glacial cycles, Palaeogeogr. Palaeocl., 568, 110280, https://doi.org/10.1016/j.palaeo.2021.110280, 2021.

Peketi, A., Mazumdar, A., Pillutla, S. P. K., Sawant, B., and Gupta, H.: Climatic and Tectonic Control on the Bengal Fan Sedimentation Since the Pliocene, Geochem. Geophy. Geosy., 22, e2020GC009448, https://doi.org/10.1029/2020GC009448, 2021.

Prell, W. L. and Kutzbach, J. E.: Sensitivity of the Indian Monsoon to forcing parameters and implications for its evolution, Nature, 360, 647–652, https://doi.org/10.1038/360647a0, 1992.

Prell, W. L., Murray, D. W., Clemens, S. C., and Anderson, D. M.: Evolution and variability of the Indian Ocean Summer Monsoon: evidence from the western Arabian Sea drilling program, in: Synthesis of results from scientific drilling in the Indian Ocean, edited by: Duncan, R. A., Rea, D. K., Kidd, R. B., von Rad, U., and Weissel, J. K., Geophysical Monograph, American Geophysical Union, Washington, DC, 447–469, https://doi.org/10.1029/GM070p0447, 1992.

Qiang, X., An, Z., Song, Y., Chang, H., Sun, Y., Liu, W., Ao, H., Dong, J., Fu, C., Wu, F., Lu, F., Cai, Y., Zhou, W., Cao, J., Xu, X., and Ai, L.: New eolian red clay sequence on the western Chinese Loess Plateau linked to onset of Asian desertification about 25 Ma ago, Science China Earth Sciences, 54, 136–144, https://doi.org/10.1007/s11430-010-4126-5, 2011.

Quade, J., Cerling, T. E., and Bowman, J. R.: Development of Asian monsoon revealed by marked ecological shift during the latest Miocene in northern Pakistan, Nature, 342, 163–166, https://doi.org/10.1038/342163a0, 1989.

Ravelo, A. C., Lawrence, K. T., Fedorov, A., and Ford, H. L.: Comment on "A 12-million-year temperature history of the tropical Pacific Ocean", Science, 346, 1467, https://doi.org/10.1126/science.1257618, 2014.

Raymo, M. E. and Ruddiman, W. F.: Tectonic forcing of Late Cenozoic climate, Nature, 359, 117–122, https://doi.org/10.1038/359117a0, 1992.

Reichart, G. J., Lourens, L. J., and Zachariasse, W. J.: Temporal variability in the northern Arabian Sea oxygen minimum zone (OMZ) during the last 225 000 years, Paleoceanography, 13, 607–621, https://doi.org/10.1029/98PA02203, 1998.

Reilly, B. T., Bergmann, F., Weber, M. E., Stoner, J. S., Selkin, P., Meynadier, L., Schwenk, T., Spiess, V., and France-Lanord, C.: Middle to Late Pleistocene Evolution of the Bengal Fan: Integrating Core and Seismic Observations for Chronostratigraphic Modeling of the IODP Expedition 354 8° North Transect, Geochem. Geophy. Geosy., 21, e2019GC008878, https://doi.org/10.1029/2019GC008878, 2020.

Reolid, J., Betzler, C., and Lüdmann, T.: The record of Oligocene – Middle Miocene paleoenvironmental changes in a carbonate platform (IODP Exp. 359, Maldives, Indian Ocean), Mar. Geol., 412, 199–216, https://doi.org/10.1016/j.margeo.2019.03.011, 2019.

Reolid, J., Betzler, C., Braga, J. C., Lüdmann, T., Ling, A., and Eberli, G. P.: Facies and geometry of drowning steps in a Miocene carbonate platform (Maldives), Palaeogeogr. Palaeocl., 538, 109455, https://doi.org/10.1016/j.palaeo.2019.109455, 2020.

Robinson, M., Bartol, M., Bolton, C., Ding, X., Gariboldi, K., Romero, O., and Scientific Party: Biostratigraphic summary, in: Proceedings of the International Ocean Discovery Program edited by: Clemens, S. C., Kuhnt, W., and LeVay, L. J., International Ocean Discovery Program, College Station, Texas, https://doi.org/10.14379/iodp.proc.353.109.2016, 2016.

Rosenthal, Y., Holbourn, A. E., Kulhanek, D. K., and Expedition 363 Scientists: Western Pacific Warm Pool, International Ocean Discovery Program, College Station, TX, https://doi.org/10.14379/iodp.proc.363.2018, 2018.

Routledge, C. M., Kulhanek, D. K., Tauxe, L., Scardia, G., Singh, A. D., Steinke, S., Griffith, E. M., and Saraswat, R.: Revised geological timescale for IODP Sites U1456 and U1457, Geol. Mag., 157, 961–978, https://doi.org/10.1017/S0016756819000104, 2020.

Sarathchandraprasad, T., Tiwari, M., and Behera, P.: South Asian Summer Monsoon precipitation variability during late Pliocene: Role of Indonesian Throughflow, Palaeogeogr. Palaeocl., 574, 110447, https://doi.org/10.1016/j.palaeo.2021.110447, 2021.

Sarr, A.-C., Donnadieu, Y., Bolton, C. T., Ladant, J.-B., Licht, A., Fluteau, F., Laugié, M., Tardif, D., and Dupont-Nivet, G.: Neogene South Asian monsoon rainfall and wind histories diverged due to topographic effects, Nat. Geosci., 15, 314–319, https://doi.org/10.1038/s41561-022-00919-0, 2022.

Schwenk, T. and Spieß, V.: Architecture and stratigraphy of the Bengal Fan as response to tectonic and climate revealed from high-resolution seismic data, External Controls on Deep-Water Depositional Systems, Special Publication-SEPM (Society of Sedimentary Geologists), 92, 107–131, https://doi.org/10.2110/sepmsp.092.107, 2009.

Seki, A., Tada, R., Kurokawa, S., and Murayama, M.: High-resolution Quaternary record of marine organic carbon content in the hemipelagic sediments of the Japan Sea from bromine counts measured by XRF core scanner, Prog. Earth Planet. Sci., 6, 1, https://doi.org/10.1186/s40645-018-0244-z, 2019.

Shen, X., Wan, S., Colin, C., Tada, R., Shi, X., Pei, W., Tan, Y., Jiang, X., and Li, A.: Increased seasonality and aridity drove the C_4 plant expansion in Central Asia since the Miocene–Pliocene boundary, Earth Planet. Sci. Lett., 502, 74–83, https://doi.org/10.1016/j.epsl.2018.08.056, 2018.

Smith, R. A., Castañeda, I. S., Groeneveld, J., De Vleeschouwer, D., Henderiks, J., Christensen, B. A., Renema, W., Auer, G., Bogus, K., Gallagher, S. J., and Fulthorpe, C. S.: Plio-Pleistocene Indonesian Throughflow Variability Drove Eastern Indian Ocean Sea Surface Temperatures, Paleoceanography and Paleoclimatology, 35, e2020PA003872, https://doi.org/10.1029/2020PA003872, 2020.

Sorrel, P., Eymard, I., Leloup, P.-H., Maheo, G., Olivier, N., Sterb, M., Gourbet, L., Wang, G., Jing, W., Lu, H., Li, H., Yadong, X., Zhang, K., Cao, K., Chevalier, M.-L., and Replumaz, A.: Wet tropical climate in SE Tibet during the Late Eocene, Sci. Rep., 7, 7809, https://doi.org/10.1038/s41598-017-07766-9, 2017.

Sprintall, J., Gordon, A. L., Koch-Larrouy, A., Lee, T., Potemra, J. T., Pujiana, K., and Wijffels, S. E.: The Indonesian seas and their role in the coupled ocean–climate system, Nat. Geosci., 7, 487–492, https://doi.org/10.1038/ngeo2188, 2014.

Steinke, S., Groeneveld, J., Johnstone, H., and Rendle-Bühring, R.: East Asian summer monsoon weakening after 7.5 Ma: Evidence from combined planktonic foraminifera Mg / Ca and δ18O (ODP Site 1146; northern South China Sea), Palaeogeogr. Palaeocl., 289, 33–43, https://doi.org/10.1016/j.palaeo.2010.02.007, 2010.

Sun, X. and Wang, P.: How old is the Asian monsoon system? Palaeobotanical records from China, Palaeogeogr. Palaeocl., 222, 181–222, https://doi.org/10.1016/j.palaeo.2005.03.005, 2005.

Sun, Z., Jian, Z., Stock, J. M., Larsen, H. C., Klaus, A., Alvarez Zarikian, C. A., and Expedition 367/368 Scientists: South China Sea Rifted Margin, International Ocean Discovery Program, College Station, TX https://doi.org/10.14379/iodp.proc.367368.2018, 2018.

Suppiah, R.: The Australian summer monsoon: a review, Prog. Phys. Geog., 16, 283–318, https://doi.org/10.1177/030913339201600302, 1992.

Suzuki, K., Yamamoto, M., and Seki, O.: Late Miocene changes in C_3, C_4 and aquatic plant vegetation in the Indus River basin: evidence from leaf wax δ13C from Indus Fan sediments, Geol. Mag., 157, 979–988, https://doi.org/10.1017/S0016756819001109, 2020.

Tada, R. and Murray, R. W.: Preface for the article collection "Land–Ocean Linkages under the Influence of the Asian Monsoon", Prog. Earth Planet. Sci., 3, 24, https://doi.org/10.1186/s40645-016-0100-y, 2016.

Tada, R., Irino, T., and Koizumi, I.: Land-ocean linkages over orbital and millennial timescales recorded in late Quaternary sediments of the Japan Sea, Paleoceanography, 14, 236–247, 1999.

Tada, R., Murray, R. W., Alvarez Zarikian, C. A., and Expedition 346 Scientists: Asian Monsoon: onset and evolution of millennial-scale variability of Asian Monsoon and its possible relation with Himalaya and Tibetan plateau, Integrated Ocean Drilling Program, College Station, TX, https://doi.org/10.2204/iodp.proc.346.2015, 2015.

Tada, R., Zheng, H., and Clift, P. D.: Evolution and variability of the Asian monsoon and its potential linkage with uplift of the Himalaya and Tibetan Plateau, Prog. Earth Planet. Sci., 3, 1–26, https://doi.org/10.1186/s40645-016-0080-y, 2016.

Tada, R., Irino, T., Ikehara, K., Karasuda, A., Sugisaki, S., Xuan, C., Sagawa, T., Itaki, T., Kubota, Y., Lu, S., Seki, A., Murray, R. W., Alvarez-Zarikian, C., Anderson, W. T., Bassetti, M.-A., Brace, B. J., Clemens, S. C., da Costa Gurgel, M. H., Dickens, G. R., Dunlea, A. G., Gallagher, S. J., Giosan, L., Henderson, A. C. G., Holbourn, A. E., Kinsley, C. W., Lee, G. S., Lee, K. E., Lofi, J., Lopes, C. I. C. D., Saavedra-Pellitero, M., Peterson, L. C., Singh, R. K., Toucanne, S., Wan, S., Zheng, H., and Ziegler, M.: High-resolution and high-precision correlation of dark and light layers in the Quaternary hemipelagic sediments of the Japan Sea recovered during IODP Expedition 346, Prog. Earth Planet. Sci., 5, 19, https://doi.org/10.1186/s40645-018-0167-8, 2018.

Tagliaro, G., Fulthorpe, C. S., Gallagher, S. J., McHugh, C. M., Kominz, M., and Lavier, L. L.: Neogene siliciclastic deposition and climate variability on a carbonate margin: Australian Northwest Shelf, Mar. Geol., 403, 285–300, https://doi.org/10.1016/j.margeo.2018.06.007, 2018.

Thiry, M.: Palaeoclimatic interpretation of clay minerals in marine deposits; an outlook from the continental origin, Earth-Sci. Rev., 49, 201–221, https://doi.org/10.1016/S0012-8252(99)00054-9, 2000.

Torfstein, A. and Steinberg, J.: The Oligo–Miocene closure of the Tethys Ocean and evolution of the proto-Mediterranean Sea, Sci. Rep., 10, 13817, https://doi.org/10.1038/s41598-020-70652-4, 2020.

Tripathi, S., Tiwari, M., Lee, J., Khim, B.-K., and IODP Expedition 355 Scientists: First evidence of denitrification visà-vis monsoon in the Arabian Sea since Late Miocene, Sci. Rep., 7, 43056, https://doi.org/10.1038/srep43056, 2017.

Vail, P. R., Mitchum, R. M., Todd, R. G., Widmier, J. M., Thompson, S. I., Sangree, J. B., Bubb, J. N., and Hatlelid, W. G.: Seismic stratigraphy and global changes of sea-level, in: Seismic Stratigraphy–Applications to Hydrocarbon Exploration, edited by: Payton, C. E., Memoir, American Association of Petroleum Geologists, Tulsa, OK, 49–212, https://doi.org/10.1306/M26490C3, 1977.

van Ufford, A. Q. and Cloos, M.: Cenozoic tectonics of New Guinea, AAPG Bull., 89, 119–140, https://doi.org/10.1306/08300403073, 2005.

Vögeli, N., Najman, Y., van der Beek, P., Huyghe, P., Wynn, P. M., Govin, G., Veen, I. v. d., and Sachse, D.: Lateral variations in vegetation in the Himalaya since the Miocene and implications for climate evolution, Earth Planet. Sci. Lett., 471, 1–9, https://doi.org/10.1016/j.epsl.2017.04.037, 2017.

Wan, S., Li, A., Clift, P. D., and Stuut, J.-B. W.: Development of the East Asian monsoon: Mineralogical and sedimentologic records in the northern South China Sea since 20 Ma, Palaeogeogr. Palaeocl., 254, 561–582, https://doi.org/10.1016/j.palaeo.2007.07.009, 2007.

Wan, S., Clift, P. D., Li, A., Li, T., and Yin, X.: Geochemical records in the South China Sea: implications for East Asian summer monsoon evolution over the last 20 Ma, in: Monsoon Evolution and Tectonics–Climate Linkage in Asia, edited by: Clift, P. D., Tada, R., and Zheng, H., Special Publication, Geological Society, London, 245–263, https://doi.org/10.1144/SP342.14, 2010.

Wang, B. (Ed.): The Asian Monsoon, Springer-Verlag, Berlin, 795 pp., https://doi.org/10.1007/3-540-37722-0, 2006.

Wang, B., Liu, J., Kim, H.-J., Webster, P. J., Yim, S.-Y., and Xiang, B.: Northern Hemisphere summer monsoon intensified by mega-El Niino/southern oscillation and Atlantic multidecadal oscillation, P. Natl. Acad. Sci. USA, 110, 5347–5352, https://doi.org/10.1073/pnas.1219405110, 2013.

Wang, H. and Mehta, V. M.: Decadal variability of the Indo-Pacific warm pool and its association with atmospheric and oceanic variability in the NCEP-NCAR and SODA reanalyses, J. Climate, 21, 5545–5565, 2008.

Wang, P.: Cenozoic deformation and the history of sealand interactions in Asia, in: Continent-Ocean Interactions in the East Asian Marginal Seas, edited by: Clift, P., Wang, P., Kuhnt, W., and Hayes, D., American Geophysical Union, Washington, DC, 1–22, https://doi.org/10.1029/149GM01, 2004.

Wang, P., Prell, W. L., Blum, P., Arnold, E. M., Buehring, C. J., Chen, M.-P., Clemens, S. C., Clift, P. D., Colin, C. J. G., Farrell, J. W., Higginson, M. J., Jian, Z., Kuhnt, W., Laj, C. E., Lauer-Leredde, C., Leventhal, J. S., Li, A., Li, Q., Lin, J., McIntyre, K., Miranda, C. R., Nathan, S. A., Shyu, J.-P., Solheid, P. A., Su, X., Tamburini, F., Trentesaux, A., Wang, L., Wang, P., Prell, W. L., Blum, P., Arnold, E. M., Buehring, C. J., Chen, M.-P., Clemens, S. C., Clift, P. D., Colin, C. J. G., Farrell, J. W., Higginson, M. J., Jian, Z., Kuhunt, W., Laj, C. E., Lauer-Leredde, C., Leventhal, J. S., Li, A., Li, Q., Lin, J., McIntyre, K., Miranda, C. R., Nathan, S. A., Shyu, J.-P., Solheid, P. A., Su, X., Tamburini, F., Trentesaux, A., and Wang, L.: Leg 184, Ocean Drilling Program, College

Station, TX, Proc. Ocean Drill. Prog., Pt A: Init. Rpt., 184, 1–77, https://doi.org/10.2973/odp.proc.ir.184.2000, 2000.

Wang, W., Zhang, P., Garzione, C. N., Liu, C., Zhang, Z., Pang, J., Wang, Y., Zheng, D., Zheng, W., and Zhang, H.: Pulsed rise and growth of the Tibetan Plateau to its northern margin since ca. 30 Ma, P. Natl. Acad. Sci. USA, 119, e2120364119, https://doi.org/10.1073/pnas.2120364119, 2022.

Weber, M. E., Lantzsch, H., Dekens, P., Das, S. K., Reilly, B. T., Martos, Y. M., Meyer-Jacob, C., Agrahari, S., Ekblad, A., Titschack, J., Holmes, B., and Wolfgramm, P.: 200 000 years of monsoonal history recorded on the lower Bengal Fan - strong response to insolation forcing, Glob. Planet. Change, 166, 107–119, https://doi.org/10.1016/j.gloplacha.2018.04.003, 2018.

Webster, P. J., Magaña, V. O., Palmer, T. N., Shukla, J., Tomas, R. A., Yanai, M., and Yasunari, T.: Monsoons: Processes, predictability, and the prospects for prediction, J. Geophys. Res., 103, 14451–14510, https://doi.org/10.1029/97JC02719, 1998.

Wei, G., Li, X.-H., Liu, Y., Shao, L., and Liang, X.: Geochemical record of chemical weathering and monsoon climate change since the early Miocene in the South China Sea, Paleoceanography, 21, PA4214, https://doi.org/10.1029/2006PA001300, 2006.

Westerhold, T., Marwan, N., Drury, A. J., Liebrand, D., Agnini, C., Anagnostou, E., Barnet, J. S. K., Bohaty, S. M., De Vleeschouwer, D., Florindo, F., Frederichs, T., Hodell, D. A., Holbourn, A. E., Kroon, D., Lauretano, V., Littler, K., Lourens, L. J., Lyle, M., Pälike, H., Röhl, U., Tian, J., Wilkens, R. H., Wilson, P. A., and Zachos, J. C.: An astronomically dated record of Earth's climate and its predictability over the last 66 million years, Science, 369, 1383–1387, https://doi.org/10.1126/science.aba6853, 2020.

Whipple, K. X.: The influence of climate on the tectonic evolution of mountain belts, Nat. Geosci., 2, 1–8, https://doi.org/10.1038/ngeo413, 2009.

Yan, Y. Y.: Intertropical Convergence Zone (ITCZ), in: Encyclopedia of World Climatology, edited by: Oliver, J. E., Springer Netherlands, Dordrecht, 429–432, https://doi.org/10.1007/1-4020-3266-8_110, 2005.

Yang, C., Dang, H., Zhou, X., Zhang, H., Wang, X., Wang, Y., Qiao, P., Jiang, X., and Jian, Z.: Upper ocean hydrographic changes in response to the evolution of the East Asian monsoon in the northern South China Sea during the middle to late Miocene, Glob. Planet. Change, 201, 103478, https://doi.org/10.1016/j.gloplacha.2021.103478, 2021.

Yang, X., Groeneveld, J., Jian, Z., Steinke, S., and Giosan, L.: Middle Miocene Intensification of South Asian Monsoonal Rainfall, Paleoceanography and Paleoclimatology, 35, e2020PA003853, https://doi.org/10.1029/2020PA003853, 2020.

Yoshida, K., Nakajima, T., Matsumoto, Y., Osaki, A., Rai, L. K., Cruz, J. W., and Sakai, H.: Miocene provenance change in Himalayan foreland basin and Bengal Fan sediments, with special reference to detrital garnet chemistry, Island Arc, 30, e12408, https://doi.org/10.1111/iar.12408, 2021.

Zachos, J. C., Dickens, G. R., and Zeebe, R. E.: An early Cenozoic perspective on greenhouse warming and carbon-cycle dynamics, Nature, 451, 279–283, https://doi.org/10.1038/nature06588, 2008.

Zhang, P., Xu, J., Holbourn, A., Kuhnt, W., Beil, S., Li, T., Xiong, Z., Dang, H., Yan, H., Pei, R., Ran, Y., and Wu, H.: Indo-Pacific Hydroclimate in Response to Changes of the Intertropical Convergence Zone: Discrepancy on Precession and Obliquity Bands Over the Last 410 kyr, J. Geophys. Res.-Atmos., 125, e2019JD032125, https://doi.org/10.1029/2019JD032125, 2020.

Zhang, R., Jiang, D., Zhang, Z., and Zhang, C.: Effects of Tibetan Plateau Growth, Paratethys Sea Retreat and Global Cooling on the East Asian Climate by the Early Miocene, Geochem. Geophy. Geosy., 22, e2021GC009655, https://doi.org/10.1029/2021GC009655, 2021.

Zhang, Y. G., Pagani, M., and Liu, Z.: Response to Comment on "A 12-million-year temperature history of the tropical Pacific Ocean", Science, 346, 1467, https://doi.org/10.1126/science.1257930, 2014a.

Zhang, Y. G., Pagani, M., and Liu, Z.: A 12-Million-Year Temperature History of the Tropical Pacific Ocean, Science, 344, 84–87, https://doi.org/10.1126/science.1246172, 2014b.

Zhao, H., Qiang, X., Xu, X., and Sun, Y.: Iron oxide characteristics of the Chinese loess-red clay sequences and their implications for the evolution of the East Asian summer monsoon since the Late Oligocene, Palaeogeogr. Palaeocl., 543, 109604, https://doi.org/10.1016/j.palaeo.2020.109604, 2020.

Zheng, H., Wei, X., Tada, R., Clift, P. D., Wang, B., Jourdan, F., Wang, P., and He, M.: Late Oligocene–early Miocene birth of the Taklimakan Desert, P. Natl. Acad. Sci. USA, 112, 7662–7667, https://doi.org/10.1073/pnas.1424487112, 2015.

Zhou, P., Ireland, T., Murray, R. W., and Clift, P. D.: Marine Sedimentary Records of Chemical Weathering Evolution in the Western Himalaya since 17 Ma, Geosphere, 17, 824–853, https://doi.org/10.1130/GES02211.1, 2021.

Sci. Dril., 31, 31–49, 2022
https://doi.org/10.5194/sd-31-31-2022

Scientific Drilling
Open Access

ICDP drilling of the Eger Rift observatory: magmatic fluids driving the earthquake swarms and deep biosphere

Tomáš Fischer[1], Pavla Hrubcová[2], Torsten Dahm[3], Heiko Woith[3], Tomáš Vylita[1], Matthias Ohrnberger[4], Josef Vlček[1], Josef Horálek[2], Petr Dědeček[2], Martin Zimmer[3], Martin P. Lipus[3], Simona Pierdominici[3], Jens Kallmeyer[3], Frank Krüger[4], Katrin Hannemann[5], Michael Korn[6], Horst Kämpf[3], Thomas Reinsch[3,7], Jakub Klicpera[2], Daniel Vollmer[4], and Kyriaki Daskalopoulou[3,4]

[1]Faculty of Science, Charles University, 128 43 Prague, Czech Republic
[2]Institute of Geophysics, Czech Academy of Sciences, 141 31 Prague, Czech Republic
[3]GFZ German Research Centre for Geosciences, Telegrafenberg, 14473 Potsdam, Germany
[4]Institute of Earth and Environmental Sciences, University of Potsdam, Golm Campus, 14476 Potsdam, Germany
[5]Institut für Geophysik, Westfälische Wilhelms-Universität Münster, 48149 Münster, Germany
[6]Institut für Geophysik und Geologie, Universität Leipzig, 04103 Leipzig, Germany
[7]Fraunhofer IEG, Fraunhofer Research Institution for Energy Infrastructures and Geothermal Systems IEG, 44801 Bochum, Germany

Correspondence: Pavla Hrubcová (pavla@ig.cas.cz)

Received: 11 March 2022 – Revised: 6 May 2022 – Accepted: 9 May 2022 – Published: 28 October 2022

Abstract. The new in situ geodynamic laboratory established in the framework of the ICDP Eger project aims to develop the most modern, comprehensive, multiparameter laboratory at depth for studying earthquake swarms, crustal fluid flow, mantle-derived CO_2 and helium degassing, and processes of the deep biosphere. In order to reach a new level of high-frequency, near-source and multiparameter observation of earthquake swarms and related phenomena, such a laboratory comprises a set of shallow boreholes with high-frequency 3-D seismic arrays as well as modern continuous real-time fluid monitoring at depth and the study of the deep biosphere.

This laboratory is located in the western part of the Eger Rift at the border of the Czech Republic and Germany (in the West Bohemia–Vogtland geodynamic region) and comprises a set of five boreholes around the seismoactive zone. To date, all monitoring boreholes have been drilled. This includes the seismic monitoring boreholes S1, S2 and S3 in the crystalline units north and east of the major Nový Kostel seismogenic zone, borehole F3 in the Hartoušov mofette field and borehole S4 in the newly discovered Bažina maar near Libá. Supplementary borehole P1 is being prepared in the Neualbenreuth maar for paleoclimate and biological research. At each of these sites, a borehole broadband seismometer will be installed, and sites S1, S2 and S3 will also host a 3-D seismic array composed of a vertical geophone chain and surface seismic array. Seismic instrumenting has been completed in the S1 borehole and is in preparation in the remaining four monitoring boreholes. The continuous fluid monitoring site of Hartoušov includes three boreholes, F1, F2 and F3, and a pilot monitoring phase is underway. The laboratory also enables one to analyze microbial activity at CO_2 mofettes and maar structures in the context of changes in habitats. The drillings into the maar volcanoes contribute to a better understanding of the Quaternary paleoclimate and volcanic activity.

Published by Copernicus Publications on behalf of the IODP and the ICDP.

1 Main goals, overview processes and settings

What are the physical and chemical processes leading to earthquake activity and fluid mobility? What are the pathways of fluids through the crust and how are they influenced by tectonic stress variations? How can geological processes influence the deep biosphere and the evolution of early life at depth? These are the open questions tackled by the ICDP project aimed at drilling in the Eger Rift region.

The western Eger Rift, cutting the Bohemian Massif in the westernmost part of the Czech Republic and the adjacent area in Germany, represents the West Bohemia–Vogtland region, which is one of the most unique European intracontinental geodynamic areas (Fig. 1). The geodynamic activity is represented by active magmatic underplating, mid-crustal earthquake swarms and massive diffuse degassing of mantle-derived CO_2 (e.g., Bräuer et al., 2003; Horálek and Fischer, 2008). The region is also characterized by numerous mineral springs, mofettes, Tertiary–Quaternary volcanism, and neotectonic crustal movements located at the intersection of major intraplate fault and tectonic zones around the Cheb Basin. The close proximity and intensity of the different geodynamic processes in an intracontinental massif far from plate boundaries are outstanding, and it is likely that all of these phenomena are related to a common driver in the lithospheric upper mantle. Currently, it is well accepted that many earthquake swarms are driven by fluids in the crust. Nowadays, fluid migration and its control by tectonics are recognized in many regions worldwide under different tectonic and volcanic settings. The ICDP Eger Rift project provides extraordinary observations that help to unravel the relations between magmatic underplating, trans-crustal CO_2 flux, earthquake swarms and their relation to volcanism and microbiology.

The evolution of the Eger Rift, a 300 km long, 50 km wide, ENE–WSW-trending zone and an active element of the European Cenozoic Rift System (Prodehl et al., 1995), is connected with the post-orogenic extension and the alkaline magmatic activity during the Cenozoic. The Cheb Basin developed at its southwestern end and dips to ∼ 300 m depth towards the east, where it is delimited by the escarpment of the Mariánské Lázně Fault. The basement of the Cheb Basin and its surroundings include the crystalline schists of the Saxothuringian unit and the granitoids of the Smrčiny Pluton, whereas the sedimentary fill of the Cheb Basin consists of Paleogene to Quaternary sediments (Kvaček and Teodoridis, 2007). Quaternary intraplate alkaline volcanism is documented at the western flank of the Cheb Basin in small volcanoes dated to 0.78–0.12 Ma (Mrlina et al., 2007; Wagner et al., 2002), whereas the CO_2-dominated hydrothermal activity is dated to 0.23–0 Ma (Vylita et al., 2007). They comprise two Quaternary scoria cones (Železná hůrka/Eisenbühl and Komorní hůrka/Kammerbühl) and two volcanic maars (Mýtina and Neualbenreuth), where the eruptions are associated with phreatomagmatic and phreato-Strombolian activity (Geissler et al., 2005; Mrlina et al., 2009; Flechsig et al., 2015; Rohrmüller et al., 2017; Lied et al., 2020). The crustal structure of the area is complex with a wide zone of increased reflectivity at the crust–mantle transition (e.g., Tomek et al., 1997; Hrubcová et al., 2005, 2013; Hrubcová and Geissler, 2009). These lower crustal features may be interpreted as low-angle shear zones partly filled with fluids and/or small magmatic intrusions or partial melting as confirmed by mantle xenoliths (Geissler et al., 2005). In the upper crust, very distinct and highly reflective features ("bright spots") were identified (Klemt, 2013; Schimschal, 2013; Mullick et al., 2015; Hrubcová et al., 2016), which can be related to the spatial–temporal behavior of seismic swarm activity and its fluid-driven origin.

The seismicity in the area is characterized by earthquake swarms, intensive long-lasting and low-magnitude seismicity, which contrasts with more typical mainshock–aftershock sequences. Such seismicity can be felt by the population and sometimes causes damage to buildings. It has been recognized in different areas worldwide, such as volcanic and geothermal fields (e.g., Dahm and Brandsdottir, 1997; Wyss et al., 1997; Lees, 1998; Dreger et al., 2000) and at the margins of tectonic plates (e.g., Einarsson, 1991), and can occur as a precursor to larger earthquakes, such as during the recent L'Aquila 2009 earthquake in Italy. However, the controlling processes and possible consequences of this kind of seismicity are still not fully disclosed.

In the western Eger Rift, the highest concentration of earthquake activity and CO_2 degassing occurs in the area of the Cheb Basin, at the intersection of major tectonic lines with four Quaternary volcanoes. The ENE–WSW-trending Eger Graben and the N–S-trending earthquake zone between Vogtland and Leipzig (Grünthal et al., 2019), the Cheb–Domažlice Graben, and the morphologically expressed Mariánské Lázně Fault intersect at one location close to the main seismically active Nový Kostel (NK) zone (Fig. 1). It seems that the earthquake activity is related to the reactivation of a complex system of faults and tectonic zones, triggered by the ascent of magmatic fluids caused by ongoing magmatic process (Fischer et al., 2014; Bräuer et al., 2014) in which fluid channels to depth (CO_2 conduits) play an important role (Kämpf et al., 2019). However, the understanding of magmatic activity, fluid ascent and earthquake-stimulating processes as well as their interconnections are not clear.

Fluid degassing of CO_2 in the Cheb Basin and surrounding areas is in the form of wet and dry mofettes and mineral springs. High portions of mantle-derived helium and CO_2 indicate a magmatic origin and fluid transport from the depleted lithospheric mantle (Weinlich et al., 1999; Bräuer et al., 2009), possibly related to active magmatic underplating (Hrubcová et al., 2017). On their way to the surface, fluids penetrate through faults, interact with the medium and are related to earthquake activity (Kämpf et al., 2013, 2019; Nickschick et al., 2015, 2019; Fischer et al., 2017; Liu et al., 2020). Subsurface life, protected from the intense radiation in the atmosphere, represents an ambience of the Earth's early

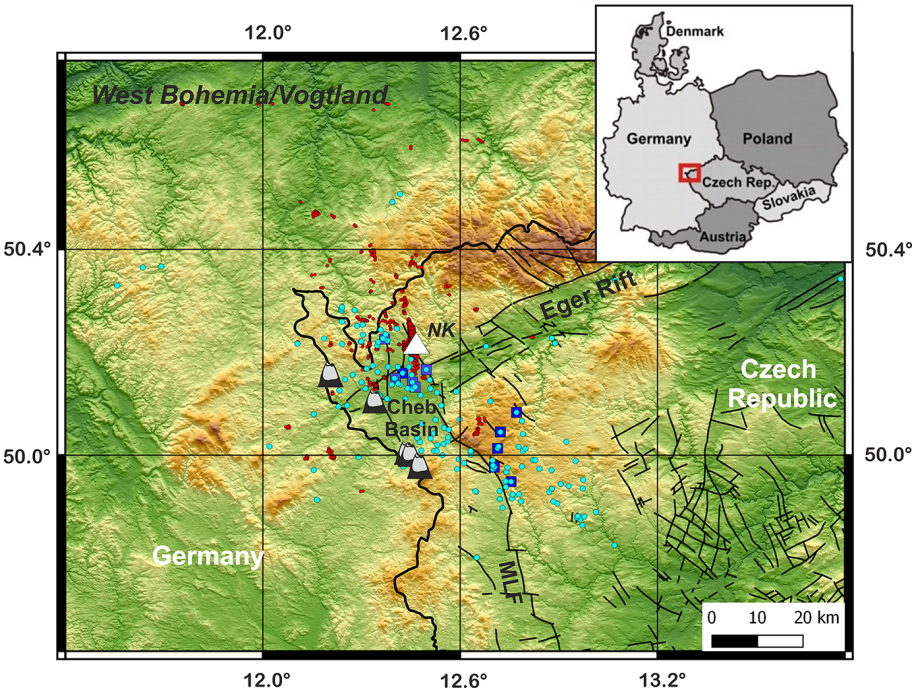

Figure 1. The West Bohemia–Vogtland geodynamic region in the westernmost part of the Eger Rift: the epicenters of earthquakes from 1991 to 2021 are marked by red circles; cyan circles represent CO_2 degassing; blue squares represent mofettes; the white triangle marks the Nový Kostel (NK) focal zone; the positions of five Quaternary volcanoes are indicated.

biotopes; on the other hand, the microbial ecosystems abundant in the subsurface react to changes in the composition of fluids or to their long-term exposure.

Because of these phenomena (and their concentration in a rather small region), the West Bohemia–Vogtland (the western Eger Rift) area is a unique site worldwide and offers an ideal possibility for interdisciplinary study. The earthquake swarms and long-term degassing of mineral-rich waters and gases in granitic and sedimentary layers makes this area perfectly suited to study the fluid composition and fluid-induced source processes along with the effect of CO_2 on the deep biosphere and the development of early life at depth. Long-term monitoring of the smallest signals and trend changes is essential to understand these phenomena and their interactions. This points to establishing a new level of multidisciplinary investigation. A modern, comprehensive, high-resolution observatory at depth with unique multiparameter observation can interconnect fields of primary research; advance the interactions among earthquakes, fluids, rocks and the biosphere; and contribute to answering related questions.

2 Current state, scientific aims and experimental approach

The seismicity in West Bohemia–Vogtland, also documented in macroseismic observations, occurs in the form of earthquake swarms, with the largest local magnitudes not exceeding M_L 5 (e.g., 1875 or 1908). The largest instrumentally recorded earthquake occurred in the 1985–1986 swarm and reached a magnitude of M_L 4.6 (Vavryčuk, 1993). Since 1985, seismicity has been concentrated in the Nový Kostel (NK) focal zone, where more than 80 % of seismic energy has been released within the last 30 years (Fischer and Michálek, 2008). The seismicity is generally shallow, with the event hypocenters occurring in the upper and middle crust, mainly between 5 and 15 km (Horálek and Fischer, 2008). Since 1997, the seismicity cluster beneath NK has been slowly but steadily growing, laterally more to the north and upwards, along a nearly planar structure (see Fig. 2).

The surface earthquake recordings are of excellent quality (e.g., Fischer et al., 2014); however, they suffer from high-frequency wave damping by the near-surface weathered layers and site scattering, resulting in a smoothing of the wave signal details. A monitoring depth of a few hundred meters will avoid high-frequency attenuation and significantly improve the possibility of studying low-magnitude earthquakes in the crust and of resolving small-scale heterogeneities. This offers the possibility of analyzing the fluid-induced source processes and the anatomy of earthquake swarms and their migration in unprecedented detail. The fact that earthquake swarms in the Eger Rift region occur regularly and persistently in known spots of activity with known radiation patterns offers the opportunity to design and tune a borehole-based monitoring network for optimized analysis.

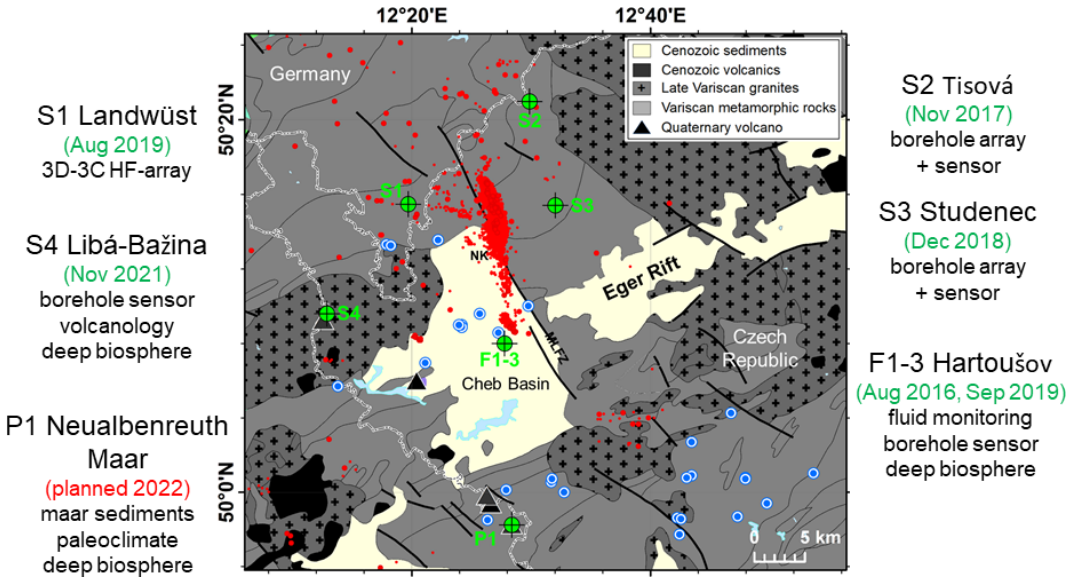

Figure 2. The drilling sites and their prime scientific targets: S1 – Landwüst, S2 – Tisová, S3 – Studenec (seismological monitoring), S4 – Libá (seismological monitoring, volcanology and the deep biosphere in volcanic maar crater), F1–3 – Hartoušov (fluid, earthquake and deep-biosphere monitoring) and P1 (a planned borehole for paleoclimate and biosphere investigation). The time of realization is indicated in parentheses. Red circles represent the seismicity of the main Nový Kostel (NK) focal zone; blue circles represent mofettes and mineral springs with a gas discharge of more than 1 L min^{-1}; Quaternary volcanoes are indicated by black triangles.

Systematic fluid probing and analyses at springs and mofettes in the western Eger Rift region have been performed for decades (Weise et al., 2001; Bräuer et al., 2003, 2005a, b, 2008, 2014; Schuessler et al., 2016). The results of the fluid isotope systematic monitoring have been capable of detecting trend changes in $^3He / ^4He$, which may indicate silent magmatic intrusions in the lower crust and upper mantle (e.g., Bräuer et al., 2009; Kämpf et al., 2013). However, the data obtained have not been sufficient to reach the objectives. The well-studied sites of massive CO_2 degassing in mofettes offer the possibility of building a new generation of continuous real-time fluid monitoring systems at different depth levels. Such monitoring can separate the effects of surface and deep processes related to the composition and rate of fluids. It can also demonstrate the correlations between isotope composition and seismic activity (e.g., Bräuer et al., 2003, 2008, 2014) or reveal the link between an earthquake swarm and microbial activities (e.g., Bräuer et al., 2008).

Microbiological studies show the existence of diverse and active microbial ecosystems in the deep subsurface (e.g., Parkes et al., 1994, 2000; Lehman, 2007). This is a vast ambience, as between 75 % and 94 % of all microbes on the Earth occur in deeply buried marine and terrestrial sediments (Kallmeyer et al., 2012). Moreover, the deep subsurface harbors a huge carbon reservoir, equivalent to that of all plants on the Earth; thus, deeply buried microbial communities are very important for driving carbon and nutrient cycling as well as catalyzing a multitude of reactions among sediments, rocks and fluids. The Eger Rift area hosts a diverse lithology of surficial sediments overlying crystalline rocks as well as active CO_2 degassing and high flow rates of mineral-rich fluids and gases (e.g., methane). The first studies of its mineral water and fluids (Alawi et al., 2015; Schuessler et al., 2016; Krauze et al., 2017; Liu et al., 2018, 2020) have indicated that the active fault systems of the Eger Rift area can be classified as a "hot spot" for microbial subsurface life. Microbial ecosystems abundant in the subsurface may react to changes in the composition of fluids. Thus, the long-term degassing of mineral-rich waters and gases in granitic and sedimentary layers makes this area ideally suited to study the effect of CO_2 on the deep biosphere and the development of life at depth (Bussert et al., 2017). The maar-diatreme volcanos, as paleoconduit structures, are considered to be important pathways of magmatic fluids to study past activities under conditions in which the first biological molecules and later the first life forms originated (Schreiber et al., 2012). Thus, the Eger Rift area provides an environment for geo-microbiological studies and studies on the origin of deep life.

Such goals can be fulfilled by the development of a modern, comprehensive laboratory at depth to study the interconnected areas of primary research. Specifically, such a laboratory comprises the novel concept of 3-D seismic arrays with a set of shallow boreholes in order to reach a new level of high-frequency, near-source and multiparameter observation of earthquake swarms, real-time fluid monitoring at different depths and related phenomena. Such a network brings a new high detection capability, which improves the earthquake and fluid recordings. This offers the possibility

to study extremely low-magnitude earthquakes and analyze the fluid-induced source processes. Repeated fluid probing at the surface can be complemented by a new generation of continuous real-time fluid monitoring in a safe and logistically accessible area. The variability in the local geological site conditions can meet the interdisciplinary targets for volcanologic, microbiological and paleoclimate research.

This initiative was introduced and discussed by Dahm et al. (2013) during the second ICDP Eger Rift workshop, resulting in a conceptual drilling approach to address the key scientific questions related to these processes. It was discussed among approximately 50 scientists from Germany, the Czech Republic, the USA, the UK and Poland; from these scientists, three scientific groups were identified based on their interests: (i) a seismological group, (ii) a fluid group, and (iii) a group interested in volcanology/petrology, paleoclimate and microbiology. Although each group is responsible for its field, together they comprise the unique interdisciplinary laboratory with a potential to better understand the following:

- fluid–rock interactions and the mechanism of fluid-induced earthquake swarms,
- the structure of fluid pathways from the upper mantle to the surface,
- physical, chemical, and biological interrelations between geological processes, mantle-derived fluids and the biosphere down to 400 m depth,
- the "fault-valve" mechanism and its relevance for earthquake triggering, seismic hazard, degassing and the activity of the deep biosphere,
- the impact of CO_2-rich mantle-derived fluids on the geo–bio interaction in the western Eger Rift,
- the Quaternary paleoclimate and volcanic activity in the western Eger Rift region.

3 Description of drillings, monitoring and scientific concepts

The in situ Eger comprehensive laboratory is currently being established by the International Continental Scientific Drilling Program (ICDP) in the framework of the interdisciplinary project "Drilling the Eger Rift: Magmatic Fluids Driving the Earthquake Swarms and the Deep Biosphere (EGER)". Specifically, this laboratory at depth comprises a set of five new, distributed, shallow (less than 500 m deep) boreholes (Fig. 2). The drilling sites were selected to be distributed around the Nový Kostel (NK) focal zone; geophysical and geological surveys contributed to the selection of the exact locations. The drill holes are denoted S1–S4 (seismological monitoring) and F1–F3 (fluid monitoring), indicating the primary field of interest of each well (Fig. 2). The planned drill hole P1 will be the main record for paleoclimate studies.

The drillings S1–S4 are designed for seismological monitoring in order to reach a new level of high-frequency, near-source observations of earthquake swarms and related phenomena, like seismic noise and tremors generated by fluid movements. The drilling of S1 (Landwüst, depth 402 m), which is the only drill hole located in German territory, was completed in August 2019 and is supplemented by a 3-D high-frequency seismic array. The S2 site (Tisová, depth 460 m) was finished in November 2017, and the S3 site (Studenec, depth 408 m) was completed in December 2018; both S2 and S3 are planned with borehole seismic arrays. The drilling of S4 (Libá, depth 400 m) was accomplished in December 2021 in the recently discovered maar crater near the Czech–German border and will be equipped with a borehole seismometer.

The drill holes F1–F3 are primary designed for fluid monitoring in the framework of a multilevel gas monitoring system built in the Hartoušov mofette field. This mofette represents a gas emission site where CO_2 ascends through crustal-scale conduits from as deep as the upper mantle; thus, the site can provide a natural window into ongoing magmatic processes at the mantle depth level. It is located at the crossing of the Eger Rift with the Počátky–Plesná zone (PPZ) tectonic lineament, which is the fault possibly related to the main Nový Kostel focal zone (Fig. 1). In particular, two existing monitoring wells, F1 and F2 (Bussert et al., 2017; Fischer et al., 2020), were complemented by the F3 drill hole; these three adjacent boreholes, F1 (30 m), F2 (70 m) and F3 (230 m), provide continuous monitoring of fluids at high sampling rates to acquire fluid parameters (gas flow, water temperature and water level/pressure) as well as chemical (CO_2, Ar, N_2, O_2, He, H_2 and CH_4) and isotopic ($\delta^{13}C_{CO_2}$, $\delta^{18}O_{CO_2}$ and ^{222}Rn) gas content (Woith et al., 2020). Additionally, samples for laboratory analysis of He, Ne and Ar isotopes are taken repeatedly (roughly every 2 months), as theses isotopes are useful tracers for constraining the fluid origins and mixing ratios of mantle components. Moreover, the fluid monitoring at different depths separates the effects of surface and deep processes related to the composition and ascent rate of fluids. The drill site is also prepared for seismological monitoring to complement the monitoring network.

All boreholes were cored; the coring in Tertiary–Quaternary sedimentary sequences (S4, F2 and F3) is utilized for paleoclimate research and microbiological investigation (Bussert et al., 2017). The coring of solid rocks outcropping at the surface (S1 and S3, phyllites) is utilized for structural and tectonic investigation. Moreover, the core of drill hole S4, located in the maar crater, also targets volcanology and the evaluation of the neotectonic evolution of the maar. The final supplementary borehole, P1 ($\sim$ 150 m), in another maar volcano near Neualbenreuth, Germany, at the Czech–German border is planned to support paleoclimate research and is scheduled for early 2023.

4 Drilling and specific characteristics of individual drill holes

4.1 Pre-drilling site surveys

Several geophysical experiments were conducted to map deeper and shallow crustal structure. From reflection and seismic source data, distinct and highly reflective features (bright spots) were found in the upper crust close to the main NK focal zone (Mullick et al., 2015; Hrubcová et al., 2016). Local earthquake tomography showed clear indications of a mid-crustal intrusive body beneath the NK focal zone from increased P-wave / S-wave (V_p / V_s) ratios (Alexandrakis et al., 2014; Mousavi et al., 2015). Magnetotelluric investigations found highly conductive channel-like structures above the focal zone (Muñoz et al., 2018) that were complemented by highly attenuating bodies beneath and north of NK to 11 km depth (Mousavi et al., 2017). All of these features point to fluid pathways and interconnections between seismicity and fluid degassing.

The exact positions of the drill holes were investigated by local geophysical surveying to control the quality of waveforms, the signal-to-noise ratio (SNR), and to provide structural and geological constraints for fluid pathways and their movements. This comprised electric resistivity tomography and high-resolution reflection and refraction seismic surveying along the resistivity profile, as well as seismic noise measurements (Umlauft and Korn, 2019) at the Hartoušov site, both completed in late 2017 (Nickschick et al., 2019).

4.2 Drilling and coring

The drill sites are located in a natural mineral spring and spa resource protection zone and required specific permissions to meet the strict governmental requirements prior to the commencement of work. Drilling works were performed by the German drilling company Pruy KG with the HD110 drilling rig (the S1 site and the pre-drill of F3) and the Czech drilling company Geoněmec – vrty, s.r.o. with the Christensen 140C drilling rig (sites S2–S4). The drilling of F3 was conducted within the Swedish national research infrastructure for scientific drilling (Riksriggen) at Lund University, Sweden, with the Atlas Copco CT20C drilling rig (crawler mounted). Due to potential CO_2 blowouts in the region, the drillings were performed through a blowout preventer to overcome the problem of pressurized CO_2 in the drilling shaft; however, none of the sites faced such issues during drilling. The drillings were conducted under strict site contamination control conditions; after the termination of works, all sites and access roads were restored (Fig. 3). Furthermore, the wellheads were secured by a concrete head casing, and the cased peduncle was secured by a lock (Fig. 4).

The parameters of the drilling sites are summarized in Table 1. Some innovative approaches were applied during drilling and subsequent logging to meet the specific requirements of multidisciplinary research. All boreholes are nearly vertical, reaching depths < 460 m, and they were all steel cased. After casing, the drillings were cleared (redrilled within the casing) to ensure clear passage from the head to the bottom, which is necessary for subsequent successful installation of fluid and seismic monitoring instrumentation. Seismological drill holes S1, S3 and S4 were cemented to ensure seismic coupling. The quality of the cementing was controlled by well logging, and an innovative approach using a fiber-optic cable was additionally applied to monitor the cementing at S1. Wireline coring was applied to all boreholes, and the cores were retrieved and organized in wooden boxes (Fig. 5) before being stored (except for S2) at the Research INfrastructure for Geothermal ENergy (RINGEN) center in Litoměřice and the Federal Institute for Geosciences and Natural Resources (BGR) core repository in Spandau, Berlin (S1). The core of drill hole S2 is not available to the scientific community, as the drill hole was an in-kind contribution from the Golden Pet s.r.o. exploration company to the ICDP Eger project.

Well logging was provided for all drilling sites except for S2 (the in-kind contribution from the Golden Pet s.r.o. exploration company). It comprised a complex of methods, including borehole geometry, caliper, sonic logging with full waveforms, and acoustic images to localize cracks, fractures, and/or tectonic and geological features. Gamma–gamma logging was applied to sample rock densities, neutron–neutron logging was applied for porosity and water content, natural gamma logging was used for the detection of unstable isotopes, and resistivity logging was used for the degree of rock deformation. For the records of well logging in individual boreholes, see Sect. 5.

Due to the specific requirements of microbiological research, drillings F3 and S4 were conducted under strict contamination control conditions, following the approach of Bussert et al. (2017). In the case of F3, the cores were retrieved in 3 m long polyvinyl chloride (PVC) liners to protect them from biological contamination; in the case of S4, the cores were encapsulated in aluminum. In both cases, the microbiological samples were frozen at -80 °C and sent for further analyses.

4.3 Seismological drillings – high-frequency 3-D arrays

Seismological monitoring requires the drillings to be distributed and optimized for detection, location, source mechanism and seismic wave scattering studies. The technical objectives of being able to analyze $M_L > -1$ earthquakes (and nonvolcanic tremors) need to be addressed by taking a step up from the current short-period seismic monitoring network to a high-frequency 3-D seismic array. Boreholes S1–S3 involve deploying vertical seismic arrays combined with a sur-

Figure 3. The Eger Rift drilling setup, showing **(a)** the drilling rig with drilling rods at the S3 site, **(b)** the wellhead after the termination of work at the S3 site and **(c)** an example of a diamond drill head designed for drilling in hard rocks.

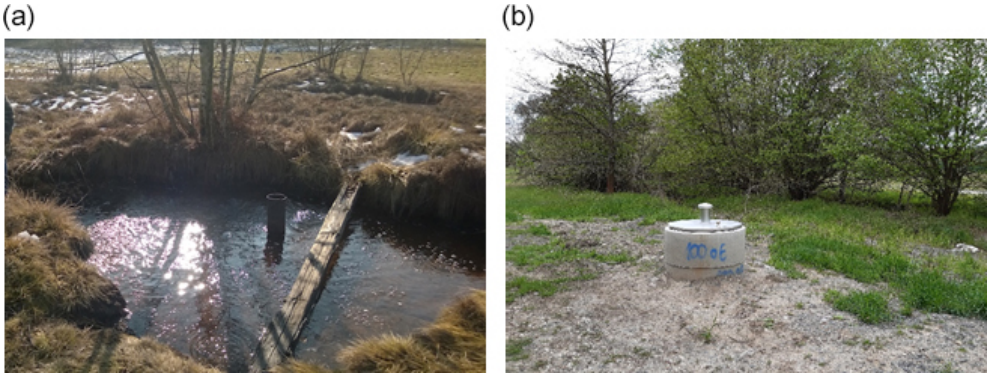

Figure 4. Panel **(a)** shows the Hartoušov mofette field, and panel **(b)** presents the F3 borehole in Hartoušov after the completion of drilling works, with the concrete head casing secured by a lock.

face small-aperture high-frequency array; a pilot observatory has already been deployed at S1. Such a configuration allows for detailed high-resolution study (at a 1 kHz sampling rate) of earthquake migration, short-term anomalies in the beginning phase of swarms, mixed-mode rupture processes, near-source scatterers, the depth distribution of events and the detection of microearthquakes along fluid channels. The location in unaltered rocks not affected by fluid ascent assures the recording of high-frequency signals of the smallest earthquakes ($M_L \geq -1$) and is supported by the pioneering tests of Hiemer et al. (2012) from a small-aperture array of short-period stations at the surface (the 6-month eight-sensor test-array deployment near S1 at Rohrbach borehole V01–V08 detecting microearthquakes from $M_L > -1.2$ from the NK focal zone).

Borehole S1 (depth 402 m, inner diameter (i.d.) 92 mm) is located in Landwüst (Germany) about 10 km northwest of the Nový Kostel (NK) focal zone in a forest area with basement rocks outcropping at the surface (metamorphosed Cambrian sediments – phyllites with quartzite layers). The test array installations and test measurements in the nearby Bad Brambach 80 m hole indicated the appropriate site conditions and excellent signal-to-noise ratios (SNRs) for weak microearthquakes with a significantly reduced S-wave damping effect. The S1 instrumentation comprises the ASIR bottomhole broadband seismometer and a vertical array of 3C bore-

Table 1. Parameters of the drill holes.

Number	Name	Lat WGS 84	Long WGS 84	Depth [m]	Inner diameter [mm]	Tilt [°]	Casing	Coring	Cement	Well-logging	Monitoring	Additional research
S1	Landwüst	50.2579	12.3291	402	92	5.0	+	+	+	+	Seismic	3-D array Fibre optic cable
S2	Tisová	50.3491	12.4948	460	76	6.4	+	-	-	-	Seismic	3-D array
S3	Studenec	50.2579	12.5185	401	76	9.0	+	+	+	+	Seismic	3-D array
F1	Hartoušov	50.1329	12.4629	28.2	115		+	+	-	-	Fluid	
F2	Hartoušov	50.1329	12.4629	108.5	100		+	+	-	+	Seismic, fluid	Microbiology
F3	Hartoušov	50.1329	12.4629	239.3	78-80	1.1	+	+	+	+	Seismic, fluid	Microbiology
S4	Libá	50.1601	12.2160	400	77	1.9	+	+	+	+	Seismic	Microbiology Paleoclimate Volcanology
P1	Neualbenreuth	49.9667	12.4667	~150			-	+	-	+		Paleoclimate Microbiology

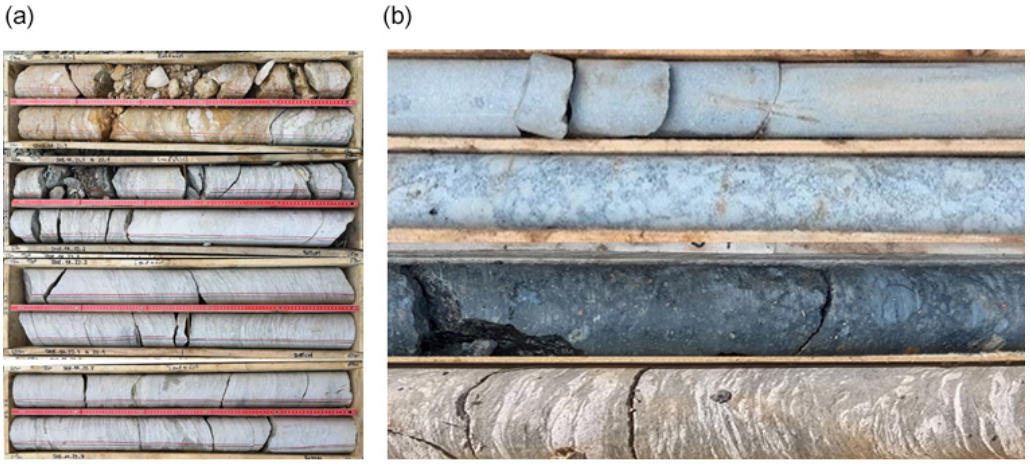

Figure 5. Panel **(a)** presents an example of drill cores stored in wooden boxes that have been marked and labeled, showing phyllitic core from S1. Panel **(b)** presents an example of different lithologies in hard rocks, showing (from top to bottom) granite from S4, granite from S4, basalt from S4 and phyllite from S3.

hole sensors between 180 and 400 m; additionally, a surface array of 3C seismic sensors is installed around the borehole (Fig. 6). The fiber-optic cable was cemented behind the borehole casing to monitor the microearthquakes as well as the quality of cementing.

Borehole S2 (depth 464 m, i.d. 76 mm) is located near Tisová (Czech Republic) about 15 km north of the Nový Kostel (NK) focal zone in weakly metamorphosed Ordovician sediments (phyllites). The thickness of the overlying weathering products (debris with rock fragments) did not exceed several meters. The noise characterization from a test array deployed indicates good SNR conditions. The instrumentation, array design and configuration are planned to be the same as for borehole S1, except for the fiber-optic cable.

Borehole S3 (depth 400 m, i.d. 76 mm) is located in Studenec (Czech Republic) about 7 km northeast of the Nový Kostel (NK) focal zone in a dynamic landscape with a minimally weathered uppermost crust on metamorphosed Cambrian sediments (phyllites). The site is in a remote area with a good SNR; this is confirmed by long-term monitoring, as the site also coincides with one seismic station (STC) of the WEBNET surface monitoring network (Horálek et al., 2000). Moreover, this coincidence provides the opportunity to compare results from both networks and use the existing operation hut. A Güralp Radian bottom-hole seismometer (Güralp Co.) is currently installed and tested at the hole bottom.

4.4 Maar drilling – seismic monitoring, paleovolcanic and microbiological research

Borehole S4 (depth 406 m, i.d. 77 mm) is located in Bažina near Libá (Czech Republic), about 17.5 km southwest of the

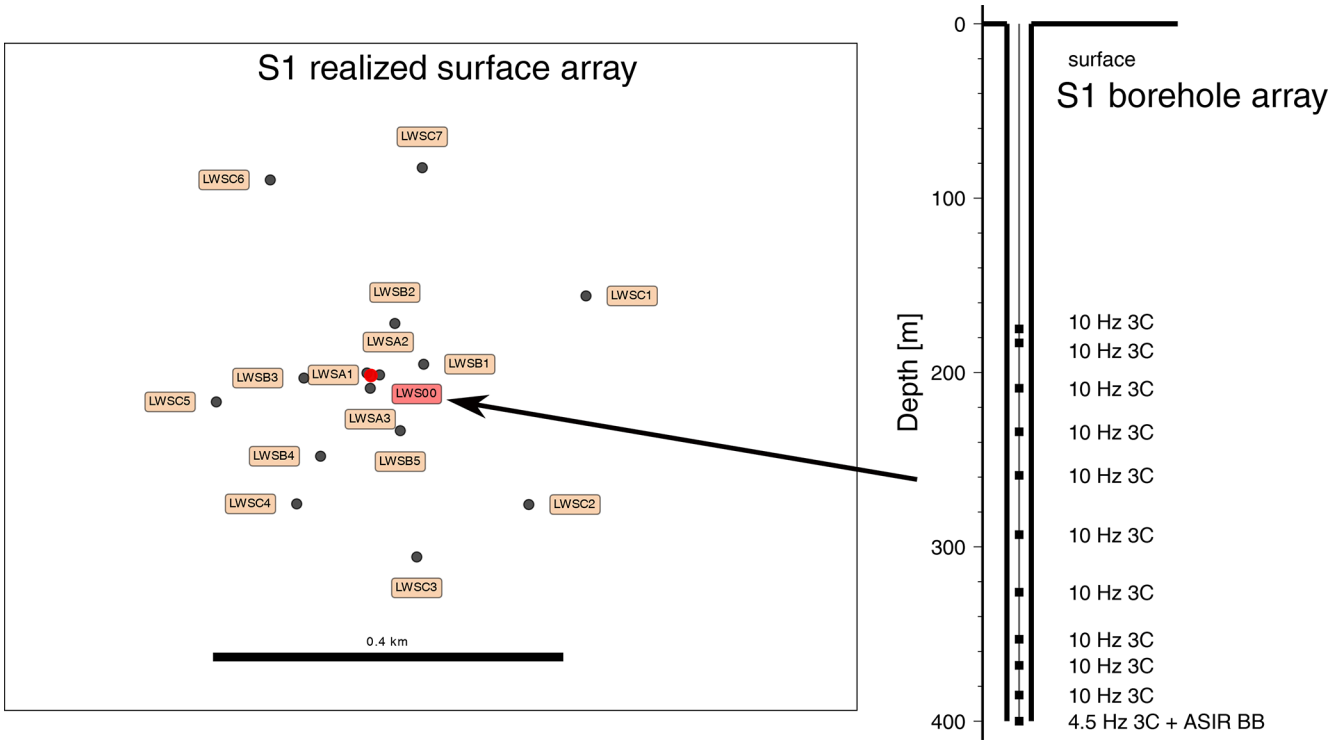

Figure 6. Surface and borehole 3-D high-frequency seismological arrays and the types of sensors realized at the S1 site. Red color denotes the S1 borehole with a surface sensor.

Nový Kostel (NK) focal zone, in a newly discovered volcanic maar structure penetrating the surrounding granitic rocks. The borehole sits in a conic maar crater and penetrates the alternating Quaternary siliciclastic and highly organic sediments of the crater. At 60 m depth, it reaches the basaltoids inside the crater; at a depth of 170 m, it reaches the contact of the crater with the surrounding granitoids (the host rocks), which continue until the bottom at 400 m depth. Because of its uppermost volcanic character, borehole S4 provides the record for combined paleovolcanic, magmatic, paleoclimate and deep-biosphere studies. As a detailed geophysical pre-site survey indicated good SNR conditions in granites, a bottom-hole seismometer is planned to be deployed in the solid granitic rocks at the bottom of the hole, along with a surface reference station.

4.5 Fluid and seismic monitoring and microbiological research – continuous sampling at different depths

Boreholes F1–F3 are located in the Hartoušov mofette field (Figs. 4, 7) in the Tertiary–Quaternary sedimentary successions of the Cheb Basin. The site appears well suited to exploring the relation between the swarm seismicity and CO_2 degassing, as a massive coseismic increase in CO_2 release has been observed here twice – in the case of the 2008 and 2014 earthquake swarms (Fischer et al., 2017). Three adjacent boreholes, F1 (depth 28 m, i.d. 115 mm), F2 (depth 108 m, i.d. 100 mm) and F3 (depth 239 m, i.d. 78 mm), supplemented by measurements in the nearby mofette (Fig. 7) allow continuous fluid monitoring at different depth levels within the basin sediments or in the CO_2-permeated weathered crystalline basement (F3). The site survey comprised seismometers and a weather station installed on-site in order to quantify the impact of earthquakes as well as the environmental effects on the fluid regime. The multilevel gas monitoring system is being installed at three wells tapping the CO_2 horizons at 20, 65 and 229 m. Continuous radon measurements while drilling revealed a promising CO_2 horizon, which was later chosen for perforations of the steel casing. Further hydraulic tests at F3 are needed to confirm whether the perforation was successful.

The F2 borehole already hosts the ASIR broadband SiA seismometer at 70 m depth. Ultimately, a borehole seismometer will be installed at the bottom of F3 and will be complemented by a capillary tube to collect "fresh" gases from the CO_2 horizon at depth, directly at the point where the fluids enter the borehole to avoid possible contamination or impact from external processes. Further details on the instrumentation of this mofette field with massive CO_2 degassing (up to 97 t d^{-1}) as well as the first monitoring results are summarized in Fischer et al. (2020), Woith et al. (2020) and Daskalopoulou et al. (2021). Once the novel monitoring system is fully operational, fluid transients will be able to be observed in great detail. We expect new insights into

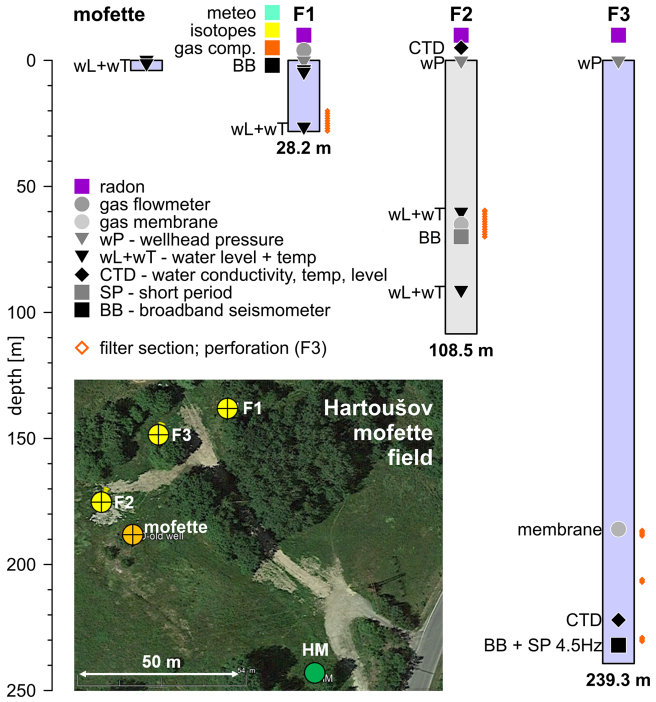

Figure 7. Fluid and seismic monitoring in the Hartoušov mofette field (after Woith et al., 2020), showing boreholes F1–F3 and a mofette site with the sensors and types of monitoring. BB denotes a broadband seismometer (borehole and/or surface), and SP represents a short-period 4.5 Hz 3C borehole sensor.

the physical processes that control the complex interplay between earthquakes, deep degassing and permeability variations along the path to the surface.

Seismic monitoring in F1–F3, located about 9 km south of the Nový Kostel (NK) focal zone (Fig. 2), complements the network of shallow boreholes. Borehole F2 (108.5 m depth) is equipped with a broadband borehole seismometer at 70 m depth; a similar sensor will be installed at the bottom of F3 (239 m depth). Moreover, a broadband surface seismic station is installed at F1 (Fig. 7).

The microbiological investigation at the Hartoušov mofette field was accomplished at the F2 and F3 drill holes. The pilot hole, F2 (HJB-1), was drilled in spring 2016, after extensive pre-drill surveys to optimize the well location (Bussert et al., 2017). The drilling through a thin caprock-like structure triggered a CO_2 blowout, indicating a CO_2 pathway. Pumping tests revealed a Na–Ca–HCO_3–SO_4-type groundwater with a total mineralization of 5870 mg L^{-1}, which is typical for the mineral waters of Františkovy Lázně Spa that is located about 8 km to the west of the drill site (Bussert et al., 2017). The first microbiological investigations included activity tests for microbial methane production, DNA extractions and cultivation experiments as well as testing of the microbial DNA extracted from samples (Bussert et al., 2017). These steps were supplemented by the investigation of the F3 borehole which involved testing for microbiological life on samples from different depths. Further analyses of F3 microbial samples are ongoing.

4.6 Drilling for paleoclimate and microbiological research

Borehole P1 is planned in the Neualbenreuth Quaternary maar structure (in Germany, at a site located about 3 km southeast of the Mýtina maar) down to ∼ 150 m depth. It will penetrate a succession of lake sediments of at least 100 m depth with varying lithologies, surrounded by Paleozoic metamorphic rocks and underlain by the diatreme. Borehole P1 will be the main record for paleoclimate studies, as it will overlap an existing 100 m drill core obtained in 2015 (Rohrmüller et al., 2017), thereby enabling the development of continuous time series. Apart from paleoclimate, the site will be exploited for microbiological and deep-biosphere studies. Due to groundwater protection issues, the well has to be closed after drilling. The geophysical pre-site survey of maar structures indicates that shallow sedimentary successions of maar craters are not suitable for high-frequency seismic monitoring; thus, the deployment of a seismic sensor in this borehole is questionable.

5 Lithologies and well logging of boreholes

The downhole logging measurements for the Eger Rift project have been performed in four of five boreholes (S1 Landwüst, S3 Studenec, S4 Libá and F3 Hartoušov). In this paper, we present the results of three seismological boreholes: S1 Landwüst, well logged by BLM Company in 2019 (Fig. 8); S3 Studenec, well logged by Aquatest in 2018 (Fig. 9); and S2 Tisová, which has not been well logged and only a stratigraphy profile is provided (Fig. 10). The following downhole logging measurements have been acquired: gamma ray, neutron–neutron, density, resistivity, temperature, P- and S-wave velocity, focus electrical resistivity (FEL), electrical conductivity, caliper, borehole deviation, and borehole azimuth direction. All logging measurements have been depth matched using the gamma ray as the reference logging present in all sondes. As the other two boreholes, S4 and F3, are the subject of further focused research, their profiles are presented in individual studies. Moreover, all records of stratigraphy and well logging in boreholes S1–S4 and F3 are depicted in Fischer et al. (2022) and in the upcoming Operational Report.

The S1 Landwüst borehole (Fig. 8) was drilled to 402 m depth and shows a southward deflection with a small deviation up to 5 ° at the bottom. The borehole encounters monotone silt–phyllite rocks with different stages of fracturing. All logs show a constant trend except at two main fractured intervals: one zone was identified from around 12.0 to 57.8 m, and the second zone was identified between 134 and 165 m. In these fractured zones, gamma ray, FEL, den-

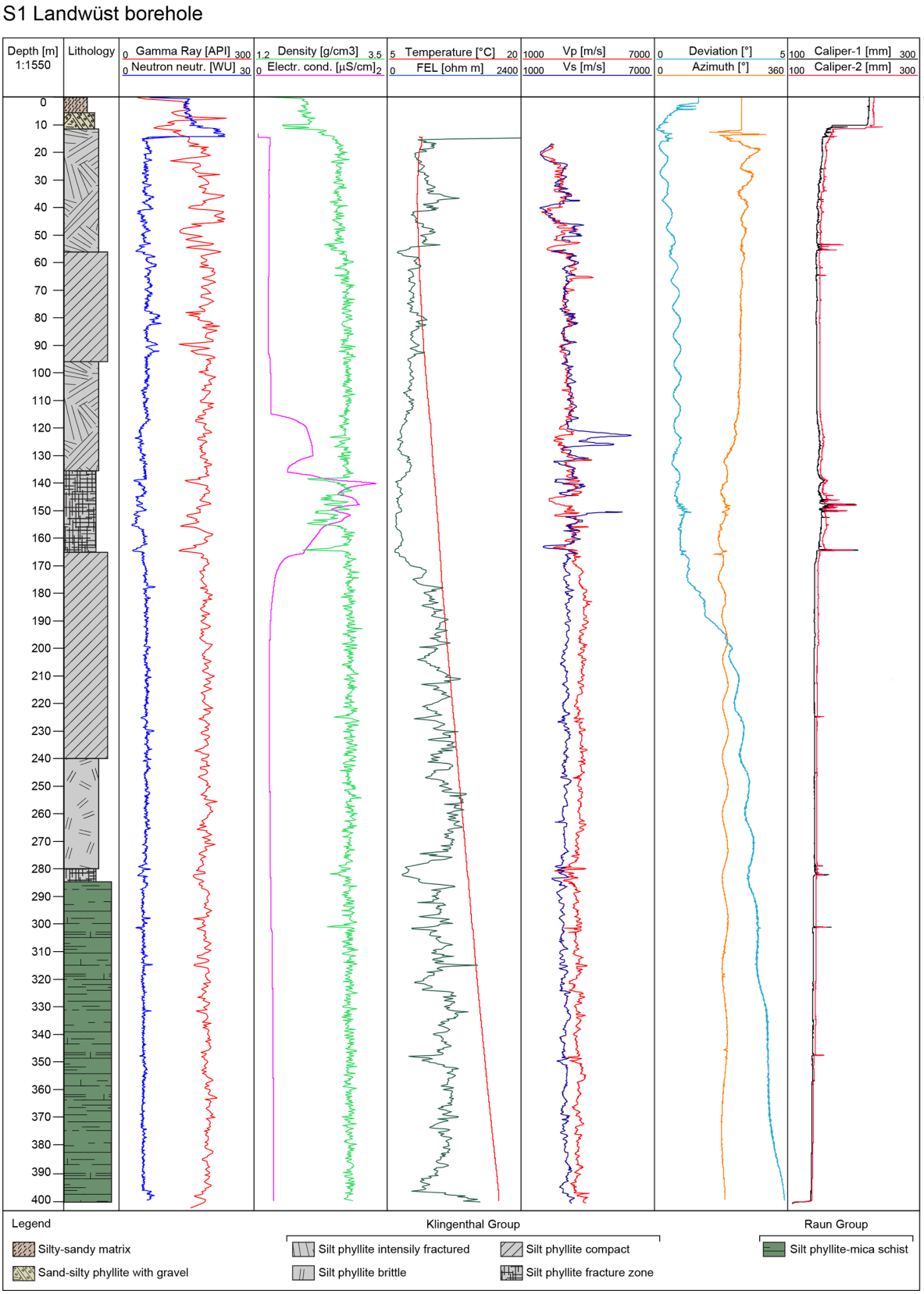

Figure 8. Logging data of the S1 Landwüst borehole and a stratigraphy profile based on the initial core description. The abbreviations used in the figure are as follows: Neutron neutr. – neutron–neutron; WU – water unit; Electr. cond. – electrical conductivity; FEL – focus electrical resistivity; V_p and V_s – P- and S-wave velocity, respectively.

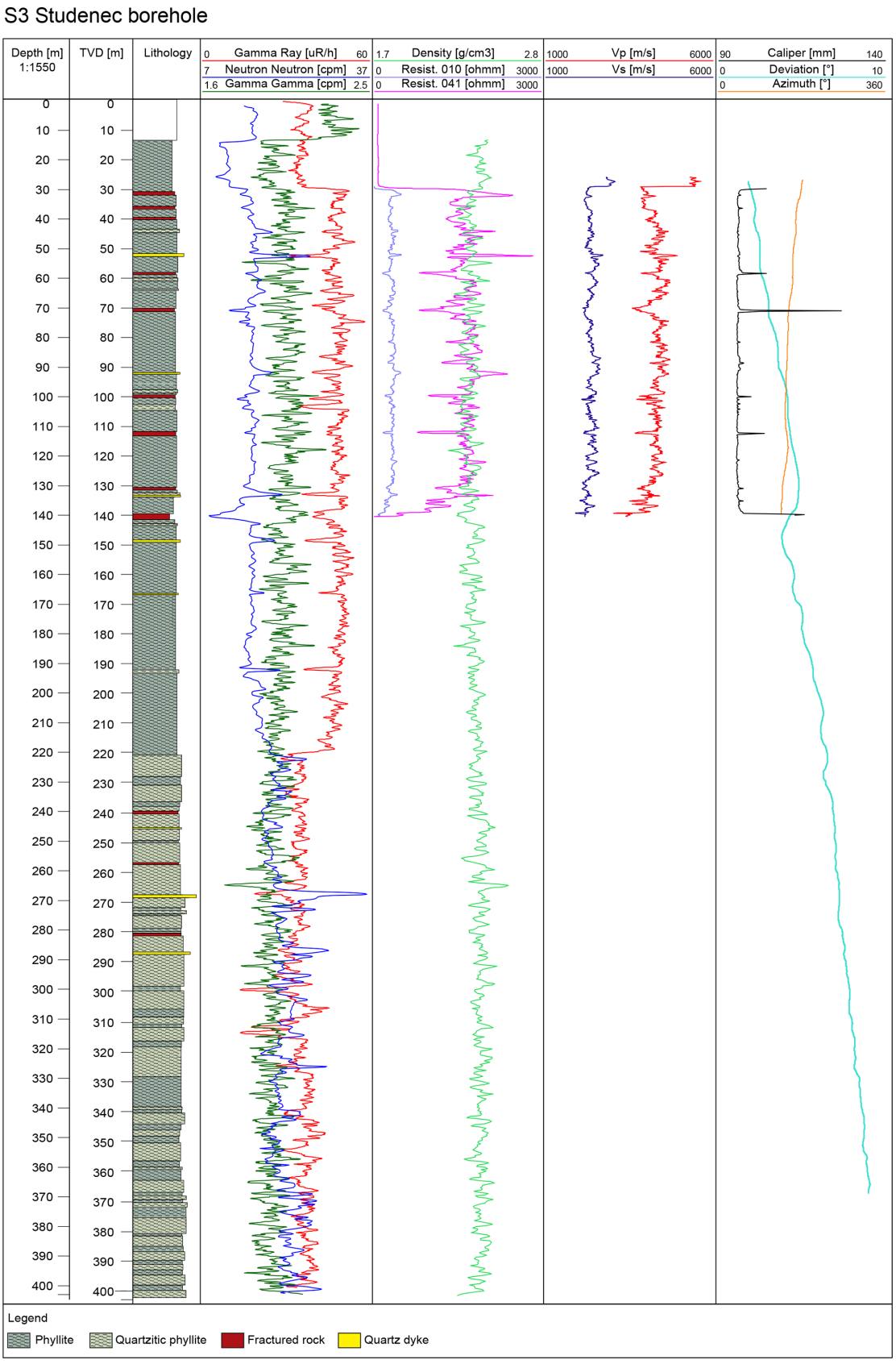

Figure 9. Logging data of the S3 Studenec borehole and a stratigraphy profile based on the initial core description. The abbreviations used in the figure are as follows: TVD – total vertical depth; Resist. – resistivity; V_p and V_s – P- and S-wave velocity, respectively.

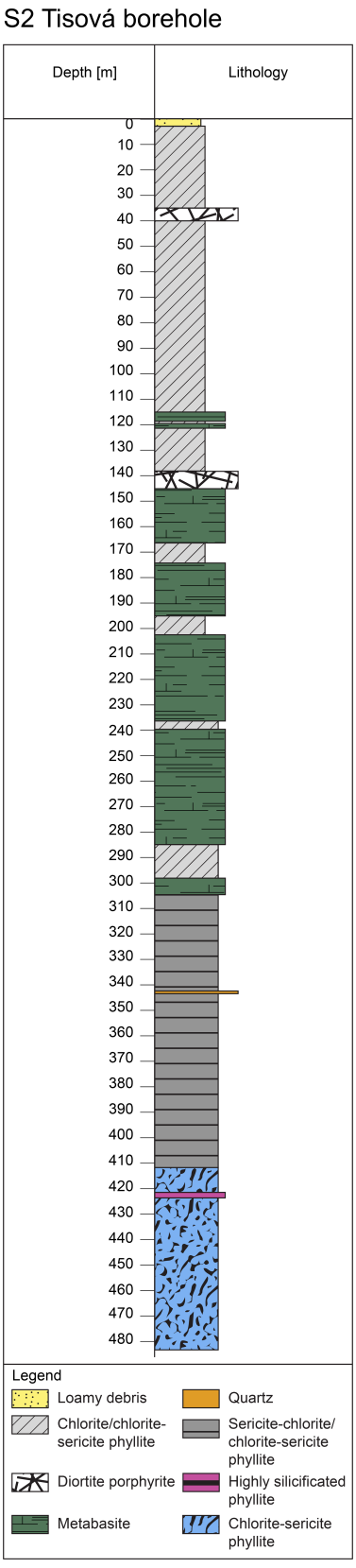

Figure 10. Stratigraphy profile based on the initial core description of borehole S2 near Tisová in weakly metamorphosed Ordovician sediments (phyllites).

sity, neutron–neutron, P- and S-wave velocity, and caliper logs show abrupt changes. In particular, in the second fracture interval, the electrical conductivity shows constant values of around 0.2 µS cm^{-1} up to 115 m that slightly increase from 0.2 to 1.8 µS cm^{-1} between 115 and 140 m. The fracturing becomes more intense between 140 and 155 m, where the electrical conductivity reaches the maximum values of around 1.8 µS cm^{-1}; the values then gradually decrease to 0.7 µS cm^{-1} at 165 m before reaching a constant value of 0.2 µS cm^{-1} at the bottom. These two main fracture zones were also detected by the caliper, which indicates an opening from 155 to 200 mm. The temperature in the borehole increases continuously from 7 °C at 25 m to 13.5 °C at 400 m depth.

The S3 Studenec borehole (Fig. 9) reached a total depth of 402.5 m, with the deviation increasing smoothly up to 9 ° at the bottom and with deflection to the southeast. The borehole encounters a sequence of phyllite rocks up to 221 m, and a quartzitic phyllite formation is then predominant in the bottom part. The variation in lithology along the borehole is well recorded by the gamma ray log. The gamma ray shows average values of 50 µR h^{-1} for the phyllite rock formation, mainly related to the higher content of clay minerals compared with the quartzitic phyllite formation which shows average values around 39 µR h^{-1}. A slight enrichment of the clay component is observed between 330 and 402.5 m. Around 139–141 m, the borehole encountered a tectonic fault that fragmented the rock of the borehole wall and caused the collapse of the section between 140 and 142.5 m. Only downhole logging measurements with nuclear sources (such as neutron–neutron and density measurements) have been run inside the pipe from 0 m to the bottom of the hole, whereas P- and S-wave velocity, caliper and resistivity logs were provided only in shallow part between 30 and 140 m. Several fracture intervals have been identified around 59, 71.0, 100, 111 and 135 m. They are detected by resistivity, P-wave velocity and gamma ray logs, showing a decrease in values compared with the general trend, whereas the caliper records show an increase in the hole size (spikes).

6 Temperature measurements and the heat flow

Due to the persistent tectonic activity and the existence of thermal springs, places with increased heat flux (Čermák, 1994) can be expected in the area. However, due to the absence of deeper boreholes penetrating sedimentary successions of the Cheb Basin to the basement crystalline rocks, detailed information is missing. For this reason, precise temperature well logging was performed in all boreholes (Fig. 11). The temperature recordings allowed for the determination of the temperature gradients, and topographic corrections were subsequently calculated for each well using 3-D numerical models. To determine the heat flow density, knowledge of the thermal conductivity of the rocks intersected by

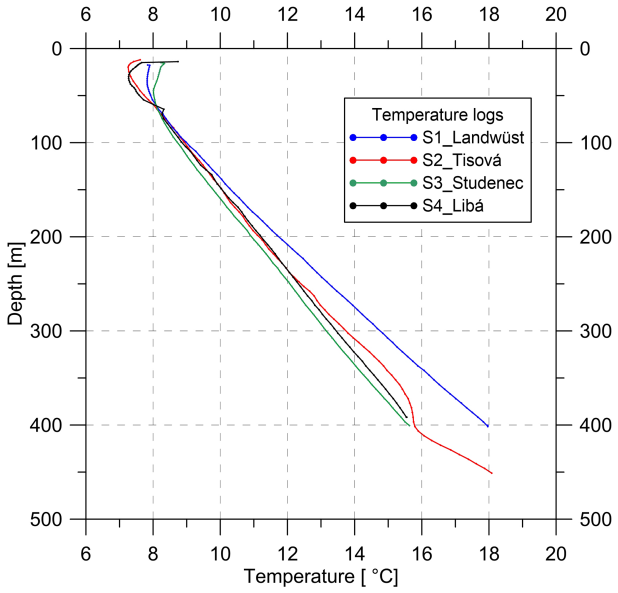

Figure 11. Temperature logs of the individual boreholes.

the boreholes was necessary. The thermal properties (thermal conductivity, thermal diffusivity and volumetric heat capacity) were measured using a high-resolution optical scanning method on several samples from each borehole. The anisotropy of the thermal properties was also assessed, which turned out to be very significant especially in the case of boreholes (S1, S2 and S3) intersecting the metamorphic rocks. Based on the above, we calculated the heat flow, which ranged from 75 mW m^{-2} for borehole S2 near Tisová to more than 100 mW m^{-2} for S1 in Landwüst.

7 Seismic monitoring concept – the 3-D high-frequency seismic array at the S1 site

The 3-D high-frequency seismic array at the S1 site has been accomplished as a pilot array for the seismic part of the ICDP Eger Rift project. The S1 instrumentation comprises the ASIR bottom-hole broadband seismometer and a vertical array of 3C borehole sensors between 180 and 400 m; additionally, a surface array of 3C seismic sensors is installed (Fig. 6). A fiber-optic cable was cemented outside of the borehole casing to monitor the microearthquakes and will provide comparison with the borehole chain. Moreover, it was also used to check the quality of the casing cementation.

7.1 Borehole array

The downhole array consists of two major parts: a 10-level high-frequency borehole chain and one additional bottom-hole seismometer. The borehole chain is assembled with high-frequency geophones for one vertical and two horizontal directions at 10 depth levels. We identified 10 Hz HG-7 geophones as the optimum sensors (little or no tilt sensitivity, high spurious and low corner frequencies and, thus, a large usable bandwidth). In order to increase the output voltage, the geophones are in sets of two sensors connected in series for each direction and depth level, which results in a total of 30 analogue channels to be handled. The analogue signals are converted by five six-channel Earth Data EDR-209 digitizers at a rate of (up to) 1 kHz. The bottom-hole equipment consists of a newly developed ASIR SiA broadband seismometer with a passband of 200 s to 1.5 kHz bundled with a 3C 4.5 Hz geophone. The analogue signals are converted by one six-channel Earth Data EDR-209 digitizer at a rate of (up to) 1 kHz. The example of waveforms of an M_L 0.1 microearthquake recorded with a borehole chain at S1 Landwüst is presented in Fig. 12.

7.2 Surface array

A small-aperture array of short-period stations at the surface consists of three rings around a central borehole station. The aperture of the first ring is 10 m, and it comprises three 3 m deep postholes that are not yet fully equipped. The second ring has an aperture of 100 m and comprises five sensors. Ring 3 is equipped with seven sensors with an aperture of 400 m. The surface sensors are positioned in shallow (50 cm deep) holes and powered by solar panels. The sensors of rings 2 and 3 are of the same type (4.5 Hz HG-6 geophones with a gain of 27.7 Vs m^{-1}). The sampling rate of 1 kHz is used with seismological data loggers (EDR-209) and near-real-time transmission of the data. The data are transmitted via mobile connection.

7.3 Fiber-optic cable – the quality of cementing

After drilling S1, a fiber-optic cable was installed behind the casing down to a depth of 397.5 m on the western side of the well. The fiber-optic cable had a tight buffer design. It contained one single-mode optical fiber (ITU-T G.652.D/657.A1) preserved in a stainless-steel metal tube and embedded in a polyamide sheath with a structured surface (outer diameter 3.2 mm) to increase the mechanical coupling between cement and cable. The cable was attached to the casing using cable ties and tape. Two fixations were used per tube joint. To improve the cement deposition and reduce the risk of micro-channels between cable and cement, 4 mm separators were installed between the cable and the casing. Figure 13a shows the fiber-optic cable (and its fixing with separators) prepared for the deployment in the well.

To verify cable integrity during installation, optical time-domain reflectometry was performed after cable installation and prior to cementation. Afterwards, the well cementation was performed to ensure the best possible coupling of the casing and the surrounding rocks. The quality of cementation was controlled by the distributed fiber-optic strain measurements along the cable with an optical backscatter reflectometer (Luna OBR 4400) previously used in borehole applica-

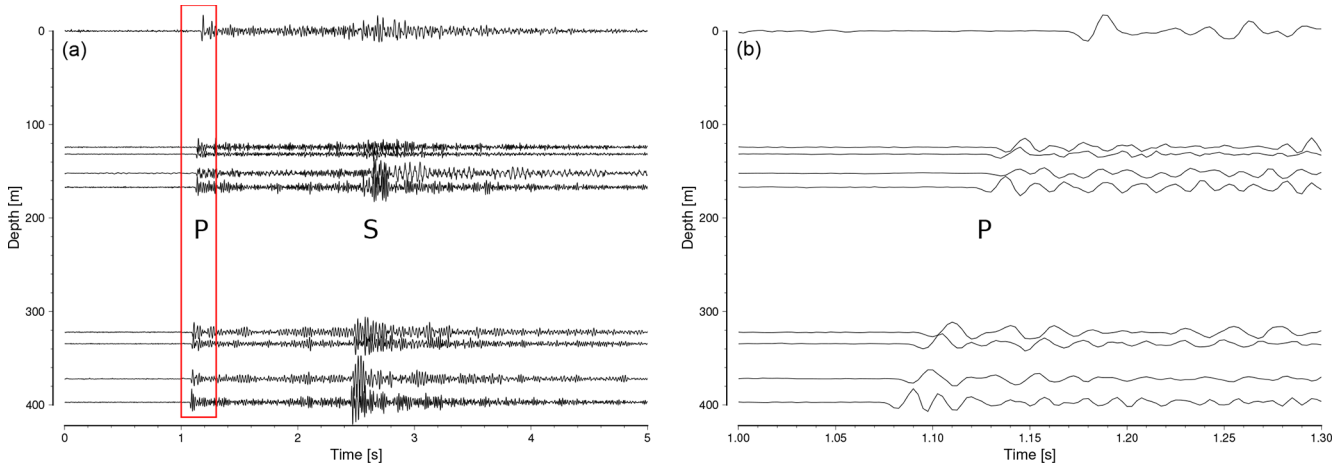

Figure 12. Example of microearthquake waveforms recorded with an 8-level borehole chain at S1 Landwüst (test installation before the deployment of the final 10-level chain) for the event on 23 January 2020, 22:21:11 UTC at 8 km depth, M_L 0.1, at an epicentral distance of 11 km (near Luby). Note the good signal-to-noise ratios (SNRs) of the recordings and their improvement with depth. The red box in panel **(a)** indicates the zoomed area in panel **(b)**.

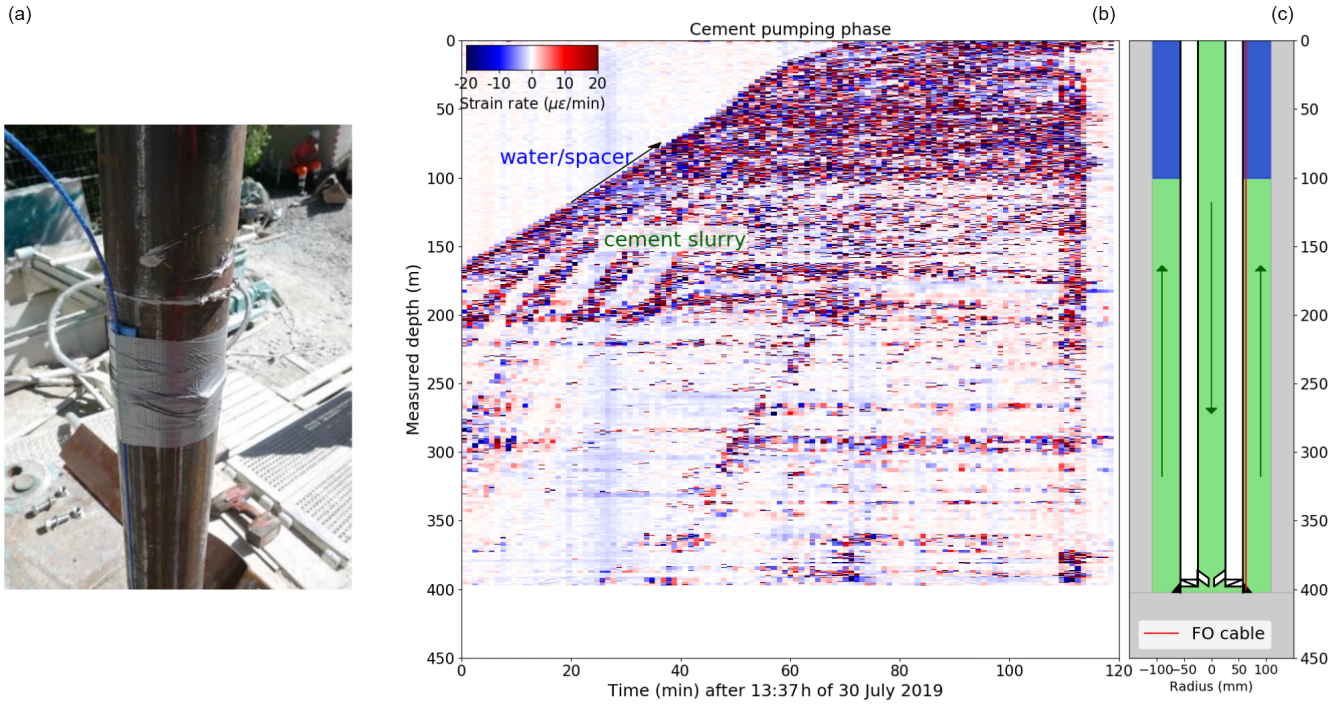

Figure 13. Panel **(a)** shows the fiber-optic cable (blue) fixed at the 4.5 in. (115 mm) borehole casing of S1. Blue separators can be seen beneath the tape to improve the cable coupling. Panel **(b)** presents the fiber-optic distributed strain rate measurements during cementing of the 4.5 in. (115 mm) casing. Panel **(c)** provides a sketch of cementing (flow indicated by arrows); the cement suspension (green) and spacer fluid (blue) are schematically depicted for the time of 26 min.

tions (e.g., Lipus et al., 2018). The OBR interrogator is based on the optical frequency domain reflectometry (OFDR) principle, following Froggatt and Moore (1998). The measurement resulted in a strain section recorded every 60 s over a time span of 2 h during the cement pumping. An example of such measurement is depicted in Fig. 13b, showing the strain change between two successive measurements.

8 Data management

The ICDP Eger project comprises a large number of continuously operating sensors for recording seismic, gas-related and meteorological data streams. In future, additional sensors also are planned for the detection of infrasonic and/or rotational seismic signals. As the project represents a long-term monitoring effort and shall be operated for at least 10–15 years, a vast amount of data has to be considered.

The major part of these data is represented by seismic monitoring at the S1–S4 and F1–F3 sites, where the 3-D arrays at the S1–S3 sites play a particularly crucial role. Each of these sites, equipped with 25 geophones/seismometers (3C instruments in all cases) with both borehole (9 geophones and 1 seismometer) and surface installations (15 geophones), produces a data stream of 75 seismic channels. With the continuous sampling rate of 1 kHz, the amount of data produced at each 3-D 3C array installation at S1–S3 will be in the order of $16\,\mathrm{GB\,d^{-1}}$ ($75\ \text{channels} \times 1000\ \text{samples} / (\text{channel} \times \text{s}) \times 86\,400\,\mathrm{s\,d^{-1}} \times 2.5\,\mathrm{B}$ per sample $= 16.2\,\mathrm{GB\,d^{-1}}$). This sums to $50\,\mathrm{GB\,d^{-1}}$ (including S4), i.e., $\sim 1.5\,\mathrm{TB}$ every month accumulating to 180 TB over a 10-year operating period. Data streams will be transmitted to Potsdam and/or partner institutions in Prague and Leipzig via 4G mobile phone standard to an open VPN server with SeedLink. The amount of data produced from gas sensors and meteorological data will be much smaller and can safely be estimated to be in the order of 1 % of the seismic data.

9 Summary

The new in situ geodynamic laboratory established in the framework of the ICDP Eger project involves five borehole sites aimed at long-term monitoring of seismic activity and CO_2 degassing in the West Bohemia–Vogtland geodynamic region (western Eger Rift). At each of these sites, a borehole broadband seismometer will be installed, and sites S1, S2 and S3 will also host a 3-D seismic array composed of a vertical geophone chain and surface seismic array. To date, all of the monitoring boreholes have been drilled. This includes the seismic monitoring boreholes S1, S2 and S3 in the crystalline units north and east of the major seismogenic zone of Nový Kostel (NK), borehole F3 in the Hartoušov mofette field south of NK and borehole S4 in the newly discovered Bažina maar near Libá west of NK. An additional borehole, P1, is being prepared in the Neualbenreuth maar, Germany, and is aimed at paleoclimate research. Seismic instrumenting has been completed in the S1 borehole and is under preparation at the four remaining monitoring borehole sites (S2, S3, S4 and F3). The continuous fluid monitoring site Hartoušov includes three boreholes, F1, F2 and F3, and a pilot monitoring phase is underway.

It is expected that the Eger Rift laboratory will result in an increasing sensitivity and discrimination capability with respect to seismic monitoring. Thanks to fluid sampling at different depths, which removes near-surface contamination, it will allow for enhanced monitoring of ongoing deep magmatic processes. This will improve our understanding of the relationships among mofette degassing, gas composition and swarms. The Eger Rift borehole laboratory also enables one to analyze microbial activity at CO_2 mofettes and maar structures in the context of changes in habitats. Last but not least, drillings into the maar volcanoes contribute to a better understanding of the Quaternary paleoclimate and volcanic activity.

Data availability. After a 3-year embargo period, beginning on the date of sampling party, the downhole logging and stratigraphy data will be available at the ICDP repository database (https://nextcloud.gfz-potsdam.de, last access: 7 June 2022; Fischer et al., 2022).

Author contributions. TF, TD, PH and HW designed, planned and executed the drillings and raised funding. TV executed the drillings and the coring. JH and JeK designed the drillings. MO, JV, PD, HK, MZ, MPL, FK, KH, TR, JaK, DV and KD performed the measurements. PH, TF, TD and HW wrote the manuscript, SP wrote the well-logging section, and all authors reviewed and edited the manuscript.

Competing interests. The contact author has declared that neither they nor their co-authors have any competing interests.

Disclaimer. Publisher's note: Copernicus Publications remains neutral with regard to jurisdictional claims in published maps and institutional affiliations.

Acknowledgements. The ICDP Eger Rift project was funded by the International Continental Scientific Drilling Program (ICDP); the Deutsche Forschungsgemeinschaft (DFG, German Research Foundation) – project nos. 419880416, 419459207 and 419909358; the Czech Science Foundation; GFZ Potsdam; a large project of the Czech infrastructure CzechGeo (CZ.02.1.01/0.0/0.0/16_013/0001800); and CzechGeo/EPOS (LM2015079). We also received co-funding from the Swedish National Research infrastructure for scientific drilling (Riksriggen) at Lund University, Sweden. The in-kind contribution of S2 drilling by the Golden Pet s.r.o. exploration company is gratefully acknowledged.

For technical support before and during drilling, we are grateful to Ulrich Harms, Thomas Wiersberg, Santiago Aldaz and Jochem Kück of the ICDP Operational Support Group. We thank the international team of drillers from Geoněmec – vrty, s.r.o., Protek Norr AB and PRUY KG, with special thanks to František Kalenda and Milan Němec (Czech Republic), Danilo Pruy (Germany), Johan Kullenberg (Sweden) and Friðfinnur K. Danielsson (Iceland). We thank also Ralf Bauz (Germany) for support during the drilling of S1 and F3.

We acknowledge Christian Cunow and Marius Isken for support during the S1 field and cable installations, and we are grateful to Marius Kriegerowski and Henning Lilienkamp for seismic noise measurements. Funding for the sensors and equipment for the S1 surface array was provided by the Saxionan State Office for Agriculture, Environment and Geology and the University of Leipzig. Special thanks go to LIAG (Germany) for well logging of F3 and Aquatest/SG Geotechnika (Czech Republic) for well logging of the other sites.

We also thank the editor Tomoaki Morishita, Ulrich Harms (the editor in chief) and the two anonymous reviewers for their comments that improved the paper.

Financial support. This research has been supported by the International Continental Scientific Drilling Program (ICDP, project no. 5008); the Deutsche Forschungsgemeinschaft (DFG, German Research Foundation, project nos. 419880416, 419459207 and 419909358); the Czech Science Foundation; GFZ Potsdam; a large project of the Czech infrastructure CzechGeo (grant no. CZ.02.1.01/0.0/0.0/16_013/0001800); and CzechGeo/EPOS (no. LM2015079). We also received co-funding from the Swedish National Research infrastructure for scientific drilling (Riksriggen) at Lund University, Sweden, and an in-kind contribution of S2 drilling from the Golden Pet s.r.o. exploration company.

Review statement. This paper was edited by Tomoaki Morishita and reviewed by two anonymous referees.

References

Alawi, M., Nickschick, T., and Kämpf, H.: Mikrobiologische Prozesse in CO_2-Aufstiegskanälen, System Erde, 5, 28–33, https://doi.org/10.2312/GFZ.syserde.05.01.5, 2015.

Alexandrakis, C., Calò, M., Bouchaala, F., and Vavryčuk, V.: Velocity structure and the role of fluids in the West Bohemia Seismic Zone, Solid Earth, 5, 863–872, https://doi.org/10.5194/se-5-863-2014, 2014.

Bräuer, K., Kämpf, H., Strauch, G., and Weise, S. M.: Isotopic evidence ($^3He/^4He$, $^{13}CCO_2$) of fluid triggered intraplate seismicity, J. Geophys. Res., 108, 2070, https://doi.org/10.1029/2002JB002077, 2003.

Bräuer, K., Kämpf, H., Faber, E., Koch, U., Nitzsche, H.-M., and Strauch, G.: Seismically triggered microbial methane production relating to the Vogtland NW Bohemia earthquake swarm period 2000, Central Europe, Geochem. J., 39, 441–450, https://doi.org/10.2343/geochemj.39.441, 2005a.

Bräuer, K., Kämpf, H., Niedermann, S. and Strauch, G.: Evidence for ascending upper mantle-derived melt beneath the Cheb basin, central Europe, Geophys. Res. Lett., 32, L08303, https://doi.org/10.1029/2004GL022205, 2005b.

Bräuer, K., Kämpf, H., Niedermann, S., Strauch, G., and Tesař, J.: The natural laboratory NW Bohemia – Comprehensive fluid studies between 1992 and 2005 used to trace geodynamic processes, Geochem. Geophy. Geosy., 9, Q04018, https://doi.org/10.1029/2007GC001921, 2008.

Bräuer, K., Kämpf, H., and Strauch, G.: Earthquake swarms in non-volcanic regions: What fluids have to say, Geophys. Res. Lett., 36, L17309, https://doi.org/10.1029/2009GL039615, 2009.

Bräuer, K., Kämpf, H., and Strauch, G.: Seismically triggered anomalies in the isotope signatures of mantle-derived gases detected at degassing sites along two neighbouring faults in NW Bohemia, Central Europe, J. Geophys. Res.-Sol. Ea., 119, 5613–5632, https://doi.org/10.1002/2014JB011044, 2014.

Bussert, R., Kämpf, H., Flechsig, C., Hesse, K., Nickschick, T., Liu, Q., Umlauft, J., Vylita, T., Wagner, D., Wonik, T., Flores, H. E., and Alawi, M.: Drilling into an active mofette: pilot-hole study of the impact of CO_2-rich mantle-derived fluids on the geo–bio interaction in the western Eger Rift (Czech Republic), Sci. Dril., 23, 13–27, https://doi.org/10.5194/sd-23-13-2017, 2017.

Čermák, V.: Results of heat flow studies in Czechoslovakia, in Crustal structure of the Bohemian Massif and the West Carpathians, in: Exploration of the Deep Continental Crust, edited by: Bucha, V. and Blížkovský, M., Berlin, Springer-Verlag, 85–120, ISBN 3540579869, 1994.

Dahm, T. and Brandsdottir, B.: Moment tensors of microearthquakes from the Eyjafjallajökull volcano in South Iceland, Geophys. J. Int., 130, 183–192, 1997.

Dahm, T., Hrubcová, P., Fischer, T., Horálek, J., Korn, M., Buske, S., and Wagner, D.: Eger Rift ICDP: an observatory for study of non-volcanic, mid-crustal earthquake swarms and accompanying phenomena, Sci. Dril., 16, 93–99, https://doi.org/10.5194/sd-16-93-2013, 2013.

Daskalopoulou, K., Woith, H., Zimmer, M., Niedermann, S., Barth, J. A. C., Frank, A. H., Vieth-Hillebrand, A., Vlček, J., Bağ, C. D., and Bauz, R.: Insight into Hartoušov Mofette, Czech Republic: Tales by the Fluids, Front. Earth Sci., 9, 615766, https://doi.org/10.3389/feart.2021.615766, 2021.

Dreger, D. S., Tkalcic, H., and Jonston, M.: Dilational processes accompanying earthquakes in the Long Valley Caldera, Science, 288, 122–125, 2000.

Einarsson, P.: Earthquakes and present-day tectonism in Iceland, Tectonophysics, 189, 261–279, 1991.

Fischer, T. and Michálek, J.: Post 2000-swarm microearthquake activity in the principal focal zone of West Bohemia/Vogtland: space-time distribution and waveform similarity analysis, Stud. Geophys. Geod., 52, 493–511, https://doi.org/10.1007/s11200-008-0034-y, 2008.

Fischer, T., Horálek, J., Hrubcová, P., Vavryčuk, V., Bräuer, K., and Kämpf, H.: Intra-continental earthquake swarms in West-Bohemia and Vogtland: A review, Tectonophysics, 611, 1–27, https://doi.org/10.1016/j.tecto.2013.11.001, 2014.

Fischer, T., Matyska, C., and Heinicke, J.: Earthquake-enhanced permeability – evidence from carbon dioxide release following the ML 3.5 earthquake in West Bohemia, Earth Planet. Sci. Lett., 460, 60–67, https://doi.org/10.1016/j.epsl.2016.12.001, 2017.

Fischer, T., Vlček, J., and Lanzendörfer, M.: Monitoring crustal CO_2 flow: methods and their applications to the mofettes in West Bohemia, Solid Earth, 11, 983–998, https://doi.org/10.5194/se-11-983-2020, 2020.

Fischer, T., Hrubcová, P., Dahm, T., Woith, H., Vylita, T., Ohrnberger, M., Vlček, J., Horálek, J., Dedeček, P., Zimmer, M., Lipus, M. P., Pierdominici, S., Kallmeyer, J., Krüger, F., Hannemann, K., Korn, M., Kämpf, H., Reinsch, T., Klicpera, J., Vollmer, D., and Daskalopoulou, K.: ICDP Drilling of the Eger

Rift Observatory: Operational Data Sets, GFZ Data Services [data set], https://doi.org/10.5880/ICDP.5008.001, 2022.

Flechsig, C., Heinicke, J., Mrlina, J., Kämpf, H., Nickschick, T., Schmidt, A., Bayer, T., Günther, T., Rücker, C., Seidel, E., and Seidl, M.: Integrated geophysical and geological methods to investigate the inner and outer structures of the Quaternary Mýtina maar (W-Bohemia, Czech Republic), Int. J. Earth Sci., 104, 2087–2105, https://doi.org/10.1007/s00531-014-1136-0, 2015.

Froggatt, M. and Moore, J.: High-spatial-resolution distributed strain measurement in optical fiber with Rayleigh scatter, Appl. Optics, 37, 1735–1740, https://doi.org/10.1364/AO.37.001735, 1998.

Geissler, W. H., Kämpf, H., Kind, R., Klinge, K., Plenefisch, T., Horálek, J., Zedník, J., and Nehybka, V.: Seismic structure and location of a CO_2 source in the upper mantle of the western Eger (Ohře) Rift, central Europe, Tectonics, 24, TC5001, https://doi.org/10.1029/2004TC001672, 2005.

Grünthal, G., Stromeyer, D., Bosse, C., Cotton, F., and Bindi, D.: Erdbebengefährdung Deutschlands – neu bewertet für aktuelle Baunorm, System Erde, 9, 1, 26–31, https://doi.org/10.2312/GFZ.syserde.09.01.4, 2019.

Hiemer, S., Roessler, D., and Scherbaum, F.: Monitoring the West Bohemian earthquake swarm in 2008/2009 by a temporal small-aperture seismic array, J. Seismol., 16, 169–182, https://doi.org/10.1007/s10950-011-9256-5, 2012.

Horálek, J. and Fischer, T.: Role of crustal fluids in triggering the West Bohemia/Vogtland earthquake swarms: just what we know (a review), Stud. Geophys. Geod., 52, 455–478, https://doi.org/10.1007/s11200-008-0032-0, 2008.

Horálek, J., Fischer, T., Boušková, A., and Jedlička, P.: The Western Bohemia/Vogtland Region in the light of the Webnet network, Stud. Geophys. Geod., 44, 107–125, https://doi.org/10.1023/A:1022198406514, 2000.

Hrubcová, P. and Geissler, W. H.: The crust-mantle transition and the Moho beneath the Vogtland/West Bohemian region in the light of different seismic methods, Stud. Geophys. Geod., 53, 275–294, https://doi.org/10.1007/s11200-009-0018-6, 2009.

Hrubcová, P., Środa, P., Špičák, A., Guterch, A., Grad, M., Keller, G.R., Brückl, E., and Thybo, H.: Crustal and uppermost mantle structure of the Bohemian Massif based on CELEBRATION 2000 data, J. Geophys. Res., 110, B11305, https://doi.org/10.1029/2004JB003080, 2005.

Hrubcová, P., Vavryčuk, V., Boušková, A., and Horálek, J.: Moho depth determination from waveforms of microearthquakes in the West Bohemia/Vogtland swarm area, J. Geophys. Res.-Sol. Ea., 118, 120–137, https://doi.org/10.1029/2012JB009360, 2013.

Hrubcová, P., Vavryčuk, V., Boušková, A., and Bohnhoff, M.: Shallow crustal discontinuities inferred from waveforms of microearthquakes: Method and application to KTB Drill Site and West Bohemia Swarm Area, J. Geophys. Res.-Sol. Ea., 121, 881–902, https://doi.org/10.1002/2015JB012548, 2016.

Hrubcová, P., Geissler, W. H., Bräuer, K., Vavryčuk, V., Tomek, Č., and Kämpf, H.: Active magmatic underplating in western Eger Rift, Central Europe, Tectonics, 36, 2846–2862, https://doi.org/10.1002/2017TC004710, 2017.

Kallmeyer, J., Pockalny, R., Adhikari, R. R., Smith, D. C., and D'Hondt, S.: Global distribution of microbial abundance and biomass in subseafloor sediment, P. Natl. Acad. Sci. USA, 109, 16213–16216, 2012.

Kämpf, H., Bräuer, K., Schumann, J., Hahne, K., and Strauch, G.: CO_2 discharge in an active, non-volcanic continental rift area (Czech Republic): characterisation ($\delta^{13}C$, ^3He / ^4He) and quantification of diffuse and vent CO_2 emissions, Chem. Geol., 339, 71–83, https://doi.org/10.1016/j.chemgeo.2012.08.005, 2013.

Kämpf, H., Broge, A. S., Marzban, P., Allahbakhshi, M., and Nickschick, T.: Nonvolcanic carbon dioxide emission at continental rifts: the Bublak Mofette Area, Western Eger Rift, Czech Republic, Geofuids, 2019, 1–19, https://doi.org/10.1155/2019/4852706, 2019.

Klemt, C.: Seismic imaging of the crustal structure in the central European Variscan orogen by reprocessing of the deep seismic reflection profiles GRANU9501 und GRANU9502, MS thesis, TU Bergakademie, Freiberg, 2013.

Krauze, P., Kämpf, H., Horn, F., Liu, Q., Voropaev, A., Wagner, D., and Alawi, M.: Microbiological and geochemical survey of CO_2-dominated mofette and mineral waters of the Cheb Basin, Czech Republic, Front. Microbiol., 8, 2446, https://doi.org/10.3389/fmicb.2017.02446, 2017.

Kvaček, Z. and Teodoridis, V.: Tertiary macrofloras of the Bohemian Massif: a review with correlations within Boreal and Central Europe, Bull. Geosci., 82, 383–408, 2007.

Lees, J. M.: Multiplet analysis at Coso geothermal, Bull. Seismol. Soc. Am., 88, 1127–1143, 1998.

Lehman, R. M.: Microbial distribution and their potential controlling factors in terrestrial subsurface environments, in: The spatial distribution of microbes in the environment, edited by: Franklin, R. B. and Mills, A. L., Springer, 135–178, https://doi.org/10.1007/978-1-4020-6216-2, 2007.

Lied, P., Kontny, A., Nowaczyk, N., Mrlina, J., and Kämpf, H.: Cooling rates of pyroclastic deposits inferred from mineral magnetic investigations: a case study from the Pleistocene Mýtina Maar (Czech Republic), Int. J. Earth Sci., 109, 1707–1725, https://doi.org/10.1007/s00531-020-01865-1, 2020.

Lipus, M. P., Reinsch, T., Schmidt-Hattenberger, C., Henninges, J., and Reich, M.: Gravel pack monitoring with a strain sensing fiber optic cable, Oil Gas-Eur. Mag., 44, 179–185, https://doi.org/10.19225/181202, 2018.

Liu, Q., Kämpf, H., Bussert, R., Krauze, P., Horn, F., Nickschick, T., Plessen, B., Wagner, D., and Alawi, M.: Influence of CO_2 degassing on the microbial community in a dry mofette field in Hartoušov, Czech Republic (Western Eger Rift), Front. Microbiol., 9, 2787, https://doi.org/10.3389/fmicb.2018.02787, 2018.

Liu, Q., Adler, K., Lipu, D., Kämpf, H., Bussert, R., Plessen, B., Schulz, H.-M., Krauze, P., Horn, F., Wagner, D., Mangelsdorf, K., and Alawi, M.: Microbial Signatures in Deep CO_2-Saturated Miocene Sediments of the Active Hartoušov Mofette System (NW Czech Republic), Front. Microbiol., 11, 543260, https://doi.org/10.3389/fmicb.2020.543260, 2020.

Mousavi, S., Bauer, K., Korn, M., and Hejrani, B.: Seismic tomography reveals a mid-crustal intrusive body, fluid pathways and their relation to the earthquake swarms in West Bohemia/Vogtland, Geophys. J. Int., 203, 1113–1127, https://doi.org/10.1093/gji/ggv338, 2015.

Mousavi, S., Haberland, C., Bauer, K., Hejrani, B., and Korn, M.: Attenuation tomography in West Bohemia/Vogtland, Tectonophysics, 695, 64–75, https://doi.org/10.1016/j.tecto.2016.12.010, 2017.

Mrlina, J., Kämpf, H., Geissler, W. H., and van den Bogaard, P.: Proposed Quaternary maar structure at the Czech/German boundary between Mýtina and Neualbentreuth (western Eger Rift, Central Europe): geophysical, petrochemical and geochronological indications, Z. Geol. Wiss., 35, 213–230, 2007.

Mrlina, J., Kämpf, H., Kroner, C., Mingram, J., Stebich, M., Brauer, A., Geissler, W. H., Kallmeyer, J., Matthes, H., and Seidl, M.: Discovery of the first Quaternary maar in the Bohemian Massif, Central Europe, based on combined geophysical and geological surveys, J. Volcanol. Geoth. Res., 182, 97–112, https://doi.org/10.1016/j.jvolgeores.2009.01.027, 2009.

Mullick, N., Buske, S., Hrubcová, P., Růžek, B. Shapiro, S., Wigger, P., and Fischer, T.: Seismic imaging of the geodynamic activity at the western Eger rift in central Europe, Tectonophysics, 647–648, 105–111, https://doi.org/10.1016/j.tecto.2015.02.010, 2015.

Muñoz, G., Weckmann, U., Pek, J., Kováčiková, S., and Klanica, R.: Regional two-dimensional megnetotelluric profile in West Bohemia/Vogtland reveals deep conductive channel into the earthquake swarm region, Tectonophysics, 727, 1–11, https://doi.org/10.1016/j.tecto.2018.01.012, 2018.

Nickschick, T., Kämpf, H., Flechsig, C., Mrlina, J., and Heinicke, J.: CO_2 degassing in the Hartousov mofette area, western Eger Rift, imaged by CO_2 mapping and geoelectrical and gravity surveys, Int. J. Earth Sci., 104, 2107–2129, https://doi.org/10.1007/s00531-014-1140-4, 2015.

Nickschick, T., Flechsig, C., Mrlina, J., Oppermann, F., Löbig, F., and Günther, T.: Large-scale electrical resistivity tomography in the Cheb Basin (Eger Rift) at an International Continental Drilling Program (ICDP) monitoring site to image fluid-related structures, Solid Earth, 10, 1951–1969, https://doi.org/10.5194/se-10-1951-2019, 2019.

Parkes, R. J., Cragg, B. A., Bale, S. J., Getliff, J. M., Goodman, K., Rochelle, P. A., Fry, J. C., Weightman, A. J., and Harvey, S. M.: Deep bacterial biosphere in Pacific Ocean sediments, Nature, 371, 410–413, 1994.

Parkes, R. J., Cragg, B. A., and Wellsbury, P.: Recent studies on bacterial populations and processes in subseafloor sediments: a review, Hydrogeol. J., 8, 11–28, 2000.

Prodehl, C., Mueller, S., and Haak, V.: The European Cenozoic Rift System, in: Continental rifts: evolution, structure, tectonics, in: Dev. Geotecton, edited by: Olsen, K. H., Elsevier, 133–212, ISBN 9780080529837, 1995.

Rohrmüller, J., Kämpf, H., Geiß, E., Großmann, J., Grun, I., Mingram, J., Mrlina, J., Plessen, B., Stebich, M., Veress, C., Wendt, A., and Nowaczyk, N.: Reconnaissance study of an inferred Quaternary maar structure in the western part of the Bohemian Massif near Neualbenreuth, NE-Bavaria (Germany), Int. J. Earth Sci., 107, 1381–1405, https://doi.org/10.1007/s00531-017-1543-0, 2017.

Schimschal, S.: Seismic imaging of the crustal structure in the Münchberg/Vogtland/Erzgebirge area by reprocessing of the deep seismic reflection profile MVE90', MS thesis, TU Bergakademie, Freiberg, 2013.

Schreiber, U., Locker-Grütjen, O., and Mayer, C.: Hypothesis: origin of life in the deep-reaching tectonic faults, Orig. Life Evol. Biosph., 42, 47–54, https://doi.org/10.1007/s11084-012-9267-4, 2012.

Schuessler, J. A., Kämpf, H., Koch, U., and Alawi, M.: Earthquake impact on iron isotope signatures recorded in mineral spring water, J. Geophys. Res.-Sol. Ea., 121, 8548–8568, https://doi.org/10.1002/2016JB013408, 2016.

Tomek, Č., Dvořáková, V., and Vrána, S.: Geological interpretation of the 9HR and 503M seismic profiles in Western Bohemia, in: Geological Model of Western Bohemia Related to the KTB Borehole in Germany, edited by: Vrána, S. and Štedrá, V., J. Geol. Sci. Prague, 47, 43–50, 1997.

Umlauft, J. and Korn, M.: 3-D fluid channel location from noise tremors using matched field processing, Geophys. J. Int., 219, 1550–1561, https://doi.org/10.1093/gji/ggz385, 2019.

Vavryčuk, V.: Crustal anisotropy from local observations of shear-wave splitting in West Bohemia, Czech Republic, Bull. Seism. Soc. Am., 83, 1420–1441, 1993.

Vylita, T., Žák, K., Cílek, V., Hercman, H., and Mikšíková, L.: Evolution of hot-spring travertine accumulation in Karlovy Vary/-Carlsbad (Czech Republic) and its significance for the evolution of Teplá valley and Ohře/Eger rift, Z. Geomorphol. N.F., 51, 427–442, 2007.

Wagner, G. A., Gögen, K., Jonckhere, R., Wagner, I., and Woda, C.: Dating of Quaternary volcanoes Komorní hůrka (Kammerbühl) and Železná hůrka (Eisenbühl), Czech Republic, by TL, ESR, alpha-recoil and fission track chronometry, Z. Geol. Wiss., 30, 191–200, 2002.

Weinlich, F. H., Bräuer, K., Kämpf, H., Strauch, G., Tesař, J., and Weise, S. M.: An active subcontinental mantle volatile system in the western Eger rift, Central Europe: Gas flux, isotopic (He, C, and N) and compositional fingerprints, Geochim. Cosmochim. Ac., 63, 3653–3671, 1999.

Weise, S. M., Bräuer, K., Kämpf, H., Strauch, G., and Koch, U.: Transport of mantle volatiles through the crust traced by seismically released fluids: A natural experiment in the earthquake swarm area Vogtland/NW Bohemia, central Europe, Tectonophysics, 336, 137–150, 2001.

Woith, H., Daskalopoulou, K., Zimmer, M., Fischer, T., Vlček, J., Trubač, J., Rosberg, J.-E., Vylita, T., and Dahm, T.: Multi-Level Gas Monitoring: A New Approach in Earthquake Research, Front. Earth Sci., 8, 585733, https://doi.org/10.3389/feart.2020.585733, 2020.

Wyss, M., Shimazaki, K., and Wiemer, S.: Mapping active magma chambers by b values beneath the off-Ito volcano, Japan, J. Geophys. Res., 102, 20413–20422, https://doi.org/10.1029/97JB01074, 1997.

Sci. Dril., 31, 51–70, 2022
https://doi.org/10.5194/sd-31-51-2022

Scientific Drilling
Open Access

Drilling Overdeepened Alpine Valleys (ICDP-DOVE): quantifying the age, extent, and environmental impact of Alpine glaciations

Flavio S. Anselmetti[1], Milos Bavec[2], Christian Crouzet[3], Markus Fiebig[4], Gerald Gabriel[5,6], Frank Preusser[7], Cesare Ravazzi[8], and DOVE scientific team✚

[1]Institute of Geological Sciences and Oeschger Centre for Climate Change Research, University of Bern, 3012 Bern, Switzerland
[2]Geological Survey of Slovenia, 1000 Ljubljana, Slovenia
[3]Department of Geology, Université Savoie Mont Blanc, Université Grenoble Alpes, CNRS, IRD, ISTerre, Chambéry, France
[4]Department of Civil Engineering and Natural Hazards, Institute of Applied Geology, University of Natural Resources and Life Sciences, Vienna (BOKU), 1190 Vienna, Austria
[5]Department 1: Seismics, Gravimetry & Magnetics, Leibniz Institute for Applied Geophysics, 30655 Hanover, Germany
[6]Institute of Geology, Leibniz University Hanover, 30167 Hanover, Germany
[7]Institute of Earth and Environmental Sciences, University of Freiburg, 79104 Freiburg, Germany
[8]CNR – Institute of Environmental Geology and Geoengineering (IGAG), 20126 Milan, Italy
✚A full list of authors appears at the end of the paper.

Correspondence: Flavio S. Anselmetti (flavio.anselmetti@geo.unibe.ch)

Received: 11 April 2022 – Revised: 26 July 2022 – Accepted: 6 September 2022 – Published: 28 October 2022

Abstract. The sedimentary infill of glacially overdeepened valleys (i.e., structures eroded below the fluvial base level) is an excellent but yet underexplored archive with regard to the age, extent, and nature of past glaciations. The ICDP project DOVE (Drilling Overdeepened Alpine Valleys) Phase 1 investigates a series of drill cores from glacially overdeepened troughs at several locations along the northern front of the Alps. All sites will be investigated with regard to several aspects of environmental dynamics during the Quaternary, with focus on the glaciation, vegetation, and landscape history. Geophysical methods (e.g., seismic surveys), for example, will explore the geometry of overdeepened structures to better understand the process of overdeepening. Sedimentological analyses combined with downhole logging, analysis of biological remains, and state-of-the-art geochronological methods, will enable us to reconstruct the erosion and sedimentation history of the overdeepened troughs. This approach is expected to yield significant novel data quantifying the extent and timing of Middle and Late Pleistocene glaciations of the Alps. In a first phase, two sites were drilled in late 2021 into filled overdeepenings below the paleolobe of the Rhine Glacier, and both recovered a trough filling composed of multiphase glacial sequences. Fully cored Hole 5068_1_C reached a depth of 165 m and recovered 10 m molasse bedrock at the base. This hole will be used together with two flush holes (5068_1_A, 5068_1_B) for further geophysical cross-well experiments. Site 5068_2 reached a depth of 255 m and bottomed out near the soft rock–bedrock contact. These two sites are complemented by three legacy drill sites that previously recovered filled overdeepenings below the more eastern Alpine Isar-Loisach, Salzach, and Traun paleoglacier lobes (5068_3, 5068_4, 5068_5). All analysis and interpretations of this DOVE Phase 1 will eventually lay the ground for an upcoming Phase 2 that will complete the pan-Alpine approach. This follow-up phase will investigate overdeepenings formerly occupied by paleoglacier lobes from the western and southern Alpine margins through drilling sites in France, Italy, and Slovenia. Available geological information and infrastructure make the Alps an ideal area to study overdeepened structures; however, the expected results of this study will not be restricted to the Alps. Such features are also

known from other formerly glaciated mountain ranges, which are less studied than the Alps and more problematic with regards to drilling logistics. The results of this study will serve as textbook concepts to understand a full range of geological processes relevant to formerly glaciated areas all over our planet.

1 Introduction

Overdeepened valleys and basins are commonly found below the present landscape surface in areas formerly affected by glaciations. As overdeepened structures reach below the fluvial base level (Fig. 1, left), they are interpreted as being of glacial origin, presumably formed by pressurized subglacial meltwater and ice-contact processes (e.g., Alley et al., 2019; Huuse and Lykke-Andersen, 2000). Limited awareness of subglacial erosion features historically posed severe challenges such as the accident in 1908 in the Bernese Alps (Switzerland) when a tunnel engineering project unexpectedly drilled into unconsolidated Quaternary sediments full of pressurized groundwater in an unknown overdeepening, causing 25 casualties (Fig. 1, right). In the Alps, overdeepened features are mainly associated with tectonic structures, weak lithologies, and/or Quaternary ice confluence and diffluence situations. Overdeepenings occur in buried elongated valleys, mainly oriented parallel to former ice flow, and in basins in the ablation area of glaciers (Preusser et al., 2010). The role of tectonics is still to be assessed, as regional differential uplift, fold growth, and active thrusting might induce drainage changes and promote or prevent overdeepening.

The sedimentary fillings of overdeepened structures are excellent archives of glaciations and environmental history but have received relatively little scientific attention so far, despite some initiatives on the southern margin of the Scandinavian Ice Sheet (e.g., Gabriel et al., 2003; Jørgensen and Sandersen, 2006; Buechi et al., 2018). In particular, controversy surrounds the age of overdeepening. Buried, deeply incised valleys on the southern side of the Alps likely formed during the Messinian salinity crisis (Bini et al., 1978; Finckh, 1978), but this mechanism actually represents fluvial incision caused by base-level drop. In comparison, beneath the former Scandinavian Ice Sheet, the first overdeepening apparently occurred during the Elsterian glaciation (Kuster and Meyer, 1979). For the Alps, lithostratigraphic records and preliminary dating suggest that some overdeepened valleys were repeatedly occupied and excavated by glaciers (Preusser et al., 2010; Ellwanger et al., 2011; Pomper et al., 2017). Coring and dating first glacial events represent a starting point in the reconstruction of the history of subsequent overdeepening phases. However, only few drill cores have been investigated in detail with regards to the age of original formation (e.g., Dehnert et al., 2012; Fiebig et al., 2014; Schwenk et al., 2022), and the subsequent depositional and erosional history of overdeepened structures in the Alps remains largely unknown.

The question of the age of overdeepening is causally linked to the controversy of when Alpine glaciers first reached into the foreland and how often (Fig. 2). Penck and Brückner (1901) distinguished four glaciations during the Quaternary, and wiggle matching to deep-sea records predicts the onset of glaciation at ∼ 650 ka (van Husen and Reitner, 2011). For the Rhine Glacier lobe, Ellwanger et al. (2011) suggest the first glaciation reached this area ∼ 1 Ma, but major overdeepening occurred only during three glaciations of the Middle and Late Pleistocene. An age of 870 ka for the onset of glaciation is proposed in northern Italy (Muttoni et al., 2003), with a total of nine glacial advances identified in the Ivrea Morainic Amphitheatre (Gianotti et al., 2015). In Bavaria, gravel deposits of potential glacial origin imply the onset of glaciation during the Early Pleistocene and a minimum of six glaciations, part of which probably comprise more than one glacial advance (Doppler et al., 2011; Fiebig et al., 2011). In northern Switzerland, at least 15 glaciations, starting around 2.5–2.0 Ma ago, are postulated (Preusser et al., 2011). In the Western Alps, information on Early and Middle Pleistocene deposits is scarce. Overdeepening seems to be limited to Alpine valleys and mainly filled with deposits of the last glaciation (Nicoud et al., 2002; Buoncristiani and Campy, 2011); the last maximum of glaciation is expected to date at ∼ 65 ka (e.g., Gribenski et al., 2021). At this time, glaciers were apparently much smaller in Switzerland but still reached the foreland, while in the Austrian Alps, glaciers are expected to have barely reached the main inner-Alpine valleys (cf. Ivy-Ochs et al., 2008).

The apparent differences regarding the timing and extent of glaciations in the Alps are stunning and need to be verified and explained – a main objective of this project. A potential explanation is a different pattern of atmospheric circulation over Europe during glacial times (Florineth and Schlüchter, 2000; Kuhlemann et al., 2008; Monegato et al., 2017). DOVE will provide primary data from ice-proximal sites from overdeepened structures and establish a broad-scale picture by integrating published information from distal, non-glaciated basins in the sphere of the Alps and by comparison with the global marine ice-volume record (Fig. 2). In addition, overdeepened troughs are important for applied aspects such as groundwater-resource management, geothermal exploitation, and radioactive waste disposal. In this regard, geophysical imaging will play an important role in upscaling the information gained in boreholes. In particular, a multi-method approach (Hellman et al., 2017), with modern numerical techniques (Jordi et al., 2018), to integrate

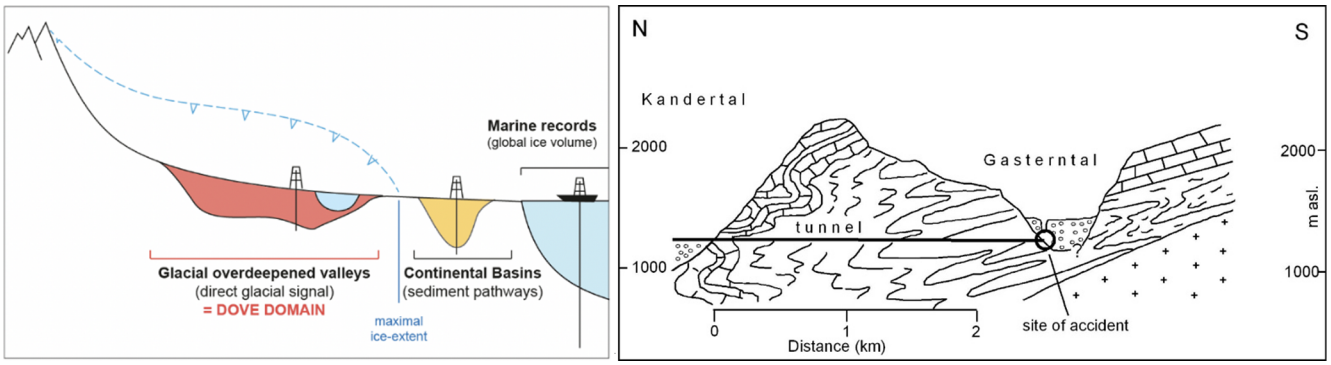

Figure 1. Left: schematic sketch (not to scale) of the formation of overdeepened valleys by erosion below glaciers (dashed blue line) reaching deeper than fluvial base level. After glaciation, troughs either are filled with sediment (red) or remain unfilled, thus forming lakes. Together with the distal non-glaciated basins (yellow) and the marine ice-volume records, they provide the sedimentary archives of glaciation history and are the targets of this project. Right: schematic cross-section through Gastern Valley (Bernese Alps, Switzerland) where in 1908 during a railway-tunnel construction, an overdeepened valley was unexpectedly encountered. The breakout of the water-saturated pressurized Quaternary sediments caused 25 casualties (after Preusser et al., 2010).

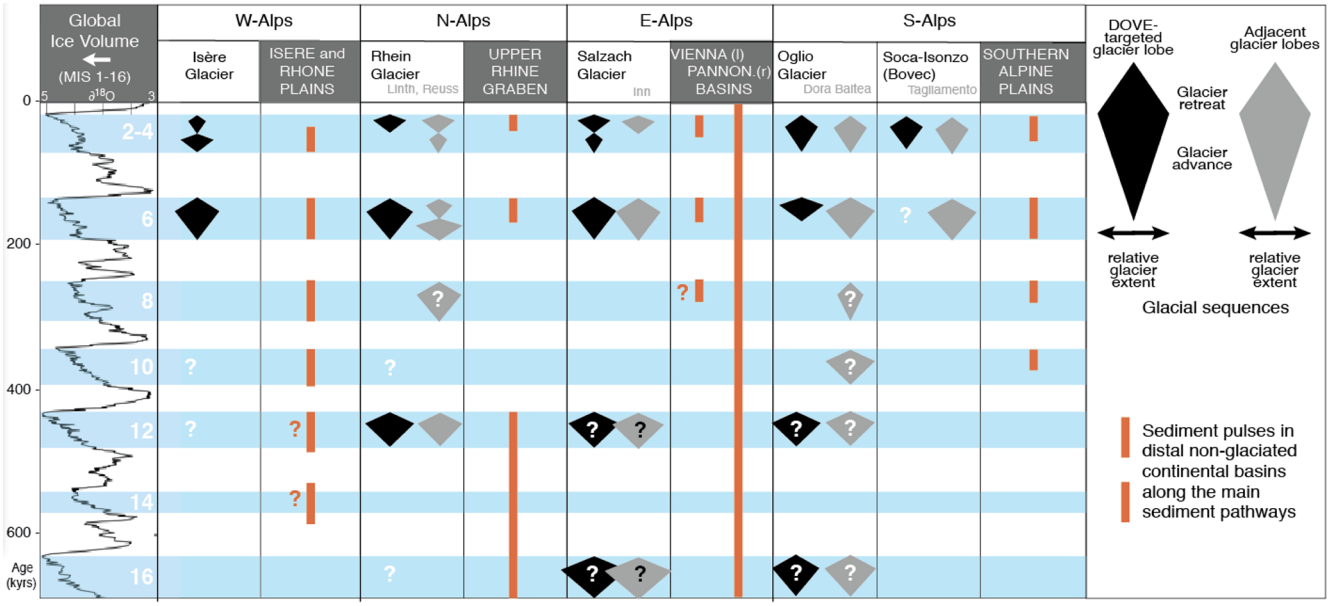

Figure 2. Present knowledge of the Quaternary glacial history of the Alps. Correlation of glaciation evidence with marine isotope record (Lisiecki and Raymo, 2005) is tentative; i.e., there is partly little confidence in presence and age as indicated by unfilled time spans and "?". "Adjacent glacier lobes" indicate glacial catchments not directly targeted by DOVE but in the same Alpine domain that likely responded in a similar manner. Data for W-Alps: Mandier (1988), Nicoud et al. (2002), and Buoncristiani and Campy (2011); N-Alps: Preusser et al. (2011), Ellwanger et al. (2011), and Dehnert et al. (2012); E-Alps: Gabris and Nador (2007), van Husen and Reitner (2011), and Salcher et al. (2012); S-Alps: Bavec et al. (2004), Scardia et al. (2006), Pini et al. (2009), and Gianotti et al. (2015).

borehole data with surface geophysics is desired. Investigation of overdeepened phenomena in the densely populated Alps is hence timely from both a scientific and applied perspective.

2 Objectives of the drilling program

On 3–4 April 2013, the ICDP Workshop DOVE "Drilling Overdeepened Alpine Valleys" was held at Villa del Grumello, on the southwestern shore of Lake Como (northern Italy), followed by a field trip on 5 April 2013. The meeting, organized by CNR–IDPA Milan, was attended by 46 scientists from nine European nations (Austria, Denmark, Germany, France, Italy, Slovenia, Sweden, Switzerland, and the

Netherlands) and the USA. The outcome of the workshop was a series of hypotheses and scientific questions as well as a drilling strategy for the DOVE drilling program, consisting of a novel approach by investigating several complementary sites along the foreland around an entire mountain range. In the Alps, geophysical surveys and previous boreholes provide a comprehensive picture of the distribution and geometry of overdeepened structures that is not available for any other mountain range. However, available borehole descriptions are not detailed enough for thorough sedimentological interpretation. Furthermore, dating the sedimentary infill has not been possible until very recently, due to the lack of suitable methods. By using a multidisciplinary approach to decipher sedimentary facies and past environmental conditions, and in combination with state-of-the-art dating methods, DOVE will address the following major scientific questions.

- (Q1) What were the timing and extent of past Alpine glaciations?

  The questions of how many glaciations occurred in the Alps and when they started are highly controversial but of fundamental importance to understand the Quaternary dynamics of natural climate and environmental change. Investigating cores will provide major new insights, as they comprise sediments and erosional features that are rarely accessible in outcrops. Furthermore, the timing and extent of past glaciations could vary substantially along and across the Alpine arc. To date, very few projects have applied multidisciplinary approaches, and collaboration between scientists from different regions has been rather limited. Consequently, only an international initiative comprising various case studies on the scale of an entire mountain range will yield sufficient ("non-local") homogenous information. The key will be to identify cycles of erosion, glacial deposition, and post-glacial infill by carrying out sequence stratigraphy, establishing reliable age control, and relating them to regional and global records (i.e., marine isotope stages, MISs).

- (Q2) How did atmospheric circulation patterns control ice flow across the Alps?

  During glacial periods, the Alps were situated in a particular setting with regards to past atmospheric circulation, and a southward shift of the polar front turned the northern foreland into an Arctic desert, while the southern foreland still received sufficient precipitation to support local forests. This likely caused substantial differences in glacial advances, on both temporal and spatial scales that are still poorly understood (e.g., Luetscher et al., 2015; Monegato et al., 2017). Hinderer et al. (2013) suggest that higher humidity led to stronger glacial conditioning and topographic accentuation of the Western Alps, which is reflected in a modern erosion rate approximately 3-fold higher, with respect to the Eastern Alps. Comparison of the timing and extent of past glaciations through multiple boreholes around the Alps will provide new insights into the regional temperature and precipitation conditions and the related changes in circulation patterns at the temporal scale of several glacial–interglacial periods. The evidence of varying area-specific precipitation patterns collected in this project will then allow for reconstruction of moisture pathways during past glacial periods that will be cross-checked with climate and ice-flow models (e.g., Seguinot et al., 2018).

- (Q3) How were mountain ranges and their foreland shaped by repetitive glaciations?

  There is a gap between established timescales of post-glacial sediment transfer and exhumation rates that prohibits elucidating the response of erosional systems to repeated glaciations (Wittman et al., 2007; Salcher et al., 2014, 2021). An expanded circum-Alpine chronology of Quaternary sediments will fill this gap, identify times of high and low erosion rates, and compare them with climate forcing and with the timing of the topographic evolution of the Alps. Repetitive glacial loading and unloading may have caused a flexure of the lithosphere and/or reactivation of basement faults, thus affecting long-term landscape evolution. While numerical modeling provides a useful tool to estimate slip rates along major faults, it needs to be validated by geological records, in order to localize and quantify deformation. The influence of peripheral lithospheric forebulges and ice loading on the reactivation of faults and structures will be evaluated in the context of landscape evolution on glacial–interglacial timescales. Investigating the bedrock contact will help to illuminate the process of overdeepening. Observations so far have distinguished simple or multiple-phase bedrock-erosion surfaces that are characterized sometimes with pieces of dislocated bedrock and/or massive diamicts (LGRB, 2015). DOVE will build upon these results with systematic investigations and by integrating sedimentological and geophysical data.

DOVE will be accompanied by a series of geophysical investigations, before and after the coring, that will be carried out to extend the punctual information provided from boreholes into 2D/3D. In the last years, the sites Tannwald and Basadingen were already covered by high-resolution reflection seismic surveys that imaged a rich seismic stratigraphic architecture of the trough fill and allowed for ideal drill-site location (Burschil et al., 2018, 2019, 2020; Brandt, 2020). Additional geophysical exploration work, comprising com-

plementary methods and investigations at other sites, will be closely linked to borehole information. Thus, DOVE will contribute to a deeper insight into the origin of geophysical signatures. For instance, it can be studied how major unconformities, which are related to the general development of overdeepened structures, are imaged in reflection seismic data (e.g., Büker et al., 1998; Burschil et al., 2018) or how depositional environments are imaged by different seismic facies (e.g., Büker et al., 1998; Reitner et al., 2010). In addition, electrical resistivities can distinguish between different sediment facies (e.g., Rumpel et al., 2009; Reitner et al., 2010). Geophysical surveys will allow for upscaling of the parameters gained in the boreholes to the entire valley extent using structural constraints and geostatistical information for geophysical inversion and contribute towards a better understanding of valley formation and sedimentological processes. This knowledge will also help to improve the interpretation of data from sites where no boreholes are available.

Within DOVE, a series of additional research goals is also foreseen:

1. It is planned to investigate, through pollen analysis, changes in Alpine vegetation structure, plant biodiversity, and phylogeographic patterns, which are likely driven by glacial–interglacial cycles and region-specific climate variability. Within the first DOVE phase, the target is to identify suitable sections in the cores by screening for the biotic content (pollen grains, spores, pollen slide charcoal fragments, algae, and other organic particles).

2. This project also provides the unique opportunity to identify present-day subsurface biological activity (cf. Lee et al., 2010), which will be addressed in more detail, depending on the results of the screening.

3. Once the data acquisition part of the overall DOVE project has reached an advanced stage, separate projects will address modeling landscape response, glacial erosion, and climate.

3 Proof of concept: the Niederweningen site

DOVE uses a multi-method approach by combining geophysics, core sedimentology, laboratory sediment characterization, geochronology, and biological proxy (mainly pollen) that has seen little application in glacial settings so far. To prove the suitability of this concept, a pilot study is described here in some detail that has been executed on cores from Niederweningen (Figs. 3, 4 and 5). This village, located north of Zürich in northern Switzerland, is well known for its rich finds of Pleistocene faunal and floral remains, including several bones of wooly mammoth (Furrer et al., 2007). It is located just 2 km outside the maximum limits of the last glaciation of the foreland (Fig. 6). The gentle valley of Niederweningen is embedded between the easternmost spur of the

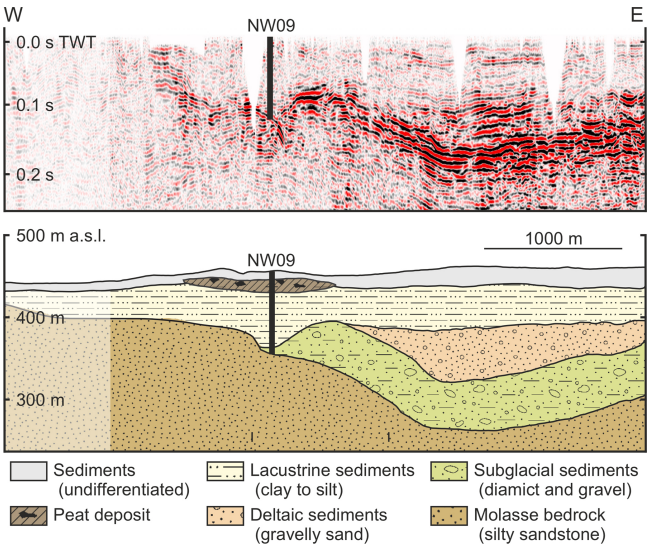

Figure 3. Top: seismic survey data along a NW–SE profile parallel to the main valley axis. Bottom: sedimentary facies model of the overdeepened trough of Niederweningen (modified after Dehnert et al., 2012).

Jura Mountains to the south (buildup of limestone) and a ridge of Molasse sandstone to the north, which is covered by older Pleistocene glacial deposits. After a first core with a length of 30 m was investigated (Anselmetti et al., 2010), reconstruction of the sedimentary history was executed on a second 93.6 m deep scientific drilling (Dehnert et al., 2012). First, a sedimentary facies model of the subsurface was constructed, based on seismic surveys conducted using an explosive source (Dehnert et al., 2012) and a number of available geotechnical drill holes (Fig. 3). This revealed the presence of a trough carved into Molasse bedrock, reaching almost 200 m below the present surface. As the eastern part of the trough is apparently filled by subglacial deposits and deltaic sediments, the longest sequence with lacustrine deposits was the target of coring using a combination of rotary and of percussion drilling techniques. A large coring diameter of 326 mm was used at the surface part, slimming down to 145 mm at the bottom part of the core. The applied coring techniques allowed for an almost complete recovery and excellent quality of the cores.

After drilling, the liners were cut into 1 m segments and split. The surface of one half-core was carefully prepared, digitally photographed, and described macroscopically to define lithotypes and stratigraphic units. Smear slides (two for each 1 m segment) were prepared to identify the major lithologic constituents, and shear strength was measured every 30 cm using a manual Eijkelkamp vane shear device. The second half-core was used for further subsampling and U-channel extraction. The latter were used to measure bulk magnetic susceptibility and wet bulk density (gamma-ray-based ^{137}Cs source) with a multi-sensor core logger (MSCL).

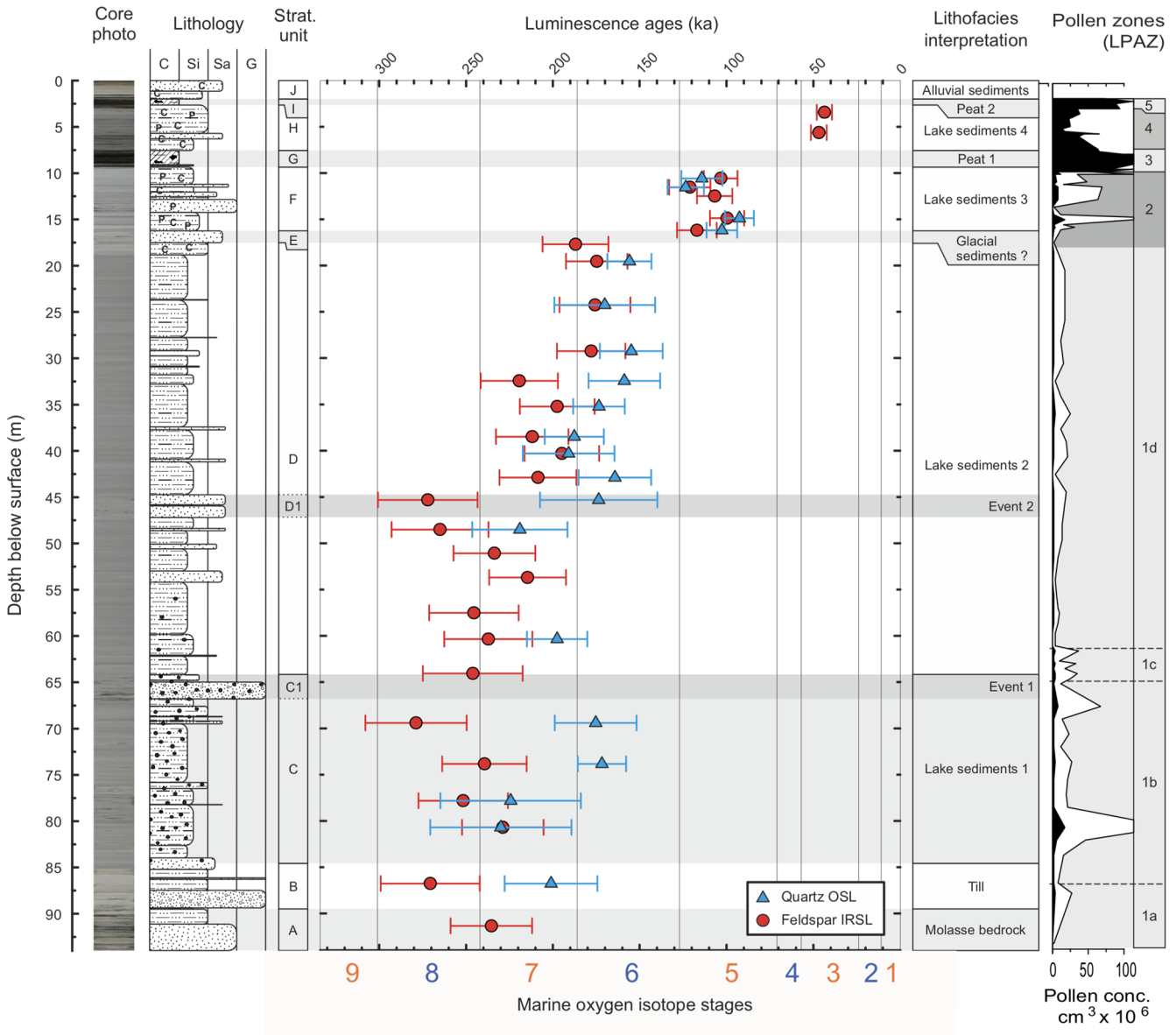

Figure 4. Core photograph, grain-size coded stratigraphic column, geochronology, and interpretation of depositional environment of the Niederweningen site (modified after Dehnert et al., 2012) with indicated marine isotope stages at the bottom (Bassinot et al., 1994) and lithofacies interpretation of the stratigraphic units. Pollen concentration data are shown on the right: white areas represent exaggeration × 10 of the pollen concentration curve. LPAZ indicates local pollen assemblage zones: LPAZ 1 – reworked pollen; LPAZ 2 – Alpine meadow, initial phase of Late Glacial reforestation; LPAZ 3 – Eemian or second Early Würmian interstadial; LPAZ 4 – increasingly inundated by water; LPAZ 5: very wet Cyperaceae/moss peat.

Laboratory analyses included determining total inorganic carbon, total organic carbon, total sulfur, and total nitrogen content as well as laser optical grain-size measurement. The U-channel material was also used to measure the directions and intensities of the natural remanent magnetization. A total of 372 sediment samples were taken, of which 99 were analyzed for their pollen content. From the consolidated (lacustrine) sediments, where the inner parts of the core had not been exposed to light, 29 samples were taken for luminescence dating. The nature of the sediment required application of the fine-grain technique (using silt-size grains 4–11 µm; cf. Preusser et al., 2008). Both optically stimulated luminescence (OSL) of the quartz and infrared stimulated luminescence (IRSL) of the polymineral (feldspar) fraction were used for dating.

The macroscopic description in combination with laboratory sediment analyses allowed for the identification of 10 lithological units within the core (A–J in Fig. 4). This com-

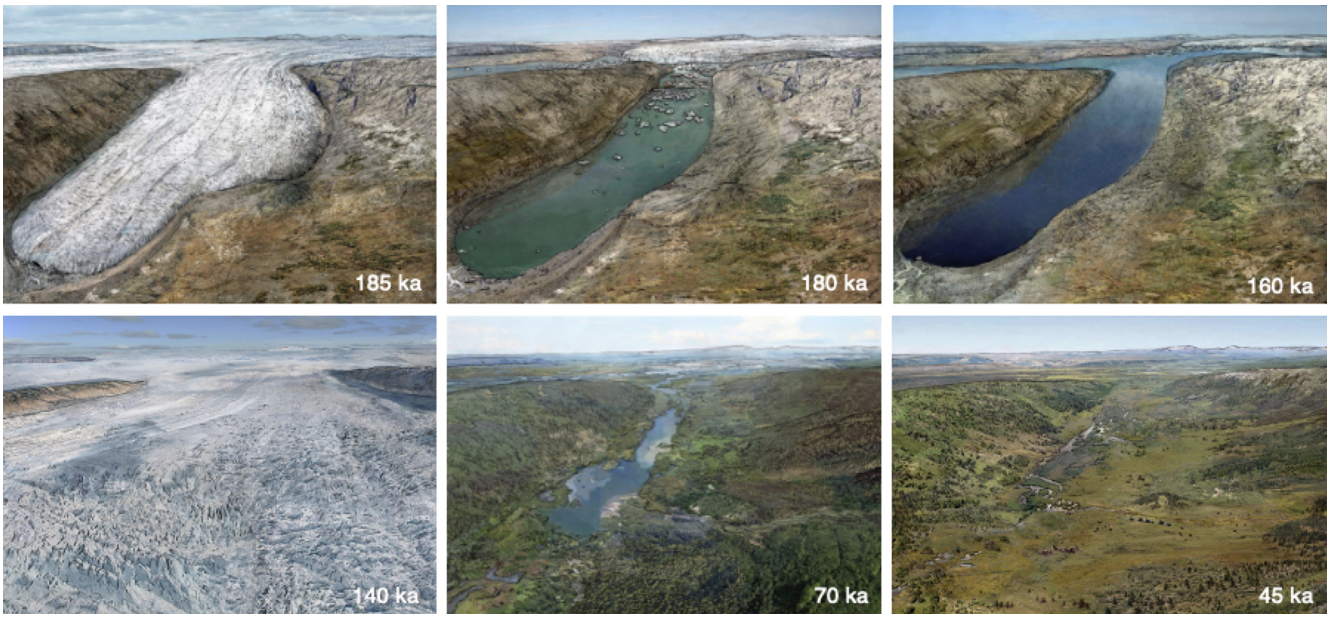

Figure 5. Landscape reconstruction with glacial advance and retreat sequences, based on drill-core analysis at Niederweningen (modified after Dehnert et al., 2012).

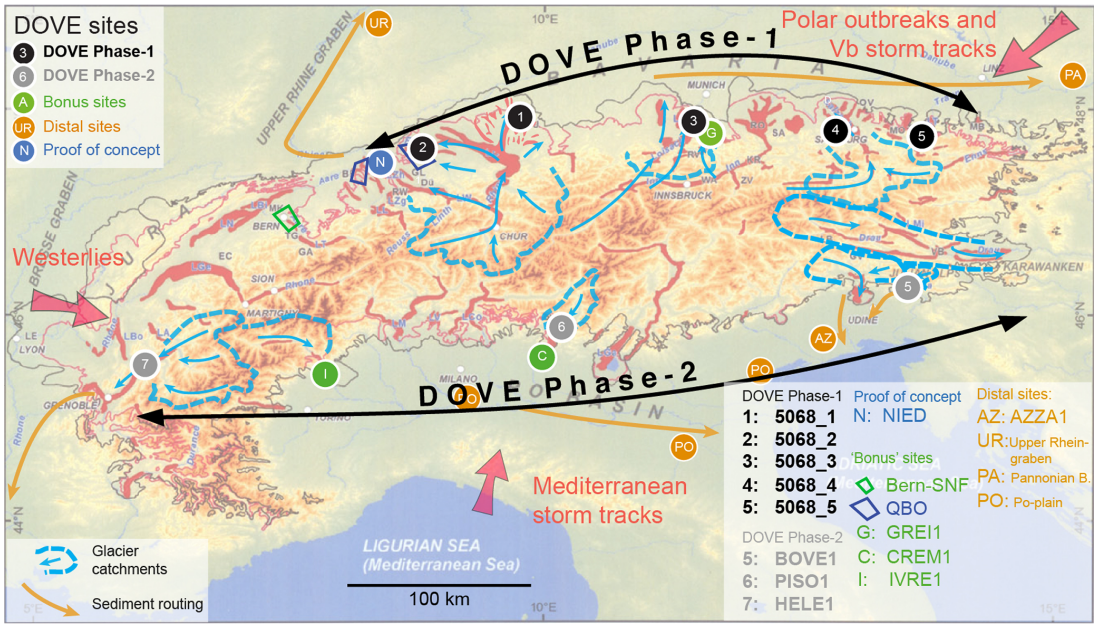

Figure 6. Location of primary DOVE Phase 1 sites (black), Nagra QBO sites (11 sites within the blue areas), Phase 2 sites (grey), and bonus sites (green) in the Alpine region, with limit of the Last Glacial Maximum (pink line), maximum limit of Pleistocene glaciation (black line), location of overdeepened structures (red) and pathways of major moisture sources (red arrows) (after Preusser et al., 2010). Indicated are glacial catchments related to the drill-site areas (dashed blue lines) and main paleo-ice-flow directions (blue arrows). Orange circles indicate distal continental basins that lie in the fluvial sediment pathways (arrows) and provide a more continuous but indirect record of glaciations.

prises direct glacial (till) and proglacial lacustrine deposits as well as peat and alluvial sediments in the upper part of the sequence. The lithological units were attributed to certain facies based on general appearance and characteristic properties such as the state of consolidation and the presence of drop-stones. Pollen extracted from the sediments has a good to excellent stage of preservation and allows five main local pollen assemblage zones to be defined, including some sub-zones (Fig. 4). The luminescence ages reveal some scatter and offset between OSL and IRSL ages, the latter being

mainly higher than the first. This can be explained by the presence of partial bleaching, leading to overestimation of the IRSL age estimates (Dehnert et al., 2012). Hence, the chronology is based on the quartz OSL ages, in combination with information derived from palynology and sediment properties (i.e., unconformities).

The entire dataset gathered during the project was integrated and eventually transferred into visual snapshots of the environmental history, carried out by artists that were advised by members of the scientific team (also available online at http://www.mammutmuseum.ch, last access: 24 September 2022). Figure 5 shows visual snapshots that summarize the glaciation and environmental history of the region, as deduced by the full suite of drill-core analysis. The earliest phase recorded is till resting directly on top of molasse bedrock, which indicates that the glacier either carved out a new basin or at least completely removed all previous Quaternary deposits. Melting of the ice body is reflected by lake sediments, showing the transition from a proximal, dropstone-dominated facies towards a more distal facies, dominated by silty dropstone-free deposits. According to quartz OSL ages, the area became ice-free around 180 ka. Two breaks in sedimentation are observed within the lake deposits and have major implications for the glaciation history of the area. The first break is identified by disturbed sediment structures, a gradual increase in shear strength, and an offset in both the OSL and IRSL ages. The latter imply this event dates to ∼ 150–140 ka, which is interpreted as the grounding of ice by a cold-based glacier (Dehnert et al., 2012). The second break in sedimentation is indicated by the absence of thermophile pollen that represents the Last Interglacial (Eemian), in concert with a gap of some 10 000 years recorded in the age data (Fig. 4). Luminescence dating and palynology point towards the deposition to be attributed to the second Early Würmian interstadial (Odderade). However, it is not clear whether the gap represents either no deposition or an erosional phase. The upper part of the sequence is composed of peat dated to ∼ 45 ka, hence representing the layer dated in outcrops (Hajdas et al., 2007; Preusser and Degering, 2007) and accompanied with faunal remains (Furrer et al., 2007). The environment is interpreted as wetlands, which represent the final phase of lake development that is finally covered by alluvial deposits transferred downslope during periglacial conditions (Fig. 5). While these artistic reconstructions are based on evidence observed at the site and its surroundings, the visualization includes a certain degree of interpretation.

4 DOVE approach

The DOVE program is designed to be executed in two phases (Fig. 6), with Phase 1 comprising boreholes along the Northern Alpine front and Phase 2 targeting the western and southern margin of the Alps, thus allowing for a complete trans-Alpine dataset. Eventually, a series of drilling and research proposals were funded and integrated with activities investigating the storage of nuclear waste disposals in the Swiss Alpine foreland (National Cooperative for the Disposal of Radioactive Waste) as well as with the geological surveys of Austria, Baden-Württemberg, and Bavaria. Funding granted by ICDP and other partners in 2021 allowed the drilling of two sites (5068_1 (TANN) and 5068_2 (BASA)) and the revisiting of three legacy cores previously drilled at two sites in Bavaria (5068_3 (SCHA) and 5068_4 (FREI) and in an inner-Alpine overdeepening (5068_5 (BADA)). Information from these sites will be complemented by similar drilling programs in glacial overdeepenings in northwestern Switzerland (Fig. 6; QBO – Quaternary drill holes: Gegg et al., 2021; SNF-Bern: Schwenk et al., 2022), and DOVE Phase 1 will eventually comprise more than 20 sites. In addition, ICDP has indicated they will provide funding for the remaining four DOVE sites along the southern transect (DOVE Phase 2), if DOVE Phase 1 is successful and matching funds can be secured.

4.1 ICDP Site 5068_1 (TANN)

Site 5068_1 is situated to the north of Lake Constance, in an area previously covered several times by ice of Rhine Glacier but outside the limits of the last glaciation (Figs. 6, 7). A research drilling in the area carried out in the early 1990s, located ∼ 1300 m south of Site 5068_1 and described in Ellwanger et al. (2011), reached molasse bedrock at a depth of ∼ 209 m. The sequence comprises 13 m of allochthonous molasse underlain by gravel and diamicts of presumed subglacial origin. The ∼ 150 m on top represents bottomsets, which turn into foresets of a lake filling sequence. The middle part of the fine-grained sediments contains pollen reflecting the Holsteinian Interglacial, which implies the formation of the basin is assigned to the Hosskirchian glaciation (Ellwanger et al., 2011).

Detailed geophysical surveys have contributed to decipher the geometry of the overdeepened structure (Fig. 7; Burschil et al., 2018) and to define the drilling location of Site 5068_1. Drilling began on 6 April 2021 and finished on 3 December 2021. Two flush boreholes (5068_1_A+B) and one core drilling (5068_1_C) were drilled to depths of 163, 155 and 165 m, which reached the base of the Quaternary valley at 153, 154, and 155 m, respectively. The reason for the three boreholes being just 28–40 m apart, which were all subsequently finished as wells with 80 mm PVC casing, is their availability for cross-hole seismic experiments as well as water sampling. The core drilling began using a ramming system, but, especially in the upper 40 m, it was found that either the crown of the corer wore down very quickly or/and a large number of hammer counts were made to achieve a meter of core. Finally, after trying unsuccessfully to ram through highly consolidated sand at 82 m, the coring method was changed to rotary coring. The core drilling took nearly

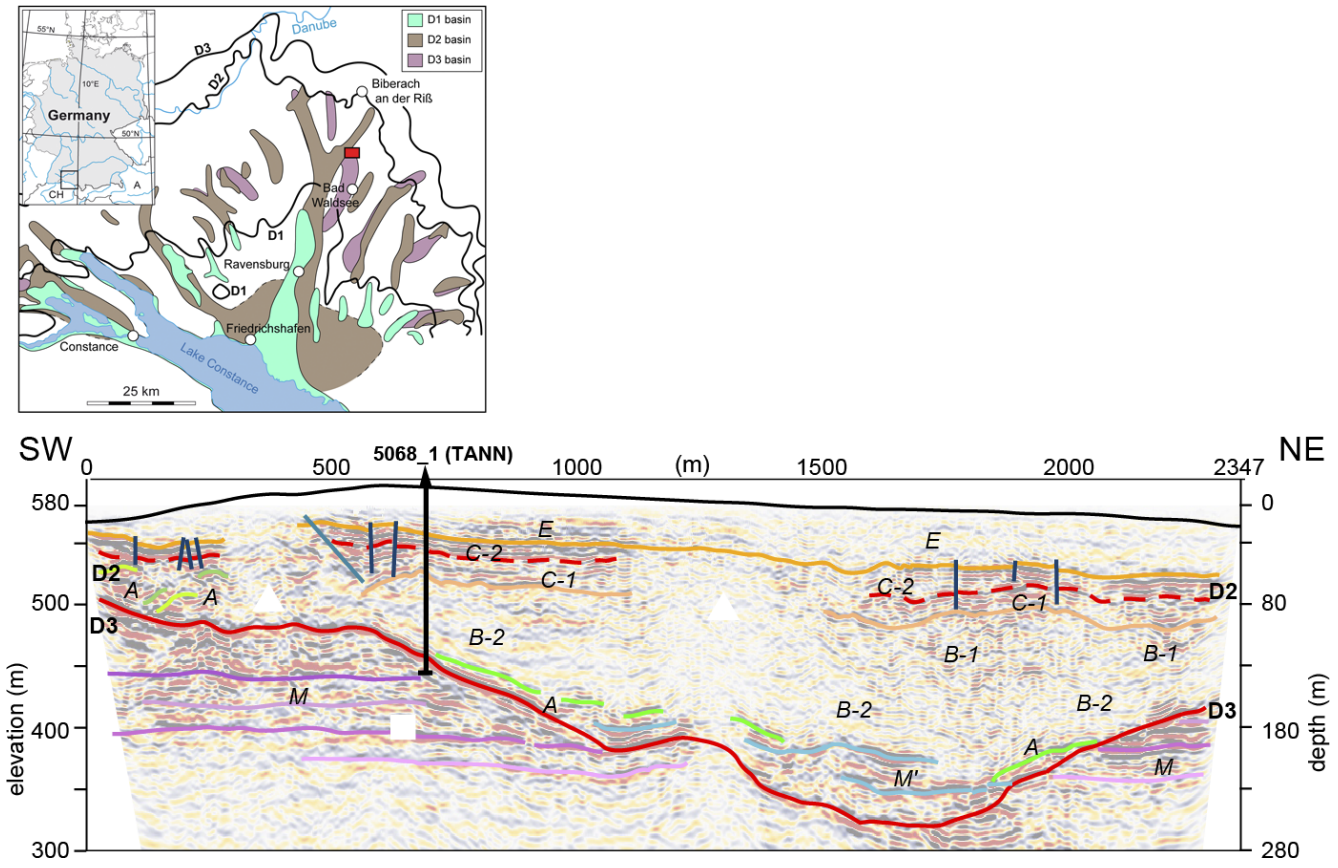

Figure 7. Top: maps displaying the location of the DOVE Phase 1 site 5068_1 (TANN) with relation to different generations of overdeepened basins (after Ellwanger et al., 2011). Bottom: interpreted seismic section and superimposed interpretation of profile 1 across the Tannwald basin (from Burschil et al., 2018). Elevation (black line) and faults with offsets > 2 m (dark blue). D3 (base of basin) and D2 are regional discontinuities that separate major sedimentological units. Seismic facies: M upper freshwater molasse, M' allochthonous molasse, A lodgement till, B basin fines, C till sequence, and E fluvial deposits.

15 weeks. Drill cores were recovered and stored in opaque PVC liners. During the core drilling, the core catchers were sampled for noble-gas analysis, and geomicrobial samples were taken to study the deep biosphere.

The core-catcher-based lithologic succession (Fig. 8) shows the upper ∼ 39 m of Hole 5068_1_C consisting of coarse gravelly and partly diamictic sediments interpreted to partly represent direct ice contact from an overriding Rhine Glacier. This coarse succession is underlain by finer grained clayey–silty sediments with occasional sandy layers. These fine-grained lithologies extend downcore to 143 m and are interpreted to have been deposited in a lacustrine setting. From there to the bedrock contact at 159 m, variable lithologies including diamictic and gravelly layers indicate again an ice contact at the base of the overdeepening. Overall, the succession confirms that the trough and its filling represent multiple glacial stages, as supported by the seismic data (Fig. 7).

4.2 ICDP Site 5068_2 (BASA)

Drill site ICDP 5068_2 is located on the Basadingen trough, which is part of the local overdeepened channel system that was formed by the Rhine Glacier during multiple Middle–Late Pleistocene glaciations (Figs. 6, 9). A seismic survey in 2019 (Brandt, 2020) revealed a narrow valley with steep flanks that reaches a maximum depth of up to 300 m (Fig. 9). The seismic sequence analysis indicated a multiphase stacked sedimentary fill, which was targeted with the selected drill site near an old flush drilling from the 1980s. Drilling operations took place from 25 May to 13 October 2021. The final depth of 253 m was reached using a combined approach of percussion drilling in the upper 60 m and a triple-tube wireline setup below. Bedrock was not reached, but bedrock fragments occurring towards the lowermost meters of the drill core indicate close proximity to the base, as supported by the seismic data. All drill cores were recovered and stored in opaque 1 m long PVC liners. Immediately after recovery, sediment samples were taken from selected cores from the core catchers for geomicrobial and noble-gas pore-

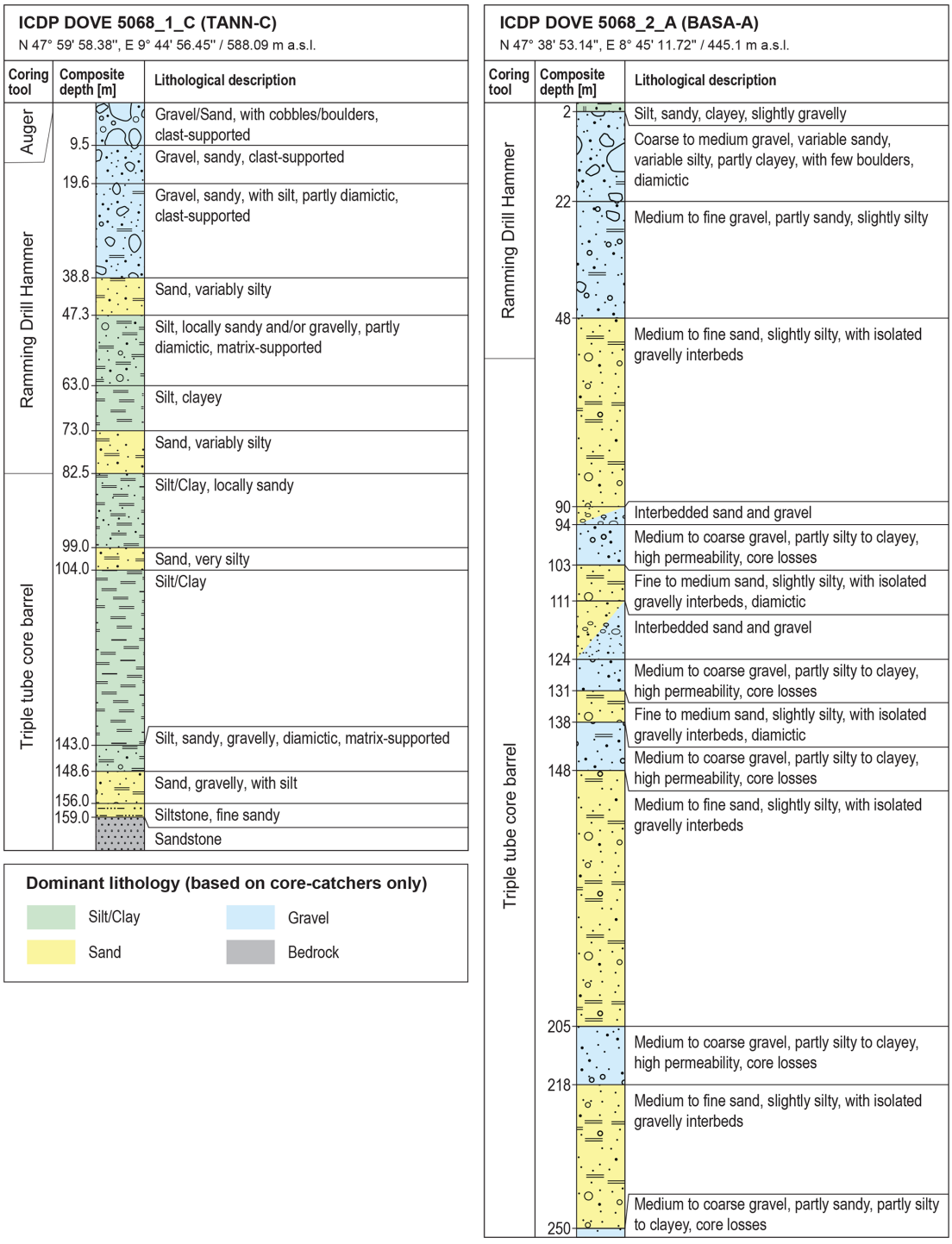

Figure 8. Core-catcher-based lithologic logs of ICDP Site 5068_1_C (Tann-C) and 5068_2_A (Basa-A) with indications of drilling technologies.

water analysis. Afterwards, all cores were sealed with caps and labeled and scanned on-site with a MSCL for wet bulk density, magnetic susceptibility, P-wave velocity, and natural gamma radiation. After scanning, the cores were transported to the University of Bern, where they will be stored at 4 °C until opening. When drilling operations were completed, a comprehensive wireline logging campaign was carried out in the borehole.

A first core-catcher-based lithologic succession (Fig. 8) of Hole 5068_2_A shows a complex stratigraphy with nu-

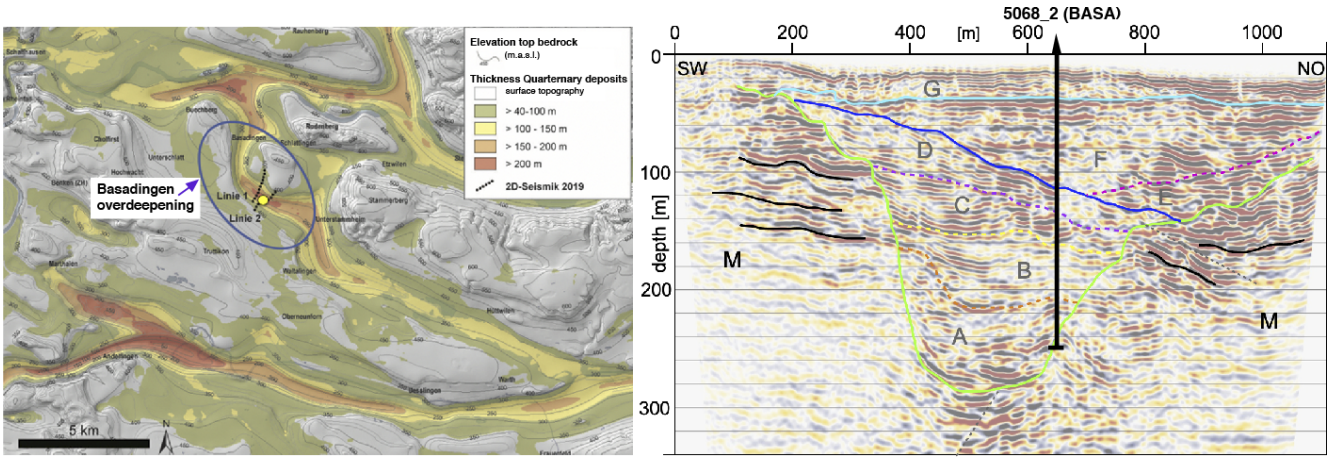

Figure 9. Left: location of primary DOVE Phase 1 site 5068_2 (BASA; yellow dot) in the overdeepened trough with a sediment thickness of up to 300 m (bedrock model by Pietsch and Jordan, 2014). The parallel and partly crosscutting overdeepenings likely represent glacial erosional pulses of different ages. They all belong to the western lobe of the Rhine Glacier. Right: seismic Line 2 crossing the Basadingen trough (Brandt, 2020). Note the complex Quaternary sequences (A–G) composing the trough-filling stratigraphy. Bedrock (M) is at ∼ 255 m depth.

merous changes between coarse gravelly and partly diamictic sections with sandy lithologies. Only minor amounts of silty lithologies are observed in the core catchers, indicating a rather ice-proximal depositional environment throughout the trough infill. In general, as at Site 5068_1, these initial results and observations support the seismic interpretation, i.e., the occurrence of the proposed multiphase glacial cycles. However, detailed analysis of the cores with a wide range of different proxies, core log, and wireline log data will help to refine the depositional and chronostratigraphic interpretation.

4.3 ICDP Site 5068_3 (SCHA)

This location is situated at the northern edge of the former Isar-Loisach Glacier, just within the limits of the maximum ice extent of the last glaciation. Overdeepening in the region was investigated by Jerz (1987), who identified a basin structure below the present town of Wolfratshausen and adjacent glacial basins in its surroundings. In order to better constrain the detailed shape of these glacial basins, the relative position of the core within the basins and its depositional structures, further geophysical data will be acquired by the Leibniz Institute of Applied Geophysics (LIAG).

Drilling was performed in 2017 by the Bavarian Environment Agency (LfU) and recovered 198.8 m of core. Coring operations had to be stopped for financial reasons, but the base of the Quaternary is assumed to be near the base of the core at ∼ 200 m below the surface. The preliminary sedimentological logging of the core was based on cuttings and investigated the top and bottom parts of the sections. According to these observations, the upper 15 m of the core consist of till, followed by ∼ 100 m of gravel of presumably Rissian and Mindelian age. The lower part of the sequence comprises basin deposits (mainly silt), which is tentatively correlated with either the Mindelian or Günzian glaciation. The cores remained closed until July 2021, when DOVE investigations started. First, all closed cores were scanned at the facilities of the Federal Institute for Geosciences and Natural Resources (BGR) in Berlin Spandau. Subsequently, the cores were cut into two half sections and transported to the sampling repository of the LfU in Hof (Bavaria). Based on the first analysis of core cuttings, the infill of the Schäftlarn Basin spans several glacial cycles. Very recently (late November to early December 2021), the detailed core logging and first sampling of the sequence was started by the DOVE team in the core repository. In 2022, the whole sequence will be sampled and investigated.

4.4 ICDP Site 5068_4 (FREI)

This site is located near the border between Germany and Austria, in an area formerly covered by ice of the Salzach foreland glacier. The research drilling was carried out by the Bavarian Environmental Agency (LfU) in a Quaternary branch basin that was diverted from the main Salzach Glacier basin to the NW. The drilled sequence was first described by Fiebig et al. (2014). The drilling sequence covers 136 m of cores; the Quaternary base was reached at 116 m below the surface. A distinct discontinuity in sedimentation was discovered at ∼ 25 m depth below surface. First age dating was conducted using quartz- and feldspar-based luminescence dating techniques (Fiebig et al., 2014). While these investigations yielded a reliable chronology up to 57 ± 6 ka for the part of the core above the discontinuity, methodological limitations prevented a reliable chronology being

established for the part of the core below the discontinuity. Both quartz and feldspar luminescence signals indicated signal saturation, providing only limited age information as all ages beyond 200 ka have to be interpreted as minimum ages. However, methodological progress, especially the development of single-grain luminescence dating techniques using potassium-rich feldspar, may now provide better age control for the older part of the core, with first tests conducted at the Vienna Laboratory for Luminescence dating (VLL) showing promising results. To create a cross-check and an overlap of independent dating methods, additional samples from the lower fine-grained part of the drilling will also be investigated using cosmogenic isotopes.

In addition to the numerical dating approaches, the core will also be reinvestigated in detail with regard to sedimentology, especially including a detailed analysis of the laminated fine lake sediments to further improve the knowledge about the infill and environment of the Pleistocene lake of Freilassing/Neusillersdorf in the Salzach foreland glacier area. Further unconformities in the sequence will be especially addressed by sediment logging and dating in 2022.

4.5 ICDP Site 5068_5 (BADA1)

This site is located in the former Traun Glacier area, inside the limits of the Alps and ∼ 80 km SE of the site 5068_4. The core was first described by van Husen and Mayer (2007) and was subdivided into two sections, with the upper section comprising ∼ 200 m of cover sediments (including glacial diamictons and coarse gravels – interpreted as "Vorstoßschotter" – below) and the lower section consisting of ∼ 700 m of lake sediments from a glacial delta situation. Based on geophysical data (Steinhauser et al., 1985), the Quaternary basin – situated in the midst of the Austrian Alps – is about 1100 m deep and thus reaches a depth below surface comparable to the present-day level of the Dead Sea. Van Husen and Mayer (2007) proposed the formation of this very deep trough below Bad Aussee to be related to dissolution of Alpine salt deposits that are mined near by. A scientific investigation concerning the chronology and mechanism of formation is planned. A new geophysical survey to resolve underground geometry is planned by the Leibniz Institute of Applied Geophysics (LIAG) to investigate the geometry of this dramatically overdeepened structure. The core will be sedimentologically reinvestigated during sample retrieval for age dating starting in early 2022. The start of detailed logging of the cores and sampling for luminescence and cosmogenic dating began in January 2022.

5 Scientific analysis

5.1 Geophysical investigations

Data retrieved from drill core or borehole logging data provide important, vertically highly resolved information of the valley fill but only for a limited spatial region. Geophysical measurements are able to project the borehole information (lithology, stratigraphic contacts, and physical properties) into cross-sections and longitudinal sections of overdeepened valley structures. This has already been done by P-wave reflection seismic data for 5068_1 (Burschil et al., 2018) and 5068_2 (Brandt, 2020), providing a very good resolution to image the valley base and some prominent unconformities. For 5068_2, S-wave data (Burschil and Buness, 2020) and two small 3D seismic surveys (P- and S-waves) were also carried out (Buness et al., 2020, 2022; Burschil and Buness, 2020; Burschil et al., 2020, 2022). Aiming to compare the different sites and, thus, catchment areas, 2-D seismic P- and S-wave surveys at the 5068_4 and 5068_5 site are envisaged.

5.1.1 Geophysical downhole logging

For most of the main DOVE and bonus sites (at the legacy sites 5068_3, 5068_3_4, and 5068_3_5, the borehole are not accessible anymore), a geophysical logging program acquired the spectral natural gamma radiation, electrical resistivity, magnetic susceptibility, and acoustic velocity (sonic) logs of the sediments. At the 5068_1 site, further parameters were logged, for example, porosity and density. Depth control and correction of core deformation that results from the process of coring itself (stretching and compression, core loss) will be achieved by comparing data from the multisensor core logger with logging data. Therefore, composite lithological profiles of the borehole sites, based on high-resolution core measurements and wireline-logging data, will be used to characterize and interpret the depositional sequences at the individual sites. Advanced geostatistical methods, such as factor and cluster analysis, will support sediment characterization and correlation, especially where complete coring cannot be obtained (Hunze and Wonik, 2009; Hunze et al., 2012; Baumgarten et al., 2014).

The characterization and interpretation of petrophysical properties include sediment composition and textures, cyclicities (if analyzable), and sequence stratigraphy. Gamma ray, magnetic properties, and porosities, etc. are sensitive to changes in clay content and grain size and thus can provide direct textural information; the significance of specific parameters as a proxy for climate or environmental change in these highly dynamic systems needs to be evaluated. The complementing approaches help to identify unconformities and glacial sediment boundaries. The dipmeter, if deployable, provides information about the orientation of sedimentary structures and thus might help to better understand the sedimentation processes. For selected borehole sections, the acoustic borehole televiewer may provide insight into sediment structures. Vertical seismic profiling (VSP) ties borehole information to the acquired surface seismic data. The compaction of the sediments caused by sediment and glacial load will also be analyzed with information from the logs. For instance, trends in compaction might be

related to individual glacial cycles. Based on the basic data and derived lithologs, the sediment characteristics of the various drill sites can then be compared with data from existing boreholes and surface geophysics and correlated to identify lateral variations of the sedimentary facies. Finally, the logging data will help to improve the interpretation of surface geophysical data.

5.1.2 Seismic cross-hole tomography

At the 5068_1 site, seismic tomography experiments, funded by the Deutsche Forschungsgemeinschaft, will help to reveal sediment properties and the sedimentation processes during the fill of the basin in more detail. Sedimentation processes may generate an anisotropic sedimentological setting. Different mechanisms that lead to seismic anisotropy of the sediments can be (1) fine layering, (2) clast alignment of fluvial sediments, (3) glacio-tectonic overprint, and (4) overconsolidation by glacial loading. Since seismic near-surface methods lack the resolution of seismic anisotropy to date, we conduct the seismic cross-hole experiment. Site 5068_1 provides a unique opportunity and the ideal setting of three boreholes ($\sim$ 160 m deep) at optimized distances of 28–40 m for such an approach. For the experiment, different source systems that are able to generate P-waves as well as differently polarized S-waves will be deployed. Polarization analyses will give evidence of shear wave splitting and direct access to anisotropy and allow us to identify the arrivals of different wave types. The first arrivals of each wave type are the input for isotropic travel time tomography between the adjacent boreholes. Isotropic full waveform inversion will further increase the resolution and accuracy of seismic velocities. Since the three boreholes enable a comparison of three azimuths of the average P- and S-wave velocities for each sedimentary unit, observed differences in the SV- and SH-wave velocities can give information about seismic anisotropy. Using borehole data, core analysis, and sedimentological interpretation, sedimentological and seismic anisotropy will be integrated to derive sedimentation processes. The findings will be included in a methodical assessment of anisotropic VSP and surface data analysis that can be used at other DOVE locations, where only one borehole is present.

5.1.3 Combined inversion of seismic and resistivity data

Geophysical imaging greatly benefits from a combination of methods that are sensitive to different properties. Electrical resistivity is a parameter that is highly sensitive to groundwater salinity, porosity, and clay content and can thus complement seismic images effectively and efficiently. At 5068_1, an electrical or electromagnetic survey is envisaged for this purpose. The limited resolution inherent in the imaging can be overcome using structural constraints in the inversion (Günther et al., 2011; Doetsch et al., 2012). Furthermore, the ambiguities in the imaging of different parameters can be greatly reduced by coupled cooperative inversion (e.g., Ronczka et al., 2017).

5.2 Core description and sedimentology

Initial analysis at the borehole site and the core repository followed standard ICDP protocols: at the 5068_2 site, a MSCL scanner was used, and at 5068_1 and 5068_2 sites, cores were opened and initially described. Available infrastructure ensures core storage in cold rooms and allows for multi-sensor core logging, cutting, scanning, and sampling, which will be carried out in a consistent manner for all drill cores. A general stratigraphy will be established, and all generated data will be uploaded to the mDIS (ICDP Digital Information System). The data will be integrated with well-log, core-log, and site-survey data, so that all scientists can use them for their respective research topics. After the usual moratorium, data will be available for non-involved scientists, who may submit sample requests to the DOVE operational committee, complemented by the repository curator.

Various sediment properties will be collected to reconstruct the depositional history through lithological, geochemical, physical, and geotechnical investigations. To correlate various sites in different catchment areas, the glacially influenced sediment records will be analyzed, interpreted, and integrated by sequence stratigraphic concepts of a glacial sequence that represents a genetic unit formed during an advance and meltdown cycle (Ellwanger et al., 2011; Powell and Cooper, 2002). These sequences will be recognized by identifying characteristic lithological and geophysical signatures. Combined with the geochronological data, this sequence stratigraphic approach will allow us to correlate sites and sediment provenance, thus addressing the key scientific goals. The proximal sites allow us to identify the direct evidence of glacial advances in the record, i.e., erosional surfaces that mark the transition from erosion to accumulation.

5.2.1 Physical and geotechnical properties

The basic sedimentological description generated during the core-opening sessions by the scientific team will be refined by detailed lithological analysis. Cores will be described using standard sediment classification schemes. Grain-size analysis, combined with observations of sedimentary structures, yields information meltwater volume and flow velocity during deposition. Sedimentological data will be integrated with the data from the multi-sensor core-logger comprising wet bulk density, P-wave velocity, magnetic susceptibility, and natural gamma ray (5068_2 only) in order to define a detailed lithological succession and separate it into various lithotypes. Establishing the glacial sequence stratigraphy in particular requires the recognition of unconformities, which relies on a detailed analysis of potential ice-contact sediments (till layers), including their geotechnical properties. Ice-contact sediments are expected at the base of

the overdeepening, where they may be used to reconstruct the mechanisms of bedrock erosion, or within the sedimentary infill, where they can be studied for the mechanisms of basin reactivation. Micromorphological sediment analysis using large thin sections will provide data to evaluate the coupled or decoupled state of the glacier bed that led to the deposition of tills and sorted gravel and sands (Menzies, 2000). This analysis will be matched with X-ray computer tomography of selected half-cores that has proved extremely valuable in analyzing diamictic fabrics and bedrock deformation (Buechi et al., 2017a; Gegg et al., 2020). Glacial sequence boundaries will be identified by investigating the geotechnical properties, such as consolidation state, which is an important parameter to determine whether the sediment was overridden by a glacier. Vane shear testing at regular intervals on the freshly opened surface will provide a quick evaluation of shear strength. Interesting areas may be selected for further geotechnical testing in the laboratory on the basis of the initial measurements. In addition to physico-sedimentological and petrophysical signatures, geochemical and mineralogical patterns provide further criteria to identify major breaks or changes in sedimentation. Total organic and inorganic carbon analysis will be routinely carried out in order to identify potential "warm-climate" lacustrine deposits. Depending on lithology, cores may be analyzed with XRD (X-ray diffraction) for mineralogical patterns and/or XRF (X-ray fluorescence)-scanned for elemental geochemical analysis that may reflect changes in the hydrogeological catchment (Anselmetti et al., 2010; Dehnert et al., 2012). Moreover, provenance studies (heavy mineral analysis and radionuclide compositional analyses) may show changes in the main drainages that could have been triggered by glacial erosion, piracy, or tectonic disturbance.

5.2.2 Screening for biologic proxies

The ultimate aim is to use biogenic remains (e.g., pollen, diatoms) to refine Pleistocene biostratigraphy, the history of mountain life, and the climatic history of the Alps and to trace fluvial erosion and glacial abrasion (reworked biological remains). As previous projects (e.g., Dehnert et al., 2012) have shown, not all fine-grained deposits are suitable archives in this context. In the initial stage we will sample only selected units to test their potential for such analysis. Detailed investigations will be carried out within follow-up proposals, once promising core sections have been identified.

5.3 Sediment dating

A key issue will be to establish reliable and independent chronologies for the different sedimentary records. While biological remains (pollen) may allow us to some extent to determine a stratigraphic setting for the investigated strata, this approach is problematic for the Middle Pleistocene due to the lack of characteristic pollen assemblages. Radiocarbon dating will be applied where appropriate, but most of the scientific questions of this project are very likely beyond its range. Magnetostratigraphy uses the "barcode" pattern of magnetic polarity reversals registered in sediment succession (Opdyke and Channell, 1996). Successful application of magnetostratigraphy to sediments relies on the detection of a number of magnetic polarity reversals or shorter-scale geomagnetic excursions in field intensity, declination, and inclination (secular variations; e.g., Channel, 2006). The main limit of the method is the presence of suitable material, i.e., fine-grained cohesive deposits. To establish a robust chronological framework, magnetostratigraphy will support the application of independent geochronological approaches. The two most promising methods for the present project are luminescence dating and terrestrial cosmogenic nuclides (TCNs). In addition, noble-gas analysis in the porewater might provide information on the age of deposition. We will cross-check results using the three approaches and amend the sampling density as appropriate. Multiple glaciation events and reworking will not substantially reduce the dating accuracy, as recent progress in dating technology allows for the identification of at least the glacial–interglacial period during which sedimentation occurs.

5.3.1 Luminescence dating

This method has already been applied to date the sediment infill of valleys in the foreland of the Alps (e.g., Preusser et al., 2005; Anselmetti et al., 2010; Buechi et al., 2017b). An internal check for reliability is available by comparing ages determined for quartz and feldspar, as the minerals have different physical properties (e.g., Dehnert et al., 2012). Depending on dose rate, standard optically stimulated luminescence (OSL) of quartz and infrared stimulated luminescence (IRSL) of feldspar may be used to date back to about 200 ka. In addition, several luminescence techniques have recently been suggested to be capable of dating older sediments of which the post-IR (pIR)-IRSL method has shown the highest potential to produce reliable ages for the time window back to ∼ 400–500 ka (Buylaert et al., 2012). This approach has also been used in the Upper Rhine Graben, revealing an onset of coarse debris accumulation, presumably related to Alpine glaciations, at at least 450 ka (Preusser et al., 2021).

In general, luminescence ages are associated with uncertainties of ∼ 10 %, and accuracy will be verified by cross-checking different techniques and by comparison with independent approaches; furthermore, interlaboratory comparisons will evidence the reliability of ages. Sampling will be done by using chips of fine-grained material or samples from opaque liners (as planned for all DOVE cores), opened under red-light conditions. Well-established techniques (IRSL/OSL, pIR-IRSL) will be applied using multiple and single-grain approaches and test the performance of different protocols, by carrying out experiments to characterize the luminescence properties (standard tests such as

dose recovery, thermal transfer, thermal stability/lifetime, and fading). Based on age estimates from previous dating studies (partly unpublished), samples from the region can be dated back to at least 200 ka (possibly to 500 ka) using both quartz and, in particular, feldspar-based methodological approaches.

5.3.2 Terrestrial cosmogenic nuclides (TCNs)

The determination of burial ages has been used to successfully assign ages to quartz-rich sediments washed into cave systems, for example, in Switzerland by Haeuselmann et al. (2007a, 2015). In addition, glaciofluvial deposits (Deckenschotter) from northern Switzerland were dated to an age range from ∼ 1 to 2 Ma (Claude et al., 2019; Knudsen et al., 2020). In Slovenia, Mihevc et al. (2016) were able to date pebbles from a cave in conglomerate to ∼ 1.8 Ma. In addition, classical sites of Mindelian and Günzian in the Bavarian Alpine foreland have been investigated and found to be between 0.6 and 2.3 Ma years old (Haeuselmann et al., 2007b). Cosmogenic depth-profile ages have been presented for northern Switzerland (Claude et al., 2017), reaching back to 1.5 Ma. The isochron technique (Balco and Rovey, 2008) will be applied to specific samples collected in the project. The actual dating strategy will depend on the sediment succession of each drill core.

5.3.3 Noble gases in porewater

Environmental tracers in the pore fluids of unconsolidated sediments indicate that the porewater that was incorporated during sedimentation can be quantitatively trapped for up to several 100 ka (e.g., Hendry et al., 2005; Hendry and Wassenaar, 2011; Wassenaar and Hendry, 2000). Recently, Tomonaga et al. (2022) demonstrated that fine-grained sediments in overdeepened valleys may preserve porewater that was trapped during sediment deposition; i.e., the sediments and originally deposited (i.e., co-eval) pore fluid were not "separated" and behave as a closed system. Due to their low retention, radiogenic noble gases such as ^{4}He or ^{40}Ar (produced within the solid matrix by the decay of U and Th or ^{40}K, respectively) accumulate in fluids, such as porewater. Therefore, concentrations of radiogenic noble gases (^{4}He, ^{40}Ar) can yield information not only on the residence time of the porewater, but also on the duration of porewater entrapment and thus on the sediment deposition (Brennwald et al., 2013; Tomonaga et al., 2014, 2017). We aim to test this novel technique to porewaters of aquitards to reconstruct the conditions under which the porewater was embedded in these low-permeable sediments.

5.4 Synthesis DOVE Phase 1

Once the drill holes have been analyzed and information on nature and age of infilling and erosional phases are available, data will be compiled and assembled along the northern Alpine transect of Phase 1. Data from the surrounding non-overdeepened landscape, such as tills, wall moraines, or glaciofluvial accumulations, will be integrated into this concept, offering a morphogenetic land-system approach (Ellwanger et al., 2011; LGRB, 2015; Fig. 6). The identified (a)synchronicities will be interpreted in terms of lateral variability of glacier activities along the front of the Alps over the last glacial cycles back into the Middle Pleistocene. These patterns then will be used as constraints for climate and glacier simulations in order to understand the regional dynamics of past atmospheric circulation patterns and their consequences for ice buildup and glacial variations. This new understanding of paleoenvironmental signatures of the past glacial epochs then will serve as a first milestone that will, if successful, justify the planning of DOVE Phase 2.

6 Conclusions

The ICDP project DOVE will apply a so far infrequently used approach to decipher the origins and environmental context of overdeepened structures in the Alps and their foreland. A key element of the project is investigating a series of drill cores taken from all around the Alps. These will be investigated using unified scientific protocols to allow for direct comparison of the data, which will be stored in online databases. Focus of the first phase of DOVE is the northern foreland of the Alps, where five locations will be addressed in great detail. This comprises the application of classical sedimentological approaches in combination with supporting laboratory analyses (e.g., grain-size determination, micromorphology, X-ray computer tomography). Constraining the age of the sedimentary filling will be done using state-of-the-art geochronological methods, mainly luminescence, TCNs, and noble-gas porewater dating. Suitable sediments will be screened for pollen content that will give insights into environmental conditions but possibly also allow us to establish a biostratigraphy. In addition, two of the recently drilled cores have been sampled to check for potential subsurface biological activity. A key element of DOVE is the application and refinement of geophysical methods that will allow us to identify the subsurface geometry of overdeepened structures. By doing so, this will allow for the upscaling of high-resolution point information gained by analyzing of the sediment sequences of the cores. Once the first phase of DOVE has proven the effectiveness of its approach, it is intended to include cores from the western, southern, and eastern parts of the Alps and by this accomplish a full circum-Alpine approach.

DOVE includes a series of connected objectives. For example, investigating the contact between bedrock and the

basal part of the sedimentary filling is expected to add new insights into the mechanisms of formation of overdeepening. Analyzing the facies and age of the sedimentary filling of the structures will allow us to unravel the environmental context. Since several of the overdeepenings remained under-filled for quite some time after their formation, they will also provide information about phases subsequent to the glaciation in which the structure was initially formed. Hence, all this information will help to improve our understanding of the glaciation history of the Alps that, according to recent publications, appears much more complex than often assumed previously. Overall, the data gained during the DOVE project will help to better understand how mountain ranges and their foreland have been shaped by glaciers during the Quaternary. In addition, it has been shown during the past 2 decades that changes in atmospheric circulation very likely had a decisive impact on the glaciation pattern in the Alps. While this is to some extent understood for the Late Pleistocene, knowledge beyond this time is rather limited. Identifying regional differences in the glaciation history during the DOVE project may help to better understand the nature of climate change and its impact during the Quaternary.

Data availability. All data from this research are published in this paper.

Team list. Daniel Ariztegui (Univ. of Geneva, Geneva, Switzerland), Sarah Beraus (LIAG Hanover, Hanover, Germany), Anna-Catharina Brandt (Univ. Hanover, Hanover, Germany), Marius Buechi (Univ. Bern, Bern, Switzerland), Herman Buness (LIAG, Hanover, Germany), Thomas Burschil (BGR Hanover, Hanover, Germany), Andreas Dehnert (ENSI, Brugg, Switzerland), Gaudenz Deplazes (Nagra, Wettingen, Switzerland), Gregor Go¨tzl (GBA, Vienna, Austria), Gustav Firla (BOKU Vienna, Vienna, Austria), Lukas Gegg (Univ. Freiburg, Freiburg, Germany), Hans Rudolf Graf (Dr. von Moos AG, Gächlingen, Switzerland), Katja Heeschen (ICDP-OSG, Potsdam, Germany), Rolf Kipfer (Eawag, Dübendorf, Switzerland), Ernst Kroemer (LfU, Augsburg, Germany), Christopher Lu¨thgens (BOKU Vienna, Vienna, Austria), Giovanni Monegato (CNR-IGG, Padova, Italy), Stephanie Neuhuber (BOKU Vienna, Vienna, Austria), Roberta Pini (CNR-IGAG, Milan, Italy), Ju¨rgen Reitner (GBA, Vienna, Austria), Bernhard Salcher (Univ. Salzburg, Salzburg, Austria), Sebastian Schaller (Univ. Bern, Bern, Switzerland), Clemens Schmalfuss (BOKU Vienna, Vienna, Austria), Cedric Schmelzbach (ETH Zu¨rich, Zu¨rich, Switzerland), Robert Scholger (Univ. Leoben, Leoben, Austria), Bennet Schuster (Univ. Freiburg, Freiburg, Germany), Andrew Stumpf (Univ. Illinois, Champaign, USA), David C. Tanner (LIAG, Hanover, Germany), Camille Thomas (Univ. Geneva, Geneva, Switzerland), Yama Tomonaga (Eawag, Dübendorf, Switzerland), Ulrike Wieland-Schuster (LGRB, Freiburg, Germany), and Thomas Wonik (LIAG, Hanover, Germany).

Author contributions. All co-authors are co-proponents of the ICDP drilling proposal and contributed to the design and fundraising of the overall DOVE initiative. They all led the discussion on specific topics at the ICDP workshop. Initial text fragments were written by FSA and FP with input from all co-authors and the DOVE science team. The entire text was reviewed by all co-authors.

Competing interests. The contact author has declared that none of the authors has any competing interests.

Disclaimer. Publisher's note: Copernicus Publications remains neutral with regard to jurisdictional claims in published maps and institutional affiliations.

Acknowledgements. We are grateful for continuing support of the International Scientific Continental Drilling Program (ICDP), including logistic support from the ICDP Operational Support Group. We are grateful to drilling companies, Fretus AG and H. Anger's Söhne GmbH, for providing us with high-quality drill cores in Basadingen and Tannwald, respectively. We also acknowledge strong support by the communities of Basadingen-Schlattingen and Winterstettenstadt, respectively. Technical staff of LIAG assisted with the seismic pre-site surveys and the downhole logging. We acknowledge all ICDP workshop participants in Como, who contributed to realizing this larger DOVE initiative.

Financial support. This research has been supported by ICDP, the Deutsche Forschungsgemeinschaft (DFG, grant nos. KR2073/3-1, BU 2467/1-2, GA749/5-1, BU2467/3-1, BU 3894/2-1, BU3894/3-1, and PR 957/6-1), Nagra, ENSI, LGRB, LFU, LIAG, BOKU Vienna, and University of Bern.

Review statement. This paper was edited by Thomas Wiersberg and reviewed by two anonymous referees.

References

Alley, R., Cuffey, K., and Zoet, L.: Glacial erosion: Status and outlook, Ann. Glaciol., 60, 1–13, https://doi.org/10.1017/aog.2019.38, 2019.

Anselmetti, F. S., Drescher-Schneider, R., Furrer, H., Graf, H. R., Lowick, S. E., Preusser, F., and Riedi, M. A.: A ∼180'000 years sedimentation history of a perialpine overdeepened glacial trough (Wehntal, N-Switzerland), Swiss J. Geosci., 103, 345–361, https://doi.org/10.1007/s00015-010-0041-1, 2010.

Balco, G. and Rovey II, C. W.: An isochron method for cosmogenic-nuclide dating of buried soils, American J. Sci., 308, 1083–1114, https://doi.org/10.2475/10.2008.02, 2008.

Bassinot, F. C., Labeyrie, L. D., Vincent, E., Quidelleur, X., Shackleton, N. J., and Lancelot, Y.: The astronomical theory of climate and the age of the Brunhes-Matuyama magnetic reversal, Earth Planet. Sci. Let., 126, 91–108, https://doi.org/10.1016/0012-821X(94)90244-5, 1994.

Bavec, M., Tulaczyk, S. M., Mahan, S. A., and Stock, G. M.: Late Quaternary glaciation of the Upper Soča River Region (Southern Julian Alps, NW Slovenia), Sediment. Geol., 165, 265–283, https://doi.org/10.1016/j.sedgeo.2003.11.011, 2004.

Baumgarten, H., Wonik, T., and Kwiecien, O.: Facies characterization based on physical properties from downhole logging for the sediment record of Lake Van, Turkey, Quaternary Sci. Rev., 104, 85–96, https://doi.org/10.1016/j.quascirev.2014.03.016, 2014.

Bini, A., Cita, M. B., and Gaetani, M.: Southern alpine lakes - hypothesis of an erosional origin related to the Messinian entrenchment, Mar. Geol., 27, 289–302, https://doi.org/10.1016/0025-3227(78)90035-X, 1978.

Brandt, A.-C.: Erkundung des alpinen, glazial-übertieften Basadingen-Beckens mithilfe von P-Wellen-Seismik, BSc thesis, Leibniz Universität Hannover, unpublished, 2020.

Brennwald, M. S., Vogel, N., Scheidegger, Y., Tomonaga, Y., and Kipfer, R.: Noble gases as environmental tracers in porewater of lacustrine or oceanic sediments and in fluid inclusions of stalagmites, in: Advances in Isotope Geochemistry, edited by: Burnard, P., Springer, 123–155, https://doi.org/10.1007/978-3-642-28836-4_6, 2013.

Buechi, M., Frank, S., Graf, H.-R., Menzies, J., and Anselmetti, F. S.: Subglacial emplacement of tills and meltwater deposits at the base of overdeepened bedrock troughs, Sedimentology, 64, 658–685, https://doi.org/10.1111/sed.12319, 2017a.

Buechi, M. W., Lowick, S. E., and Anselmetti, F. S.: Luminescence dating of glaciolacustrine silt in overdeepened basin fills beyond the last interglacial, Quat. Geochronol., 37, 55–67, https://doi.org/10.1016/j.quageo.2016.09.009, 2017b.

Buechi, M. W., Graf, H. R., Haldimann, P., Lowick, S. E., and Anselmetti, F. S.: Multiple Quaternary erosion and infill cycles in overdeepened basins of the northern Alpine foreland, Swiss J. Geosci., 111, 133–167, https://doi.org/10.1007/s00015-017-0289-9, 2018.

Büker, F., Green, A. G., and Horstmeyer, H.: Shallow seismic reflection study of a glaciated valley, Geophysics, 63, 1395–1407, https://doi.org/10.1190/1.1444441, 1998.

Buness, H., Burschil, T., and Tanner, D.: Imaging glacial sediments and tectonics with a small-scale 3-D reflection seismic survey, 26th European Meeting of Environmental and Engineering Geophysics, 7–8 December 2020, online, 1, 1–4, https://doi.org/10.3997/2214-4609.202020094, 2020.

Buness, H., Tanner, D. C., Burschil, T., Gabriel, G., and Wielandt-Schuster, U.: Cuspate-lobate folding in glacial sediments revealed by a small-scale 3-D seismic survey, J. Appl. Geophy., 200, 104614, https://doi.org/10.1016/j.jappgeo.2022.104614, 2022.

Buoncristiani, J.-F. and Campy, M.: Quaternary Glaciations in the French Alps and Jura, Develop. Quat. Sci., 15, 117–126, https://doi.org/10.1016/B978-0-444-53447-7.00010-6, 2011.

Burschil, T. and Buness, H.: S-wave seismic imaging of near-surface sediments using tailored processing strategies, J. Appl. Geophy., 173, 103927, https://doi.org/10.1016/j.jappgeo.2019.103927, 2020.

Burschil, T., Buness, H., Tanner, D., Wielandt-Schuster, U., Ellwanger, D., and Gabriel, G.: High-resolution reflection seismics reveal the structure and the evolution of the Quaternary glacial Tannwald Basin, Near Surf. Geophy., 16, 593–610, https://doi.org/10.1002/nsg.12011, 2018.

Burschil, T., Tanner, D., Reitner, J., Buness, H., and Gabriel, G.: Unravelling the complex stratigraphy of an overdeepened valley with high-resolution reflection seismics: The Lienz Basin (Austria), Swiss J. Geosci., 112, 341–355, https://doi.org/10.1007/s00015-019-00339-0, 2019.

Burschil, T., Buness, H., and Schmelzbach, C.: 3-D Multi-Component S-Wave Survey in the Tannwald Basin: Data processing and component rotation, 26th European Meeting of Environmental and Engineering Geophysics, 7–8 December 2020, online, 1, 1–4, https://doi.org/10.3997/2214-4609.202020103, 2020.

Burschil, T., Buness, H., and Schmelzbach, C.: Near-surface 3-dimensional multi-component source and receiver S-wave survey in the Tannwald Basin, Germany: acquisition and data processing, Near Surf. Geophys., 20, 331–348, https://doi.org/10.1002/nsg.12214, 2022.

Buylaert, J.-P., Jain, M., Murray, A. S., Thomsen, K. J., Thiel, C., and Sohbati, R.: A robust feldspar luminescence dating method for Middle and Late Pleistocene sediments, Boreas, 41, 435–451, https://doi.org/10.1111/j.1502-3885.2012.00248.x, 2012.

Channel, J. E. T: Late Brunhes polarity excursions (Mono Lake, Laschamp, Iceland Basin and Pringle Falls) recorded at ODP Site 919 (Irminger Basin), Earth Planet. Sci. Let., 244, 378–393, https://doi.org/10.1016/j.epsl.2006.01.021, 2006.

Claude, A., Akçar, N., Ivy-Ochs, S., Schlunegger, F., Rentzel, P., Pümpin, C., Tikhomirov, D., Kubik, P. W., Vockenhuber, C., Dehnert, A., Rahn, M., and Schlüchter, C.: Chronology of Quaternary terrace deposits at the locality Hohle Gasse (Pratteln, NW Switzerland), Swiss J. Geosci., 110, 793–809, https://doi.org/10.1007/s00015-017-0278-z, 2017.

Claude, A., Akcar, N., Ivy-Ochs, S., Schlunegger, F., Kubik, P. W., Christl, M., Vockenhuber, C., Kuhlemann, J., Rahn, M., and Schluechter, C.: Changes in landscape evolution patterns in the northern Swiss Alpine Foreland during the mid-Pleistocene revolution, GSA Bulletin, 131, 2056–2078, https://doi.org/10.1130/B31880.1, 2019.

Dehnert, A., Lowick, S. E., Preusser, F., Anselmetti, F. S., Drescher-Schneider, R., Graf, H. R., Heller, F., Horstmeyer, H., Kemna, H. A., Nowaczyk, N. R., Züger, A., and Furrer, H.: Evolution of an overdeepened trough in the northern Alpine Foreland at Niederweningen, Switzerland, Quaternary Sci. Rev., 34, 127–145, https://doi.org/10.1016/j.quascirev.2011.12.015, 2012.

Doetsch, J., Linde, N., Pessognelli, M., Green, A. G., and Günther, T.: Constraining 3-D electrical resistance tomography with GPR reflection data for improved aquifer characterization, J. Appl. Geophys., 78, 68–76, https://doi.org/10.1016/j.jappgeo.2011.04.008, 2012.

Doppler, G., Kroemer, E., Rögner, K., Wallner, J., Jerz, H., and Grottenthaler, W.: Quaternary Stratigraphy of Southern Bavaria, E&G Quaternary Sci. J., 60, 23, https://doi.org/10.3285/eg.60.2-3.08, 2011.

Ellwanger, D., Wielandt-Schuster, U., Franz, M., and Simon, T.: The Quaternary of the southwest German Alpine Foreland (Bodensee-Oberschwaben, Baden-Württemberg, Southwest Germany), E&G Quaternary Sci. J., 60, 22, https://doi.org/10.3285/eg.60.2-3.07, 2011.

Fiebig, M., Ellwanger, D., and Doppler, G.: Pleistocene glaciations of southern Germany, Develop. Quat. Sci., 15, 163–173, https://doi.org/10.1016/B978-0-444-53447-7.00014-3, 2011.

Fiebig, M., Herbst, P., Drescher-Schneider, R., Lüthgens, C., Lomax, J., and Doppler, G.: Some remarks about a new Last Glacial record from the western Salzach foreland glacier basin (Southern Germany), Quatern. Int., 328–329, 107–119, https://doi.org/10.1016/j.quaint.2013.12.048, 2014.

Finckh, P.: Are southern Alpine lakes former Messinian canyons? Geophysical evidence for preglacial erosion in the southern Alpine lakes, Mar. Geol. 27, 289–302, https://doi.org/10.1016/0025-3227(78)90036-1, 1978.

Florineth, D. and Schlüchter, C.: Alpine evidence for atmospheric circulation patterns in Europe during the Last Glacial Maximum, Quaternary Res., 54, 295–308, https://doi.org/10.1006/qres.2000.2169, 2000.

Furrer, H., Graf, H. R., and Mäder, A.: The mammoth site of Niederweningen, Switzerland, Quatern. Int., 164–165, 85–97, https://doi.org/10.1016/j.quaint.2006.10.012, 2007.

Gabriel, G., Kirsch, R., Siemon, B., and Wiederhold, H.: Geophysical investigation of buried Pleistocene subglacial valleys in Northern Germany, J. Appl. Geophys., 53, 159–180, https://doi.org/10.1016/j.jappgeo.2003.08.005, 2003.

Gabris, G. and Nador, A.: Long term fluvial archives in Hungary: response of the Danube and Tisza rivers to tectonic movements and climatic changes during the Quaternary: a review and new synthesis, Quaternary Sci. Rev., 26, 2758–2782, https://doi.org/10.1016/j.quascirev.2007.06.030, 2007.

Gegg, L., Buechi, M. W., Ebert, A., Deplazes, G., Madritsch, H., and Anselmetti, F. S.: Brecciation of glacially overridden palaeokarst (Lower Aare Valley, northern Switzerland): result of subglacial water-pressure peaks?, Boreas 49, 813–827, https://doi.org/10.1111/bor.12457, 2020.

Gegg, L., Deplazes, G., Keller, L., Madritsch, H., Spillmann, T., Anselmetti, F. S., and Buechi, M. W.: 3D morphology of a glacially overdeepened trough controlled by underlying bedrock geology, Geomorphology, 394, 107950, https://doi.org/10.1016/j.geomorph.2021.107950, 2021.

Gianotti, F., Forno, M.G., Ivy-Ochs, S., Monegato, G., Pini, R., and Ravazzi, C.: Stratigraphy of the Ivrea Moranic Amphitheatre (NW Italy): An updated synthesis, Alp. Mediter. Quat., 28, 29–58, 2015.

Gribenski, N., Valla, P., Preusser, F., Roattino, T., Crouzet, C., and Buoncristiani, J.-F.: Out-of-phase Late Pleistocene glacier advances in the western Alps reflect past changes in North Atlantic atmospheric circulation, Geology, 49, 1096–1101, https://doi.org/10.1130/G48688.1, 2021.

Günther, T., Musmann, P., Schaumann, G., and Grinat, M.: Imaging of a fault zone by a large-scale dc resistivity experiment and seismic structural information, 17th EAGE European Meeting of Environmental and Engineering Geophysics, 12–14 September 2011, Leicester, UK, Ext. Abstr., https://doi.org/10.3997/2214-4609.20144450, 2011.

Haeuselmann, P., Granger, D., Jeannin, P.-Y., and Lauritzen, S.-E.: Abrupt glacial valley incision at 0.8 Ma dated from cave deposits in Switzerland, Geology, 35, 143–146, https://doi.org/10.1130/G23094A, 2007a.

Haeuselmann, P., Fiebig, M., Kubik, P. W., and Adrian, H.: A first attempt to date the original "Deckenschotter" of Penck and Brückner with cosmogenic isotopes, Quatern. Int., 164–165, 33–42, https://doi.org/10.1016/j.quaint.2006.12.013, 2007b.

Haeuselmann, P., Mihevc, A., Pruner, P., Horacek, I., Cermak, S., Hercman, H., Sahy, D., Fiebig, M., Hajna, N. Z., and Bosak, P.: Snežna jama (Slovenia): Interdisciplinary dating of cave sediments and implications for landscape evolution, Geomorphology, 247, 10–24, https://doi.org/10.1016/j.geomorph.2014.12.034, 2015.

Hajdas, I., Bonani, G., Furrer, H., Mäder, A., and Schoch, W.: Radiocarbon chronology of the mammoth site at Niederweningen, Switzerland: results from dating bones, teeth, wood, and peat, Quatern. Int., 164–165, 98–105, https://doi.org/10.1016/j.quaint.2006.10.007, 2007.

Hellman, K., Ronczka, M., Günther, T., Wennermark, M., Rücker, C., and Dahlin, T.: Structurally coupled inversion of ERT and refraction seismic data combined with cluster-based model integration, J. Appl. Geophy., 143, 169–181, https://doi.org/10.1016/j.jappgeo.2017.06.008, 2017.

Hendry, M. J. and Wassenaar, L. I.: Millennial-scale diffusive migration of solutes in thick clay-rich aquitards: evidence from multiple environmental tracers, Hydrogeol. J., 19, 259–270, https://doi.org/10.1007/s10040-010-0647-4, 2011.

Hendry, M. J., Kotzer, T. G., and Solomon, D. K.: Sources of radiogenic helium in a clay till aquitard and its use to evaluate the timing of geologic events, Geochim. Cosmochim. Ac., 69, 475–483, https://doi.org/10.1016/j.gca.2004.07.001, 2005.

Hinderer, M., Kastowski, M., Kamelger, A., Bartolini, C., and Schlunegger, F.: River loads and modern denudation of the Alps – A review, Earth Sci. Rev., 118, 11–44, https://doi.org/10.1016/j.earscirev.2013.01.001, 2013.

Hunze, S. and Wonik, T.: Sediment Input into the Heidelberg Basin as determined from Downhole Logs, E&G Quaternary Sci. J., 57, 367–381, https://doi.org/10.3285/eg.57.3-4.5, 2009.

Hunze, S., Gabriel, G., Wiederhold, H., Buness, H., and Wonik, T.: Research borehole Paffrather Mulde 1: characterisation of sediments and structures of the Upper Devonian (Bergisches Land, Germany) by downhole logs, and gravimetric and seismic investigations, Z. dt. Ges. Geowiss., 163, 153–164, https://doi.org/10.1127/1860-1804/2012/0163-0153, 2012.

Huuse, M. and Lykke-Andersen, H.: Overdeepened Quaternary valleys in the eastern Danish North Sea: morphology and origin, Quaternary Sci. Rev., 19, 1233–1253, https://doi.org/10.1016/S0277-3791(99)00103-1, 2000.

Ivy-Ochs, S., Kerschner H., Reuther, A., Preusser, F., Heine, K., Kubik, P. W., Maisch, M., and Schlüchter, C.: Chronology of the last glacial cycle in the European Alps, J. Quat. Sci., 23, 559–573, https://doi.org/10.1002/jqs.1202, 2008.

Jerz, H.: Geologische Karte von Bayern 1 : 25 000, Blatt 8034 Starnberg Süd, Bayerisches Geologisches Landesamt, München, 1987.

Jordi, J., Doetsch, J., Günther, T., Schmelzbach, C., and Robertsson, J. O. A.: Geostatistical regularization operators for geophysical inverse problems on irregular meshes, Geophys. J. Int., 213, 1374–1386, https://doi.org/10.1093/gji/ggy055, 2018.

Jørgensen, F. and Sandersen, P. B. E.: Buried and open tunnel valleys in Denmark – erosion beneath multiple ice sheets, Quaternary Sci. Rev., 25, 1339–1363, https://doi.org/10.1016/j.quascirev.2005.11.006, 2006.

Knudsen, M. F., Nørgaard, J., Grischott, R., Kober, F., Egholm, D. L., Mejer Hansen, T., and Jansen J. D.: New cosmogenic nuclide burial-dating model indicates onset of major glaciations in the

Alps during Middle Pleistocene Transition, Earth Planet. Sci. Lett., 549, 116491, https://doi.org/10.1016/j.epsl.2020.116491, 2020.

Kuhlemann, J., Rohling, E. J., Krumrei, I., Kubik, P., Ivy-Ochs, S., and Kucera, M.: Regional synthesis of Mediterranean atmospheric circulation during the Last Glacial Maximum, Science 321, 1338–1340, https://doi.org/10.1126/science.1157638, 2008.

Kuster, H. and Meyer, K.-D.: Glaziäre Rinnen im mittleren und nördlichen Niedersachsen, E&G Quaternary Sci. J., 29, 135–156, https://doi.org/10.3285/eg.29.1.12, 1979.

Lee, H. J., Ho, M. R., Bhuwan, M., Hsu, C. Y., Huang, M. S., Peng, H. L., and Chang, H. Y.: Enhancing ATP-based bacteria and biofilm detection by enzymatic pyrophosphate regeneration, Anal. Biochem., 399, 168–173, https://doi.org/10.1016/j.ab.2009.12.032, 2010.

LGRB (Landesamt für Geologie, Rohstoffe und Bergbau Baden-Württemberg): Lithostratigraphische Entwicklung des baden-württembergischen Rheingletschergebiets: Übertiefte Becken- und Moränen-Landschaft, LGRB-Fachbericht 2015/4, 2015.

Lisiecki, L. E. and Raymo, M. E.: A Pliocene-Pleistocene stack of 57 globally distributed benthic δ^{18}O records, Paleoceanography 20, PA1003, https://doi.org/10.1029/2004PA001071, 2005.

Luetscher, M., Boch, R., Sodemann, H., Spötl, C., Cheng, H., Edwards, R. L., Frisia, S., Hof, F., and Müller, W.: North Atlantic storm track changes during the Last Glacial Maximum recorded by Alpine speleothems, Nat. Commun., 6, 6344, https://doi.org/10.1038/ncomms7344, 2015.

Mandier, P.: Le relief de la moyenne vallée du Rhône au Tertiaire et au Quaternaire, Essai de synthèse paléogéographique. Thèse de Doctorat d'Etat présentée devant l'université de Lyon II., 654 pp., unpublished, 1988.

Menzies, J.: Micromorphological analyses of microfabrics and microstructures indicative of deformation processes in glacial sediments, Geol. Soc. London Spec. Pub., 176, 245–257, https://doi.org/10.1144/GSL.SP.2000.176.01.19, 2000.

Mihevc, A., Bavec, M., Haeuselmann, P., and Fiebig, M.: Dating of the Udin Boršt conglomerate terrace and implications for tectonic uplift in the Northwestern Part of the Ljubljana Basin (Slovenia), Acta Carsologica, 44, 169–176, https://doi.org/10.3986/ac.v44i2.2033, 2016.

Monegato, G., Scardia, G., Hajdas, I., Rizzini, F., and Piccin, A.: The Alpine LGM in the boreal ice-sheets game, Sci. Rep., 7, 2078, https://doi.org/10.1038/s41598-017-02148-7, 2017.

Muttoni, G., Carcano, C., Garzanti, E., Ghielmi, M., Piccin, A., Pini, R., Rogledi, S., and Sciunnach, D.: Onset of major Pleistocene glaciations in the Alps, Geology, 31, 989–992, https://doi.org/10.1130/G19445.1, 2003.

Nicoud, G., Royer, G., Corbin, J.-C., Lemeille, F., and Paillet, A.: Creusement et remplissage de la vallée de l'Isère au Quaternaire récent, Géologie de la France, 4, 39–49, 2002.

Opdyke, N. D. and Channell, J. E. T.: Magnetic Stratigraphy, Academic Press, San Diego, ISBN 0-12-527470-X , 1996.

Penck, A., and Brückner, E.; Die Alpen im Eiszeitalter, Tauchnitz, Leipzig, 1901.

Pietsch, J. and Jordan, P.: Digitales Höhenmodell Basis Quartär der Nordschweiz – Version 2014 und ausgewählte Auswertungen, Technical report, Nagra Arbeitsbericht NAB, 14-02, 2014.

Pini, R., Ravazzi, C., and Donegana, M.: Pollen stratigraphy, vegetation and climate history of the last 215 ka in the Azzano Decimo core (plain of Friuli, northeastern Italy), Quaternary Sci. Rev., 28, 1268–1290, https://doi.org/10.1016/j.quascirev.2008.12.017, 2009.

Pomper, J., Salcher, B. C., Eichkitz, C., Prasicek, G., Lang, A., Lindner, M., and Götz J.: The glacially overdeepened trough of the Salzach Valley, Austria: Bedrock geometry and sedimentary fill of a major Alpine subglacial basin, Geomorphology, 295, 147–158, https://doi.org/10.1016/j.geomorph.2017.07.009, 2017.

Powell, R. D. and Cooper, J. M.: A glacial sequence stratigraphic model for temperate, glaciated continental shelves, Geol. Soc. London Spec. Pub., 203, 215–244, https://doi.org/10.1144/GSL.SP.2002.203.01.12, 2002.

Preusser, F. and Degering, D.: Luminescence dating of the Niederweningen mammoth site, Switzerland, Quatern. Int., 164–165, 106–112, https://doi.org/10.1016/j.quaint.2006.12.002, 2007.

Preusser, F., Drescher-Schneider, R., Fiebig, M., and Schlüchter, C.: Re-interpretation of the Meikirch pollen record, Swiss Alpine Foreland, and implications for Middle Pleistocene chronostratigraphy, J. Quat. Sci., 20, 607–620, https://doi.org/10.1002/jqs.930, 2005.

Preusser, F., Degering, D., Fuchs, M., Hilgers, A., Kadereit, A., Klasen, N., Krbetschek, M., Richter, D., and Spencer, J. Q. G.: Luminescence dating: basics, methods and applications, E&G Quaternary Sci. J., 57, 95–149, https://doi.org/10.3285/eg.57.1-2.5, 2008.

Preusser, F., Reitner, J., and Schlüchter, C.: Distribution, geometry, age and origin of overdeepened valleys and basins in the Alps and their foreland, Swiss J. Geosci., 103, 407–426, https://doi.org/10.1007/s00015-010-0044-y, 2010.

Preusser, F., Graf, H. R., Keller, O., Krayss, E., and Schlüchter, C.: Quaternary glaciation history of northern Switzerland, E&G Quaternary Sci. J., 60, 21, https://doi.org/10.3285/eg.60.2-3.06, 2011.

Preusser, F., Büschelberger, M., Kemna, H. A., Miocic, J., Mueller, D., and May, J.-H.: Exploring possible links between Quaternary aggradation in the Upper Rhine Graben and the glaciation history of northern Switzerland, Int. J. Earth Sci. (Geol. Rundsch.) 110, 1827–1846, https://doi.org/10.1007/s00531-021-02043-7, 2021.

Reitner, J. M., Gruber, W., Römer, A., and Morawetz, R.: Alpine overdeepenings and paleo-ice flow changes: an integrated geophysical-sedimentological case study from Tyrol (Austria), Swiss J. Geosci., 103, 385–405, https://doi.org/10.1007/s00015-010-0046-9, 2010.

Ronczka, M., Hellman, K., Günther, T., Wisén, R., and Dahlin, T.: Electric resistivity and seismic refraction tomography: a challenging joint underwater survey at Äspö Hard Rock Laboratory, Solid Earth, 8, 671–682, https://doi.org/10.5194/se-8-671-2017, 2017.

Rumpel, H.-M., Binot, F., Gabriel, G., Siemon, B., Steuer, A., and Wiederhold, H.: The benefit of geophysical data for hydrogeological 3D modelling – an example using the Cuxhaven buried valley, Z. dtsch. Ges. Geowiss., 160, 259–269, https://doi.org/10.1127/1860-1804/2009/0160-0259, 2009.

Salcher, B., Meurers, B., Smit, J., Decker, K., Hölzel, M., and Wagreich, M.: Strike-slip tectonics and Quaternary basin formation along the Vienna Basin fault system inferred from Bouguer gravity derivates, Tectonics, 31, TC3004, https://doi.org/10.1029/2011TC002979, 2012.

Salcher, B., Kober, F., Kissling, E., and Willett, S. D.: Glacial impact on short-wavelength topography and long-lasting effects on the denudation of a deglaciated mountain range, Glob. Planet. Change, 115, 59–70, https://doi.org/10.1016/j.gloplacha.2014.01.002, 2014.

Salcher, B., Prasicek, G., Baumann, S., and Kober, F.: Alpine relief limited by glacial occupation time, Geology, 49, 10, 1209–1213, https://doi.org/10.1130/G48639.1, 2021.

Scardia, G., Muttoni, G., and Sciunnach, D.: Subsurface magnetostratigraphy of Pleistocene sediments from the Po Plain (Italy): Constraints on rates of sedimentation and rock uplift, GSA Bulletin, 118, 1299–1312, https://doi.org/10.1130/B25869.1, 2006.

Schwenk, M. A., Schläfli, P., Bandou, D., Gribenski, N., Douillet, G. A., and Schlunegger, F.: From glacial erosion to basin overfill: a 240 m-thick overdeepening–fill sequence in Bern, Switzerland, Sci. Dril., 30, 17–42, https://doi.org/10.5194/sd-30-17-2022, 2022.

Seguinot, J., Ivy-Ochs, S., Jouvet, G., Huss, M., Funk, M., and Preusser, F.: Modelling last glacial cycle ice dynamics in the Alps, The Cryosphere, 12, 3265–3285, https://doi.org/10.5194/tc-12-3265-2018, 2018.

Steinhauser, P., Meurers, B., and Aric, K.: Geophysikalische Detailuntersuchungen der Schwereanomalie von Bad Aussee, Geophysikalischer Forschungsbericht Nr. 18, Institut für Meteorologie und Geophysik, Universität Wien, internal report, 1985.

Tomonaga, Y., Brennwald, M. S., Meydan, A. F., and Kipfer, R.: Noble gases in the sediments of Lake Van – Solute transport and palaeotemperature reconstruction, Quaternary Sci. Rev., 104, 117–126, https://doi.org/10.1016/j.quascirev.2014.09.005, 2014.

Tomonaga, Y., Brennwald, M. S., Livingstone, D. M., Kwiecien, O., Randlett, M.-E., Stockhecke, M., Unwin, K., Anselmetti, F., Beer, J., Haug, G., Schubert, C., Sturm, M., and Kipfer, R.: Porewater salinity reveals past lake-level changes in Lake Van, the Earth's largest soda lake, Sci. Rep., 7, 313, https://doi.org/10.1038/s41598-017-00371-w, 2017.

Tomonaga, Y., Buechi, M., Deplazes, G., and Kipfer, R.: ^{4}He / U–Th dating of pore waters from Quaternary sediments of the Swiss Midland, 31st Annual V.M. Goldschmidt Conference, 4–9 July 2021, virtual conference, https://doi.org/10.7185/gold2021.5714, 2021.

Van Husen, D. and Mayer, M.: The hole of Bad Ausssee – An unexpected overdeepened area in NW Steiermark, Austria, Aust. J. Earth Sci., 100, 128–136, 2007.

Van Husen, D. and Reitner, J. M.: An Outline of the Quaternary Stratigraphy of Austria, E&G Quaternary Sci. J., 60, 24, https://doi.org/10.3285/eg.60.2-3.09, 2011.

Wassenaar, L. I. and Hendry, M. J.: Mechanisms controlling the distribution and transport of ^{14}C in a clay-rich till aquitard, Ground Water, 38, 343–349, https://doi.org/10.1111/j.1745-6584.2000.tb00219.x, 2000.

Wittmann, H., Blanckenburg, F. V., Kruesmann, T., Norton, K. P., and Kubik, P.W.: Relation between rock uplift and denudation from cosmogenic nuclides in river sediment in the Central Alps of Switzerland, J. Geophys. Res., 112, F04010, https://doi.org/10.1029/2006JF000729, 2007.

Sci. Dril., 31, 71–84, 2022
https://doi.org/10.5194/sd-31-71-2022

Scientific Drilling
Open Access

A channel sampling strategy for measurement of mineral modal and chemical composition of drill cores: application to lower oceanic crustal rocks from IODP Expedition 345 to the Hess Deep rift

Robert P. Wintsch[1,2], Romain Meyer[3], David L. Bish[4], Ryan T. Deasy[5], Toshio Nozaka[6], and Carley Johnson[7]

[1]Department of Earth and Environmental Sciences, Wesleyan University, Middletown, CT 06459, USA
[2]Connecticut Geological Survey, 79 Elm Street, Hartford, CT 06106-5127, USA
[3]Geological Survey of Luxembourg, Ministry of Mobility and Public Works, 23, Rue du Chemin de Fer, 8057 Bertrange, Luxembourg
[4]Department of Chemistry, Indiana University, Bloomington, IN 47405, USA
[5]U.S. Geological Survey, Florence Bascom Geoscience Center, 12201 Sunrise Valley Dr., MS 926A, Reston, VA 20192, USA
[6]Department of Earth Sciences, Okayama University, 3-1-1 Tsushima-naka, Okayama 700-8530, Japan
[7]Marathon Oil Corporation, Room #3545, 5555 San Felipe St., Houston, TX 77056, USA

Correspondence: Robert P. Wintsch (rwintsch@wesleyan.edu)

Received: 5 November 2021 – Revised: 17 February 2022 – Accepted: 8 April 2022 – Published: 28 October 2022

Abstract. We report a new sampling strategy for collecting representative samples of drill core. By splitting the core with a diamond saw into working and archive halves, the saw cuttings constitute a "channel" sample, the best subsample from which to obtain an average mineralogical and geochemical composition of a core. We apply this procedure to sampling core of the lower oceanic crust in the Hess Deep obtained during Expedition 345 of the Integrated Ocean Drilling Program (now International Ocean Discovery Program).

Our results show that particles produced by sawing range from sand to clay sizes. Sand- and silt-sized cuttings can be sampled with a spatula, whereas clay-sized particles remained in suspension after 12 h and could be collected only by settling, aided by centrifuge. X-ray diffraction (XRD) analysis and Rietveld refinement show that phyllosilicates were fractionated into the clay-sized fraction. Thus, collection of both the sedimented fraction and the clay-sized suspended fraction (commonly > 15 wt % of the total) is necessary to capture the whole sample. The strong positive correlation between the recovered sample mass (in grams) and length of core cut demonstrates that this sampling protocol was uniform and systematic, with almost 1.4 g sediment produced per centimeter of core cut. We show that major-element concentrations of our channel samples compare favorably with the compositions of billet-sized samples analyzed aboard the *JOIDES Resolution*, but the results show that individual billet analyses are rarely representative of the whole core recovered. A final test of the validity of our methods comes from the strong positive correlation between the loss on ignition (LOI) values of our channel samples and the H_2O contents calculated from the modal mineralogy obtained by X-ray diffraction and Rietveld refinement. This sampling procedure shows that grain-sized fractionation modifies both mineralogical and chemical compositions; nevertheless, this channel sampling method is a reliable method of obtaining representative samples of bulk cores. With the ever-increasing precision offered by modern analytical instrumentation, this sampling protocol allows the accuracy of the analytical results to keep pace.

Published by Copernicus Publications on behalf of the IODP and the ICDP.

1 Introduction

Fundamental questions about the dynamics of plate tectonics require the most statistically robust knowledge of the composition of the oceanic crust produced with variable spreading rates. Slow spreading rates may produce more alkali-rich magmas, whereas fast spreading may produce more mafic magmas with higher percentages of melting (e.g., Regelous et al., 2016). In addition, the state of alteration to hydrated minerals may play an important role in defining the density and seismic properties of the oceanic crust. An understanding of the consequences of the destruction of oceanic crust during subduction at convergent plate margins requires detailed knowledge of the extent of hydration and related alteration mineralogy of the recycled slab. These variables control the flux of fluids returned to the mantle. This in turn affects both petrologic (e.g., hydration melting) and geophysical (e.g., dehydration embrittlement) behavior of these rocks (e.g., Raleigh and Paterson, 1965; Meade and Jeanloz, 1991; Hacker et al., 2003; Bourdon et al., 2003; Manning, 2004; Ranero et al., 2005).

Progress in defining the properties of the oceanic crust has been stymied by the lack of knowledge of the composition of the lower oceanic crust. Our knowledge of the chemical and mineralogical composition of the oceanic crust is biased toward the more accessible volcanic rocks and sheeted dikes from mid-ocean ridge basalt (MORB) (e.g., Stewart et al., 2002, 2005; Blackman et al., 2011; White and Klein, 2014). Analysis of lower crustal lithologies by core and dredged samples provides some answers (e.g., Mével and Stamoudi, 1996; Natland and Dick, 1996; Pedersen et al., 1996; Dick et al., 1999; Manning et al., 1996; Lissenberg et al., 2013), but such studies are limited by small individual sample size and by lack of structural context. In particular, the chemical composition and especially the modal mineralogy of lower plutonic oceanic crust at fast-spreading axes are not as well known as slower spreading centers (Arai and Matsukage, 1996; Coogan et al., 2002; Arai and Takemoto, 2007; Gillis et al., 2014e). There is a large body of literature on the use of reflectance spectroscopy for determining the mineralogy of rocks from the planetary scale (e.g., remote sensing of Mars and Earth) to the microscopic scale. For example, micro-imaging infrared spectroscopy as applied to the Samail ophiolite, Oman (Kelemen et al., 2020), is an advance in detecting whole-core mineralogy but is so far only semi-quantitative. Greenberger et al. (2021) used the X-ray diffraction (XRD) data from Kelemen et al. (2020) to map mineral distributions in oceanic crust from Oman. They were able to determine spatial distributions of a number of minerals and mineral groups in core, with claimed accuracy of 68 %–100 % compared with XRD identifications. Micro-imaging infrared spectroscopy can identify mineral families (Greenberger et al., 2021) with a spatial resolution of $\sim 250\,\mu m$, but the method does not discriminate well among important mineral groups (e.g., quartz from two feldspars, phyllosilicates, oxides, sulfides, zeolites).

This gap in data from the lower crust was one of the primary motivations for drilling the lowermost ocean crust at the fast-spreading East Pacific Rise on Expedition 345 to the Hess Deep (Gillis et al., 2014e). First-order questions addressed there included (1) what are the compositions of the primitive plutonic rocks that comprise the lower magmatic crust, and (2) what is the state of alteration of that crust? Different approaches used to calculate the bulk major-element compositions of oceanic crust (e.g., Gillis et al., 2014a) are presently still debated (White and Klein, 2014). The major point of contention relates to the composition of the lower oceanic crustal component of the total crust (e.g., Coogan, 2014). Here the lack of quantitative data for the gabbroic lower oceanic crust leads to additional uncertainty.

In this study we describe a sampling strategy that allows us to acquire representative samples of all the cores of lower crustal rocks recovered from Expedition 345 to the Hess Deep. We provide results demonstrating the viability of the sampling method, we present data on the modal mineralogy and major-element compositions of these cores, and we compare our results with those of traditional methods of analyzing centimeter-sized billets subjectively sampled from parts of cores. Deasy et al. (2021) presented the quantitative chemical results of our study and applied them to interpreting magmatic processes in the lower crust and in an updated estimate of the composition of fast-spreading oceanic crust.

2 Background on sampling protocols

Samples of oceanic crustal rocks are available from limited coring, dredging, and collecting from submersible dives, but sample size and sample density are typically small, yielding to the conflicting interests and needs of different scientific experiments, as well as to the preservation of the archival half of the core. In the absence of other analytical data, sample selection for chemical analysis is necessarily subjective and as such can be statistically unsystematic. The analysis of a small specimen may be representative of only that particular sample, and extrapolations to the composition of a related outcrop, core, igneous unit, and especially crustal segment can only be made with increasing uncertainty (e.g., Potts, 1987).

Small sample sizes employed for the analysis of hydrothermal alteration are especially limiting. Reactions and structures responsible for alteration have been identified (e.g., Lecuyer and Reynard, 1996; Manning and MacLeod, 1996; Manning et al., 1996; Frost et al., 2008; Meyer et al., 2013; Deasy et al., 2014; Nozaka and Fryer, 2011; Marks et al., 2013, 2014; Nozaka et al., 2016, 2017), but their net effect on modifying the bulk mineralogy of the protolith is not well understood (e.g., Gillis et al., 2005) and stands to be improved. In fact, no analyst, with even the best analytical methods, will be able to correct data for errors related

to unsystematic sampling (Heinrichs and Hermann, 1990). An analysis of an entire core comes much closer to producing the data needed to assess the effects of alteration on bulk compositions.

Representative sampling strategies are well established in geochemical ore prospecting (e.g., Heinrichs and Hermann, 1990). Linear sampling, i.e., channel sampling, provides representative samples for mineralogy and chemical analysis (Sinclair and Blackwell, 2002), and such linear sampling has been widely applied in the metal mining and coal industries (e.g., Agterberg, 2012; Stanton, 1986; Swanson and Huffman, 1976). In surface exposures this involves cutting a linear channel, typically 10 cm deep, across the fresh outcrop face (Cornish, 1966). The exact shape of the channel has little influence on the sample quality, but a uniform volume of sample needs to be guaranteed over the total length of the channel (Heinrichs and Hermann, 1990). An additional representative sampling method in ore prospecting equivalent to a channel sample is the "Bohrmehlprobe", where the fine-grained material obtained from drilling rock-blasting holes is collected for analysis (Heinrichs and Hermann, 1990). NASA has recently used a similar drilling sampling strategy with the Curiosity rover on Mars for quantitative mineral compositions with the CheMin instrument (Bish et al., 2004, 2013). Finally, Hart et al. (1999) followed the philosophy of a linear channel sample within the scientific drilling community by trimming a 1 cm wide wedge off the edges of several lengths of Ocean Drilling Program (ODP) core. Their highly successful "strip" sample did produce representative samples of core, but it also consumed a large percentage of the precious core recovered and so was never repeated within the ocean drilling programs.

Identifying a sample representative of the mineral or chemical composition of an entire length of core was especially challenging for the recent IODP Expedition 345, Site U1415, to the Hess Deep for several reasons. First, the billets (typically $2 \times 3 \times 3$ cm, 15 to 30 g) used in chemical analysis (Gillis et al., 2014d) are too small to adequately sample the many varieties of gabbroic rocks that contained oikocrysts of clinopyroxene up to 5 cm in diameter. The same is true for samples with modal variations and layering that occur on the scale of up to 10 cm (Gillis et al., 2014d; Koepke et al., 2013). The most limiting property of the core is the heterogeneous distribution of alteration. It is typically associated with fractures and faults whose occurrence is equally heterogeneous, and the scales of alteration vary from micrometers to meters in width. The scale and distribution of these structures is much too large to be captured proportionally in typical IODP sample pieces, and the alteration typically dismembers the core into irregular-sized pieces. Moreover, billets are typically cut from well-indurated core, thereby biasing sampling against altered material. Thus, the analysis of billets cannot be representative of the bulk rock or even the drilled units.

Another uncertainty in the study of IODP cores stems from the method of obtaining modal mineralogy. Modal mineralogy is typically determined by "visual core descriptions" (VCDs; Gillis et al., 2014c), where a scientist estimates by eye the volume percent of each magmatic and alteration mineral. These are subject to uncertainties derived from the several scientists involved in both identifying the mineralogy correctly and in estimating modal percentages of each mineral accurately. These errors are not systematic, because six or more scientists may be involved in the estimate of magmatic and alteration mineralogy of the many pieces of core. In addition, it is often difficult, if not impossible, to obtain an accurate identification let alone an accurate modal estimate of fine-grained alteration minerals. It is well known from oil reservoir characterization studies that visual estimates are often twice as high as point-counted values (Lucia, 2007). As a result, visual estimates can be inaccurate if not calibrated with point-counted methods.

Here we describe a new method of obtaining a representative sample of hard-rock core: a channel sample of the drill core. These samples were obtained by meticulously collecting all of the cuttings, slurries, and rinse water from the linear or "channel sample" of the core produced by the saw as it cut each of the 42 cores into working and archive halves on IODP Expedition 345 to the Hess Deep (Gillis et al., 2014c). A distinct advantage of this method is that it did not consume any new volume of core. These representative samples were then used to determine (1) the modal mineralogy by collecting X-ray powder diffraction data and using Rietveld refinement methods to determine the total wt % of each mineral (Wintsch et al., 2013), (2) the major- and trace-element compositions (Deasy et al., 2021), and (3) Sr isotopic compositions (Deasy et al., 2014; Wintsch et al., 2019). This new method has distinct advantages over traditional methods used in past IODP expeditions as described below.

3 Methods

In this section we provide detail on new methods of channel sampling, i.e., the systematic collection of rock material removed during the separation of cores into working and archive halves. The chemical analytical methods are described in Deasy et al. (2021). During IODP Expedition 345, 42 cores were recovered "in situ" with the label "R." Other samples were of rock that collapsed into the hole and commonly produced "pebbly" material, having been ground by the rotary drilling process. These "ghost" or "G" samples (Gilles et al., 2014c) were maintained but were not systematically sampled in this study, because their position in the hole could not be firmly established. The results of these mineralogical and chemical analyses confirm that this is a robust method of sample collection.

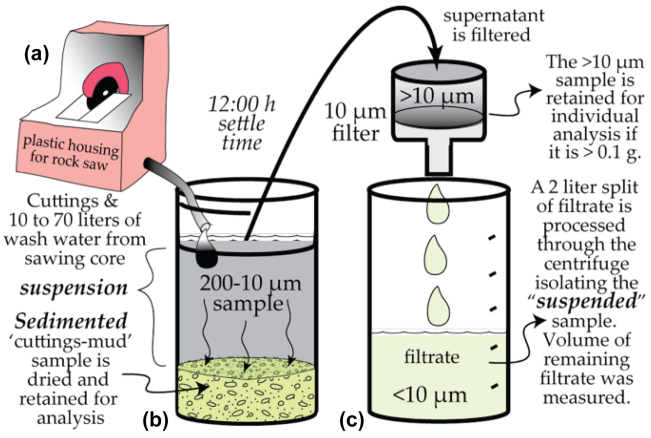

Figure 1. A schematic diagram showing the processes involved in collecting the channel sample of the drill core. Larger particles produced in cutting the core **(a)** are sedimented in the plastic housing, whereas smaller particles are flushed into a large carboy **(b)**. A coarser-grained sedimented subsample is produced by allowing the sample to settle for 12 h. Clay-sized particles remaining in suspension **(c)** are isolated by using a centrifuge.

3.1 Sample collection

In accordance with IODP procedures (see Gillis et al., 2014c), all 42 cores recovered during IODP Expedition 345 were cut in half lengthwise to produce an archive half and a working half. The sawing process cut a channel ∼ 1.5 mm wide in the 57 mm diameter core. The fragments produced by sawing were typically < 200 µm in diameter. Some fragments were up to 2 mm in diameter, and many particles were reduced to clay size. The standard procedure aboard the D/V *JOIDES Resolution* (JR) had been to discard these cuttings back to the ocean, thereby wasting the opportunity to acquire this precious and otherwise "free" sample.

Our sampling procedure on the JR was as follows: after the core was removed from its plastic casing, the core pieces were thoroughly washed and rinsed of all drilling mud using the distilled water produced on the JR. Beyond cleaning the core of contaminants, it had to be optically clean for digital imaging purposes. The samples were then cut on a new diamond saw that was enclosed on five sides by a plastic housing (Fig. 1a). Together with the spray guard at the front of the saw, all water and cuttings sprayed from the sample were contained within the housing or collected through a drain into buckets or carboys (Fig. 1b).

After all pieces in any one core (typically 0.5 to 1.5 m long) were cut, we collected all of the particles produced from sawing the slot. The coarser grains, including millimeter-sized fragments, sedimented to the bottom of the plastic housing of the saw, and as much as possible of this sedimented material was collected using a plastic spatula. Any remaining particles were collected by rinsing the shuttle, mounts, and farther reaches of the housing with a strong spray of distilled water and capturing this rinse water through the drain into buckets or carboys (Fig. 1b). Final rinsing ensured the complete capture of all particles of all grain sizes in any given section of core. This procedure effectively collected all of the material in the 1.5 mm wide saw cut, averaged over the entire 0.5 to 1.5 m core. Furthermore, the final wash left the saw and housing clean for cutting the next section of core and for the collection of the next channel sample.

The resulting slurry of particles, or cuttings and rinse water was left to settle for at least 12 h to allow all silt-sized and larger particles (those greater than ∼ 4 µm) to settle to the bottom of the 37 cm tall bucket (e.g., Lewis, 1984; Fig. 1b). The supernatant suspension was then decanted from the bucket, leaving a thick slurry of particle sizes ranging from ∼ 4 µm up to several millimeters. This slurry was then air-dried, weighed, and retained for X-ray diffraction and chemical analysis.

The suspension, then free of silt-sized particles, was passed through a 10 µm sieve to capture any lingering coarser particles (Fig. 1c). In practice the material on the sieve never exceeded 0.1 g. This material was later added to the sedimented 4 to 200 µm subsample. A 2 L aliquot of the remaining 5 to 35 L of suspension was then decanted into 50 mL centrifuge tubes, which were centrifuged at 2000 rpm for 10 min, removing particles < 4 µm. This clay-sized material was then washed in alcohol, dried in air, and weighed, producing the yield of < 4 µm material in grams per 2 L. The volume of the remaining suspension was then measured in a burette to ±5 mL. Excess suspension water could then be discarded, minimizing the need to store more than a few buckets of rinse water at a time. The total mass of clay-sized particles was then calculated. The final weight of the bulk samples of each core was calculated by weighted averages of the sedimented and suspended subsamples; that is, bulk sample = suspended sample + sedimented sample.

3.2 X-ray diffraction

Sedimented subsamples for this analysis were reground under acetone to a fine powder using an agate mortar and pestle. Powdered samples were loaded into Ti mounts with cavities 35 mm × 28 mm × 1 mm depth and analyzed on an automated Bruker D8 diffractometer with a Cu anode and a SolX energy-dispersive detector at room temperature and ∼ 20 % relative humidity. Samples were measured from 2–70° 2θ with a step size of 0.02°. Rietveld refinements (Bish and Post, 1993) were performed using the TOPAS 5 software package (Bruker AXS). The limits of detection by XRD methods are ∼ 1 wt %m depending on the mineral and the count time used for data collection.

The Rietveld method allows for the independent refinement of modeled mineral properties, including the preferred orientations of grains in the sample mount as well as compositional parameters such as Fe / Mg occupancy in olivine, pyroxenes, amphibole, and chlorite, and the Ca / Na ratio in

plagioclase. To maximize the fit of the model to the measured diffraction signal, the effects of crystallite size and crystal strain on peak shape were also considered.

3.3 Loss on ignition (LOI)

Each sample was first dried for 10–12 h at 100 °C. Next, 2.5 and 0.1200 g of the sedimented and suspension subsamples, respectively, were weighed on a Mettler Toledo™ balance. Ignition at 1000 °C took place for 2 h within a Carbolite™ 1100 °C chamber furnace. The weight difference in percent between the pre-ignited powder and the ignited material is reported as loss on ignition (LOI). The 2.5 g procedure is routinely used at the Bergen Geoanalytical Facility of the University of Bergen for igneous rocks. The analytical quality control for the 0.1200 g sample material method was performed while measuring two commercially available international reference materials: basalt BIR-1 (−0.5 wt %) and gabbro MRG-1 (1.2 wt %). These data overlap with reported reference values for these materials within the GeoReM database (http://georem.mpch-mainz.gwdg.de, last access: 21 October 2021).

4 Assessment of methods and results

In the sections above, we report in detail the methods by which we collected and processed channel samples of drill core. In this section we analyze the results of our sampling in several ways to evaluate whether our methods have been appropriate, systematic, or even necessary. We follow this by exploring mineral and chemical fractionation between the sedimented and suspended subsamples, and we then compare our analyses of major elements in channel samples with those obtained by analyzing selected billets on board the JR.

4.1 Recovery of cuttings

To evaluate whether our sampling methods were systematic, we compare the total recovered channel sample (sedimented + suspended subsamples) with the length of core cut using data from all 42 cores. As most pieces of core were cylindrical, measurements of the length of core are a good proxy for the volume of core consumed by the cut. The correlation of the mass of sample recovered with the length of core cut (Fig. 2) is rather good with an R^2 value of 0.86; the best correlation is with cores longer than ∼ 1 m. There is a weak correlation of length of core to total alteration, and that could explain the higher yield of grams recovered from these crumbly cores. The good correlation demonstrates that our methods were systematic, leading to a surprisingly large ∼ 1.3 g of sample recovered per centimeter of core cut. With a 1.5 mm slot cut into the 57 mm diameter core, the amount of material recovered is 3.3 % of the core.

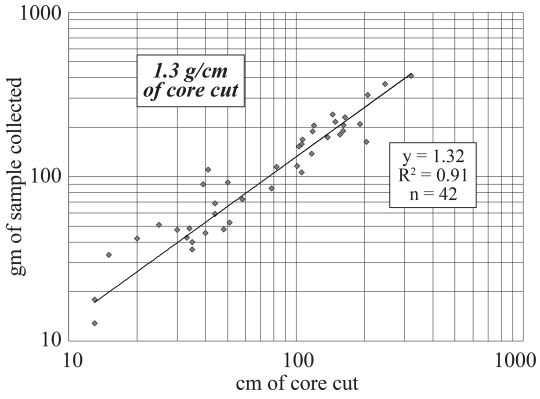

Figure 2. The relationship between total grams of sample collected and centimeters of core cut, illustrating that the sampling methods were systematic and that ∼ 1.3 g cm^{-1} of cut core was recovered from this process.

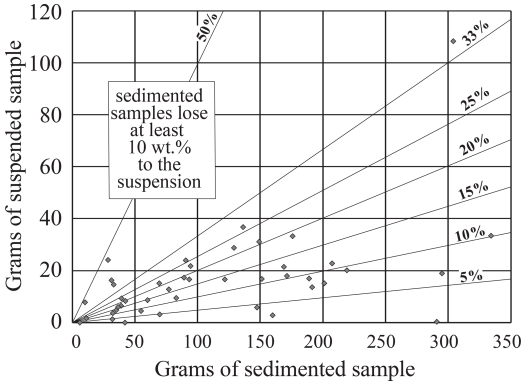

Figure 3. Graph comparing the weights of sedimented and suspended fractions in 42 core samples from Site 1415, Hess Deep. Equal weight fractions would follow the 50 % line. The data show that the suspended sample was generally > 10 % of the total sample, but some samples produced a suspended subsample that was > 30 % of the sedimented subsample.

4.2 Sedimented vs. suspended subsamples

To determine if collection of the suspended sediment in addition to the sedimented sample is quantitatively necessary, we compare the mass of sedimented particles recovered (Fig. 1b) with the mass of clay-sized suspended particles (Fig. 1c) for all 42 cores recovered. This comparison (Fig. 3) shows that a typical core produced between 30 and 200 g of sedimented sample. It also shows that between 5 and 40 g of suspended subsample were extracted from the suspension. This constitutes between 5 and 20 % of the total sample and over 33 % of the bulk in very short cores. There is a weak correlation between short cores and percent alteration minerals, which could explain the higher yield of suspended material in the short cores. We conclude that the relative amount of suspended material can be significant, and its collection is necessary for the characterization of the total sample.

4.3 Potential contamination

Several sources of contamination of our samples are possible. Cuttings created by the active drilling were flushed into the ocean with seawater and did not interfere with ship-board analyses. Cores were brought to the surface in plastic pipes, insulating them from the metal drill stems. After the core was extracted from the plastic pipe, it was thoroughly washed and rinsed with distilled water produced on board the JR. In addition to avoiding contamination, the cores needed to be devoid of particles to allow for whole-round photographic recording. We employed a new saw with new blades to eliminate contamination from samples cut on prior expeditions. The lubricating fluid for the saw was distilled water that provided no inorganic contaminants. A comparison of the concentrations of Ni vs. V (Fig. 4d) measured in our channel samples and in the billet samples shows that the range of channel sample compositions lies within the field defined by the billet concentrations. Neither data set shows outliers that could suggest contamination by any drilling or sawing tools that would contain these metals.

One last source of contamination could be the drilling mud that was used in "mud sweeps" to flush out sidewall fragments that may have fallen into the hole. To explore this possibility of contamination by drilling mud that might have survived washing of the core, we tested for the presence of Ba in the suspended and sedimented subsamples. Given the high concentration of barite in the mud, its presence would signal lingering contamination in the core. We expected barite to fractionate into the sedimented subsample because of its high density. Evidence that density contributes to fractionation between the sedimented and suspension subsamples comes from the higher concentration of Cr (Fig. 4c) and V (Fig. 4a), presumably in oxides, by up to a factor of 2 into the sedimented sample (Fig. 4c). Barium, however, does not follow this fractionation relationship. In contrast its concentration in the suspended fraction is more than 2 times that in the sedimented faction (Fig. 4a). Furthermore, the concentrations are not larger than found in billets analyzed on board the JR (Gillis et al., 2014b, their Table T1). We infer from these results that neither barite nor drilling mud contaminated our samples (see also Sect. 4.6).

4.4 Mineral fractionation between suspended and sedimented samples

To determine whether any mineral fractionation occurred between the coarser sedimented subsample and the suspended clay-sized subsample, mineral modes of both size fractions were determined by X-ray diffraction and Rietveld refinement (Fig. 5). The results of these analyses show that the same suite of minerals is present in both the sediment and the suspension fractions, but that the magmatic minerals are fractionated into the coarser sedimented subsample. Plagioclase and clinopyroxene are enriched by 50 % in the sediment, whereas olivine (modeled as Fe-forsterite in the Rietveld refinement) is 2 to 5 times more abundant in the sediment. In contrast, the phyllosilicates are fractionated into the suspension. Chlorite and serpentine are nearly twice as abundant in the suspension, and talc and amphibole can be more than 5 times as abundant. Prehnite analcime and Ca-thomsonite show the least tendency to fractionate.

Such fractionation is not unexpected. Phyllosilicates would predictably cleave easily along their basal cleavage planes, producing thin, small-diameter platelets. These would thus dominate the clay-sized fraction in the mineralogy of the suspension. Fragments of plagioclase, clinopyroxene, and olivine with weaker or no cleavage would remain coarser and would dominate the sedimented sample. Prehnite, where abundant, might be expected to follow these magmatic minerals as it also has only one good direction of cleavage, but it fractionates into the suspended sample where it is present in low concentrations. This might be explained by its fine grain size in some samples where it is associated with plagioclase alteration (e.g., Früh-Green et al., 1996; Frost et al., 2008; Fig. 6). The conclusion from these results is that the collection of the suspended subsample is imperative to recover representative samples of these altered mafic rocks to avoid bias against the alteration minerals.

4.5 Chemical fractionation between suspended and sedimented samples

With the identification of the phyllosilicate fractionation into the suspended subsample, a sympathetic chemical fractionation is expected. Both FeO and MgO occur in magmatic and alteration minerals, but the phyllosilicates are concentrated in the suspended subsample. A comparison of the concentrations of these elements (Fig. 7a, b) shows no significant fractionation in olivine gabbro and troctolite in Hole P. However, in rocks from the more highly altered Hole J, FeO, MgO, Co (Fig. 4a), Eu (Fig. 4b), and Ni (Fig. 4c) do fractionate into the suspension to varying degrees. The Mg# (atomic MgO / (MgO + FeO)) is also higher in the suspended subsample, likely due to its higher concentration of serpentine (see Fig. 5). This is obvious where Mg#s of suspended and sedimented subsamples are compared (Fig. 7c). Nevertheless, the Mg# of the bulk rock is largely determined by the sedimented sample (Fig. 7d).

A comparison of CaO with Na_2O concentrations shows that CaO is fractionated into the sedimented subsample (Fig. 8a), whereas Na_2O is concentrated into the suspended subsample (Fig. 8b). This reflects the higher concentrations of Ca-rich plagioclase, clinopyroxene, and prehnite in the former and of Na-rich clay minerals in the latter. This interpretation is consistent with the fractionation of V, Sc, Cr, and most rare-earth elements (REEs) also into the sedimented subsamples and of Ba and Eu into the suspended fraction (Fig. 4). The modest fractionation of Sr into the sedimented sample (Fig. 4a) is a surprise given that its likely host, pla-

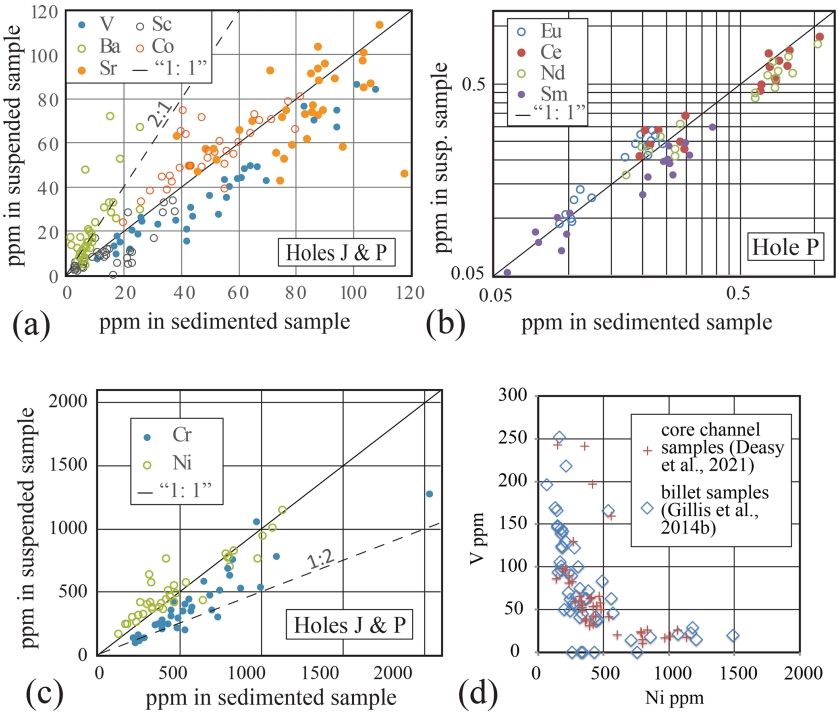

Figure 4. Graphs showing the distribution of selected trace elements between the suspension subsample and the sedimented subsample. **(a)** Ba is strongly fractionated into the suspension subsample, whereas the reverse occurs with V. **(b)** Little fractionation of REEs occurs with the possible exception of Eu into the suspended subsample. **(c)** Little fractionation occurs with Ni, but Cr is fractionated into the sedimented subsample. **(d)** The correlation of the concentrations of Ni and V measured in our channel samples and in the billet samples is very good, suggesting no detectable contamination in the channel samples.

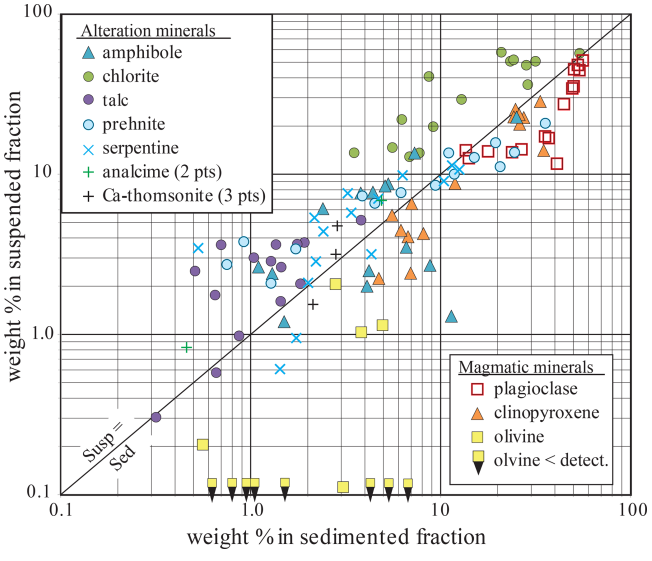

Figure 5. Graph comparing the weight percent (wt %) of the minerals in the sedimented subsample with the weight percent of the clay-sized minerals in the suspended subsample in cores from Hole J as determined by X-ray diffraction and Rietveld refinement. The graph shows that magmatic minerals fractionated into the sedimented subsample whereas phyllosilicates fractionated into the suspended subsample.

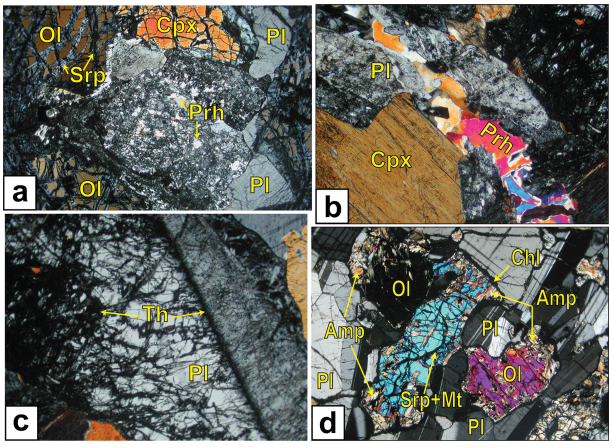

Figure 6. Cross-polarized light images of minerals from Hole J, Site U1415. **(a)** A sample of troctolite from Unit III (J19R1_39-45), showing prehnite (Prh) replacing plagioclase (Pl) and serpentine (Srp) replacing olivine (Ol), forming a mesh texture in a plagioclase + clinopyroxene (Cpx) host. **(b)** A prehnite vein cutting Pl and Cpx in gabbro from Unit II (J8R3_114-116). **(c)** Ca-thomsonite (Th, very low birefringence) replacing Pl in gabbro Unit II (J8R3 114–116). **(d)** The alteration of Ol by amphibole (Amp) and by serpentine + magnetite (Mt) and the alteration of Pl + Ol by chlorite (Chl) in sample J7G1 44–46.

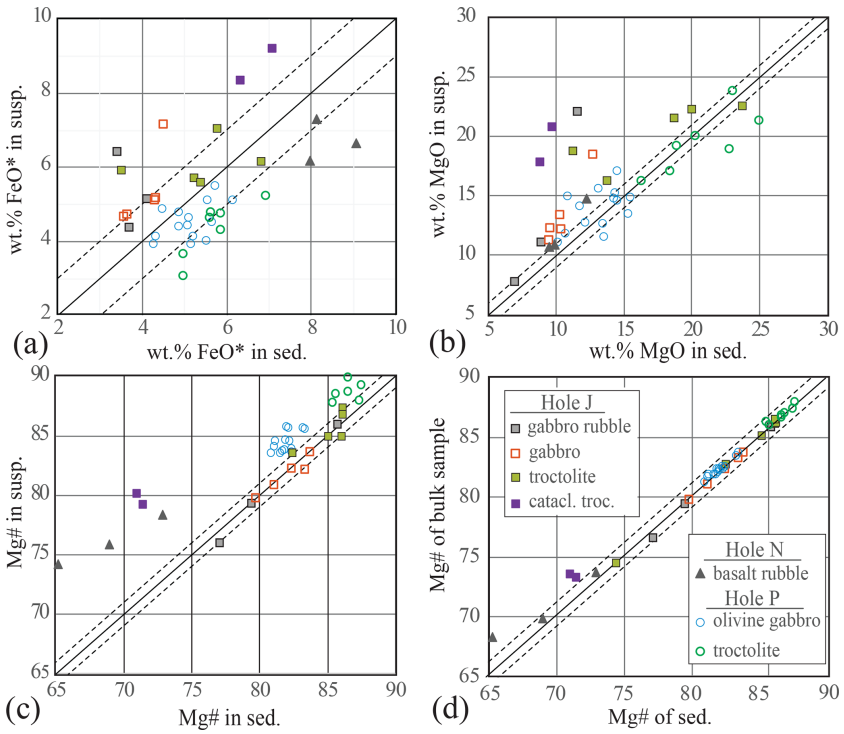

Figure 7. A comparison of the concentrations of MgO and FeO* (total) in sedimented and suspended fractions of the channel samples. Solid line: 1 to 1, no fractionation. Dashed lines: ±1 % envelope. **(a)** Graph showing that there is no systematic fractionation of FeO* between sedimented and suspended samples. **(b)** Graph showing that MgO tends to be fractionated into the suspended sample, reflecting the relatively high concentration of MgO-rich phyllosilicates. **(c)** The comparison of the Mg# between suspended and sedimented samples shows the effect of phyllosilicates raising the Mg# in the suspended sample. **(d)** Graph showing that the larger mass of the sedimented sample dominates the Mg# of bulk sample.

gioclase, is fractionated into the sediment (Fig. 5). The Sr content of prehnite and zeolite partially fractionated into the suspended sample probably contributes to this behavior. Figure 8c shows the corresponding higher Ca#s (atomic Ca / (Ca + Na)) in the sedimented subsample. However, as was found in the Mg system, the Ca# is dominated by the sedimented sample because of the relatively low concentration of CaO and Na_2O in the suspended subsample. Consequently, the Ca# of the bulk sample follows that of the sedimented sample (Fig. 8d).

4.6 Comparison of chemical compositions of channel samples and billets

We compare the chemical compositions of billets (typically 2 × 3 × 3 cm) from Hole J analyzed aboard the JR (Gilles et al., 2014b) with the chemical compositions of bulk channel samples analyzed by Deasy et al. (2021). Instrumental analytical analysis in both studies was similar with the inductively coupled plasma atomic emission spectroscopy (ICP-AES) method on the JR and ICP-AES (major elements) with inductively coupled plasma mass spectroscopy (ICP-MS, trace element) measurements reported in Deasy et al. (2021). This comparison for SiO_2 (Fig. 9), MgO (Fig. 10), and two trace elements (Fig. 11) shows a general agreement between the two data sets, in spite of the differing sampling strategies. The agreement improves where averages of billet compositions are compared to the respective channel sample of the same core. In particular, the average concentrations of SiO_2, MgO, Sr, and V of five billet compositions from Core 8R come close to recovering the composition of the channel sample (Figs. 9, 10, 11). The results for Sr and V from Core 8 (Fig. 11) also show that where five billets are analyzed their average more closely approaches the concentrations in the channel sample. The results also support the conclusion in Sect. 4.3 that there is no evidence for contamination in the concentration of trace elements analyzed in the channel samples.

On the other hand, individual billets are the only way to target anomalies in bulk compositions. For example, two billets from Core 13R sampled anorthosite and troctolite with very different MgO contents (Fig. 10) and moderately differing SiO_2 contents (Fig. 9), while the average of MgO concentration did come close to the concentration in the channel sample. Clearly, the advantage to analyzing billet-sized samples of a core is to identify heterogeneity in the composition of a core. However, the average of these local compositions

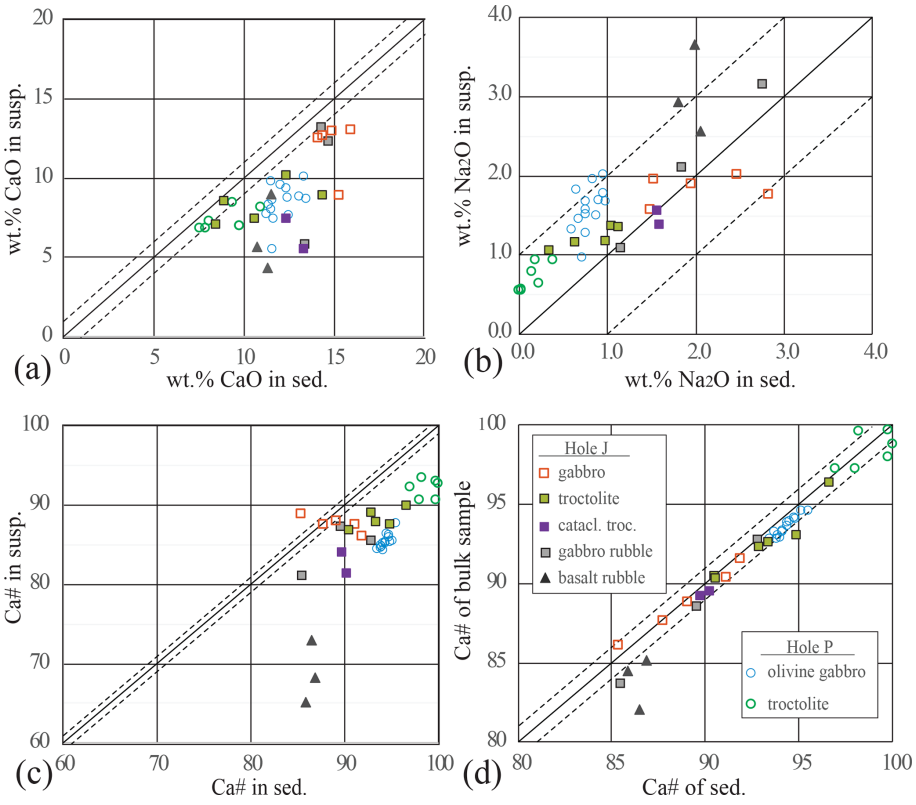

Figure 8. A comparison of the concentrations of CaO and Na_2O in sedimented and suspended fractions of the channel samples. Solid line: 1 to 1, no fractionation. Dashed lines: ±1 % envelope. **(a)** The higher concentration of CaO in the sedimented subsample reflects the higher concentration of CaO in plagioclase, clinopyroxene, and prehnite. **(b)** Na_2O is fractionated into the suspended subsample, reflecting its phyllosilicate host. **(c)** Graph showing the higher Ca# in the sedimented subsamples, consistent with the higher concentration of Ca in magmatic minerals. **(d)** A comparison of the Ca# in the sedimented subsample with the Ca# in the total sample. The similarity snows that the sedimented subsample dominates the Ca# in the total sample.

does not necessarily produce a representative composition of a longer length of core.

The agreement between values of loss on ignition (LOI) measured in billets with H_2O calculated from crystallography is not good (Fig. 12). In this case the LOI of the billets is significantly less than the values measured for the channel samples. This relationship is probably best explained by the fact that the billets were selected for the cohesive nature of the material being sampled. By avoiding veins and altered fractures, these billets provide a better estimate of the composition of the unaltered igneous rocks. However, if the goal is to estimate the composition of a lithology as captured in the core, alteration and all, then the channel sample provides a better estimate by sampling more of the altered material. Still, the core did separate during drilling along some altered fractures and even the analyses of the channel samples gives a minimum estimate of the altered material and the LOI that would have been sampled by the full core.

4.7 Correlation of modal mineralogy with geochemistry

One goal of the channel sampling described here is to analyze the bulk mineralogy and the bulk chemical composition independently. To determine if the chemical and XRD methods employed are consistent with each other, we compare their results. Unfortunately, this comparison is not straightforward, because the XRD methods with Rietveld refinement provide quantitative estimates of the wt % of each mineral and the compositions of many solid solutions. An exception is plagioclase in which the unit cell volumes of albite and anorthite differ by less than 1 %, such that X-ray peak positions are not sensitive to composition. The H_2O content, however, offers an exception that does allow this comparison. The wt % of each hydrated mineral can be used to calculate the wt % of H_2O in that mineral. We compare the sum of these values with the LOI for the same sample as reported by Deasy et al. (2021) in Fig. 13. The comparison does show a strong correlation but with the LOI slightly higher than the H_2O calculated from crystallography. It is possible that small amounts of hydrated minerals below the detection limit of XRD methods (< 1 wt %) are present but at such a low con-

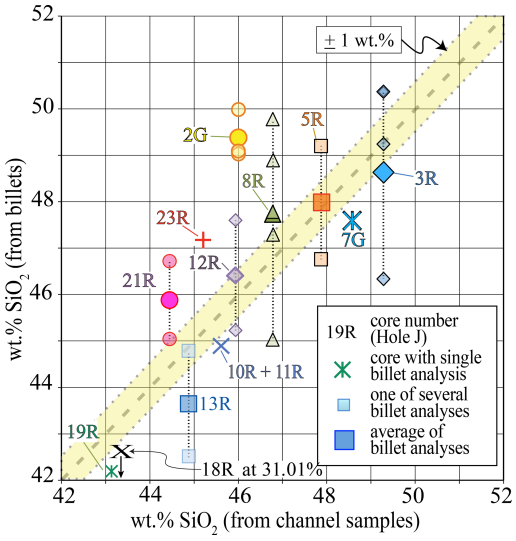

Figure 9. The comparison of bulk SiO_2 analyses of channel samples (x axis) from core from Hole J with the analyses of billets (y axis) analyzed aboard the JR from the same cores. Where more than one billet was analyzed from a single core, they are joined by dotted vertical lines that correspond to the SiO_2 concentrations of the channel samples. Average compositions of the billets are indicated by the bolder symbols. The close correspondence among many samples shows a general agreement of the two sampling methods. However, the averages or single billet compositions of 6 out of 11 samples lie outside a 1.0 wt % band (yellow), showing that average compositions of billets do not yield representative compositions of the whole core.

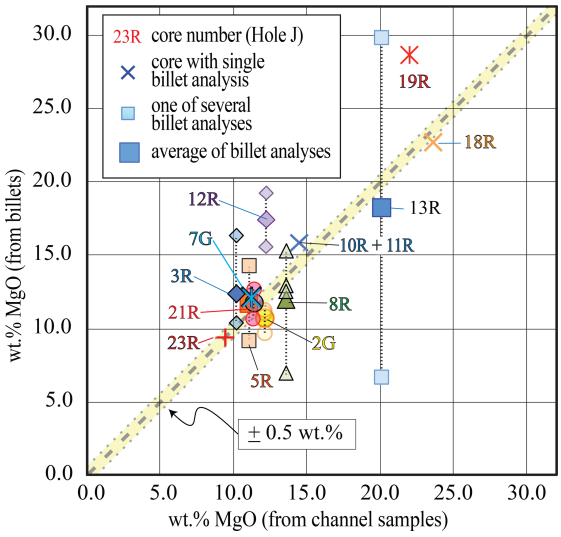

Figure 10. The comparison of bulk MgO concentrations of channel samples from core from Hole J with the analyses of billets analyzed aboard the JR from the same cores. The concentrations of MgO in single billets and from averages of billets from 9 out of 11 cores differ by more than 0.5 wt % (yellow band) from the compositions of the channel samples of the same cores, showing that analyses of billets do not yield representative compositions of the whole core.

centration that their presence could not explain the discrepancy in Fig. 13. However, a comparison of the LOI with the actual measured H_2O on the JR (Gillis et al., 2014b, their Table T1) shows the same higher value for LOI. This demonstrates that the LOI is responding to the weight loss of not only structural H_2O but also of CO_2, SO_2, halogens, and H_2O adsorbed on surfaces. Thus, the good fit of LOI with wt % H_2O calculated from crystallographic data supports a conclusion that each method is responding to the same material equally.

5 Recommendations

In order to make collection of this valuable channel sample of core more efficient and less labor intensive, we recommend the following modifications to the methods described above. The volume of water used to capture the suspended fine fraction should be minimized. This can be accomplished by recycling and filtering the (distilled) lubricating water from the bottom of the saw housing with a pump. Although rinse water for washing the saw and housing would still be required, recycling would minimize the volume of water holding the suspension by as much as 75 % for a long core. For ease in cleaning, the saw housing should be coated with Teflon.

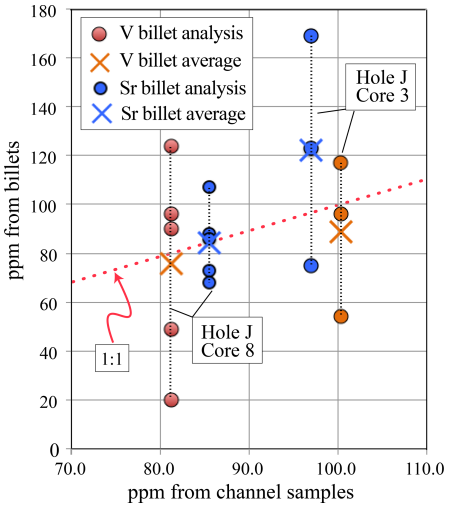

Figure 11. A comparison of the concentrations of Sr and V in channel samples from Cores 3 and 8 in Hole J with the analyses of billets analyzed aboard the JR from the same cores. The average concentrations of Sr and V in five billets from Core 8 approaches the concentrations in the channel sample more closely than does the average of the concentrations in three billets from Core 3.

A major rate-limiting step in sampling was the time needed for collection of the suspended material using a normal tube centrifuge. When the rate of core recovery was high, the rate of production of rinse water was much higher than could be processed by filtering and centrifuging the water.

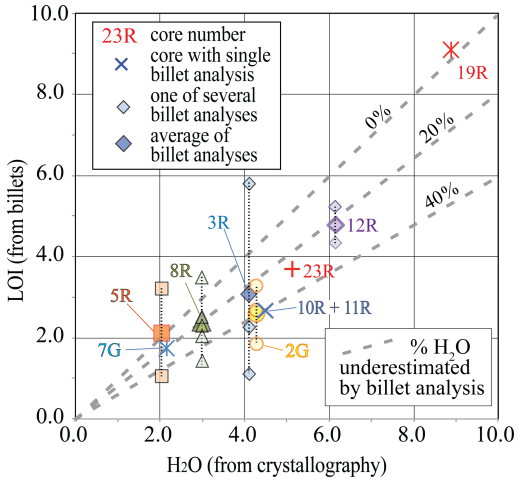

Figure 12. The comparison of the values of weight loss on ignition (LOI) from channel samples of the bulk cores from Hole J (this study) with values analyzed aboard the JR from billets cut from the same cores. The values of LOI from billets are as much as 40 % smaller than found in the bulk core samples.

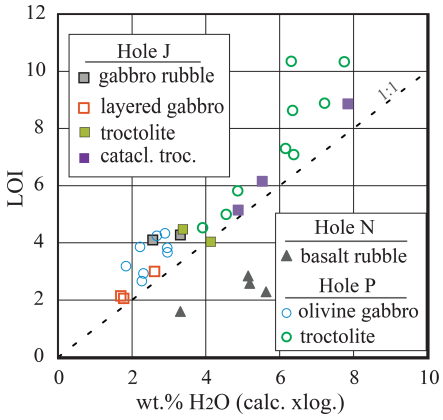

Figure 13. A comparison of the measured weight loss on ignition (LOI) with the wt % H_2O calculated from the sum of the wt % of each hydrated mineral calculated using the Rietveld refinement (this study). The diagram shows that LOI values slightly exceed the calculated H_2O contents (see text).

Use of a continuous-flow centrifuge would greatly increase the efficiency of the onboard collection of the suspended material. The slow recovery of core on Expedition 345 gave us time to collect the suspended samples, but this situation will hopefully not be repeated.

Staffing would also need to be increased. During Expedition 345, scientists from petrology and geochemistry took on double shifts to accomplish this sampling. With a greater rate of core recovery, a minimum of three scientists would be necessary for 24 h sample recovery. A fourth scientist would probably be necessary with continuous core recovery. If analytical work were to be performed on board, then one scientist would be sufficient to conduct all the XRD studies, but three geochemists would be needed for the greatly increased number of samples to be analyzed.

Improvements in our analytical instruments are giving us ever-increasing precision in the compositions of rocks and minerals, even to the parts per trillion (ppt) levels of detection. However, without improvements in our sampling protocol, the accuracy of any analytical result will not improve. We have presented here a sampling strategy that will keep pace with advancements in analytical capabilities that will lead to both a more precise and a more accurate understanding of Earth materials in general, as well as to a deeper understanding of the mineralogical and chemical composition of the lower oceanic crust.

6 Discussion and conclusions

The results above show that the method of channel sampling produces a reliable, representative data set of the core involved without consuming any new split of the valuable core. In fact, the yield is a significant $\sim 1.3\,\mathrm{g\,cm^{-1}}$ of cut core (Fig. 2), a recovery of 3.3 vol % of the core. We find no evidence for contamination of our channel samples (Figs. 4, 9, 10, 11). Bulk chemical compositions of core are not attainable through an average of the compositions of subjectively selected billet-sized samples (Figs. 9, 10). An important result of this work is the discovery that there is significant mineral and thus also chemical fractionation between the sedimented material and the suspended clay-sized particles produced during cutting the core; thus, both size fractions must be sampled and analyzed to produce a representative sample of the bulk core. The collection of the suspended subsample is time-consuming, but because it commonly makes up > 10 % of the bulk sample (Fig. 3) and because phyllosilicates are selectively fractionated into it (Fig. 5), it cannot be ignored. Thus, neither the sedimented subsample nor the suspended subsample alone is representative of the bulk core composition. The results also show that the proportion of the sample in the suspension cannot be predicted, because there is no correlation between the mass of the sediment and suspended fractions. Added together, however, there is a good correlation between the total grams sampled and the centimeters of core cut (Fig. 2). Thus, the data demonstrate that only the weighted average of the two size fractions yields a representative bulk sample.

Data availability. The data from this research are available in Deasy et al. (2021, https://doi.org/10.1093/petrology/egab019).

Author contributions. RPW, RM, and TN designed and executed sample collection aboard the JR. RM analyzed volatile content aboard the JR, developed the wet chemistry procedure, prepared samples, and supervised the chemical analysis onshore. DLB supervised the XRD analysis and Rietveld refinements. RTD conducted

much of the chemical analysis. CJ and RTD prepared the samples and conducted the XRD analysis. Petrographic analysis was performed by TN, who also provided images in the text. RPW prepared the article with contributions from all co-authors.

Competing interests. The contact author has declared that neither they nor their co-authors have any competing interests.

Disclaimer. Any use of trade, firm, or product names is for descriptive purposes only and does not imply endorsement by the U.S. Government.

Publisher's note: Copernicus Publications remains neutral with regard to jurisdictional claims in published maps and institutional affiliations.

Acknowledgements. We thank the drilling and operational crew of the *JOIDES Resolution* for cooperation, as we sampled the cuttings at all hours, and the IODP Expedition 345 scientific community, especially Jon Snow for encouragement and helpful discussion aboard the JR. This work was partially supported by IODP start-up funds (grant no. 0123456). Romain Meyer was at the Centre for Geobiology, Department of Earth Science, University of Bergen, during some of this research.

Financial support. This research has been supported by IODP start-up funds (grant no. 0123456) and the Norges forskningsråd.

Review statement. This paper was edited by Thomas Wiersberg and reviewed by Thomas Belgrano and one anonymous referee.

References

Agterberg, F. P.: Sampling and analysis of chemical element concentration distribution in rock units and orebodies, Nonlin. Processes Geophys., 19, 23–44, https://doi.org/10.5194/npg-19-23-2012, 2012.

Arai, S. and Matsukage, K.: Petrology of gabbro-troctolite-peridotite complex from Hess Deep, equatorial Pacific: implications for mantle-melt interaction within the oceanic lithosphere, in: Proc. ODP, Sci. Results, College Station, TX (Ocean Drilling Program), edited by: Mével, C., Gillis, K. M., Allan, J. F., and Meyer, P. S., 147, 135–155, https://doi.org/10.2973/odp.proc.sr.147.008.1996, 1996.

Arai, S. and Takemoto, Y.: Mantle wehrlite from Hess Deep as a crystal cumulate from an ultra-depleted primary melt in East Pacific Rise, Geophys. Res. Lett., 34, L08302, https://doi.org/10.1029/2006GL029198, 2007.

Bish, D. L. and Post, J. E.: Quantitative mineralogical analysis using the Rietveld full-pattern fitting method, Am. Min., 78, 932–940, 1993.

Bish, D. L., Sarrazin, P., Chipera, S. J., Vaniman, D. T., and Blake, D.: Quantitative mineralogical analysis of Mars analogues using CHEMIN data and Rietveld refinement, 35th Lunar and Planetary Science Conf., 2004: The Future of Mars Surface Exploration, 15–19 March 2004, League City, Texas, USA, 35, 1404, ID: 20040065952, 2004.

Bish, D. L., Blake, D. F., Vaniman, D. T., Chipera, S. J., Morris, R. V., Ming, D. W., Treiman, A. H., Sarrazin, P., Morrison, S. M., Downs, R. T. Achilles, C. N., A. S. Yen, Bristow, T. F. Crisp, J. A., Morookian, J. M., Farmer, J. D., Rampe, E. B., Stolper, E. M., Spanovich, N., and the MSL Science Team: X-ray Diffraction Results from Mars Science Laboratory: Mineralogy of Rocknest at Gale Crater, Science, 341, 1476–1477, https://doi.org/10.1126/science.1238932, 2013.

Blackman, D. K., Ildefonse, B., John, B. E., Ohara, Y., Miller, D. J., Abe, N., Abratis, M., Andal, E. S., Andreani, M., Awaji, S., Beard, J. S., Brunelli, D., Charney, A. B., Christie, D., Collins, M. J., Delacour, A. G., Delius, H., Drouin, M., Einaudi, F., Escartín, J., Frost, B. R., Früh-Green, G., Fryer, P. B., Gee, J. S., Godard, M., Grimes, C. B., Halfpenny, A., Hansen, H. E., Harris, A. C., Tamura, A., Hayman, N. W., Hellebrand, E., Hirose, T., Hirth, J. G., Ishimaru, S., Johnson, K. T. M., Karner, G. D., Linek, M., MacLeod, C. J., Maeda, J., Mason, O. U., McCaig, A. M., Michibayashi, K., Morris, A., Nakagawa, T., Nozaka, T., Rosner, M., Searle, R. C., Suhr, G., Tominaga, M., von der Handt, A., Yamasaki, T., and Zhao X.: Drilling constraints on lithospheric accretion and evolution at Atlantis Massif, Mid-Atlantic Ridge 30° N, J. Geophys. Res., 116, B07103, https://doi.org/10.1029/2010JB007931, 2011.

Bourdon, B., Turner, S., and Dosseto, A.: Dehydration and partial melting in subduction zones: Constraints from U-series disequilibria, J. Geophys. Res., 108, 2291, https://doi.org/10.1029/2002JB001839, 2003.

Coogan, L. A.: The Lower Oceanic Crust, in: Treatise on Geochemistry, edited by: Holland, H and Turekian, K., 2nd edn., The crust, 4.14, 497–541, ISBN 9780080959757, 2014.

Coogan, L. A., Gillis, K. M., MacLeod, C. J., Thompson, G. M., and Hékinian, R.: Petrology and geochemistry of the lower ocean crust formed at the East Pacific Rise and exposed at Hess Deep: a synthesis and new results, Geochem. Geophy. Geosy., 3, 8604, https://doi.org/10.1029/2001GC000230, 2002.

Cornish, E. C.: Sampling ore deposits, Colorado School of Mines Mineral Industries Bulletin 9, 2, 15 pp., ISSN 0010-1745, 1966.

Deasy, R. T., Wintsch, R. P., Meyer, R. Bish, D. L., Gasaway, C., and Heimdal, T.: Decoupling of serpentinization and prehnitization in Lower East Pacific Rise Crust at Hess Deep, Fall Meeting, AGU, 15–19 December 2014, San Francisco, Calif., USA, Abs. V52A-04, Accession Number: 2016-012344, 2014.

Deasy, R. T., Wintsch, R. P., and Meyer, R.: Bulk composition of fast-spreading oceanic crust: insights from the lower cumulates of the East Pacific Rise and from Cocos-Nazca Rift basalts, Hess Deep, J. Petrol. 62, egab019, https://doi.org/10.1093/petrology/egab019, 2021.

Dick, H. J. B., Natland, J. H., Miller, D. J., Alt, J. C., Bach, W., Bideau, D., Gee, J. S., Haggas, S., Hertogen, J. G. H., Hirth, G., Holm, P. N., Ildefonse, B., Iturrino, G. J., John, B. E., Kelley, D. S. Kikawa, E., Kingdon, A., Le Roux, P. J., Maeda, J., Meyer, P. S., Naslund, H. R., Niu, Y., Robinson, T. P., Snow, J. E., Stephen, R. A., Trimby, P. W., Worm, H.-U., and Yoshinobu, A.: Initial Reports, Proceed-

ings ODP, College Station, TX (Ocean Drilling Program), 176, https://doi.org/10.2973/odp.proc.ir.176.1999, 1999.

Frost, B. R., Beard, J. S., McCaig, A., and Condliffe, E.: The Formation of Micro-Rodingites from IODP Hole U1309D: Key To Understanding the Process of Serpentinization, J. Pet., 49, 1579–1588, 2008.

Früh-Green, G. L., Plas, A., and Dell'Angelo, L. N.: Mineralogic and stable isotope record of polyphase alteration of upper crustal gabbros of the East Pacific Rise (Hess Deep, Site 894), in: Proc. ODP, Sci. Results, College Station, TX (Ocean Drilling Program), edited by: Mével, C., Gillis, K. M., Allan, J. F., and Meyer, P. S., 147, 235–254, https://doi.org/10.2973/odp.proc.sr.147.015.1996, 1996.

Gillis, K. M., Coogan, L. A., and Pedersen, T, R.: Strontium isotope constraints on fluid flow in the upper oceanic crust at the East Pacific Rise, Earth Planet. Sc. Lett., 232, 83–94, 2005.

Gillis, K. M., Snow, J. E., Klaus, A., Guerin, G., Abe, N., Akizawa, N., Ceuleneer, G., Cheadle, M. J., Adrião, Á., Faak, K., Falloon, T. J., Friedman, S. A., Godard, M. M., Harigane, Y., Horst, A. J., Hoshide, T., Ildefonse, B., Jean, M. M., John, B. E., Koepke, J. H., Machi, S., Maeda, J., Marks, N. E., McCaig, A. M., Meyer, R., Morris, A., Nozaka, T., Python, M., Saha, A., and Wintsch, R. P.: Expedition 345 summary, in: Proceedings of the Integrated Ocean Drilling Program, College Station, TX (Integrated Ocean Drilling Program), edited by: Gillis, K. M., Snow, J. E., Klaus, A., and the Expedition 345 Scientists, 345, 1–49, https://doi.org/10.2204/iodp.proc.345.101.2014, 2014a.

Gillis, K. M., Snow, J. E., Klaus, A., Guerin, G., Abe, N., Akizawa, N., Ceuleneer, G., Cheadle, M.J., Adrião, Á., Faak, K., Falloon, T. J., Friedman, S.A., Godard, M. M., Harigane, Y., Horst, A. J., Hoshide, T., Ildefonse, B., Jean, M. M., John, B. E., Koepke, J. H., Machi, S., Maeda, J., Marks, N. E., McCaig, A. M., Meyer, R., Morris, A., Nozaka, T., Python, M., Saha, A., and Wintsch, R. P.: Geochemistry summary, in: Proc. IODP, College Station, TX (Integrated Ocean Drilling Program), edited by: Gillis, K. M., Snow, J. E., Klaus, A., and the Expedition 345 Scientists, 345, 7 pp., https://doi.org/10.2204/iodp.proc.345.114.2014, 2014b.

Gillis, K. M., Snow, J. E., Klaus, A., Guerin, G., Abe, N., Akizawa, N., Ceuleneer, G., Cheadle, M.J., Adrião, Á., Faak, K., Falloon, T. J., Friedman, S. A., Godard, M. M., Harigane, Y., Horst, A. J., Hoshide, T., Ildefonse, B., Jean, M. M., John, B. E., Koepke, J. H., Machi, S., Maeda, J., Marks, N. E., McCaig, A. M., Meyer, R., Morris, A., Nozaka, T., Python, M., Saha, A., and Wintsch, R. P.: Methods Chapter, in: Proceedings of the Integrated Ocean Drilling Program, College Station, TX (Integrated Ocean Drilling Program), edited by: Gillis, K. M., Snow, J. E., Klaus, A., and the Expedition 345 Scientists, 345, 1–63, https://doi.org/10.2204/iodp.proc.345.115.2014, 2014c.

Gillis, K. M., Snow, J. E., Klaus, A., Guerin, G., Abe, N., Akizawa, N., Ceuleneer, G., Cheadle, M. J., Adrião, Á., Faak, K., Falloon, T. J., Friedman, S. A., Godard, M. M., Harigane, Y., Horst, A. J., Hoshide, T., Ildefonse, B., Jean, M. M., John, B. E., Koepke, J. H., Machi, S., Maeda, J., Marks, N. E., McCaig, A. M., Meyer, R., Morris, A., Nozaka, T., Python, M., Saha, A., and Wintsch, R. P.: Primitive layered gabbros from fast-spreading lower oceanic crust, Nature, 505, 204–207, https://doi.org/10.1038/nature12778, 2014d.

Gillis, K. M., Snow, J. E., Klaus, A., Guerin, G., Abe, N., Akizawa, N., Ceuleneer, G., Cheadle, M. J., Adrião, Á., Faak, K., Falloon, T. J., Friedman, S. A., Godard, M. M., Harigane, Y., Horst, A. J., Hoshide, T., Ildefonse, B., Jean, M. M., John, B. E., Koepke, J. H., Machi, S., Maeda, J., Marks, N. E., McCaig, A. M., Meyer, R., Morris, A., Nozaka, T., Python, M., Saha, A., and Wintsch, R. P.: Proceedings of the Integrated Ocean Drilling Program; Hess Deep plutonic crust; exploring the plutonic crust at a fast-spreading ridge; new drilling at Hess Deep, Expedition 345 of the riserless drilling platform; Puntarenas, Costa Rica, to Balboa, Panama; Site U1415, 11 December 2012–12 February 2013, Proceedings of the Integrated Ocean Drilling Program, College Station, TX (Integrated Ocean Drilling Program), 345, variously paginated, 2014e.

Greenberger R. N., Harris M., Ehlmann B. L., Crotteau M., Kelemen P. B., Manning C. E., and Teagle D. A.: Hydrothermal alteration of the ocean crust and patterns in mineralization with depth as measured by micro-imaging infrared spectroscopy, J. Geophys. Res.-Sol. Ea., 128, e2021JB021976, https://doi.org/10.1029/2021JB021976, 2021.

Hacker, B. R., Peacock, S. M., Abers, G. A., and Holloway, S. D.: Subduction factory, 2, Are intermediate-depth earthquakes in subducting slabs linked to metamorphic dehydration reactions?, J. Geophys. Res., 108, 2030, https://doi.org/10.1029/2001JB001129, 2003.

Hart, S. R., Blusztajn, J., Dick, H. J. B., Meyer, P. S., and Muehlenbachs, K.: The fingerprint of seawater circulation in a 500-meter section of ocean crust gabbros, Geochim. Cosmochim. Ac., 63, 4059–4080, 1999.

Heinrichs, H. and Hermann, A. G.: Praktikum der Analytischen Geochemie, Springer, New York, 669 pp., ISBN 978-3-540-51874-7, 1990.

Kelemen, P. B., Matter, J. M., Teagle, D. A. H., Coggon, J. A., and the Oman Drilling Project Science Team: Proceedings of the Oman Drilling Project, College Station, TX (International Ocean Discovery Program), 19 Chapters, variously paginated, https://doi.org/10.14379/OmanDP.proc.2020, 2020.

Koepke J., Abe, N., Akizawa, N., Falloon, T. J., Hoshide, T., Jean, M. M., and Snow, J. E.: IODP EXP 345: Orthopyroxene omnipresent in layered gabbros from the Hess Deep, RPR, 2013 Fall Meeting, AGU, 9–13 December 2013, San Francisco, Calif., USA, Abstract OS43A-1875, 2013.

Lecuyer, C. and Reynard, B.: High-temperature alteration of oceanic gabbros by seawater (Hess Deep, Ocean Drilling Program Leg 147): evidence from oxygen isotopes and elemental fluxes, J. Geophys. Res.-Sol. Ea., 101, 15883–15897, https://doi.org/10.1029/96JB00950, 1996.

Lewis, D. W.: Practical Sedimentology, Hutchinson Ross Publishers, Stroudsburg, PA, 277 pp., ISBN 978-0-87933-443-7, 1984.

Lissenberg, C. J., MacLeod, C. J., Howard, K. A., and Godard, M.: Pervasive reactive melt migration through fast-spreading lower oceanic crust (Hess Deep, equatorial Pacific Ocean), Earth Planet. Sc. Lett., 361, 436–447, 2013.

Lucia, F. J.: Carbonate Reservoir Characterization, An Integrated Approach, Springer, Berlin, 336 pp., ISBN 978-3-540-72740-8, 2007.

Manning, C. E.: The chemistry of subduction-zone fluids, Earth Planet. Sc. Lett., 223, 1–16, 2004.

Manning, C. E. and MacLeod, C. J.: Fracture-controlled metamorphism of Hess Deep gabbros, Site 894: constraints on the roots of mid-ocean-ridge hydrothermal systems at fast-

spreading centers, in: Proc. ODP, Sci. Results, College Station, TX (Ocean Drilling Program), edited by: Mével, C., Gillis, K. M., Allan, J. F., and Meyer, P. S., 147, 189–212, https://doi.org/10.2973/odp.proc.sr.147.011.1996, 1996.

Manning, C. E., Weston, P. E., and Mahon, K. I.: Rapid high-temperature metamorphism of East Pacific Rise gabbros from Hess Deep, Earth Planet. Sc. Lett., 144, 123–132, https://doi.org/10.1016/0012-821X(96)00153-7, 1996.

Marks, N., Gillis, K. M., Lindvall, R. E., and Schorzman, K.: IODP Expedition 345: Characterizing Hydrothermal Alteration of Fast-Spreading EPR Lower Crust using O, Sr and Nd isotopics, 2014 AGU Fall Meeting, 15–19 December 2014, San Francisco, USA, V22A-07, 2014.38, Accession Number: 2015-088474, 2014.

Marks, N. E., Faak, K., Gillis, K. M., McCaig, A. M., Nozaka, T., and Python, M.: IODP Expedition 345: Hydrothermal Alteration of Fast-Spreading EPR Lower Crust, 2013 AGU Fall Meeting, 9–13 December 2013, San Francisco, USA, OS43A-1879, Accession Number: 2015-070549, 2013.

Meade, C. and Jeanloz, R.: Deep-focus earthquakes and recycling of water into the Earth's mantle, Science, 252, 68–72, 1991.

Mével, C. and Stamoudi, C.: Hydrothermal Alteration of the Upper-Mantle Section at Hess Deep, in: Proceedings of the Ocean Drilling Program, Scientific Results, edited by: Mével, C, Gillis, K. M., Allan, J. F., and Meyer, P. S., chap. 15, 147, 293–309, https://doi.org/10.2973/odp.proc.sr.147.017.1996, 1996.

Meyer, R., Wintsch, R. P., Nozaka, T., Gillis, K. M., and Snow, J. E., and the Scientific Crew of the Joides Resolution,: Deep fast-spread Oceanic Crust – Fluid Interactions: Petrography and Volatiles from IODP Expedition 345 Hess Deep Plutonic Crust, Min. Mag., 77.5, 1750, https://doi.org/10.1180/minmag.2013.077.5.13, 2013.

Natland, J. H. and Dick, H. J. B.: Melt migration through high-level gabbroic cumulates of the East Pacific Rise at Hess Deep: the origin of magma lenses and the deep crustal structure of fast-spreading ridges, in: Proceedings ODP, Scientific Results, College Station, TX (Ocean Drilling Program), edited by: Mével, C., Gillis, K. M., Allan, J. F., and Meyer, P. S., 147, 21–58, https://doi.org/10.2973/odp.proc.sr.147.002.1996, 1996.

Nozaka, T. and Fryer, P.: Alteration of the oceanic lower crust at a slow-spreading axis: insight from vein-related zoned halos in olivine gabbro from Atlantis Massif, Mid-Atlantic Ridge, J. Petrol., 52, 643–664, https://doi.org/10.1093/petrology/egq098, 2011.

Nozaka, T., Meyer, R., Wintsch, R. P., and Wathen, B.: Hydrothermal spinel, corundum and diaspore in lower oceanic crustal troctolites from the Hess Deep Rift, Contri. Min. Pet., 171, 1–14, https://doi.org/10.1007/s00410-016-1266-4, 2016.

Nozaka, T., Wintsch, R. P., and Meyer, R.: Serpentinization of olivine in troctolites and olivine gabbros from the Hess Deep Rift, Lithos, 282, 201–214, 2017.

Pedersen, R. B., Malpas, J., and Falloon, T.: Petrology and geochemistry of gabbroic and related rocks from Site 894, Hess Deep, in: Proceedings ODP, Scientific Results, College Station, TX (Ocean Drilling Program), edited by: Mével, C., Gillis, K. M., Allan, J. F., and Meyer, P. S., 147, 3–19, https://doi.org/10.2973/odp.proc.sr.147.001.1996, 1996.

Potts, P. J.: A handbook of silicate rock analysis, Chapman & Hall, New York, NY, USA, 622 pp., ISBN 0412008815, 1987.

Raleigh, C. B. and Paterson, M. S.: Experimental deformation of serpentinite and its tectonic implications, J. Geophys. Res.-Sol. Ea., 70, 3965–3985, 1965.

Ranero, C. R., Villasenõr, A., Phipps Morgan, J., and Weinrebe, W.: Relationship between bend-faulting at trenches and intermediate-depth seismicity, Geochem. Geophy. Geosy., 6, Q12002, https://doi.org/10.1029/2005GC000997, 2005.

Regelous, M., Weinzierl, C. G., and Haase, K. M.: Controls on melting at spreading ridges from correlated abyssal peridotite–mid-ocean ridge basalt compositions, Earth Planet. Sc. Lett., 449, 1–11, 2016.

Sinclair, A. J. and Blackwell. G. H.: Applied Mineral Inventory Estimation, Cambridge University Press, Cambridge, 381 pp., ISBN 978-0-521-79103-8, 2002.

Stanton, R.: Channel and core sampling of coal beds: purposes, methods, and value, Proceedings of the International Coal Testing Conference, 11–13 February 1986, Lexington, KY, USA, 63–68, Accession Number: 1992-004533, 1986.

Stewart, M. A., Klein, E. M., and Karson, J. A.: Geochemistry of dikes and lavas from the north wall of the Hess Deep Rift: insights into the four-dimensional character of crustal construction at fast-spreading mid-ocean ridges, J. Geophys. Res.-Sol. Ea., 107, 2238, https://doi.org/10.1029/2001JB000545, 2002.

Stewart, M. A., Karson, J. A., and Klein, E. M.: Four-dimensional upper crustal construction at fast-spreading mid-ocean ridges: a perspective from an upper crustal cross-section at the Hess Deep Rift, J. Vol. Geoth. Res. 144, 287–309, https://doi.org/10.1016/j.jvolgeores.2004.11.026, 2005.

Swanson, V. E. and Huffman Jr., C.: Guidelines for Sample Collecting and Analytical Methods Used in the U.S. Geological Survey for Determining Chemical Composition of Coal, US Geological Survey Circular 735, 18 pp., ISSN 03646017, 1976.

White, W. M. and Klein, E. M.: Composition of the Oceanic Crust, in: Treatise on Geochemistry, 2nd edn., edited by: Holland, H. and Turekian, K., The crust, 4.13, 457–492, ISBN 978-0080448473, 2014.

Wintsch, R. P., Bish, D. L., and Meyer, R.: IODP Expedition 345: Bulk Mineralogy From Lower Oceanic Crustal Rocks of the Hess Deep, in: 2013 AGU Fall Meeting, 9–13 December 2013, San Francisco, USA, OS43A-1880, Accession Number: 2015-070550, 2013.

Wintsch, R. P., Deasy, R. T., Bish, D. L., and Meyer, R.: Stepped alteration of lower oceanic crust at Hess Deep from whole rock $^{87}Sr/^{86}Sr$ data and quantitative modal mineralogy, in: AGU Fall Meeting, 9–13 December 2019, San Francisco, USA, V33E-022, 2019.

Sci. Dril., 31, 85–91, 2022
https://doi.org/10.5194/sd-31-85-2022

Scientific Drilling
Open Access

Simple evaluation of the fold axis, axial plane, and interlimb angle from a borehole image log

Yohei Hamada[1], **Yoshinori Sanada**[2], **and Takehiro Hirose**[1]

[1]Kochi Institute for Core Sample Research (X-Star), Japan Agency for Marine-Earth Science and Technology, 200 Monobe Otsu, Nankoku, Kochi 783-8502, Japan
[2]Institute for Marine-Earth Exploration and Engineering, Japan Agency for Marine-Earth Science and Technology, 2-15 Natsushimacho, Yokosuka, Kanagawa 237-0061, Japan

Correspondence: Yohei Hamada (yhamada@jamstec.go.jp)

Received: 21 February 2022 – Revised: 27 April 2022 – Accepted: 9 May 2022 – Published: 28 October 2022

Abstract. Folds and fractures are important structures that preserve information on the past stress evolution; however, folds remain largely unexplored. Studying folds remains challenging, as no simple and unified method can be used to evaluate fold parameters, which include the fold axis, axial plane, and interlimb angle with depth. In this study, we propose a method to calculate the fold parameters of cylindrical concentric folds by considering the point at which the bedding trend changes as an inflexion point of the fold. The inflexion point is identified from the analysis of bedding orientation, which can be obtained by borehole image log. The orientation of the fold axis and the axial plane were geometrically calculated based on the inflexion surfaces at both ends of the folds. The application of this method is illustrated using a simulated fold model. It is shown that these fold parameters are calculated using the depth of the fold and are reliable to a certain extent, despite the uncertainty of the inflexion points. Although the extraction method assumes cylindrical concentric folds, it can be applied to symmetric folds to estimate the orientation of the fold axis and axial planes. The method developed in this study is expected to have a wide range of applications in structural geology as it can estimate the fold parameters of each fold traversed by a borehole.

1 Introduction

Borehole imaging is a logging technique for the azimuthal surface scan of a borehole wall (Zemanek et al., 1969). It provides information on strikes and dips on features, such as bedding, lithology, grading, fractures, and breakouts. They are utilized in a wide range of geological disciplines including sedimentology, structural geology, metamorphic and volcanic petrology, and geomechanics (e.g. Prensky, 1999). The structural interpretation using stratigraphic orientation data is fundamental for the understanding of the geology around a drilling site. It is a common practice to reconstruct 2D/3D geological structures from the bedding or fracture orientation that is obtained from borehole images and compare them with those obtained by seismic exploration (log-seismic integration; Goldberg, 1997; Moore et al., 2014). Furthermore, geological modelling methods that consider structures such as folds and faults have also been proposed (Etchecopar and Bonnetain, 1992; Etchecopar and Dubas, 1992; Yamada et al., 2016). On the other hand, the resolution of borehole images has developed in recent years, and it is presently possible to recognize sedimentary facies down to a few centimetres. Hence, a borehole can be regarded as a continuous outcrop without the influence of vegetation or topography. This has led to field-like fracture analysis and geological interpretation (Ienaga et al., 2006; Blake and Davatzes, 2012; Lai et al., 2018). However, as for folds, which record past and present stresses, as well as fractures, such mesoscale and outcrop-scale descriptions and analyses have not been commonly performed, which is contrary to the aforementioned extension to large-scale structures.

In borehole images, folded structures are recognized from eye-shaped structures and continuous changes in the orientation of bedding planes on tadpole plots (Vickerman and

Spratt, 2011; Crow and Ladevèze, 2015). By extracting this series of changes in orientation and processing statistically on stereographic plotting, the orientations of the fold axes and axial planes can be derived similar to geological outcrop surveys (Holdsworth, 1988). As the eye mark represents the hinge of the fold obliquely aligned with the borehole, it is possible to determine the fold axis azimuth simply by measuring the direction of the eye. Note that this method cannot be used if the hinge line is parallel to the borehole, as the eye mark will not appear. The fold axes, axial planes, and interlimb angles are measured by these methods; however, these methods lack information on the depth of each fold and their spatial variation. Although the small-scale fold is a powerful indicator of the stress orientation (Ramsay and Huber, 1987; Mayer and Albat, 1990; Scott and Selley, 2004), this conventional approach does not focus on their location and is not suitable for investigating local–regional stress evolution. Due to the limited exposure of continuous folds in the field and the measurement of fold parameters being time-consuming, it is important to obtain fold parameters effortlessly in continuous borehole images.

Therefore, this study aims to develop a simple and continuous method for obtaining fold parameters such as the fold axis, axial plane, and interlimb angle based on borehole image data. The proposed method was applied to a folded geological model to examine its effectiveness and feasibility.

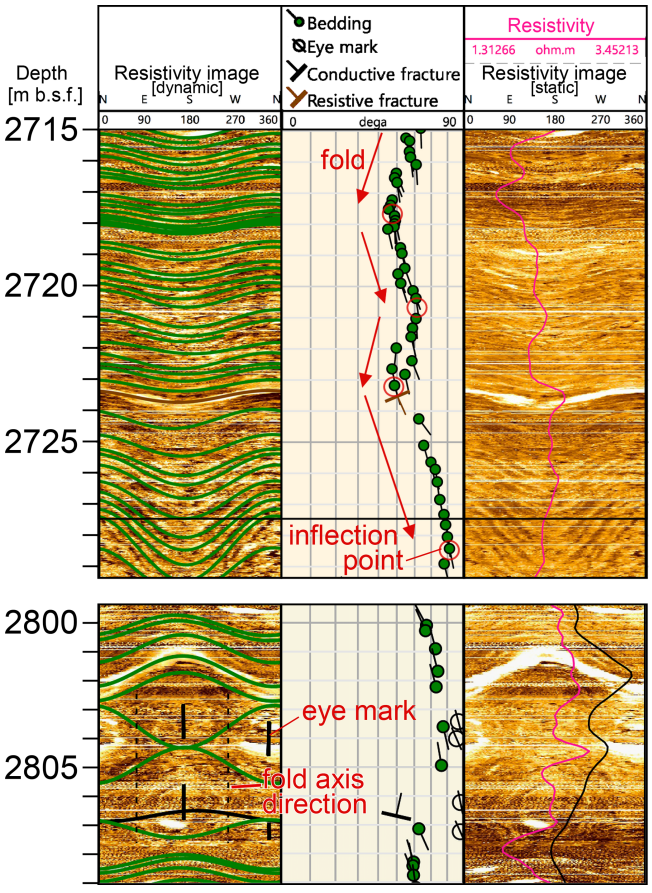

Figure 1. Example of fold appearance in a borehole wall image. Bedding planar interpretation, fold inflexion points, and eye marks are interpreted in the electrical resistivity image of the interior of the accretionary complex that was acquired from the IODP (Integrated Ocean Drilling Program) Expedition 348 (Tobin et al., 2015). Green lines in the dynamic resistivity image are fitted using a bedding plane, and its orientations are plotted in tadpole plot. The pink line in the static image is the shallow resistivity value. The folds appear as a systematic increase or decrease in the dip of the bedding. The eye, the hinge of the fold, can also be observed. The orientation of the fold axis is orthogonal to the eye direction and is indicated by the dotted line in the lower column.

2 Method

The fold structure in the borehole image is observed as a continuous change in the strike and dip of the bedding on the tadpole plot and eye marks (Fig. 1). Although the eye orientation indicates the azimuth of the fold axis and that the axis surface is almost orthogonal to the borehole, the plunge of the axis and the axial plane orientation cannot be obtained. The bedding dip and strike trend on the tadpole plot represent more detailed information on the folds. At the point where one wave of a fold ends and the next one begins (red circle in Fig. 1), the trend of the strike and dip changes. The key to obtaining the fold parameters is to describe this point as the inflexion point of the fold and to identify the inflexion surface at this point. In the case of a symmetric fold, the axial plane is represented as the bisector of the inflexion surface, and the interlimb angle is the angle between two bedding planes at the inflexion point. To formulate them, we consider a cylindrical concentric fold, as shown in Fig. 2. The top of the borehole was set to $[0, 0, 0]$ for simplicity. The borehole and an inflexion point on stratum A of this fold intersect at i_A $[x_1, y_1, z_1]$. In addition, another inflexion point on stratum B intersects the borehole at I_B $[x_2, y_2, z_2]$. The normal vector of the bedding plane at point i_A is $\boldsymbol{n}_1$, and similarly, the normal vector of the bedding at point I_B is $\boldsymbol{n}_2$. The normal vector is expressed as follows, using the strike (θ) and dip (ϕ) of the bedding planes at the inflexion points that can be extracted from the borehole image.

$$\begin{aligned}\boldsymbol{n}_i &= \left[\boldsymbol{n}_{xi}, \boldsymbol{n}_{yi}, \boldsymbol{n}_{zi}\right] \\ &= \left[\sin\phi_i \cos\left(\theta_i + \frac{\pi}{2}\right), \sin\phi_i \sin\left(\theta_i + \frac{\pi}{2}\right), -\cos\phi_i\right]. \quad (1)\end{aligned}$$

Note that the normal vector is a unit vector that does not include the spatial coordinates of the measured point. The direction vector of the fold axis $\boldsymbol{e}$ appears as the intersection of the following two planes:

$$\boldsymbol{e} = \boldsymbol{n}_1 \times \boldsymbol{n}_2. \quad (2)$$

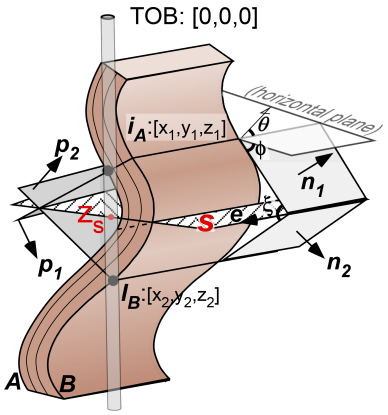

Figure 2. Schematic illustration of a cylindrical concentric fold and a borehole. TOB is the top of the borehole. A and B represent folded bedding planes. $\boldsymbol{n}$ and p are the normal vectors of the bedding plane and inflexion surface, respectively. $\boldsymbol{e}$ is the direction vector of fold axis. S is the axial plane. i_A, I_B, and Z_s are the intersection points of the borehole and A, B, and the axial plane. θ, ϕ, and ξ indicate strike, dip, and interlimb angle, respectively.

The interlimb angle of a fold (ξ), the angle between the bedding planes, can be expressed as follows:

$$\xi = \arccos\left(\frac{\boldsymbol{n}_1 \cdot \boldsymbol{n}_2}{|\boldsymbol{n}_1||\boldsymbol{n}_2|}\right). \tag{3}$$

Thus, the fold and interlimb angles can be easily inferred by identifying the inflexion points on any bedding plane. The axial plane and its location can be calculated if the inflexion points are identified on the same bed. However, such cases can only occur when the axial plane is perpendicular to the borehole, and it is rarely possible to calculate the axial surface in a simple way. To identify an axial plane, we consider an inflexion surface p that is perpendicular to the stratum surface at the inflexion point and parallel to the fold axis (Fig. 2). The normal vector of plane p and the equation of the surface are expressed as follows:

$$p_i = \left[p_{xi}, p_{yi}, p_{zi}\right] = \boldsymbol{e} \times \boldsymbol{n}_i \tag{4}$$

$$p_i \cdot \begin{bmatrix} x - x_i \\ y - y_i \\ z - z_i \end{bmatrix} = 0. \tag{5}$$

Due to the assumption of concentric folding, the inflexion surface p is the plane that passes through the inflexion points on all bedding planes and not just on bedding planes A and B. The axial plane is the bisector plane of p_1 and p_2. Thus, the equation of the axial plane s is expressed as follows:

$$\pm p_1 \cdot \begin{bmatrix} x - x_1 \\ y - y_1 \\ z - z_1 \end{bmatrix} + p_2 \cdot \begin{bmatrix} x - x_2 \\ y - y_2 \\ z - z_2 \end{bmatrix} = 0. \tag{6}$$

The strike (θ_3) and dip angle (ϕ_3) of the axial plane are as follows:

$$\theta_3 = \arcsin\left(\frac{\pm p_{y1} + p_{y2}}{|s| \sin\phi_3}\right) \tag{7}$$

$$\phi_3 = \arccos\left(\frac{\pm p_{z1} + p_{z2}}{|s|}\right). \tag{8}$$

Note that there are two bisecting surfaces. One of these is the axial plane. As the axial plane passes between inflexion points, it is sufficient to confirm that the intersection point Z_s of the drilled hole and the axial plane are included between i_A and I_B. If the borehole is considered to be vertical ($x_1 = x_2 = 0$ and $y_1 = y_2 = 0$ at all times), then the coordinates of the intersection of the axial plane and borehole (z_3) can be calculated as follows:

$$z_3 = \frac{\pm p_{z1} z_1 + p_{z2} z_2}{\pm p_{z1} + p_{z2}}. \tag{9}$$

The distribution of folds along the borehole can be obtained by calculating the location of the axial planes in the borehole for each fold.

3 Example of the application for a simulated fold model

To check the feasibility of the proposed method, an artificial fold was created, and the fold parameters were calculated and compared to a conventional method. A schematic geological model with loose folds was used to illustrate the application of the method proposed in this study. The geological model, including folds, was created based on the arc method described by Busk (1929; Wojtal, 1988), for mapping cylindrical concentric folds, and extended to three dimensions. First, we draw several spherical shells, L, centred at an arbitrary point O in space. The folded stratum surface is obtained by calculating the tangent surfaces at each intersection of L and an arbitrary line l and projecting them onto a line segment that simulates a borehole (Fig. 3). The intersection of the outermost spherical shell and the inner spherical shell ($L11$ and $L13$ in Fig. 3) with l becomes the inflexion point of the fold. For the next deeper fold, the spherical shells and line are arbitrarily set and projected into the borehole in the same manner. To simulate the continuous development of folds, these two folds were set up to share an inflexion point (the layer enclosed by the square in Fig. 3).

In this study, 10 folds were created to examine the proposed method. In total, seven spherical shells corresponding to the seven strata were utilized for each fold. There were two structural units with significantly different trends established for each of the five folds, and the fold structures were non-continuous between these units. Figure 4a and b display the stratigraphic model and the tadpole plot of the bedding strike and dip obtained from the interpretation of the borehole image logging. In Fig. 4b, the green line in the cross section

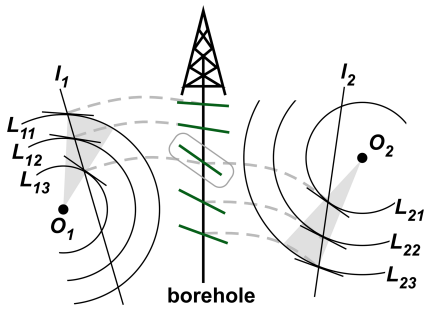

Figure 3. Schematic diagram of the procedure for creating a simulated fold model. The grey hatch in the figure represents a fold created based on an arbitrary point O, and the green lines are the stratigraphic surface projected onto the borehole.

indicates the bedding plane, and the grey dotted line and red points in the tadpole plot exhibit the inflexion plane and inflexion points of the folding strata, respectively. The fold axis is simply calculated by applying the Bingham axial distribution method (Fisher et al., 1987) to the unit-by-unit strike and dip data of this formation. The results of the general calculation, the azimuth, and plunge of the fold axis for units A and B were obtained to be 345, 13.3, and 282.1, 27.7, respectively.

The fold axis, axial plane, and interlimb angle were calculated for each fold according to its depth by applying the proposed method to the model data (red points in Fig. 4c). The axes calculated by the general Bingham axial distribution method are also plotted as grey rectangles in the plot of the fold axis in Fig. 4c. The proposed method provides considerable information on the fold components than the previous method. With the availability of axial planes, it is possible to estimate the stress direction in three dimensions (Fig. 4d). In addition, the amount of fold shortening can be determined from the interlimb angle. As each piece of information can be obtained continuously in the depth direction, it can also be used to detect the presence of local stress distribution or an overprinting fold by capturing changes in the axis or axial plane in a certain direction, as seen in unit B (Fig. 4d).

On the other hand, inflexion points do not always appear on the image log because of missing data or thick strata. For such cases, we also examined the way the estimated fold information would be affected by picking incorrect inflexion points. We performed calculations when the true inflexion point (red point) in Fig. 4b did not appear in the log, and the blue point was interpreted as the inflexion point. In this case, the shifting of an inflexion point causes a certain fold to contain a shortened section or to include strata of a different fold trend. The calculation results (blue points in Fig. 4c), however, exhibit no significant difference between the case where the wrong inflexion point is identified, and the case where the true inflexion point is selected. In particular, there is little change in the trend with depth or the value of the dip angle. However, it should be noted that the calculated depth of the folds may change, the interlimb angle can be overestimated (resulting in loose folds), and the observation error at this inflexion point may be difficult to estimate in practice. The values of the orientation of the simulated bedding planes and the evaluated fold parameters in the above calculations are provided in the Supplement.

4 Discussion

The proposed method focuses only on the inflection points of the folds (maximum and minimum values in tadpole plots) and aims to mainly extract the fold parameters along the borehole. In this respect, it differs from the graphical representation of 2D/3D fold structures, including the Busk (1929) method, which uses continuous bedding data (e.g. Yamada et al., 2016). The advantage of our method is that, unlike previous methods aimed at reconstructing structures, it is simple and allows numerical data on continuous folds in the direction of the borehole to be calculated, even for small structures. The proposed method for deriving fold parameters assumes cylindrical concentric folds and can be applied to other cylindrical folds to some extent. In the case of parallel and symmetrical folds, the folding parameters can be calculated in the same way as for concentric folds, since the characteristics of the inflectional surfaces are the same as for concentric folds. In the case of a similar fold, the orientations of the fold and axial planes calculated by the same process would be equal to the actual fold parameters. The intersection of the axial plane and the borehole, corresponding to the calculated location of the fold, will be somewhat off, although it will be limited to between the inflexion point depths (see the Supplement). However, most folds in nature are cylindrical or conical folds, as pointed out by Wilson (1967). When this method is applied to conical folds, it results in the identification of meaningless axes. However, if the fold is symmetric, it is possible to evaluate a plausible axial plane. Other situations where this method is difficult to apply include those where the angle between the axial plane and the borehole is small, and those where the interlimb is nearly 0°. This is because the variation in the bedding orientation due to folding is difficult to capture, and the frequency of crossing inflexion points may decrease. Very fine folds, such as those found in outcrops (e.g. Alexander and Watkinson, 1989) may be overlooked, or the heterogeneity of the stratum surface can be picked up in borehole images. In addition, errors can be introduced by incorrectly selecting inflection points (Fig. 4), and pseudo-folds can be identified due to the assumption that the strata are continuous. Caution should be exercised in attempting to estimate a wide range of precise fold structures using single borehole wall images. It may be necessary to identify several folds to focus on trends and perform statistical processing in these situations.

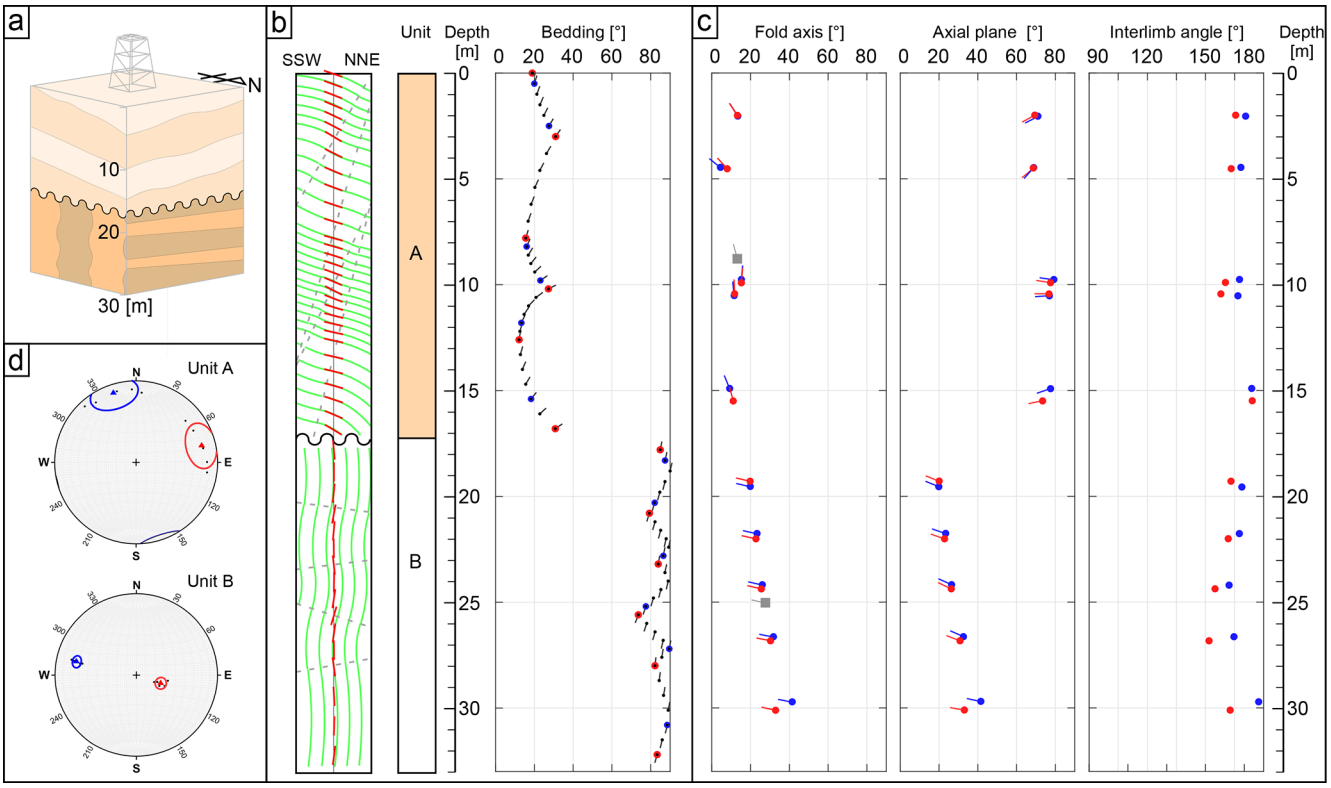

Figure 4. Results of applying the proposed method to the simulated fold model. **(a)** Schematic image of the simulated fold model. **(b)** Cross section of the simulated fold model, structural units, and a tadpole plot of the orientation of bedding planes that would be interpreted if the simulated formation is drilled. Points identified as inflexion points are indicated by red/blue circles. **(c)** Fold axes, axial planes, and interlimb angles obtained by applying the proposed method. The grey squares represent the orientation of the fold axes calculated using the Bingham axial distribution for each unit. The difference between the red and blue circles is the same as the colour of the inflexion points used in the calculation. **(d)** Stereonet of calculated fold parameters. The mean direction (Fisher et al., 1987) of the poles of the axial planes is shown in red and that of the fold axis in blue, representing the direction of maximum principal stress and intermediate stress during fold formation, respectively. Curves of the same colour as the mean vector represent 95 % confidence cone for the mean direction (Fisher et al., 1987).

The proposed method will become even more effective for its use in detailed fold analysis by considering the seismic images and surrounding tectonics. Seismic imaging, however, may not be able to illustrate significant geological structures for the following reasons: lack of resolution, high dip angle of the bedding planes, and small differences in acoustic impedance (Serra, 2003). The proposed method using borehole and logging data will also be effective, especially in such cases, to clarify the invisible formation. The strength of this method is in the fact that it uses borehole images to quantitatively determine the location of the folded structures in the borehole. This can be utilized to create more realistic geological models, geological interpretation focusing on structural changes at depth, and structural geological interpretation, such as the estimation of present and past stress directions. Comparisons with other structural exploration methods, such as seismic reflection methods, and the use of data from multiple boreholes will enable the above strengths to be more robustly exploited.

5 Conclusions

The method described herein enables the determination of the azimuth and plunge of the fold axis, the strike and dip of the axial plane, the interlimb angle, and their depths from the bedding orientation acquired from the borehole image. To apply this method, we require marking the position of the inflexion point in the depth profile of the dip/strike of the bedding. It was confirmed that these fold parameters did not vary significantly, even when the inflexion points could not be reliably determined. This method was designed to be applied to cylindrical concentric folds, and it is also appropriate for the calculation of the axial plane orientation of symmetric folds. As it is difficult to limit the type of folds in borehole images, the method should be implemented with an understanding of the type of error that will occur if the actual formation is not a cylindrical fold. This method, which can obtain fold parameters continuously in the depth direction, will develop a geological interpretation using borehole image logs. If combined with other methods that can add information from a

tadpole plot with regards to whether a fold is similar or not, then the result will be more advanced and user-friendly.

Data availability. All data, including simulated dip and strike data used for fold calculations and the results of fold parameter evaluations, are shown in Sect. 3 and the Supplement.

Supplement. The supplement related to this article is available online at: https://doi.org/10.5194/sd-31-85-2022-supplement.

Author contributions. YS and YH curated research data. YH and TH developed the model code and performed the simulations. YH prepared the paper with contributions from all co-authors.

Competing interests. The contact author has declared that neither they nor their co-authors have any competing interests.

Disclaimer. Publisher's note: Copernicus Publications remains neutral with regard to jurisdictional claims in published maps and institutional affiliations.

Acknowledgements. We are grateful to Yuzuru Yamamoto and Takamitsu Sugihara, for their helpful discussions. We would like to thank Editage for the English language editing. This work was partly supported by the Japan Society for the Promotion of Science KAKENHI (grant nos. JP21H05201, 20K14587, 19K21907, 19H02006, 19H00717, and JP16H06476) in the Scientific Research on Innovative Areas as part of the "Science of Slow Earthquakes" project.

Financial support. This research has been supported by the Japan Society for the Promotion of Science (grant nos. JP21H05201, 20K14587, 19K21907, 19H02006, 19H00717, and JP16H06476).

Review statement. This paper was edited by Ulrich Harms and reviewed by Maria Jose Jurado and one anonymous referee.

References

Alexander, J. I. D. and Watkinson, A. J.: Microfolding in the Permian Castile formation: An example of geometric systems in multilayer folding, Texas and New Mexico, Geol. Soc. Am. Bull., 101, 742–750, 1989.

Blake, K. and Davatzes, N. C.: Borehole image log and statistical analysis of FOH-3D, Fallon Naval Air Station, NV Proceedings Thirty-Seven Stanford University Geothermal Workshop, 30 January–1 February 2012, Stanford, California, USA, https://pangea.stanford.edu/ERE/db/IGAstandard/record_detail.php?id=8231 (last access: 30 May 2022), 2012.

Busk, H. G.: Earth flexures, Cambridge University Press, London, 106 pp., ISBN 9781107663190, 1929.

Crow, H. L. and Ladevèze, P.: Downhole geophysical data collected in 11 boreholes near St-Édouard-de-Lotbinière, Québec, Geological Survey of Canada, Open File 7768, 48 pp., https://doi.org/10.4095/297047, 2015.

Etchecopar, A. and Bonnetain, J. L.: Cross sections from Dipmeter Data 1, AAPG Bull., 76, 621–637, https://doi.org/10.1306/BDFF888A-1718-11D7-8645000102C1865D, 1992.

Etchecopar, A. and Dubas, M. O.: Methods for geological interpretation of dips, SPWLA, SPWLA-1992-J 33rd Annual Logging Symposium, 14–17 June 1992, Oklahoma City, Oklahoma, USA, https://onepetro.org/SPWLAALS/proceedings-abstract/SPWLA-1992/All-SPWLA-1992/SPWLA-1992-J/18977 (last access: 30 May 2022), 1992.

Fisher, N. I., Lewis, T. L., and Embleton, B. J.: Statistical Analysis of Spherical Data, Cambridge University Press, 329 pp., ISBN 9780511623059, 1987.

Goldberg, D.: The role of downhole measurements in marine geology and geophysics, Rev. Geophys., 35, 315–342, https://doi.org/10.1029/97RG00221, 1997.

Holdsworth, R. E.: The stereographic analysis of facing, J. Struct. Geol., 10, 219–223, 1988.

Ienaga, M., McNeill, L. C., Mikada, H., Saito, S., Goldberg, D., and Casey Moore, J.: Borehole image analysis of the Nankai Accretionary Wedge, ODP Leg. 196: Structural and stress studies, Tectonophysics, 426, 207–220, https://doi.org/10.1016/j.tecto.2006.02.018, 2006.

Lai, J., Wang, G., Wang, S., Cao, J., Li, M., Pang, X., Han, C., Fan, X., Yang, L., He, Z., and Qin, Z.: A review on the applications of image logs in structural analysis and sedimentary characterization, Mar. Petrol. Geol., 95, 139–166, https://doi.org/10.1016/j.marpetgeo.2018.04.020, 2018.

Mayer, J. J. and Albat, H. M.: An appraisal of the significance of small-scale fold structures in the contorted bed of the area of the Vredefort, S. Afr. J. Geol., 93, 311–317, 1990.

Moore, G. F., Kanagawa, K., Strasser, M., Dugan, B., Maeda, L., Toczko, S., and the IODP Expedition 338 Scientific Party: IODP Expedition 338: NanTroSEIZE Stage 3: NanTroSEIZE plate boundary deep riser 2, Sci. Dril., 17, 1–12, https://doi.org/10.5194/sd-17-1-2014, 2014.

Prensky, S. E.: Advances in borehole imaging technology and applications, Geological Society, London, Special Publications, edited by: Lovell, M. A., Williamson, G., and Harvey, P. K., Geological Society, London, 159, 1–43, https://doi.org/10.1144/GSL.SP.1999.159.01.01, 1999.

Ramsay, J. G. and Huber, M. I.: The techniques of modern structural geology, in: Folds and Fractures, vol. 2, Academic Press, London, ISBN 0125769024, 1987.

Scott, R. J. and Selley, D.: Measurement of fold axes in drill core, J. Struc. Geol., 26, 637–642, https://doi.org/10.1016/j.jsg.2003.08.016, 2004.

Serra, O. L.: Well Logging and Geology, Editions Serralog, Mery Corbon, France, ISBN 9782951561618, 2003.

Tobin, H., Hirose, T., Saffer, D., Toczko, S., Maeda, L., Kubo, Y., Boston, B., Broderick, A., Brown, K., Crespo-Blanc, A., Even, E., Fuchida, S., Fukuchi, R., Hammerschmidt, S., Henry, P., Josh, M., Jurado, M. J., Kitajima, H., Kitamura, M.,

Maia, A., Otsubo, M., Sample, J., Schleicher, A., Sone, H., Song, C., Valdez, R., Yamamoto, Y., Yang, K., Sanada, Y., Kido, Y., and Hamada, Y.: Site C0002, in: Integrated Ocean Drilling Program. Proceedings IODP, 348, edited by: Tobin, H., Hirose, T., Saffer, D., Toczko, S., Maeda, L., Kubo, Y., and the Expedition 348 Scientists, College Station, TX, https://doi.org/10.2204/iodp.proc.348.103.2015, 2015.

Vickerman, K. and Spratt, D.: Measuring minor structures in borehole image logs, CSPG CSEG CWLS Convention, 9–11 May 2011, Calgary, Alberta, Canada, https://cseg.ca/resources/abstracts/2011-conference-abstracts-m-to-z (last access: 30 May 2022), 2011.

Wilson, G.: The geometry of cylindrical and conical folds, P. Geologist. Assoc., 78, 179–209, https://doi.org/10.1016/S0016-7878(67)80043-9, 1967.

Wojtal, S.: Chapter 13 Objective methods for constructing profiles and block diagrams of folds, in: Basic Methods of Structural Geology, edited by: Marshak, S. and Mitra, G., Prentice-Hall, Englewood Cliffs, NJ, USA, 269–302, ISBN 0130652105, 1988.

Yamada, T., Le Nir, I., Moscardi, E., and Etchecopar, A.: A new parallel fold construction method from borehole dip for structural delineation, AAPG Annual Convention and Exhibition, 19–22 June 2016, Calgary, Alberta, Canada, https://www.searchanddiscovery.com/pdfz/documents/2016/41969yamada/ndx_yamada.pdf.html (last access: 30 May 2022), 2016.

Zemanek, J., Caldwell, R. L., Glenn, E. E., Jr Holcomb, S. V., Nortom, L. F., and Siraus, A. D. J.: The Borehole Televiewer – A New Logging Concept for Fracture Location and Other Types of Borehole Inspection, J. Petrol. Technol., 264, 762–774, https://doi.org/10.2118/2402-pa, 1969.

Sci. Dril., 31, 93–110, 2022
https://doi.org/10.5194/sd-31-93-2022

Scientific Drilling
Open Access

Mediterranean–Black Sea gateway exchange: scientific drilling workshop on the BlackGate project

Wout Krijgsman[1], Iuliana Vasiliev[2], Anouk Beniest[3], Timothy Lyons[4], Johanna Lofi[5], Gabor Tari[6], Caroline P. Slomp[1], Namik Cagatay[7], Maria Triantaphyllou[8], Rachel Flecker[9], Dan Palcu[10], Cecilia McHugh[11,12], Helge Arz[13], Pierre Henry[14], Karen Lloyd[15], Gunay Cifci[16], Özgür Sipahioglu[17], Dimitris Sakellariou[18], and the BlackGate workshop participants✚

[1]Department of Earth Sciences, Utrecht University, 3584 CB Utrecht, the Netherlands
[2]Senckenberg Biodiversity and Climate Research Centre (SBiK-F), 60325 Frankfurt am Main, Germany
[3]Department of Geosciences, Vrije Universiteit Amsterdam, 1081 HV Amsterdam, the Netherlands
[4]Department of Earth Sciences, University of California, Riverside, CA 92521, USA
[5]Géosciences Montpellier, CNRS, Université de Montpellier, 34095 Montpellier CEDEX 05, France
[6]OMV Upstream, Exploration, 1020 Vienna, Austria
[7]EMCOL Research Centre, Department of Geological Engineering, Istanbul Technical University, Ayazaga Campus, 34469 Istanbul, Turkey
[8]Faculty of Geology and Geoenvironment, National and Kapodistrian University of Athens, Panepistimioupolis, 15784 Athens, Greece
[9]BRIDGE, School of Geographical Sciences and Cabot Institute, University of Bristol, Bristol BS8 1SS, UK
[10]Instituto Oceanográfico, Universidade do São Paulo, 05508-120 São Paulo, Brazil
[11]Queens College, City University of New York, Flushing, NY 11367, USA
[12]Lamont-Doherty Earth Observatory of Columbia University, Palisades, NY 10964, USA
[13]Marine Geology, Leibniz Institute for Baltic Sea Research Warnemünde (IOW), 18119 Rostock, Germany
[14]Aix-Marseille University, CNRS, IRD, INRAE, Coll France, CEREGE, 13545 Aix-en-Provence, France
[15]Department of Microbiology, University of Tennessee, Knoxville, TN 37996, USA
[16]Dokuz Eylül Üniversitesi, Deniz Bilimleri ve Teknolojisi Enstitüsü, İnciraltı, 35340 İzmir, Turkey
[17]Exploration Department, Türkiye Petrolleri Anonim Ortakliği (TPAO), 06530 Çankaya-Ankara, Turkey
[18]Institute of Oceanography, Hellenic Centre for Marine Research, 19103 Anavyssos, Greece
✚A full list of authors appears at the end of the paper.

Correspondence: Wout Krijgsman (w.krijgsman@uu.nl)

Received: 21 April 2022 – Revised: 29 June 2022 – Accepted: 18 July 2022 – Published: 28 October 2022

Abstract. The MagellanPlus workshop "BlackGate" addressed fundamental questions concerning the dynamic evolution of the Mediterranean–Black Sea (MBS) gateway and its palaeoenvironmental consequences. This gateway drives the Miocene–Quaternary circulation patterns in the Black Sea and governs its present status as the world's largest example of marine anoxia. The exchange history of the MBS gateway is poorly constrained because continuous Pliocene–Quaternary deposits are not exposed on land adjacent to the Black Sea or northern Aegean. Gateway exchange is controlled by climatic (glacio-eustatic-driven sea-level fluctuations) and tectonic processes in the catchment as well as tectonic propagation of the North Anatolian Fault Zone (NAFZ) in the gateway area itself. Changes in connectivity trigger dramatic palaeoenvironmental and biotic turnovers in both the Black Sea and Mediterranean domains. Drilling a Messinian to Holocene transect across the MBS gateway will recover high-amplitude records of continent-scale hydrological changes during glacial–interglacial cycles and allow us to reconstruct marine and freshwater fluxes, biological turnover events, deep biospheric

processes, subsurface gradients in primary sedimentary properties, patterns and processes controlling anoxia, chemical perturbations and carbon cycling, growth and propagation of the NAFZ, the timing of land bridges for Africa and/or Asia–Europe mammal migration, and the presence or absence of water exchange during the Messinian salinity crisis. During thorough discussions at the workshop, three key sites were selected for potential drilling using a mission-specific platform (MSP): one on the Turkish margin of the Black Sea (Arkhangelsky Ridge, 400 m b.s.f., metres below the seafloor), one on the southern margin of the Sea of Marmara (North İmrali Basin, 750 m b.s.f.), and one in the Aegean (North Aegean Trough, 650 m b.s.f.). All sites target Quaternary oxic–anoxic marl–sapropel cycles. Plans include recovery of Pliocene lacustrine sediments and mixed marine–brackish Miocene sediments from the Black Sea and the Aegean. MSP drilling is required because the *JOIDES Resolution* cannot pass under the Bosporus bridges. The wider goals are in line with the aims and scope of the International Ocean Discovery Program (IODP) "2050 Science Framework: Exploring Earth by Scientific Ocean Drilling" and relate specifically to the strategic objectives "Earth's climate system", "Tipping points in Earth's history", and "Natural hazards impacting society".

1 Introduction

Marine gateways are lifelines for restricted basins like the Mediterranean and Black seas, as they govern the regional and global expressions of first-order hydrologic, climatic, and environmental change (Thunell et al., 1988). They play a critical role in the exchange of water, heat, salt, and nutrients between oceans and seas; hence, they impact regional and global climate and marine and terrestrial biodiversity (e.g. Flecker et al., 2015). The complex evolution of the Mediterranean gateways over the past 7 Myr caused environmental challenges that severely impacted marine and terrestrial biota in Eurasia. During the Messinian, the Black Sea gateway opened, and the Atlantic gateway progressively closed as the Mediterranean developed into a largely desiccated saline basin and later into a brackish water "lake-sea" (Lago Mare) during the Messinian salinity crisis (MSC; 5.97–5.33 Ma) (Roveri et al., 2014; Andreetto et al., 2021). Two-way exchange with the Black Sea probably persisted (Vasiliev et al., 2013; Grothe et al., 2020), and its brackish water faunas expanded over the entire Mediterranean as far west as the Malaga Basin adjacent to Gibraltar (Guerra-Merchán et al., 2010). The exact hydrologic fluxes remain uncertain because the dimensions of the Black Sea gateway are poorly constrained (Fig. 1).

The global importance of dynamic Mediterranean connectivity changes is realized by the scientific community, and several projects are currently directed at a better understanding of the Mediterranean gateway system: the European Training Network (ETN) SALTGIANT initiative, funded by the European Union (EU), focuses on the formation of thick evaporite units in the Mediterranean; the International Ocean Discovery Program (IODP)–International Continental Drilling Program (ICDP) amphibious IMMAGE (Investigate Miocene Mediterranean–Atlantic Gateway Exchange) project will be directed at the evolution of the Mediterranean–Atlantic connection; and the IODP project "DEMISE of a salt giant: climatic-environmental transitions during the terminal Messinian Salinity Crisis" aims to unravel halite deformation of the eastern Mediterranean salt deposits. The missing link for a comprehensive understanding of the Mediterranean hydrologic and environmental evolution is the poor comprehension of the hydrological fluxes from the Black Sea domain. For example, the Mediterranean–Black Sea gateway determines the freshwater flux for continental Eurasia (from the Alps in Germany to the Himalayas in western China), which may significantly influence salinity, temperature, and stratification in the Mediterranean. At the same time, these gaps limit our understanding of Black Sea evolution and its broader value in studies of abrupt marine–non-marine transitions and widespread anoxia through history. The gateway influences circulation patterns in the Black Sea ($\leq$ 2000 m deep) and its status as the world's largest modern example of marine anoxia. This condition dominated the global ocean for the first 90 % of Earth's history as well as intermittently over the last 500 Myr (Lyons et al., 2014), including ocean-scale anoxic events (OAEs) that are often marked by mass extinction.

2 Gateway impact on the Mediterranean and Black Sea

The Mediterranean region is one of the most vulnerable and rapidly responding areas to present-day climate change. Future warming will likely enhance its salinity and reduce its deep-water formation, all leading to water column stratification and higher mass mortality in marine fauna (Coma et al., 2009). MBS gateway dynamics impact the Mediterranean circulation system as well (Sperling et al., 2003; Filippidi et al., 2016). Salinity variations of Aegean water, largely regulated by lower-salinity-water inflow from the Black Sea, are known to have displaced Mediterranean bottom waters upwards, creating Mediterranean deep-water ventilation and overturn perturbations (Roether et al., 1996; Incarbona et al., 2016). The onset of modern Mediterranean ventilation most likely occurred in the Quaternary, but the influence of Black

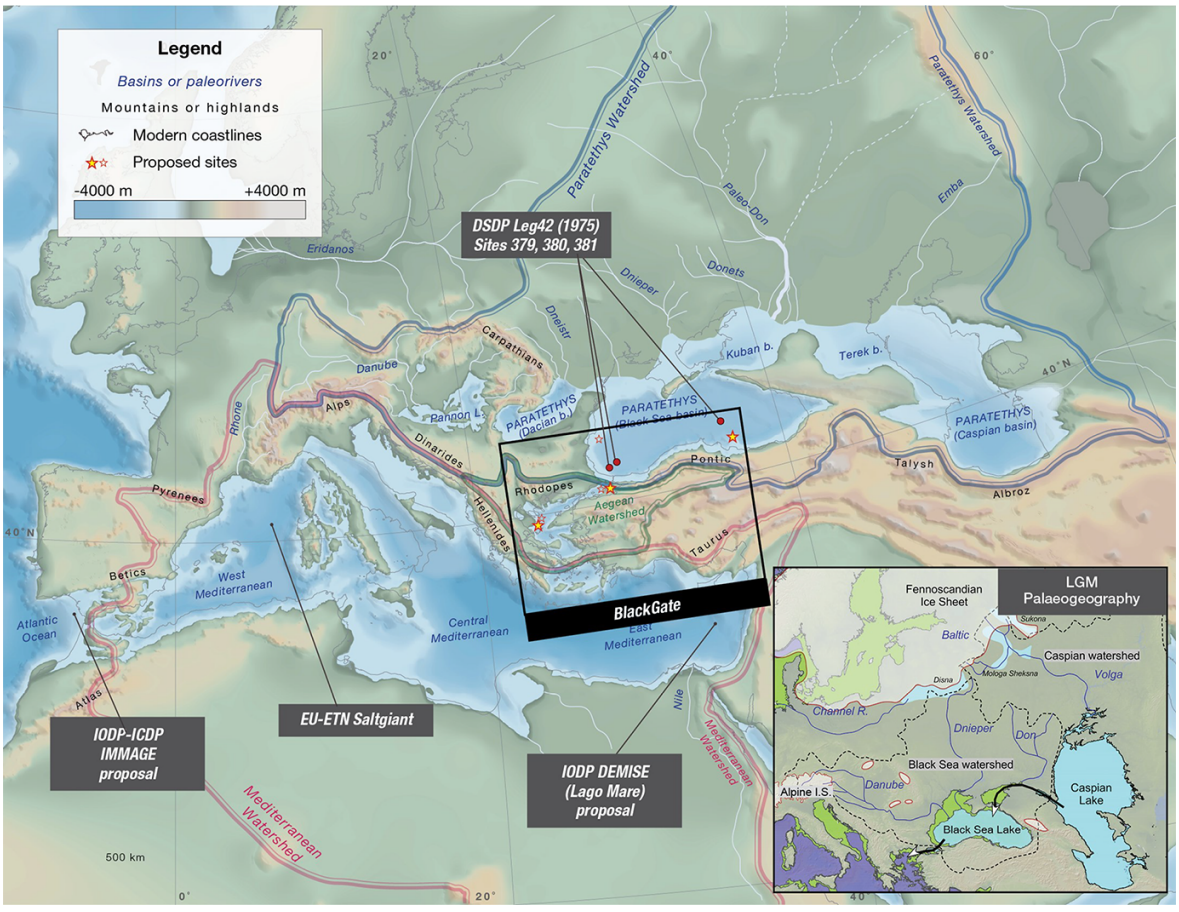

Figure 1. Late-Miocene palaeogeography of Eurasia showing the context of BlackGate (after Palcu et al., 2021). The inset shows the palaeogeographic configuration during the Last Glacial Maximum.

Sea ingressions on Mediterranean hydrology is still largely unknown. The late-Miocene Mediterranean is characterized by the cyclic development of organic-rich sapropelic layers that reflect climatic and hydrological changes resulting in water column stratification and episodes of anoxic conditions in the deep basins (Rohling et al., 2015). A stratified Mediterranean water mass is also envisaged during the enigmatic Messinian salinity crisis (MSC) halite and gypsum precipitation when the Mediterranean was transformed into a saline basin (García-Veigas et al., 2018). Deciphering the palaeoenvironmental evolution of the Mediterranean–Aegean gateway basin over the past 10 Myr will be crucial to understanding the critical thresholds of ancient and modern corridors, and thus our ability to make environmental and biotic projections for the ocean in the near future under increasing anthropogenic influence.

The Black Sea is the world's largest modern anoxic basin (Arthur and Dean, 1998). This condition results from an estuarine-type circulation driven by riverine inputs and marine Mediterranean inflow through the Bosphorus Strait. The present-day gateway is marked by bottom inflow of dense Aegean water below a surface outflow of fresher Black Sea water. The salty northern Aegean inflow sinks to the deeper parts of the basin and does not mix with the oxygen-rich upper water column. The result is a strongly stratified vertical structure in the Black Sea water column, with 90 % of the deep basin consisting of an anoxic dead zone (Fig. 2; Eckert et al., 2013). A ∼ 100 m thick oxygenated surface layer isolates the strongly sulfidic deep waters from the atmosphere. Bacteria producing hydrogen sulfide (H_2S) at high rates make the Black Sea the world's largest H_2S (euxinic) body, a condition rare today but common in Earth's past. Recent studies have shown that the thickness of the oxygenated layer in the Black Sea is strongly influenced by freshwater fluxes, increasing temperature, and the ingression of Mediterranean seawater (Capet et al., 2016). Relatively minor changes in connectivity may cause wholesale turnover in basin hydrology, bringing sulfide into the surface waters. Moreover, the geological archives from the Black Sea show multiple episodes of isolation from the Mediterranean during the Messinian to Quaternary (Schrader, 1978; Popov et al., 2006).

Change in climate and associated sea-level variation, in phase with glacial–interglacial cycles, have been suggested

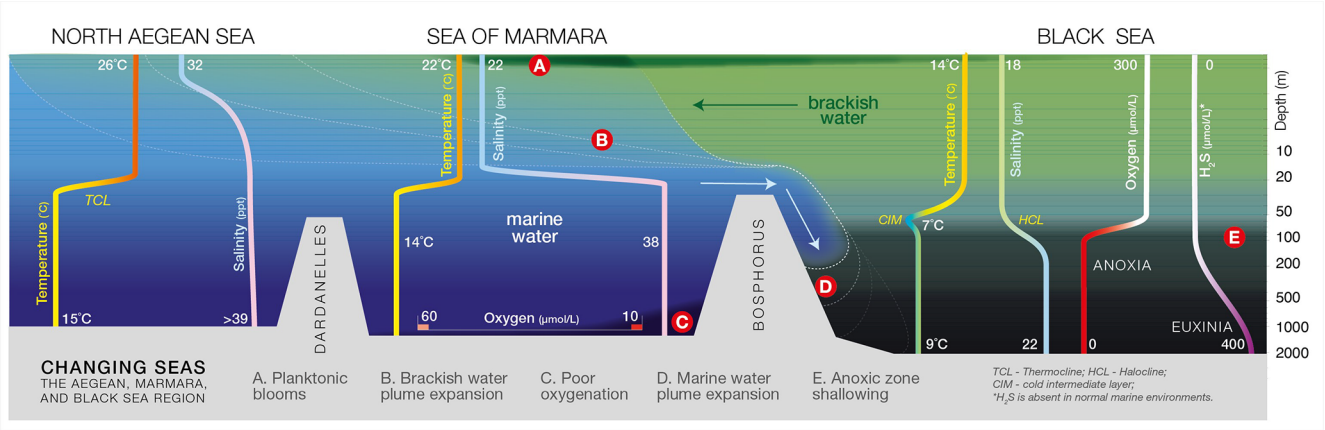

Figure 2. Schematic cross section of the water layers in the North Aegean, Sea of Marmara, and Black Sea basins (values after Yakushev et al., 2008; Keskin et al., 2011; Lagaria et al., 2017; and Çağatay et al., 2022). The huge dominant anoxic bottom layer makes the Black Sea the most poisonous sea in the world. Changing the hydrological fluxes may disturb the equilibrium and bring the deadly sulfides towards the surface waters.

as the main drivers of dynamic connectivity, with connections occurring during interglacial sea-level high stands (e.g. Çağatay et al., 2019; Hoyle et al., 2021). The recent sedimentary archives of the Black Sea document its sensitivity to rapid climatic change across a large part of the Eurasian interior (e.g. Fig. 1; Badertscher et al., 2011; Wegwerth et al., 2020). Over the past 7 Myr, however, the Black Sea has experienced a highly dynamic hydrologic history, including episodes during which its catchment tripled in size, incorporating both low-latitude monsoonal systems and high- to mid-latitude glacial cyclicity. The terrestrial signal in sediment cores from this region provides a rare continental record of hemisphere-wide orbital and millennial-scale variability on a scale suitable for robust modelling of the hydrological cycle, a widely acknowledged weakness in general circulation models (GCMs). The long-term records of sea-level change and concomitant consequences for connectivity and coupled biogeochemical processes, like carbon cycling and the development of anoxia, are so far only speculative. In the absence of recent drilling, most of the focus to date is placed on the last glacial–interglacial transition.

In addition, the MBS gateway region is deeply affected by plate tectonic processes of the Africa–Europe collision zone. Subsidence and uplift in the Bosphorus–Marmara–Dardanelles region is strongly driven by North Anatolian Fault activity, a major east–west-running strike-slip fault below the metropolis of Istanbul that shows a record of almost continuous activity throughout the last 7 Myr (Şengör et al., 2005). Tectonically induced palaeoenvironmental changes in the Aegean and Black Sea basins over million-year timescales are not well understood.

3 BlackGate MagellanPlus workshop

The BlackGate workshop was a sequel to the previously funded Magellan workshop BlackSink (2014), which aimed to identify the most suitable drill sites in the Black Sea for exploring the temporal relationships of recurring restriction events, their impact on regional palaeoclimate and palaeoenvironment, and the complex hydro-interactions with the Mediterranean Sea and the global ocean over the last 15 Myr. This prior workshop was an unqualified success, and most attendees (∼ 40 scientists) concluded that drilling the Miocene to Holocene Black Sea is long overdue and that it would have global importance in our understanding of large-scale anoxia and the causes and consequences of millennial-scale climatic and palaeoenvironmental variability, including implications for the deep biosphere. The workshop was followed by detailed investigations of the old Deep Sea Drilling Project (DSDP) cores (Grothe et al., 2014; Van Baak et al., 2015, 2016; Vasiliev et al., 2015, 2020; Feurdean and Vasiliev, 2019; Golovina et al., 2019; Hoyle et al., 2021) and several field studies of the scattered outcrops in the Black Sea region (Rybkina et al., 2015; Popov et al., 2016; Stoica et al., 2016; Vasiliev et al., 2019), but the key scientific questions about gateway exchange remained. Therefore, we considered it timely to reinvestigate the possibility of drilling the northern Aegean–Marmara–Black Sea transect to comprehensively reconstruct, in a fully interdisciplinary way, the impacts of the east Mediterranean gateway.

The BlackGate workshop was hosted by the Senckenberg Biodiversity and Climate Research Centre in Frankfurt, Germany, and was co-sponsored by the United States Science Advisory Committee (USSAC) for Scientific Ocean Drilling (five scientists from the USA) and SALTGIANT (four early-stage researchers from the EU). It took place from 21 to 24 September 2021. A total of 30 scientists personally at-

tended the workshop (and 7 participated online) from 12 different countries. The participants also represented multiple disciplines, spanning geology, palaeoclimatology, palaeontology, biogeochemistry, tectonics, and reflection seismology, including 11 early-career scientists. The workshop involved numerous scientists with expertise specifically in Black Sea–Mediterranean geology, tectonics, palaeoclimatology, palaeoenvironments, and fundamental biogeochemical processes in the system linked, for example, to changing redox (anoxia), primary production, and salinity. The workshop followed the standard format of concurrent topical breakout sessions on scientific, technical, and funding themes that subsequently reported back to the main group. Breakouts were designed to include complementary disciplines and broadly mixed expertise, but they were also planned with focused expertise in some cases, particularly to address very specific technical questions.

4 BlackGate preliminary proposal

Riding on the success of the BlackGate workshop, we quickly prepared and submitted a preliminary proposal for the IODP 1 October 2021 deadline with the following three themes:

- generation of high-resolution integrated records of continental-scale climate, sea surface temperature, salinity, anoxia, and thermohaline circulation;
- impact of Black Sea–Aegean gateway connectivity on biogeochemical processes and sub-seafloor microbial communities; and
- reconstruction of the detrital provenance and tectonic history of the gateway basins and the surrounding mountains.

To achieve these scientific goals, we propose the use of a mission-specific platform (MSP) to drill three sites: one on the Turkish margin of the Black Sea, one on the southern margin of the Sea of Marmara, and one in the northern Aegean. All sites target Quaternary oxic–anoxic marl–sapropel cycles. Pliocene lacustrine sediments and mixed marine–brackish Miocene sediments will be recovered from the Black Sea and Aegean (Fig. 1).

The gateway is linked to a wide array of critical observations and remaining questions. For example, a recent re-evaluation of the late-Miocene faunal evolution in the northern Aegean basins exposed new palaeogeographic scenarios strikingly different from conventional views, illustrating the need to improve our understanding of the timing and location of critical gateways (Krijgsman et al., 2020). There are no continuous Miocene–Quaternary successions exposed on land in the northern Aegean and Black Sea region. Previous DSDP holes in the Black Sea (Leg 42B) are all disturbed by core breaks and erosional events, and they also include substantial mass transport complexes (Tari et al., 2015), which have only recently been identified and mapped on industrial seismic data. Consequently, there are currently no Miocene–Quaternary cores available for continuous, high-resolution climate reconstruction before the penultimate glacial (Wegwerth et al., 2014). Therefore, the long-term records of hydrology and sea-level change as well as the concomitant consequences for connectivity and coupled biogeochemical processes, carbon cycling, and the development of anoxia are largely speculative. We currently have very little understanding of the impact of major climate events such as the mid-Pliocene warming and the onset of Northern Hemisphere glaciation, locally or regionally. Thus, we are targeting sites on both sides of the MBS gateway because its unique geographic, hydrographic, oceanographic, and tectonic position makes these cores particularly suited to assessing and even quantifying Eurasian palaeoenvironmental processes.

4.1 Theme A: generation of high-resolution integrated records of continental-scale climate, sea surface temperature, salinity, anoxia, and thermohaline circulation

The objectives of Theme A are as follows:

1. to understand the role of global climate and gateway morphology on northern Aegean and Black Sea surface temperature, salinity, anoxia, and thermohaline circulation; and
2. to quantify the time lag between the arrival of Atlantic waters in the Aegean, Marmara, and Black seas at the onset of marine connectivity and evaluate its environmental consequences.

Hydrological exchange between water masses is primarily controlled by salinity and temperature contrasts, but gateway morphology and net evaporation also play roles. During the Miocene–Quaternary, the MBS region experienced repeated, rapid basin-wide salinity fluctuations (e.g. Wegwerth et al., 2014; Çağatay et al., 2019). These reflect the interaction of tectonics, climate, and eustasy as well as changing catchments that at times incorporated both positive and negative water budgets (Gladstone et al., 2007). The process and extent to which these interrelated drivers of gateway exchange interacted remains unquantified. We will explore MBS hydrological interactions by reconstructing the following (Fig. 3):

1. hydrological variations (aquatic vs. terrestrial using biomarker-based compound-specific δ^2H);
2. sea surface temperatures (alkenone-based U^K_{37} and isoprenoidal glycerol dialkyl glycerol tetraether (isoGDGT-based) TEX_{86} proxies. Analysis of clumped isotopes (Δ_{47}), a novel proxy for palaeotemperature reconstructions that, unlike traditional δ^{18}O approaches, is independent of $\delta^{18}O_{water}$);

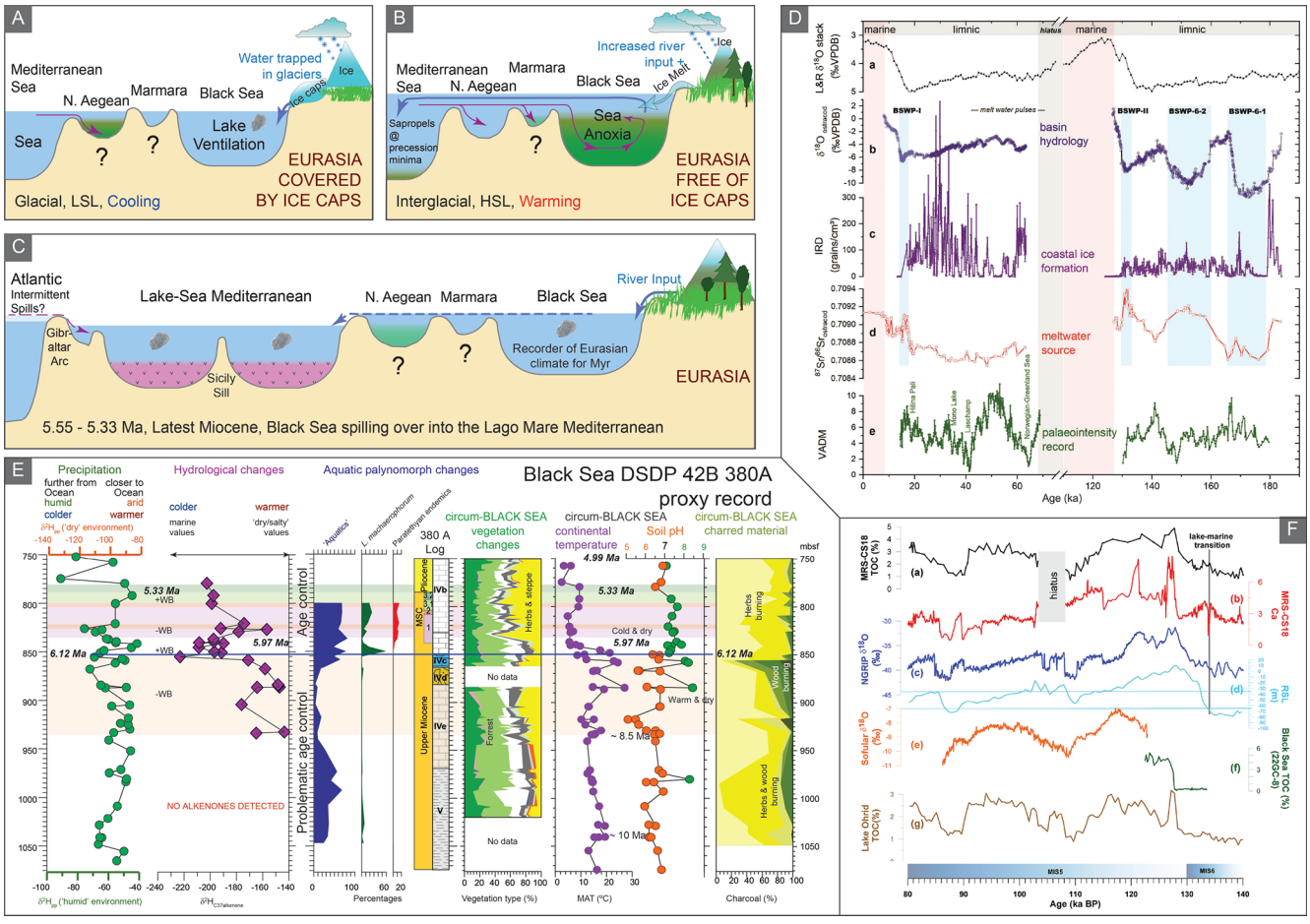

Figure 3. Schematic representation of connectivity scenarios in the BlackGate region during **(a)** glacials and **(b)** interglacials leading to Black Sea anoxia; **(c)** Atlantic–Mediterranean–Aegean–Marmara–Black Sea connectivity during the Lago Mare (5.55 to 5.33 Ma) with MSC evaporites shown using pink shading. **(d)** Example of a study that reflects major changes in the Black Sea hydrology since 185 ka from Major et al. (2006), Nowaczyk et al. (2012, 2021), Kwiecien et al. (2014), and Wegwerth et al. (2014, 2019, 2020). **(e)** Data from the Black Sea DSDP 42B 380 hole (compiled from Grothe et al., 2014; Vasiliev et al., 2015, 2020; and Feurdean and Vasiliev, 2019). **(f)** Sea of Marmara records reveal regional and global climate change (Çağatay et al., 2019).

3. continental temperatures (primarily soil-derived branched (br) GDGTs), with sea surface temperatures (SSTs) and mean annual air temperatures (MAATs) established in parallel to quantify sea–land temperature contrasts during connectivity changes (e.g. Vasiliev et al., 2013, 2019, 2020);

4. vegetation composition (compound-specific $\delta^{13}C$ and $\delta^{2}H$ of terrestrial plant-derived long-chain *n*-alkanes as well as palynology coupled with micro-charcoal; Feurdean and Vasiliev, 2019);

5. anoxia, stratification, and sapropel formation (e.g. isorenieratene; extended archaeol; archaeol; total organic carbon, TOC; C/N; $\delta^{13}C$; $\delta^{15}N$; and Mn, Fe, Mo, V, Tl, and abundances of other redox-sensitive metals and, in many cases, their isotope relationships; Rohling et al., 2014, 2015);

6. water sources and connectivity proxies ($^{87}Sr/^{86}Sr$ for continental vs. marine influx; Çağatay et al., 2006; Grothe et al., 2020);

7. environmental change within the water column ($\delta^{13}C$ and $\delta^{18}O$ on ostracods and, during connection, $\delta^{13}C$ and $\delta^{18}O$ on foraminifera; Bahr et al., 2005, 2008);

8. $^{143}Nd/^{144}Nd$ of foraminifera to constrain deep-water circulation under different climate and hydrographic forcings (Bialik et al., 2019); and

9. continuous geochemical measurements via core-scanning X-ray fluorescence (XRF) for intervals of interest.

Further, a robust chronology for the MBS system is essential. Although biostratigraphic correlations over the MBS gateway are hampered by the endemic character of Black

Sea biota, calcareous nannofossil and dinocyst biostratigraphy coupled with isotope geochemistry can provide ages during marine incursions (Karatsolis et al., 2017; Çağatay et al., 2019; Hoyle et al., 2021). Magnetostratigraphy, radiometric dating, and tephrochronology have all successfully provided age constraints for parts of these sedimentary successions (e.g. Van Baak et al., 2015, 2016; Nowaczyk et al., 2012, 2021; Çağatay et al., 2019; Liu et al., 2020; Wegwerth et al., 2020). We propose the utilization of all of these methods to construct a robust chronological framework for the MBS gateway system over the last 7 Myr.

4.2 Theme B: impact of Black Sea–Aegean gateway connectivity on biogeochemical processes and sub-seafloor microbial communities

The objectives of Theme B are as follows:

1. to understand the linkage between the hydrological connection in the MBS gateway and widespread anoxia, biological turnover, and organic carbon burial in the gateway region;

2. to interrogate environmental variability in the highly sensitive, restricted Black Sea on various timescales ranging from years (varves) to glacial–interglacial (orbital) to millions of years, driven by the interplay of climate, local and global sea level, nutrient inputs, tectonics, macro- and micro-ecology, and the regional water balance; and

3. to elucidate the effects of variations in bottom water oxygen, salinity, and input of organic carbon on microbial communities and biogeochemical processes in a deep-biosphere environment that is strongly influenced by organic-rich sedimentation and pronounced upward fluxes of methane.

The BlackGate drill cores will use state-of-the-art biogeochemical proxies to provide the first reconstruction of water column salinity, redox conditions, temperature, nutrient (re)cycling, primary productivity, (micro)biological communities, and organic matter burial over the entire Miocene–Quaternary interval. While many of these proxies have been developed or refined using samples from the present-day Black Sea often with strong anthropogenic overprints, they have not been applied to the deeper record because of a lack of suitable core samples. Hence, essential aspects of the pre-anthropogenic baseline are missing. Key parameters extracted from sediment records using biogeochemical tools that will complement palaeoenvironmental data collected in Theme A will include the following (Fig. 4):

1. palaeoredox from reactive iron, sulfur, and manganese speciation (Canfield et al., 1996; Poulton and Canfield, 2005; Lenstra et al., 2021); other redox-sensitive trace metals (e.g. molybdenum; Scott and Lyons, 2012; Matthews et al., 2017; Chiu et al., 2022); sulfur isotope systematics (Calvert et al., 1996; Lyons, 1997); carbon / phosphorus ratios (C/P) (Algeo and Ingall, 2007); and metal isotopes (Arnold et al., 2004; Owens et al., 2017);

2. palaeosalinity from alkenones (Huang et al., 2021), carbon–sulfur relationships (Lyons and Berner, 1992), and chloride concentrations (Soulet et al., 2010);

3. productivity from organic C and barium where possible (Henkel et al., 2012); and

4. the presence of specific phytoplankton/microbial groups, including those recorded as biomarkers from anoxygenic photosynthetic sulfur oxidizers (Sinninge Damsté et al., 1993) and evidence of anaerobic ammonium oxidation (Kuypers et al., 2003).

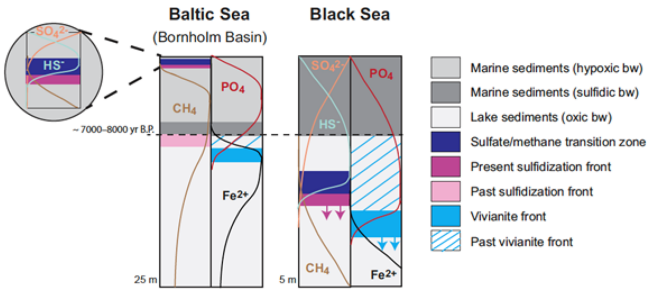

Figure 4. Simplified schematic of methane, sulfur, iron, and phosphorus diagenesis in Baltic Sea and Black Sea sediments, illustrating the location of key redox and chemical fronts relevant to post-depositional alteration of both lake and marine sediments (after Dijkstra et al., 2018).

Previous IODP drilling has shown that subsurface seafloor sediments contain a wealth of microorganisms that are metabolically active and drive a range of diagenetic reactions, albeit at low rates (Orcutt et al., 2014). This deep biosphere comprises an important fraction of Earth's total living biomass. We still know relatively little about the metabolism of the microbial groups in the subsurface, including their carbon sources and electron acceptors and donors. These relationships are particularly relevant in gateway regions, where redox, salinity, and other chemical fronts can develop within sediments leading to changes in microbial communities (Marshall et al., 2018), new mineral formation, and diagenetic overprinting of primary depositional signals (Fig. 4; Jørgensen et al., 2001, 2004; Dijkstra et al., 2018). Importantly, although geochemical profiles of solutes and solids can provide key insights into net rates of biogeochemical processes, they do not reveal the specific microbial drivers nor do they reveal cryptic processes in which substrates or products of reactions (e.g. transient intermediates) have short half-lives. For example, methane oxidation in the subsurface may be coupled to reduction of iron oxides, but whether such

a reaction truly occurs cannot be proven without insight into the specific microbes involved (Riedinger et al., 2014; Egger et al., 2017).

We will study the impacts of abrupt variations in bottom water oxygen, salinity, and organic carbon input on microbial communities and biogeochemical processes/cycles in the deep subsurface. Detailed geochemical analyses of sediments and porewaters (including C, H, and O isotopes) will reveal the positions of active redox fronts, allowing the separation of primary and secondary signals. Microbiological analyses will include cell counts (Jørgensen et al., 2020), metagenomics (Zinke et al., 2017), measurements of enzyme activities (Schmidt et al., 2021), and the use of various single-cell technologies to link function and genetic identity (Coskun et al., 2018). Our ultimate goal is to determine which microbes are active; how they function; and how they drive geochemical processes in the subsurface, including carbon cycling.

4.3 Theme C: reconstruction of the tectonic evolution of MBS gateway basins and surrounding mountains

The objectives of Theme C are as follows:

1. to unravel the tectonic history of the MBS gateway in Messinian–Quaternary times; and

2. to determine how growth and propagation of strike-slip faults in the continental domain affect gateway dynamics and geohazards.

The MBS gateway is located in a tectonically active region that has been dominated by the westward growth and propagation of the NAFZ over the past 5 Myr (Sengör, 1979; Taymaz et al., 1991; Armijo et al., 1999). Gateway basin geometries and inferred kinematics vary laterally and are heavily affected by NAFZ activity (Fig. 5). The basins in the northern Aegean domain have seen a rapid increase in tectonic activity and opening rate since the late Miocene (Brun et al., 2016), generating increased accommodation space in the past 3–5 Myr (Beniest et al., 2016), coeval with the propagation of the NAFZ into the north Aegean domain (Sakellariou and Tsampouraki-Kraounaki, 2018). Various methods have been used to estimate the age of the gateway sediments in the Aegean domain, including onshore basin stratigraphy (Beniest et al., 2016; Karakitsios et al., 2017), interpolating a Messinian age for large unconformities (Rodriguez et al., 2018; Sakellariou et al., 2018), and using seismic stratigraphy from the deep-sea drilling in the South Aegean Sea (Hsü et al., 1978); however, a robust chronological framework is absent for this region. Recovering sediments that accumulated in the gateway basins will reveal unique information about the evolution of the transform fault system, palaeo-earthquakes associated with their growth (Jolivet and Brun, 2010; Royden and Papanikolaou, 2011), and how they propagate through normal continental and thinned continental crust. Large strike-slip faults like the NAFZ pose a serious threat to society because the gateway region and the geography associated with those faults have been the focus of human activity and urban development for millennia. Specifically, two major population centres, Istanbul and Izmir in north-western Turkey, are located on this fault. A thorough understanding of the gateway's dynamic behaviour with potential temporal patterns is essential for the effective mitigation of seismic hazards.

We will use sediment chronology developed for our cores to ground truth the existing but tentative seismic-stratigraphic framework for the Marmara Trough (Sorlien et al., 2012). These surfaces, which are a sequence of low-stand deltas, have been traced throughout the Sea of Marmara basins and linked to glacial–interglacial cycles. IODP drilling through these strata, in both the Aegean and Marmara domains, coupled with extensive seismic data grids, will provide the chronology necessary for interpretation of transform basin subsidence and fault slip analyses. These results, in turn, will constrain the geometry, kinematics, and segmentation of the main fault branch over the long term, providing a much improved understanding of transform faulting and associated basin evolution. Greater knowledge of the geodynamic context of the MBS gateway basins will eventually shed new light on Miocene plate tectonics, controls on local uplift and subsidence, and active large-scale fault displacements that may lead to slope instability and subsequent mass transfer deposits and earthquake activity.

5 Conceptual drilling and coring strategy

We have identified three primary and five alternative sites on seismic lines in the northern Aegean (AEG-01A and AEG-02A), the Sea of Marmara (MAR-01A and MAR-02A), and the Black Sea basin (BSB-01A, BSB-02A, BUL-01A, and BUL-02A). Core recovery must be sufficient for high-resolution sampling with minimal gaps. Therefore, we propose the use of an advanced piston corer (APC) to refusal at each site, followed by a rotary core barrel (RCB). Limited core recovery in the single/double sites will be mitigated by the acquisition of downhole logs under open-hole conditions (see below). These data will also be used to generate comprehensive cyclostratigraphic records. More detailed information on the sites used is given in the following:

- Aegean – primary site is the North Aegean Trough (AEG-01 with $\sim$ 650 m penetration; one hole down to 650 m and one hole down to 100 m), yielding a total expected core recovery of 750 m, and the alternative site is AEG-02, which involves a lateral shift in location that shows smaller stratigraphic thickness;

- Sea of Marmara – preferred site is the North İmrali (MAR-01; one hole down to 400 m), and the alternative site is the MAR-02, which involves a lateral shift in location that shows smaller stratigraphic thickness; and

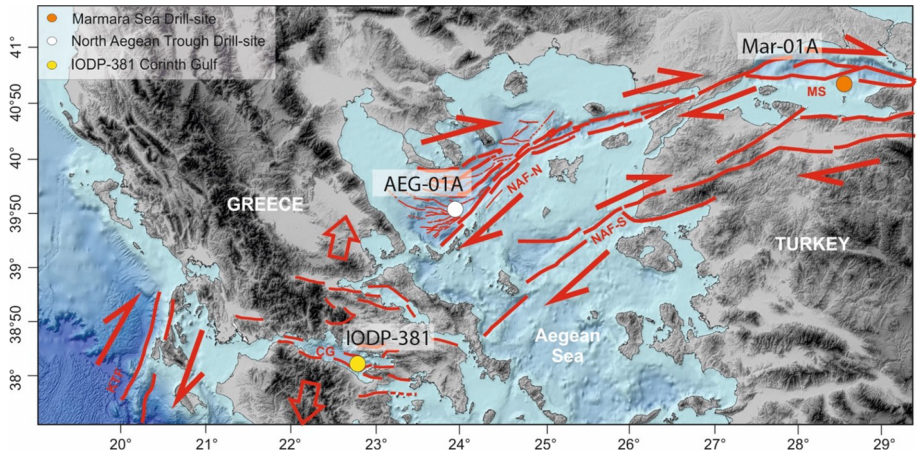

Figure 5. The Sea of Marmara–Aegean Sea transform system (map after Sakellariou and Tsampouraki-Kraounaki, 2018), where MS denotes the Sea of Marmara. The red arrows and lines indicate branches of the North Anatolian Fault (NAF) system that are observed on bathymetry and are considered active today.

– Black Sea – preferred site is the Arkhangelsky Ridge (Turkey) (BSB-01A with ∼ 400 m penetration with one hole down to 400 m and two holes down to 200 m), yielding a total expected core recovery of 800 m, and the alternative site is the Bulgarian margin (BUL-01A and BUL-02A, ∼ 750–650 m).

Downhole logging measurements will be important as they can be used to fill gaps in the sedimentary records. Moreover, they offer in situ determinations of the physical properties. At each site, we plan to acquire through-pipe gamma ray logs followed by the following logs collected under open-hole conditions: spectral gamma ray, formation resistivity and magnetic susceptibility, sonic, borehole fluid temperature and conductivity, caliper logs, and vertical seismic profiles (VSPs).

6 Site descriptions

6.1 North Aegean Sea: AEG-01A (primary) and AEG-02A (alternative)

AEG-1A is located on a relative plateau in the southern part of the North Aegean Trough (Fig. 6). At the proposed location, the seismic profile shows a continuous, undisturbed section (AEG-01A; Fig. 6c) at a water depth of 1120 m (see Fig. 6b for details). AEG-2A occupies a plateau in the central deep part of the North Aegean Trough, just south of the Sithonia Peninsula. At the proposed location, the seismic character shows parallel, continuous, undisturbed reflectors (AEG-02A; Fig. 6d) at a water depth of 960 m (see Fig. 6b for details).

6.2 Sea of Marmara: MAR-01A (primary) and MAR-02A (alternative)

MAR-01A is located on a flat plateau in the eastern İmrali Basin near the southern margin of the Sea of Marmara. At the proposed location, the seismic character shows parallel, continuous, undisturbed reflectors (MAR-01A; Fig. 7d) at a water depth of 346 m (see Fig. 7b for details). MAR-02A is located in the western part of İmrali Basin. At the proposed location, the seismic character shows parallel, continuous, undisturbed reflectors (MAR-02A; Fig. 7d) at a water depth of 346 m (see Fig. 7b for details).

6.3 Black Sea: BSB-01A (primary) and BSB-02A (alternative)

The sites are located on the south-eastern end of the north-west–south-east-extending Arkhangelsky Ridge at water depths of 375 and 370 m. The proposed drilling/coring site likely received minimum terrigenous input because it is situated on a relatively high plateau. The existing interpretations include the Messinian unconformity and other significant seismic surfaces in deeper parts of the eastern Black Sea basin (BSB-01A/-02A; Fig. 8c). The geometric relationships between the reflectors and the known geological history of the area were considered when selecting horizons at the proposed drill site.

6.4 BUL-01A and BUL-02A (alternative sites)

The sites are located on the southernmost part of Bulgarian deep-water slope. A large modern 3D seismic data set is available. Few mass transport complexes (MTCs), perhaps at 305–325 m b.s.f., within the Miocene–Quaternary sequence (Tari et al., 2015, 2016; Tishchenko et al., 2021) are expected. Potential drilling location BUL-01A/-02A (Fig. 8g,

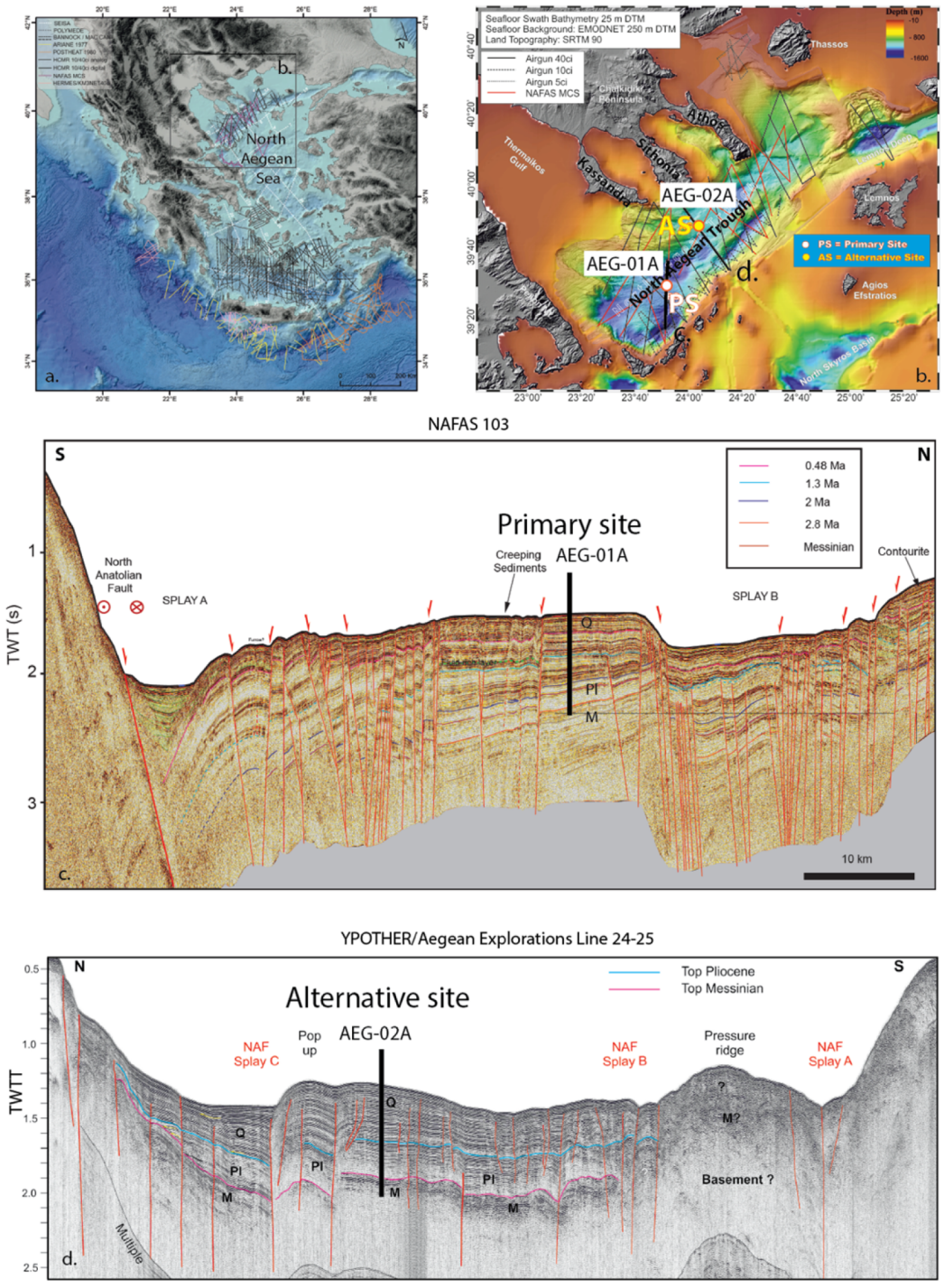

Figure 6. Existing seismic data coverage in the North Aegean Sea (the background bathymetry map is sourced from Sakellariou and Tsampouraki-Kraounaki, 2019). High-resolution bathymetry in the northern Aegean Sea with seismic data (Sakellariou et al., 2018). Panel **(c)** shows seismic line 103 from the North Anatolian Fault in the Aegean Sea (NAFAS) expedition (2017) as well as primary site AEG-01A; the shooting direction was N184°, the acquisition speed was close to 4.1 knots, the streamer length was 288 m (24 traces, 12.5 m spaced), the offset maximum was 400 m, the shot interval was 12.5 m, the sample rate was 1 ms, the trace length was 5500 ms, and the final bin spacing was 6.25 m. The data were processed with a Kirchhoff post-stack time migration. Seismic units have been identified down to the Messinian (Rodriguez et al., 2018). Panel **(d)** shows seismic line 13–14, from the YPOTHER/Aegean expeditions (2013–2015) as well as alternative site AEG-02A; the shooting direction was north-north-west–south-south-east, the streamer length was 65 m, the shot interval was 6–6.5 m, and the sample rate was 4000 ms. The data were processed with Kirchhoff post-stack time migration. The proposed ages of the units are given but not verified (Sakellariou et al., 2018). The abbreviations used in the figure are as follows: Q – Quaternary, PI – Pliocene, and M – Messinian.

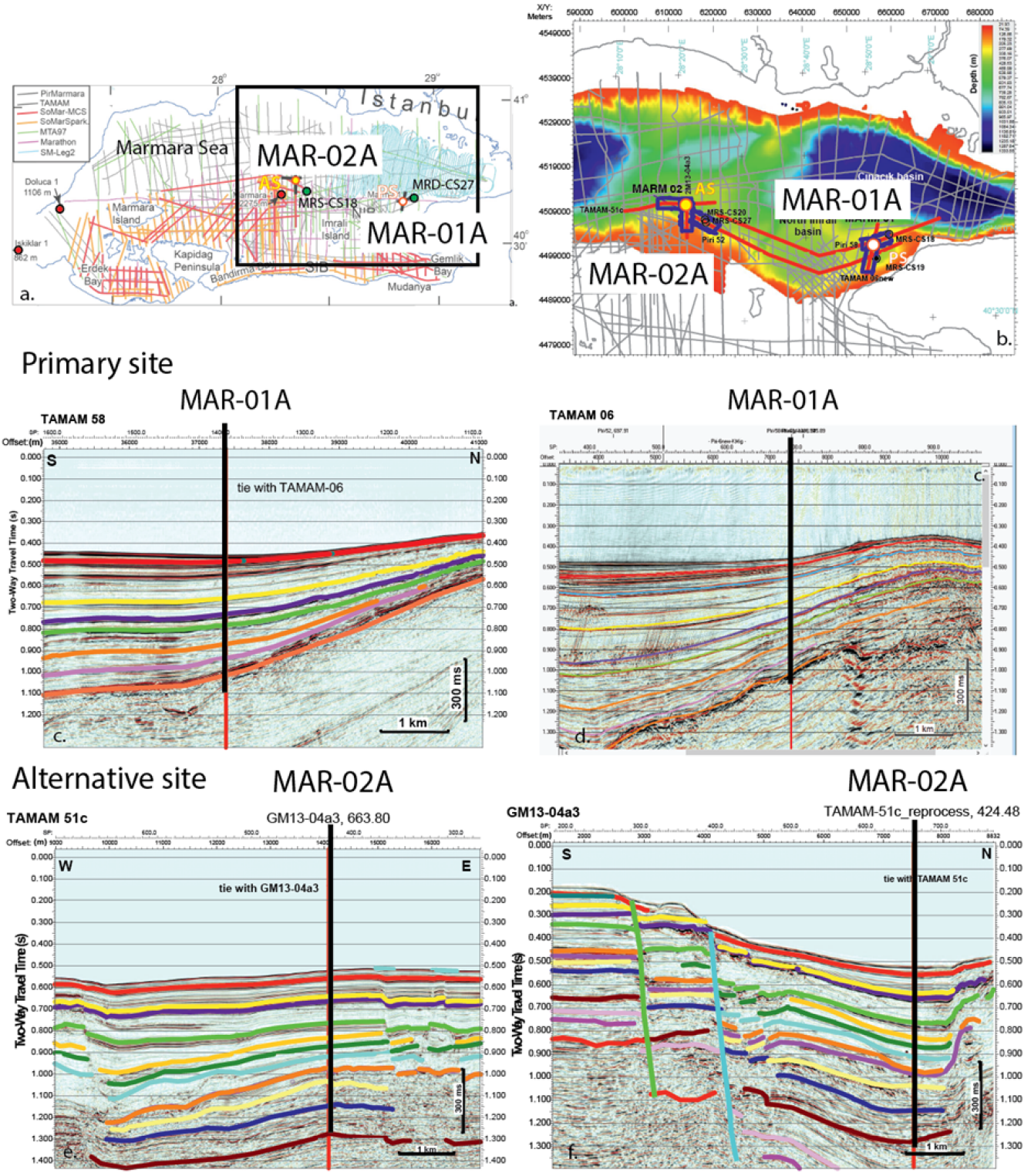

Figure 7. **(a)** MCS data coverage in the Sea of Marmara (after Çağatay et al., 2019): black solid bars show crossing lines for proposed sites MAR-01 and MAR-02, green circles mark holes MRS-CS 18 and MRD-CS 27, and red circles mark deep drill sites by the oil industry. Panel **(b)** presents a zoomed in map of proposed drill locations. Panels **(c)** and **(d)** show seismic line TAMAM 58 and 06 as well as primary site MAR-01A. Panels **(e)** and **(f)** show the seismic crossing lines GM13-04a3 and Turkish American Marmara Multichannel (TAMAM) 51 as well as alternative site MAR-02A. All seismic units have been identified but not dated. Shooting of all seismic data in panels **(c)**, **(d)**, **(e)**, and **(f)** happened during the TAMAM expedition (2008), with a streamer length of 450 m, a shot interval of 12.5 or 18.75 m, and a sample rate of 1 ms. The data were processed with detailed velocity analysis and Kirchhoff post-stack time migration.

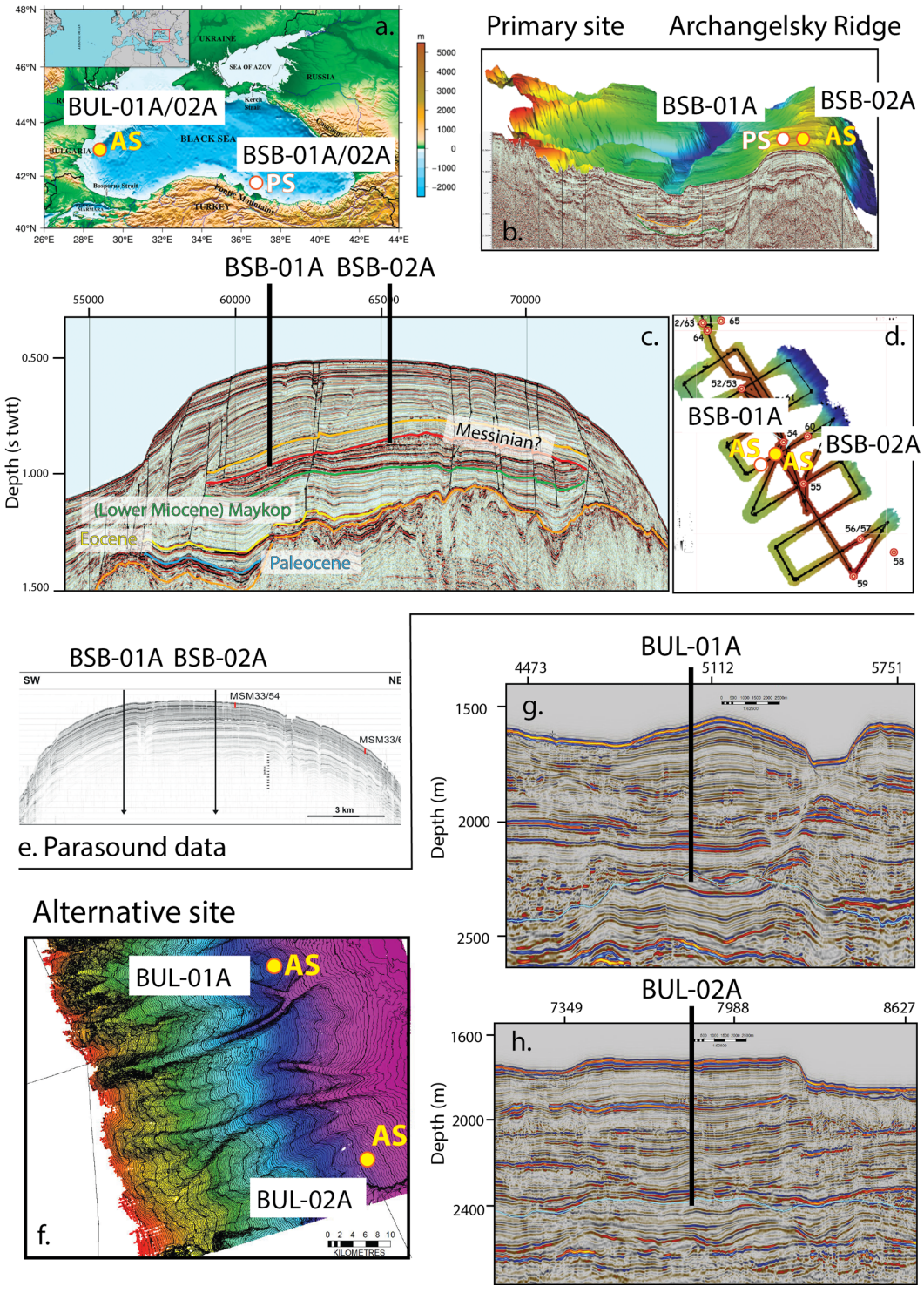

Figure 8. **(a)** Overview map of the Black Sea region with proposed primary and alternative drilling sites (after Avşar and Kutoğlu, 2020). **(b)** A zoomed in 3D image of proposed drill locations BSB-01A and BSB-2A. **(c)** Seismic line showing primary sites BSB-01A and BSB-01B; seismic units, characterized by continuous reflectors with various amplitudes, have been identified with expected ages. **(d)** Overview map of Parasound data acquired in the primary drill location. **(e)** A high-resolution Parasound profile showing primary sites BSB-01A and BSB-02A. **(f)** A zoomed in high-resolution bathymetry image showing alternative sites BUL-01A and BUL-02A. **(g, h)** Seismic line BS-20 2D acquired during "Geology Without Limits" (2011) (Nikishin et al., 2015), showing alternative sites BUL-01A and BUL-02A; the shooting direction was north-west–south-east, the streamer length was 10 200 m, and the sample rate was 4 ms. The data were processed by Kirchhoff pre-stack depth migration.

h) has been selected because of the relatively undeformed sequence between the seafloor and the Messinian unconformity. There is an unconformity at 446 m b.s.f. (Fig. 8h), which may represent up to 20–30 m of missing section within the Pliocene.

Code and data availability. No codes or data sets were used in this article.

Team list. Konstantina Agiadi (Department of Palaeontology, University of Vienna, Vienna, Austria), Federico Andreetto (Department of Earth Sciences, Utrecht University, Utrecht, the Netherlands), Helge Arz (Marine Geology, Leibniz Institute for Baltic Sea Research Warnemünde, Rostock, Germany), Anouk Beniest (Department of Geosciences, Vrije Universiteit Amsterdam, Amsterdam, the Netherlands), Diksha Bista (NERC Isotope Geosciences Laboratory, British Geological Survey, Keyworth, UK), Francesca Bulian (Department of Geology, University of Salamanca, Salamanca, Spain), Geanina Butiseaca (Senckenberg Biodiversity and Climate Research Centre, Frankfurt am Main, Germany), Namik Cagatay (EMCOL Research Centre, Department of Geological Engineering, Istanbul Technical University, Istanbul, Turkey), Gunay Cifci (Dokuz Eylül Üniversitesi, Deniz Bilimleri ve Teknolojisi Enstitüsü, İnciraltı, İzmir, Turkey), Pinar Ertepinar (Department of Geological Engineering, METU Üniversiteler, Çankaya-Ankara, Turkey), Rachel Flecker (BRIDGE, School of Geographical Sciences and Cabot Institute, University of Bristol, Bristol, UK), Luca Gasperini (Institute of Marine Science, National Research Council ISMAR-CNR, Bologna, Italy), Liviu Giosan (Woods Hole Oceanographic Institution, Woods Hole, USA), Christian Gorini (Sorbonne University, ISTEP, Paris, France), Erhan Gülyüz (Department of Neotectonics and Thermochronology, Institute of Rock Structure and Mechanics of the CAS, Prague, Czech Republic), Pierre Henry (Aix-Marseille University, CNRS, IRD, INRAE, Coll France, CEREGE, Aix-en-Provence, France), Thomas Hoyle (CASP, West Building, Cambridge, UK), Yongsong Huang (Department of Earth, Environmental and Planetary Sciences, Brown University, Providence, USA), Nuretdin Kaymakci (Department of Geological Engineering, METU Üniversiteler, Çankaya-Ankara, Turkey), Wout Krijgsman (Department of Earth Sciences, Utrecht University, Utrecht, the Netherlands), Sergei Lazarev (Carbonate Sedimentology Lab, Department of Geosciences, University of Fribourg, Fribourg, Switzerland), Johanna Lofi (Géosciences Montpellier, CNRS, Université de Montpellier, Montpellier, France), Lucas Lourens (Department of Earth Sciences, Utrecht University, Utrecht, the Netherlands), Timothy Lyons (Department of Earth Sciences, University of California, Riverside, USA), Oleg Mandic (Department of Geology and Paleontology, Natural History Museum Vienna, Vienna, Austria), Cecilia McHugh (Queens College, City University of New York, Flushing, USA), David McInroy (British Geological Survey, Keyworth, UK), Javier Molina-Hernandez (Department of Earth Sciences, Royal Holloway University of London, Egham, UK), Jimmy Moneron (Institute of Earth Sciences, The Hebrew University of Jerusalem, Jerusalem, Israel), Andreas Mulch (Senckenberg Biodiversity and Climate Research Centre, Frankfurt am Main, Germany), Dan Palcu (Instituto Oceanográfico, Universidade do São Paulo, São Paulo, Brazil), Fadl Raad (Géosciences Montpellier, CNRS, Université de Montpellier, Montpellier, France), Dimitris Sakellariou (Institute of Oceanography, Hellenic Centre for Marine Research, Anavyssos, Greece), Özgür Sipahioglu (Exploration Department, Türkiye Petrolleri Anonim Ortakliği (TPAO), Çankaya-Ankara, Turkey), Elisabeth Skampa (Faculty of Geology and Geoenvironment, National and Kapodistrian University of Athens, Athens, Greece), Caroline Slomp (Department of Earth Sciences, Utrecht University, Utrecht, the Netherlands), Gabor Tari (OMV Upstream, Exploration, Vienna, Austria), Maria Triantaphyllou (Faculty of Geology and Geoenvironment, National and Kapodistrian University of Athens, Athens, Greece), Iuliana Vasiliev (Senckenberg Biodiversity and Climate Research Centre, Frankfurt am Main, Germany), Antje Wegwerth (Marine Geology, Leibniz Institute for Baltic Sea Research Warnemünde, Rostock, Germany), Frank Wesselingh (Naturalis Biodiversity Center, Leiden, the Netherlands), and Anastasia Yanchilina (Lamont-Doherty Earth Observatory of Columbia University, Palisades, USA).

Author contributions. WK, IV, and AB convened the workshop in Frankfurt. All co-authors contributed to the text and figures that resulted in the submission of a preliminary proposal. DP provided the introductory Figs. 1 and 2. IV, HA, NC, and MT organized Theme A. CPS, TL, and KL wrote Theme B. AB, NC, CM, MT, GC, and PH focused on Theme C. GT, NC, CM, GC, ÖS, and DS provided the seismic lines and location figures. JL wrote the coring strategy. WK, IV, AB, and RF were responsible for revising, editing, and homogenizing the final version of the paper. Participants at the workshop contributed intellectual input.

Competing interests. The contact author has declared that none of the authors has any competing interests.

Disclaimer. Publisher's note: Copernicus Publications remains neutral with regard to jurisdictional claims in published maps and institutional affiliations.

Acknowledgements. The authors wish to thank the Senckenberg Biodiversity and Climate Research Centre in Frankfurt (in particular Andreas Mulch), Germany, for hosting the event and Iryna Yashchenko and Tjitske Vos for their managerial support and assistance. We are also grateful to Lucas Lourens for continued encouragement and constructive suggestions and to Nadine Hallmann and Gilbert Camoin for essential hands-on support with respect to organizing the workshop. Finally, we acknowledge all participants for their constructive input and enthusiasm. Those interested in participating in future BlackGate activities are invited to contact the authors.

Financial support. This research has been supported by ECORD/IODP (BlackGate2020 grant); the US Science Advisory Committee (five scientists from the USA); and SALTGIANT (four ESRs from the EU), a European project that has received funding from the European Union's Horizon 2020 Research and Innovation

programme, within the framework of the Marie Skłodowska-Curie Actions (grant no. 765256). Dan Palcu acknowledges the Fundação de Amparo a Pesquisa do Estado de São Paulo (FAPESP) for financial support (grant no. 2018/20733-6).

Review statement. This paper was edited by Will Sager and reviewed by Werner Piller and one anonymous referee.

References

Algeo, T. J. and Ingall, E.: Sedimentary Corg : P ratios, paleocean ventilation, and Phanerozoic atmospheric pO_2, Palaeogeogr. Palaeoclimatol. Palaeoecol., 256, 130–155, https://doi.org/10.1016/j.palaeo.2007.02.029, 2007.

Andreetto, F., Aloisi, G., Raad, F., Heida, H., Flecker, R., Agiadi, K., Lofi, J., Blondel, S., Bulian, F., Camerlenghi, A., Caruso, A., Ebner, R., Garcia-Castellanos, D., Gaullier, V., Guibourdenche, L., Gvirtzman, Z., Hoyle, T.M., Meijer, P. T., Moneron, J., Sierro, F. J., Travan, G., Tzevahirtzian, A., Vasiliev, I., and Krijgsman, W.: Freshening of the Mediterranean Salt Giant: controversies and certainties around the terminal (Upper Gypsum and Lago-Mare) phases of the Messinian Salinity Crisis, Earth-Science Rev., 216, 103577, https://doi.org/10.1016/j.earscirev.2021.103577, 2021.

Armijo, R., Meyer, B., Hubert, A., and Barka, A.: Westward propagation of the North Anatolian fault into the northern Aegean: Timing and kinematics, Geology, 27, 267, https://doi.org/10.1130/0091-7613(1999)027<0267:WPOTNA>2.3.CO;2, 1999.

Arnold, G. L., Anbar, A. D., Barling, J., and Lyons, T. W.: Molybdenum Isotope Evidence for Widespread Anoxia in Mid-Proterozoic Oceans, Science, 304, 87–90, https://doi.org/10.1126/science.1091785, 2004.

Arthur, M. A. and Dean, W. E.: Organic-matter production and preservation and evolution of anoxia in the Holocene Black Sea, Paleoceanography, 13, 395–411, https://doi.org/10.1029/98PA01161, 1998.

Avşar, N. B. and Kutoğlu, Ş. H.: Recent sea level change in the Black Sea from satellite altimetry and tide gauge observations, ISPRS Int. J. Geo.-Inf., 9, 185, https://doi.org/10.3390/ijgi9030185, 2020.

Badertscher, S., Fleitmann, D., Cheng, H., Edwards, R. L., Göktürk, O. M., Zumbühl, A., Leuenberger, M., and Tüysüz, O.: Pleistocene water intrusions from the Mediterranean and Caspian seas into the Black Sea, Nat. Geosci., 4, 236–239, https://doi.org/10.1038/ngeo1106, 2011.

Bahr, A., Lamy, F., Arz, H., Kuhlmann, H., and Wefer, G.: Late glacial to Holocene climate and sedimentation history in the NW Black Sea, Mar. Geol., 214, 309–322, 2005.

Bahr, A., Lamy, F., Arz, H. W., Major, C., Kwiecien, O., and Wefer, G.: Abrupt changes of temperature and water chemistry in the late Pleistocene and early Holocene Black Sea, Geochem. Geophy. Geosy., 9, Q01004, https://doi.org/10.1029/2007GC001683, 2008.

Beniest, A., Brun, J. P., Gorini, C., Crombez, V., Deschamps, R., Hamon, Y., and Smit, J.: Interaction between trench retreat and Anatolian escape as recorded by neogene basins in the northern Aegean Sea, Mar. Pet. Geol., 77, 30–42, https://doi.org/10.1016/j.marpetgeo.2016.05.011, 2016.

Bialik, O. M., Frank, M., Betzler, C., Zammit, R., and Waldmann, N. D.: Two-step closure of the Miocene Indian Ocean Gateway to the Mediterranean, Sci. Rep., 9, 1–10, https://doi.org/10.1038/s41598-019-45308-7, 2019.

Brun, J.-P., Faccenna, C., Gueydan, F., Sokoutis, D., Philippon, M., Kydonakis, K., and Gorini, C.: The two-stage Aegean extension, from localized to distributed, a result of slab rollback acceleration, Canadian J. Earth Sci., 53, 1–16, 2016.

Çağatay, M. N., Görür, N., Flecker, R., Sakınç, M., Tünoğlu, C., Ellam, R., Krijgsman, W., Vincent, S., and Dikbaş, A.: Paratethyan–Mediterranean connectivity in the Sea of Marmara region (NW Turkey) during the Messinian, Sediment. Geol., 188–189, 171–187, https://doi.org/10.1016/j.sedgeo.2006.03.004, 2006.

Çağatay, M. N., Eriş, K. K., Makaroğlu, Ö., Yakupoğlu, N., Henry, P., Leroy, S. A. G., Uçarkuş, G., Sakınç, M., Yalamaz, B., Bozyiğit, C., and Kende, J.: The Sea of Marmara during Marine Isotope Stages 5 and 6, Quat. Sci. Rev., 220, 124–141, https://doi.org/10.1016/j.quascirev.2019.07.031, 2019.

Çağatay, M. N., Eris ̧, K. K., and Erdem, Z.: Morphology and Late Pleistocene–Holocene sedimentation of the Strait of Istanbul (Bosphorus): a review, in: Straits and Seaways: Controls, Processes and Implications in Modern and Ancient Systems, edited by: Rossi, V. M., Longhitano, S., Olariu, C., and Chiocci, F., Geological Society, London, Special Publications, 523, https://doi.org/10.1144/SP523-2021-48, 2022.

Calvert, S. E., Thode, H. D., Yeung, D., and Karlin, R. E.: A stable isotope study of pyrite formation in the Late Pleistocene and Holocene sediments of the Black Sea, Geochim. Cosmochim. Ac., 60, 1261–1270, 1996.

Canfield, D. E., Lyons, T. W., and Raiswell, R.: A model for iron deposition to euxinic Black Sea sediments, Am. J. Sci., 296, 818–834. https://doi.org/10.2475/ajs.296.7.818, 1996.

Capet, A., Stanev, E. V., Beckers, J.-M., Murray, J. W., and Grégoire, M.: Decline of the Black Sea oxygen inventory, Biogeosciences, 13, 1287–1297, https://doi.org/10.5194/bg-13-1287-2016, 2016.

Chiu, C. F., Sweere, T. C., Clarkson, M. O., de Souza, G. F., Hennekam, R., and Vance, D.: Co-variation systematics of uranium and molybdenum isotopes reveal pathways for descent into euxinia in Mediterranean sapropels, Earth Planet. Sci Lett., 585, 117527, https://doi.org/10.1016/j.epsl.2022.117527, 2022.

Coma, R., Ribes, M., Serrano, E., Jiménez, E., Salat, J., and Pascual, J.: Global warming-enhanced stratification and mass mortality events in the mediterranean, P. Natl. Acad. Sci. USA, 106, 6176–6181, https://doi.org/10.1073/pnas.0805801106, 2009.

Coskun, Ö. K., Pichler, M., Vargas, S., Gilder, S., and Orsi, W. D.: Linking uncultivated microbial populations and benthic carbon turnover by using quantitative stable isotope probing, Appl. Environ. Microbiol., 84, e01083-18, https://doi.org/10.1128/AEM.01083-18, 2018.

Dijkstra, N., Hagens, M., Egger, M., and Slomp, C. P.: Post-depositional formation of vivianite-type minerals alters sediment phosphorus records, Biogeosciences, 15, 861–883, https://doi.org/10.5194/bg-15-861-2018, 2018.

Eckert, S., Brumsack, H. J., Severmann, S., Schnetger, B., März, C., and Fröllje, H.: Establishment of euxinic condi-

tions in the Holocene Black Sea, Geology, 41, 431–434, https://doi.org/10.1130/G33826.1, 2013.

Egger, M., Hagens, M., Sapart, C. J., Dijkstra, N., van Helmond, N. A. G. M., Mogollón, J. M., Risgaard-Petersen, N., van der Veen, C., Kasten, S., Riedinger, N., Jørgensen, B. B., and Slomp, C. P.: Iron oxide reduction in methane-rich deep Baltic Sea sediments, Geochim. Cosmochim. Ac., 207, 256–276, https://doi.org/10.1016/j.gca.2017.03.019, 2017.

Feurdean, A. and Vasiliev, I.: The contribution of fire to the late Miocene spread of grasslands in eastern Eurasia (Black Sea region), Sci. Rep., 9, 1–7, https://doi.org/10.1038/s41598-019-43094-w, 2019.

Filippidi, A., Triantaphyllou, M. V., and De Lange, G. J.: Eastern-Mediterranean ventilation variability during sapropel S1 formation, evaluated at two sites influenced by deep-water formation from Adriatic and Aegean Seas, Quat. Sci. Rev., 144, 95–106, https://doi.org/10.1016/j.quascirev.2016.05.024, 2016.

Flecker, R., Krijgsman, W., Capella, W., de Castro Martíns, C., Dmitrieva, E., Mayser, J. P., Marzocchi, A., Modestu, S., Ochoa, D., Simon, D., Tulbure, M., van den Berg, B., van der Schee, M., de Lange, G., Ellam, R., Govers, R., Gutjahr, M., Hilgen, F., Kouwenhoven, T., Lofi, J., Meijer, P., Sierro, F. J., Bachiri, N., Barhoun, N., Alami, A. C., Chacon, B., Flores, J. A., Gregory, J., Howard, J., Lunt, D., Ochoa, M., Pancost, R., Vincent, S., and Yousfi, M. Z.: Evolution of the Late Miocene Mediterranean-Atlantic gateways and their impact on regional and global environmental change, Earth-Science Rev., 150, 365–392, https://doi.org/10.1016/j.earscirev.2015.08.007, 2015.

García-Veigas, J., Cendón, D. I., Gibert, L., Lowenstein, T. K., and Artiaga, D.: Geochemical indicators in Western Mediterranean Messinian evaporites: Implications for the salinity crisis, Mar. Geol., 403, 197–214, https://doi.org/10.1016/j.margeo.2018.06.005, 2018.

Gladstone, R., Flecker, R., Valdes, P., Lunt, D., and Markwick, P.: The Mediterranean hydrologic budget from a Late Miocene global climate simulation, Palaeogeogr. Palaeoclimatol. Palaeoecol., 251, 254–267, https://doi.org/10.1016/j.palaeo.2007.03.050, 2007.

Golovina, L. A., Radionova, E. P., Van Baak, C. G. C., Krijgsman, W., and Palcu, D. V.: A Late Maeotian age (6.7–6.3 Ma) for the enigmatic "Pebbly Breccia" unit in DSDP Hole 380A of the Black Sea, Palaeogeogr. Palaeoclimatol. Palaeoecol., 533, 109269, https://doi.org/10.1016/j.palaeo.2019.109269, 2019.

Grothe, A., Sangiorgi, F., Mulders, Y. R., Vasiliev, I., Reichart, G. J., Brinkhuis, H., Stoica, M., and Krijgsman, W.: Black sea desiccation during the Messinian Salinity Crisis: Fact or fiction?, Geology, 42, 563–586, https://doi.org/10.1130/G35503.1, 2014.

Grothe, A., Andreetto, F., Reichart, G.-J., Wolthers, M., Van Baak, C. G. C., Vasiliev, I., Stoica, M., Sangiorgi, F., Middelburg, J. J., Davies, G. R., and Krijgsman, W.: Paratethys pacing of the Messinian Salinity Crisis: Low salinity waters contributing to gypsum precipitation?, Earth Planet. Sci. Lett., 532, 116029, https://doi.org/10.1016/j.epsl.2019.116029, 2020.

Guerra-Merchán, A., Serrano, F., Garcés, M., Gofas, S., Esu, D., Gliozzi, E., and Grossi, F.: Messinian Lago-Mare deposits near the Strait of Gibraltar (Malaga Basin, S Spain), Palaeogeogr. Palaeoclimatol. Palaeoecol., 285, 264–276, https://doi.org/10.1016/j.palaeo.2009.11.019, 2010.

Henkel, S., Mogollón, J. M., Nöthen, K., Franke, C., Bogus, K., Robin, E., Bahr, A., Blumenberg, M., Pape, T., Seifert, R., de Lange, G. J., and Kasten, S.: Diagenetic barium cycling in Black Sea sediments - A case study for anoxic marine environments, Geochim. Cosmochim. Acta, 88, 88–105, https://doi.org/10.1016/j.gca.2012.04.021, 2012.

Hoyle, T. M., Bista, D., Flecker, R., Krijgsman, W., and Sangiorgi, F.: Climate-driven connectivity changes of the Black Sea since 430 ka: Testing a dual palynological and geochemical approach, Palaeogeogr. Palaeoclimatol. Palaeoecol., 561, 110069, https://doi.org/10.1016/j.palaeo.2020.110069, 2021.

Hsü, K. J., Montadert, L., Bernouilli, D., Bizon, G., Cita, M., Erickson, A., Fabricius, F., Garrison, R. E., Kido, R. B., Mellieres, F., Muller, C., and Wright, R. C.: Site 378: Cretan basin, Init. Rep. Deep. Drill. Proj., 42, 321–357, 1978.

Huang, Y., Zheng, Y., Heng, P., Giosan, L., and Coolen, M. J. L.: Black Sea paleosalinity evolution since the last deglaciation reconstructed from alkenone-inferred Isochrysidales diversity, Earth Planet. Sci. Lett., 564, 116881, https://doi.org/10.1016/j.epsl.2021.116881, 2021.

Incarbona, A., Martrat, B., Mortyn, P. G., Sprovieri, M., Ziveri, P., Gogou, A., Jordà, G., Xoplaki, E., Luterbacher, J., Langone, L., Marino, G., Rodríguez-Sanz, L., Triantaphyllou, M., Di Stefano, E., Grimalt, J. O., Tranchida, G., Sprovieri, R., and Mazzola, S.: Mediterranean circulation perturbations over the last five centuries: Relevance to past Eastern Mediterranean Transient-type events, Sci. Rep., 6, 1–10, https://doi.org/10.1038/srep29623, 2016.

Jolivet, L. and Brun, J.-P.: Cenozoic geodynamic evolution of the Aegean, Int. J. Earth Sci., 99, 109–138, https://doi.org/10.1007/s00531-008-0366-4, 2010.

Jørgensen, B. B., Weber, A., and Zopfi, J.: Sulfate reduction and anaerobic methane oxidation in Black Sea sediments, Deep Sea Res. Part I Oceanogr. Res. Pap., 48, 2097–2120, 2001.

Jørgensen, B. B., Böttcher, M. E., Lüschen, H., Neretin, L. N., and Volkov, I. I.: Anaerobic methane oxidation and a deep H2S sink generate isotopically heavy sulfides in Black Sea sediments, Geochim. Cosmochim. Ac., 9, 2095–2118, 2004.

Jørgensen, B. B., Andrén, T., and Marshall, I. P. G.: Subseafloor biogeochemical processes and microbial life in the Baltic Sea, Environ. Microbiol., 22, 1688–1706, https://doi.org/10.1111/1462-2920.14920, 2020.

Karakitsios, V., Cornee, J., Tsourou, T., Moissette, P., Kontakiotis, G., Agiadi, K., Manoutsoglou, E., Triantaphyllou, M., and Koskeridou, E.: Messinian salinity crisis record under strong freshwater input in marginal, intermediate, and deep environments: the case of the North Aegean. Paleogr. Paleoclimatol. Paleoecol. 485, 316–335, https://doi.org/10.1016/j.palaeo.2017.06.023, 2017.

Karatsolis, B. T., Triantaphyllou, M. V., Dimiza, M. D., Malinverno, E., Lagaria, A., Mara, P., Archontikis, O., and Psarra, S.: Coccolithophore assemblage response to Black Sea Water inflow into the North Aegean Sea (NE Mediterranean), Cont. Shelf Res., 149, 138–150, https://doi.org/10.1016/j.csr.2016.12.005, 2017.

Keskin, C., Ordines, F., Guijarro, B., and Massutí, E.: Comparison of fish assemblages between the Sea of Marmara and the Aegean Sea (north-eastern Mediterranean), J. Mar. Biol. Assoc. United Kingdom, 91, 1307–1318, https://doi.org/10.1017/S0025315410002213, 2011.

Krijgsman, W., Palcu, D. V., Andreetto, F., Stoica, M., and Mandic, O.: Changing seas in the late Miocene Northern Aegean: A Paratethyan perspective to Mediterranean stratigraphy, Earth Sci. Rev., 210, 103386, https://doi.org/10.1016/j.earscirev.2020.103386, 2020.

Kuypers, M. M. M., Sliekers, A. O., Lavik, G., Schmid, M., Jørgensen, B. B., Kuenen, J. G., Sinninge Damsté, J. S., Strous, M., and Jetten, M. S. M.: Anaerobic ammonium oxidation by anammox bacteria in the Black Sea, Nature, 422, 608–611, 2003.

Kwiecien, O., Stockhecke, M., Pickarski, N., Heumann, G., Litt, T., Sturm, M., Anselmetti, F., Kipfer, R., and Haug, G. H.: Dynamics of the last four glacial terminations recorded in Lake Van, Turkey, Quat. Sci. Rev., 104, 42–52, https://doi.org/10.1016/j.quascirev.2014.07.001, 2014.

Lagaria, A., Mandalakis, M., Mara, P., Frangoulis, C., Karatsolis, B. T., Pitta, P., Triantaphyllou, M., Tsiola, A., and Psarra, S.: Phytoplankton variability and community structure in relation to hydrographic features in the NE Aegean frontal area (NE Mediterranean Sea), Cont. Shelf Res., 149, 124–137, https://doi.org/10.1016/j.csr.2016.07.014, 2017.

Lenstra, W. K., Klomp, R., Molema, F., Behrends, T., and Slomp, C. P.: A sequential extraction procedure for particulate manganese and its application to coastal marine sediments, Chem. Geol., https://doi.org/10.1016/j.chemgeo.2021.120538, 2021.

Liu, J., Nowaczyk, N. R., Panovska, S., Korte, M., and Arz, H. W.: The Norwegian-Greenland Sea, the Laschamps, and the Mono Lake Excursions Recorded in a Black Sea Sedimentary Sequence Spanning From 68.9 to 14.5 ka, J. Geophys. Res.-Sol. Ea., 125, e2019JB019225, https://doi.org/10.1029/2019JB019225, 2020.

Lyons, T. W.: Sulfur isotopic trends and pathways of iron sulfide formation in upper holocene sediments of the anoxic black sea, Geochim. Cosmochim. Ac., 61, 3367–3382, https://doi.org/10.1016/S0016-7037(97)00174-9, 1997.

Lyons, T. W. and Berner, R. A.: Carbon-sulfur-iron systematics of the uppermost deep-water sediments of the Black Sea, Chem. Geol., 99, 1–27, 1992.

Lyons, T. W., Reinhard, C. T., and Planavsky, N. J.: The rise of oxygen in Earth's early ocean and atmosphere, Nature, 506, 307–315, https://doi.org/10.1038/nature13068, 2014.

Major, C. O., Goldstein, S. L., Ryan, W. B. F., Lericolais, G., Piotrowski, A. M., and Hajdas, I.: The co-evolution of Black Sea level and composition through the last deglaciation and its paleoclimatic significance, Quat. Sci. Rev., 25, 2031–2047, https://doi.org/10.1016/j.quascirev.2006.01.032, 2006.

Marshall, I. P. G., Karst, S. M., Nielsen, P. H., and Jørgensen, B. B.: Metagenomes from deep Baltic Sea sediments reveal how past and present environmental conditions determine microbial community composition, Mar. Genomics, 37, 58–68, https://doi.org/10.1016/j.margen.2017.08.004, 2018.

Matthews, A., Azrieli-Tal, I., Benkovitz, A., Bar-Matthews, M., Vance, D., Poulton, S. W., Teutsch, N., Almogi-Labin, A., and Archer, C.: Anoxic development of sapropel S1 in the Nile Fan inferred from redox sensitive proxies, Fe speciation, Fe and Mo isotopes, Chem. Geol., 475, 24–39, https://doi.org/10.1016/j.chemgeo.2017.10.028, 2017.

Nikishin, A. M., Okay, A. I., Tüysüz, O., Demirer, A., Amelin, N., and Petrov, E.: The Black Sea basins structure and history: new model based on new deep penetration regional seismic data. Part 1: Basins structure and fill, Mar. Pet. Geol., 59, 638–655, 2015.

Nowaczyk, N. R., Arz, H. W., Frank, U., Kind, J., and Plessen, B.: Dynamics of the Laschamp geomagnetic excursion from Black Sea sediments, Earth Planet. Sci. Lett., 351–352, 54–69, https://doi.org/10.1016/j.epsl.2012.06.050, 2012.

Nowaczyk, N. R., Liu, J., Plessen, B., Wegwerth, A., and Arz, H. W.: A High-Resolution Paleosecular Variation Record for Marine Isotope Stage 6 From Southeastern Black Sea Sediments, J. Geophys. Res.-Sol. Ea., 126, e2020JB021350, https://doi.org/10.1029/2020JB021350, 2021.

Orcutt, B. N., LaRowe, D. E., Lloyd, K. G., Mills, H., Orsi, W., Reese, B. K., Sauvage, J., Huber, J. A., and Amend, J.: IODP Deep Biosphere Research Workshop report – a synthesis of recent investigations, and discussion of new research questions and drilling targets, Sci. Dril., 17, 61–66, https://doi.org/10.5194/sd-17-61-2014, 2014.

Owens, J. D., Nielsen, S. G., Horner, T. J., Ostrander, C. M., and Peterson, L.: Thallium-isotopic compositions of euxinic sediments as a proxy for global manganese-oxide burial, Geochim. Cosmochim. Ac., 213, 291–307, 2017.

Palcu, D. V., Patina, I. S., Sandric, I., Lazarev, S., Vasiliev, I., Stoica, M., and Krijgsman, W.: Late Miocene megalake regressions in Eurasia, Sci. Rep., 11, 1–12, https://doi.org/10.1038/s41598-021-91001-z, 2021.

Popov, S. V., Shcherba, I. G., Ilyina, L. B., Nevesskaya, L. A., Paramonova, N. P., Khondkarian, S. O., and Magyar, I.: Late Miocene to Pliocene palaeogeography of the Paratethys and its relation to the Mediterranean, Palaeogeogr. Palaeoclimatol. Palaeoecol., 238, 91–106, https://doi.org/10.1016/j.palaeo.2006.03.020, 2006.

Popov, S. V., Rostovtseva, Y. V., Fillippova, N. Y., Golovina, L. A., Radionova, E. P., Goncharova, I. A., Vernyhorova, Y. V., Dykan, N. I., Pinchuk, T. N., Iljina, L. B., Koromyslova, A. V., Kozyrenko, T. M., Nikolaeva, I. A., and Viskova, L. A.: Paleontology and Stratigraphy of the Middle–Upper Miocene of the Taman Peninsula: Part 1. Description of Key Sections and Benthic Fossil Groups, Paleontol. J., 50, 1–168, 2016.

Poulton, S. W. and Canfield, D. E.: Development of a sequential extraction procedure for iron: Implications for iron partitioning in continentally derived particulates, Chem. Geol., 214, 209–221, https://doi.org/10.1016/j.chemgeo.2004.09.003, 2005.

Riedinger, N., Formolo, M. J., Lyons, T. W., Henkel, S., Beck, A., and Kasten, S.: An inorganic geochemical argument for coupled anaerobic oxidation of methane and iron reduction in marine sediments, Geobiology, 12, 172–181, 2014.

Rodriguez, M., Sakellariou, D., Gorini, C., Chamot-Rooke, N., d'Acremont, E., Nercessian, A., Tsampouraki Kraounaki, K., Oregioni, D., Delescluse, M., and Janin, A.: Seismic profiles across the North Anatolian Fault in the Aegean Sea, Geophys. Res. Abstr., Vol. 20, EGU2018-7426, EGU General Assembly 2018.

Roether, W., Beniamino, B. M., Klein, B., Bregant, D., Georgopoulos, D., Beitzel, V., Kovačević, V., Luchetta, A., Roether, W., Manca, B. B., Klein, B., Bregant, D., Georgopoulos, D., and Beitzel, V.: Recent Changes in Eastern Mediterranean Deep Waters, Science, 271, 333–335, 1996.

Rohling, E. J., Foster, G. L., Grant, K. M., Marino, G., Roberts, A. P., Tamisiea, M. E., and Williams, F.: Sea-level and deep-sea-temperature variability over the past 5.3 million years, Nature, 508, 477–482, https://doi.org/10.1038/nature13230, 2014.

Rohling, E. J., Marino, G., and Grant, K. M.: Mediterranean climate and oceanography, and the periodic development of anoxic events (sapropels), Earth-Science Rev., 143, 62–97, https://doi.org/10.1016/j.earscirev.2015.01.008, 2015.

Roveri, M., Flecker, R., Krijgsman, W., Lofi, J., Lugli, S., Manzi, V., Sierro, F. J., Bertini, A., Camerlenghi, A., De Lange, G., Govers, R., Hilgen, F. J., Hübscher, C., Meijer, P. T., and Stoica, M.: The Messinian Salinity Crisis: Past and future of a great challenge for marine sciences, Mar. Geol., 352, 25–58, https://doi.org/10.1016/j.margeo.2014.02.002, 2014.

Royden, L. H. and Papanikolaou, D. J.: Slab segmentation and late Cenozoic disruption of the Hellenic arc, Geochem. Geophy. Geosy., 12, Q03010, https://doi.org/10.1029/2010GC003280, 2011.

Rybkina, A. I., Kern, A. N., and Rostovtseva, Y. V.: New evidence of the age of the lower Maeotian substage of the Eastern Paratethys based on astronomical cycles, Sediment. Geol., 330, 122–131, https://doi.org/10.1016/j.sedgeo.2015.10.003, 2015.

Sakellariou, D., Rousakis, G., Morfis, I., Panagiotopoulos, I., Ioakim, C., Trikalinou, G., Tsampouraki-Kraounaki, K., Kranis, H., and Karageorgis, A.: Deformation and kinematics at the termination of the North Anatolian Fault: the North Aegean Trough horsetail structure, Proc. 9th Int. INQUA Meet. Paleoseismology, Act. Tectonics Archeoseismology, 237–240, 25–27 June 2018, Possidi, Greece, 2018.

Sakellariou, D. and Tsampouraki-Kraounaki, K.: Plio-Quaternary extension and strike-slip tectonics in the Aegean, in: Transform Plate Boundaries and Fracture Zones, edited by: Duarte, J., Elsevier, 339–374, https://doi.org/10.1016/B978-0-12-812064-4.00014-1, 2018.

Schmidt, J. M., Royalty, T. M., Lloyd, K. G., and Steen, A. D.: Potential Activities and Long Lifetimes of Organic Carbon-Degrading Extracellular Enzymes in Deep Subsurface Sediments of the Baltic Sea, Front. Microbiol., 12, 702015, https://doi.org/10.3389/fmicb.2021.702015, 2021.

Schrader, H. J.: Quaternary through Neogene history of the Black Sea, deduced from the paleoecology of diatoms, silicoflagellates, ebridians, and chrysomonads, in: Initial Reports of the Deep Sea Drilling Project, edited by: Ross, D. A. and Neprochnov, Y. P., Vol. 42, Part 2, U.S. Government Printing Office, Washington, 1978.

Scott, C. and Lyons, T. W.: Contrasting molybdenum cycling and isotopic properties in euxinic versus non-euxinic sediments and sedimentary rocks: Refining the paleoproxies, Chem. Geol., 324, 19–27, 2012.

Şengör, A. M. C.: The North Anatolian transform fault: its age, onset and tectonic significance, J. Geol. Soc. London, 136, 269–282, 1979.

Şengör, A. M. C., Tüysüz, O., İmren, C., Sakınç, M., Eyidoğan, H., Görür, N., Le Pichon, X., and Claude Rangin, C.: The North Anatolian Fault. A new look, Annu. Rev. Earth Planet. Sci., 33, 1–75, 2005.

Sinninge Damsté, J. S., Wakeham, S. G., Kohnen, M. E., Hayes, J. M., and de Leeuw, J. W.: A 6,000-year sedimentary molecular record of chemocline excursions in the Black Sea, Nature, 362, 827–829, 1993.

Sorlien, C. C., Akhun, S. D., Seeber, L., Steckler, M. S., Shillington, D. J., Kurt, H., Çifçi, G., Poyraz, D. T., Gürçay, S., Dondurur, D., Küçük, H. M., and Diebold, J. B.: Uniform basin growth over the last 500ka, North Anatolian Fault, Marmara Sea, Turkey, Tectonophysics, 518–521, 1–16, https://doi.org/10.1016/j.tecto.2011.10.006, 2012.

Soulet, G., Delaygue, G., Vallet-Coulomb, C., Böttcher, M. E., Sonzogni, C., Lericolais, G., and Bard, E.: Glacial hydrologic conditions in the Black Sea reconstructed using geochemical pore water profiles, Earth Planet. Sci. Lett., 296, 57–66, https://doi.org/10.1016/j.epsl.2010.04.045, 2010.

Sperling, M., Schmiedl, G., Hemleben, C., Emeis, K. C., Erlenkeuser, H., and Grootes, P. M.: Black Sea impact on the formation of eastern Mediterranean sapropel S1? Evidence from the Marmara Sea, Palaeogeogr. Palaeoclimatol. Palaeoecol., 190, 9–21, https://doi.org/10.1016/S0031-0182(02)00596-5, 2003.

Stoica, M., Krijgsman, W., Fortuin, A., and Gliozzi, E.: Paratethyan ostracods in the Spanish Lago-Mare: More evidence for interbasinal exchange at high Mediterranean sea level, Palaeogeogr. Palaeoclimatol. Palaeoecol., 441, 854–870, https://doi.org/10.1016/j.palaeo.2015.10.034, 2016.

Tari, G., Fallah, M., Kosi, W., Floodpage, J., Baur, J., Bati, Z., and Sipahioğlu, N. O.: Is the impact of the Messinian Salinity Crisis in the Black Sea comparable to that of the Mediterranean?, Mar. Pet. Geol., 66, 135–148, https://doi.org/10.1016/j.marpetgeo.2015.03.021, 2015.

Tari, G., Fallah, M., Schell, C., Kosi, W., Bati, Z., Sipahioğlu, N. Ö., Krezsek, C., Schleder, Z., Kozhuharov, E., and Kitchka, A.:. Why are there no Messinian evaporites in the Black Sea?, Pet. Geosci., 22, 381–391, 2016.

Taymaz, T., Jackson, J., and McKenzie, D.: Active tectonics of the North and Central Aegean Sea, Geophys. J. Int., 106, 433–490, 1991.

Thunell, R. C., Locke, S. M., and Williams, D. F.: Glacio-eustatic sealevel control on Red Sea salinity, Nature, 334, 601–604, 1988.

Tishchenko, I., Tari, G., Fallah, M., and Floodpage, J.: Submarine landslide origin of a tsunami at the Black Sea coast: Evidence based on swath bathymetry and 3D seismic reflection data, Interpretation, 0, SB67-BS78, 2021.

Van Baak, C. G. C., Radionova, E. P., Golovina, L. A., Raffi, I., Kuiper, K. F., Vasiliev, I., and Krijgsman, W.: Messinian events in the Black Sea, Terra Nov., 27, 433–441, https://doi.org/10.1111/ter.12177, 2015.

Van Baak, C. G. C., Vasiliev, I., Palcu, D. V, Dekkers, M. J., and Krijgsman, W.: A Greigite-Based Magnetostratigraphic Time Frame for the Late Miocene to Recent DSDP Leg 42B Cores from the Black Sea, Front. Earth Sci., 4, 1–18, https://doi.org/10.3389/feart.2016.00060, 2016.

Vasiliev, I., Reichart, G.-J., and Krijgsman, W.: Impact of the Messinian Salinity Crisis on Black Sea hydrology—Insights from hydrogen isotopes analysis on biomarkers, Earth Planet. Sci. Lett., 362, 272–282, https://doi.org/10.1016/j.epsl.2012.11.038, 2013.

Vasiliev, I., Reichart, G.-J., Grothe, A., Sinninghe Damsté, J. S., Krijgsman, W., Sangiorgi, F., Weijers, J. W. H., and van Roij, L.: Recurrent phases of drought in the upper Miocene of the Black Sea region, Palaeogeogr. Palaeoclimatol. Palaeoecol., 423, 18–31, https://doi.org/10.1016/j.palaeo.2015.01.020, 2015.

Vasiliev, I., Reichart, G.-J., Krijgsman, W., and Mulch, A.: Black Sea rivers capture significant change in catchment-wide mean annual temperature and soil pH during the Miocene-

to-Pliocene transition, Glob. Planet. Change, 172, 428–439, https://doi.org/10.1016/j.gloplacha.2018.10.016, 2019.

Vasiliev, I., Feurdean, A., Reichart, G. J., and Mulch, A.: Late Miocene intensification of continentality in the Black Sea region, Int. J. Earth Sci., 109, 831–846, https://doi.org/10.1007/s00531-020-01832-w, 2020.

Wegwerth, A., Dellwig, O., Kaiser, J., Ménot, G., Bard, E., Shumilovskikh, L., Schnetger, B., Kleinhanns, I. C., Wille, M., and Arz, H. W.: Meltwater events and the Mediterranean reconnection at the Saalian–Eemian transition in the Black Sea, Earth Planet. Sci. Lett., 404, 124–135, 2014.

Wegwerth, A., Dellwig, O., Wulf, S., Plessen, B., Kleinhanns, I. C., Nowaczyk, N. R., Jiabo, L., and Arz, H. W.: Major hydrological shifts in the Black Sea "Lake" in response to ice sheet collapses during MIS 6 (130–184 ka BP), Quat. Sci. Rev., 219, 126–144, https://doi.org/10.1016/j.quascirev.2019.07.008, 2019.

Wegwerth, A., Kaiser, J., Dellwig, O., and Arz, H. W.: Impact of Eurasian Ice Sheet and North Atlantic Climate Dynamics on Black Sea Temperature Variability During the Penultimate Glacial (MIS 6, 130–184 ka BP), Paleoceanogr. Paleocl., 35, e2020PA003882, https://doi.org/10.1029/2020PA003882, 2020.

Yakushev, E. V., Chasovnikov, V. K., Murray, J. W., Pakhomova, S. V., Podymov, O. I., and Stunzhas, P. A.: Vertical hydrochemical structure of the black sea, Handb. Environ. Chem., Vol. 5 Water Pollut., 5 Q, 277–307, https://doi.org/10.1007/698_5_088, 2008.

Zinke, L. A., Mullis, M. M., Bird, J. T., Marshall, I. P. G., Jørgensen, B. B., Lloyd, K. G., Amend, J. P., and Kiel Reese, B.: Thriving or surviving? Evaluating active microbial guilds in Baltic Sea sediment, Environ. Microbiol. Rep., 9, 528–536, https://doi.org/10.1111/1758-2229.12578, 2017.

A Boost for Geothermal Energy Research by ICDP

Driven by a couple of proposals received and reviewed by the International Continental Scientific Drilling Program, ICDP in the past years, a new strategy was developed to guide international geothermal research groups towards ICDP support. This strategy was published by ICDP in the short brochure '**Support for geothermal drilling projects**' (https://www.icdp-online.org/fileadmin/icdp/media/doc/ICDP_Geothermal.pdf)

Until recently, ICDP focused on projects in the high and ultrahigh temperature fields including e.g., supercritical fluids (Iceland Deep Drilling Projects 1 and 2). However, the global soaring need for utilizing heat from Earth is uncovering the necessity to open additionally new research avenues in enhanced geothermal energy production as well as in low-enthalpy heat utilization. ICDP recognizes the need for additional research in the respective fields by expending its funding priorities: **World-Class Science** and **World-Class Site** remain of course valid criteria but are now being supplemented with **World-Class Opportunity**. The latter counts for opportunities to incorporate scientifically outstanding experiments in public or industry funded geothermal projects. Such piggy-backing must enable scientists to understand underlying processes of key scientific significance. Furthermore, it must address demands that are transferrable to other sites and data acquired must be made fully available to science and public.

In terms of methodological approaches, the new geothermal strategy of ICDP highlightsfour fields including

- **Monitoring** – high resolution, long-term, in situ observations on rock and fluid parameters, stress and strain, and alike
- **Simulation** – addresses the needs of modelling to illuminate complex coupled processes by using high-quality data
- **Technology Challenges** – require development of monitoring, sampling, and borehole integrity equipment withstanding hostile conditions over extended time periods
- **New Horizons** – are completely new pathways in the geothermal sector such as ultradeep drilling

Finally, **Societal Aspects** and public acceptance issues should be a vital part of any proposal submitted to ICDP.

Uli Harms

Obituary for Prof. Leanne Armand 1968–2022

We are deeply saddened to report the passing of Prof. Leanne Armand, the Director of the Australian and New Zealand IODP Consortium (ANZIC), on January 4th after a valiant battle with a highly aggressive cancer. Leanne was a major force in IODP from 2017 to 2021, both as ANZIC Program Scientist, and later as ANZIC Director, and through her engagement and questioning on committees including the JRFB. Her contributions to scientific ocean drilling were profound, as she ably guided the ANZIC Program Member Office through a critical period of setting a post-2024 vision for scientific ocean drilling. This involved the planning and implementation of ANZIC's Ocean Planet Workshop in April 2019, a multidisciplinary effort that identified key themes of interest to the ANZIC ocean drilling community, and which provided significant scientific and conceptual input into the IODP 2050 Scientific Framework.

Leanne was a micropaleontologist. She undertook her PhD on marine diatoms from the Southern Ocean at the Australian National University (ANU) and Bordeaux University. Her PhD, awarded in 1998, focused on using fossilised diatom species assemblages to determine past changes in sea-surface temperature and sea-ice extent in the Southern Ocean – the topic she then devoted the rest of her career to, contributing significantly to our understanding of the paleoceanography of the Southern Ocean.

After finishing her PhD, Leanne worked at the University of Tasmania. She returned to France in 2007 as the first Australian recipient of a European Union Incoming Marie Curie Fellowship, studying at the Centre d'Océanographie de Marseille, before moving back to Australia in 2009, where she joined the Department of Biology at Macquarie University in Sydney. She rose to the level of Deputy Director of the MQ Marine Research Centre at Macquarie, where she remained until assuming the first of her ANZIC roles in 2017.

Over her career Leanne participated and lead a number of international research voyages to the Southern Ocean and Antarctica, published over 100 papers, supervised a large number of students, and mentored many more early/mid/late career researchers (especially women in marine science). She was the driving force in the creation of the Collaborative Australian Postgraduate Sea Training Alliance Network (CAPSTAN), serving as its first Director. In 2007, she was awarded the Australian Academy of Science's prestigious Dorothy Hill Medal. She received a U.S. Antarctic Service Medal in 2014 for the Sabrina Coast Mission on the RVIB Palmer, and was the first Chief Scientist to conduct an Antarctic expedition on Australia's then-new research ship, RV Investigator, in 2017. In 2020, Leanne was promoted to Professor of Marine Micropalaeontology at ANU.

Leanne's service as leader of the ANZIC Program Member Office was marked by a keen scientific and managerial eye and her tireless support for diversity within IODP. Her expertise, energy, personal warmth, and enthusiasm were infectious. She is greatly missed.

Carl Brenner, Mike Coffin and Henk Brinkhuis, Clive Neal, Helen Bostock

Information from Obituary- Professor Leanne Armand, ANZIC Director (1968–2022) | ANU Research School of Earth Sciences

Leanne Armand's obituary https://doi.org/10.1016/j.marmicro.2022.102095.

Leanne Armand - Wikipedia

Post-2024 Scientific Ocean Drilling

The end of the International Ocean Discovery Program on 30 September 2024 will mark major change in the organization of international activities related to scientific ocean drilling, with a transition from a single international program operated by independent platform providers to independent and collaborative programs. The 2050 Science Framework (http://www.iodp.org/2050-science-framework), which represents a new and innovative approach for conducting science using a portfolio of offshore drilling platforms, must be the foundation of such future initiatives.

A major outcome of bilateral meetings between current IODP partners was the decision by ECORD and Japan to build a combined post-2024 program based on Mission-Specific Platform (MSP) expeditions, while keeping their own functioning and identity. At the IODP Forum that was held in Lamont-Doherty Earth Observatory, Palisades, New York, in September 2022, ECORD and Japan have presented the progress made to formalize their partnership. They also invited other international entities to join this initiative and share overarching resources, such as proposal and data management (the main responsibility of the current Science Support Office – SSO-) and the proposal review process (the remit of the current Science Evaluation Panel – SEP - and Environmental Protection and Safety Panel - EPSP -). ECORD and Japan anticipate that this joint program, inspired by the 2050 Framework, will begin immediately after the conclusion of the current IODP. Communication plans to inform international ocean drilling science communities about the rapidly evolving situation of the post-2024 plans will develop in the next months.

The development of post-2024 initiatives will also require continuity of core and data legacies, in order to maintain one of the key basic principles of the successive international scientific ocean drilling programs. The related agreements among current IODP partners will be formalized to ensure the continuity of legacy activities throughout the transition between the current IODP and future scientific ocean drilling initiatives.

Gilbert Camoin,
Director of the ECORD
Managing Agency
Nobu Eguchi,
Director of Operations
Dept MarE3 JAMSTEC
On behalf of the
ECORD-Japan Scientific Ocean Drilling Working Groups

Schedules

Due to the Corona pandemic situation, several expeditions and drilling projects are postponed until further notice.

IODP – Expedition schedule http://www.iodp.org/expeditions/

USIO operations	Platform	Dates	Port of origin
1 Exp 397: Iberian Margin Paleoclimate	JOIDES Resolution	Oct 11–Dec 11, 2022	Lisbon
2 Exp 398: Hellenic Arc Volcanic Field	JOIDES Resolution	Dec 11, 2022–Feb 10, 2023	Tarragona
3 Exp 399: Building Blocks of Life, Atlantis Massif	JOIDES Resolution	Apr 12–Jun 12, 2023	Heraklion

ICDP – Project schedule http://www.icdp-online.org/projects/

ICDP project	Drilling dates	Location
1 Drilling the Ivrea-Verbano ZonE (DIVE)	Oct 2022–May 2023	Northern Italy (Ornavasso, Megolo)
2 Trans-Amazon Drilling Project (TADP)	Feb–Jul 2023	Brazil (Acre and Marajo Basins)
3 Bushveld Drilling Project (BVDP)	Spring–Fall 2023	South Africa (Mpumalanga, Limpopo)
4 Eger Rift Drilling Project (EGER)	Spring 2023	Germany (Neualbenreuth)

Location

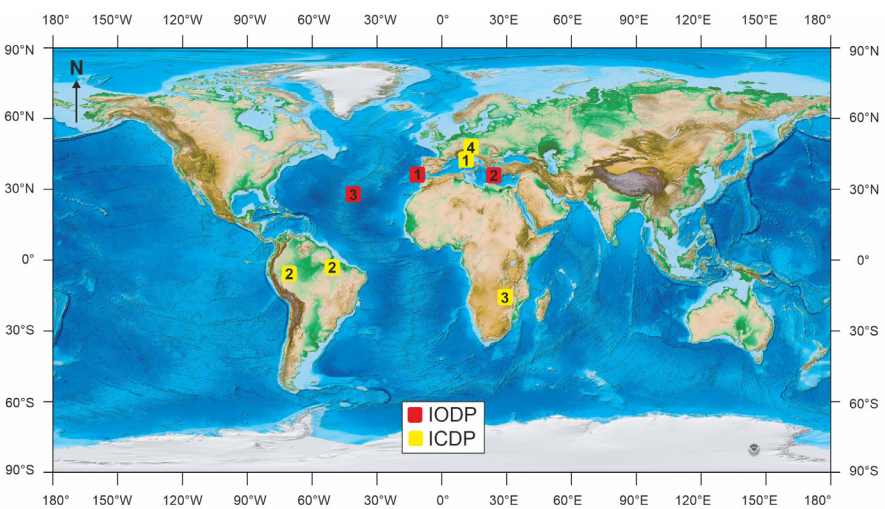

Topographic/bathymetric maps courtesy of NOAA (Amante, C. and B.W. Eakins, 2009. ETOPO1 1 Arc-Minute Global Relief Model: Procedures, Data Sources and Analysis. NOAA Technical Memorandum NESDIS NGDC-24. National Geophysical Data Center, NOAA. doi:10.7289/V5C8276M).